Geochemical Study of the Cameroon Volcanic Line: Implication for the Genesis of Passive Margin Intraplate Magmatism

2017, September

Iyasu Getachew Belay

Graduate School of Natural Science and Technology

(Doctor's Course)

OKAYAMA UNIVERSITY

ABSTRACT

The origin of hotspot magmatism has generally been explained by the plume hypothesis, namely, melting of upwelling asthenospheric mantle beneath the intraplate lithospheric mantle. The passive continental margin is one of the major hot spot location, which is most widely distributed on and western offshore of the African continent. The plume hypothesis explains the presence of recycled crustal or lithospheric mantle materials in the upwelling mantle plume to generate the large chemical and isotopic variabilities of the West African passive margin intraplate basalt (WAPM-IB). However, absence of time-progressive linear hotspot track and little distribution of high-degree of melt in WAPM-IB make it difficult to explain its genesis by the simple mantle plume hypothesis. In this thesis, I report major and trace elements and Sr, Nd, Hf, and Pb isotopic compositions for 90 mafic samples collected from five volcanic centers (Annobon, Sao Tome, Principe, Bioko, and Etinde) in the Cameroon Volcanic Line (CVL). These chemical and Sr-Nd-Hf-Pb isotopic variations explain that the parental magmas for the CVL can be generated by melting of Group 1 kimberlite source, refertilized cratonic subcontinental lithospheric mantle (SCLM). The old asthenospheric mantle-derived low degree of melt that should have metasomatized SCLM during the Mesozoic continental breakup, and the pyroxenite vein or layer in the SCLM. This result demonstrates that no external 'plume' components is necessary to form the CVL magmas. The defined source materials can also explain the isotopic variations for other WAPM-IB: Canary Islands, Atlas Mountains, and Capo Verde Islands. Our results combined with the continental rift model deciphers that the tectonically-controlled lateral mantle convection can be a heat source to melt the SCLM widely distributed beneath Africa and Atlantic Ocean. Edge-driven convection formed by the lateral mantle flow at the continent-oceanic boundary can heat the SCLM beneath the Atlantic Ocean, selectively melting the low solidus material of the SCLM. The coincident distribution of CVL and Canary-Atlas chains at the NW edge of the cratonic lithospheric mantle suggests that the heating of the SCLM by the edge-driven convection can be the most effective where the mantle flow collide near the edge of the SCLM rather than at the front collision. The edge-driven convection can occur more than several tens Mys at the same location, forming the long duration of magmatism without showing the time-progressive linear hot spot track. Consequently, the upwelling mantle plume is not necessary to form the chemical and isotopic characteristics for the passive continental margin hot spot magmatism at the WAPM.

DEDICATION

This piece of work is dedicated with sincere gratitude and affection to:

My late Mother, Wubayehu Enyew and my late Brother, Birhanu Enyew whose legacy of love continue to inspire me. May their soul continue to rest in perfect peace.

My wife Samrawit Sisay and my daughter Christian Iyasu whose warmth affection and patience brought this a success.....

ACKNOWLEDGEMENTS

I would like to express my sincere appreciation and deep gratitude to my academic supervisors; Associate Professor Ryoji Tanaka, Professor Eizo Nakamura, Professor Katsura Kobayashi, and Assistant Professor Hiroshi Kitagawa for their academic supervision, scientific guidance and providing me stimulating environment to establish myself in research. I would like to acknowledge their continuous encouragement throughout my PhD research and the financial support to the realization of this work.

I am so grateful to Professor Akio Makishima for his encouragement and for teaching me different basic courses in Geochemistry and Isotope Geology. I would like to extend my gratefulness to Associate Professor Takuya Moriguti for his guidance and encouragement. Associate Professors Tatsuki Tsujimori and Takuya Kunihiro are thanked for their encouragement and offering me various courses. My sincere thanks go to Dr. Tsutomu Ota for his support in SEM analysis and for his encouragement. I would like to express my gratefulness to Dr. Hiroshi Kitagawa for his great help in K-Ar dating.

I am deeply indebted to Ms. Chie Sakaguchi for her guidance and support in the clean room laboratory work and for her commitment in helping me in analysis of trace elements and Multi isotopic compositions of the samples. Dr. Satoshi Tokeshi and Dr. Takele Akalu are greatly acknowledged for training me in laboratory works, analytical guidance and for their valuable discussions.

My special thanks go to Dr. Tesfaye Demissie for his professional support and introducing me to the research environment. Dr. Aka Festus is acknowledged for collecting the studied samples. My gratefulness goes to Ms. X. J. Shen for her contribution in the preparation of powdered samples, thin sections and analysis of major elements. I am so thankful to Dr. Melese Gemechu, Dr. Lalindra Vishwajith Ranaweera, Abebe Asnake, Tsegereda Ayalew, Dejene Hailemariam, Marian Sapah, Dr. Ivan Pineda Velasco, Narangoo Purevjav, Dr. Morgane Ledevin, Dr. Sunyoung Ryu, Nadezda Chertkova Wang Riping, Tai Truong Nguen, Que Dinh Hoang and Xiaoyu Zhou for their warmth friendship and encouragement.

I would like to extend my deep gratitude to all the academic and administrative staff members of the Pheasant Memorial laboratory (PML) for their immeasurable support to provide me a suitable environment for research. I am sincerely grateful for the

financial support from the Pheasant Memorial Laboratory, Institute for Planetary Materials (IPM), Okayama University and the Japanese Government (Monbukagakusho) scholarships.

My deep appreciation and love goes to my wife, Samrawit Sisay for providing me love and care being on myside and for overcoming the challenge of raising our daughter, Christian Iyasu, during my absence. My sincere gratitude and affection goes to my grandmother, ALEMTSEHAY YIGZAW who has made the greatest effort to raise me with love and discipline.

I appreciate the moral and spiritual support from my Father, Mr. Getachew Belay and my Mother, Mrs. Ruth Mandefro. My special thanks go to my Father in law, Mr. Sisay Ambico and my mother in law, Mrs. Addisalem Mekonnen for their immeasurable encouragement and support in handling my family issues that concern me during my stay in Japan.

Thank you, ALMIGHTY GOD, for your guidance and inspiration.

TABLE OF CONTENTS

LIST OF FIGURES

CHAPTER 1

CHAPTER 2

CHAPTER 3

CHAPTER 4

CHAPTER 5

LIST OF TABLES

CHAPTER 4

CHAPTER 5

APPENDIX

CHAPTER 1: INTRODUCTION

1.1. Intraplate magmatism: plume vs. tectonic-controlled hypotheses

Intraplate basaltic magmatism provides valuable information to understand the chemical and physical properties of Earth's mantle. Forming the mantle-derived magma at the intraplate setting requires the temperature that exceeds its solidus, which generally constrains the thermal structure of the convecting asthenospheric mantle. Geochemical characteristics of these magmas provide the chemical and petrological properties of the source material. The intraplate basalts, except for that erupted near the plate boundary, are located in three main regions: intra-ocean (generally refereed as ocean island basalts or OIB: e.g. Hawaii and Réunion), intra-continent (e.g. Yellow stone and many volcanic centers in African continent), and ocean-continent boundary (e.g. Canary and Cameroon Volcanic Line). Whole mantle-scale upwelling mantle plume theory has generally been accepted to explain the time-progressive linear hot spot track aligned in the plate motion (e.g. Hawaii-Emperor chain) or large igneous provinces where the voluminous magmatism was occurred instantaneously within a few million years (e.g. Afar and Deccan) (Morgan, 1971). Initiation of rift-related intra-continental basalts may have generally been explained either by the upwelling mantle plume (Richards et al., 1989), lithospheric thinning (Foulger and Natland, 2003), or asthenospheric shear (Conrad et al., 2010).

The genesis of intraplate basalt has been debated for more than 40 years. Two major hypotheses have been proposed to explain intraplate magma genesis namely plume and non-plume hypotheses. The plume hypothesis (Morgan, 1971) proposed that intraplate basalt is a surface expression of melting of hot and buoyant mantle plume originated from core-mantle boundary. To evaluate the deep mantle-derived plume hypothesis, Courtillot (2003) examined the geological, geophysical, and geochemical features of hotspots on the Earth based on the five criteria: the presence of (1) an age-progressive linear volcanic chain, (2) the flood basalt at the initial stage of hotspot track, (3) a large buoyancy flux, (4) a high $^{3}He/^{4}He$ lava, and (5) a significant low shear wave velocity in the underlying mantle. They concluded that only seven out of 49 hotspots (Hawaii, Easter, Louisville, Iceland, Afar, Reunion, and Tristan) can be regarded as formed by lower mantle derived upwelling plume, and the others were originated either from upper and lower mantle transition zone (N~20) or by the upper mantle features which may link to the small

convection in the upper mantle or passive response from the lithospheric mantle (N~20).

The seismic tomography image provides a deep-rooted mantle plume connected to the core mantle boundary. Tomography of Ritsema and Allen (2003) presented the vertically continuous low share velocity zones for eight regions (Afar, Bowie, Easter, Hawaii, Iceland, Louisville, McDonald, and Samoa) and the P-wave velocity tomographic image of Montelli et al. (2004) suggested at least six well-resolved deep mantle plumes (Ascension, Azores, Canary, Easter, Samoa, and Tahiti). The recent whole-mantle shear wave velocity model indicated 27 hotspots are connected to the core-mantle boundary via the vertical plume conduit (French and Romanowicz, 2015). Although the numbers and locations are different among the studies, the root of the plume at the core-mantle boundary coincident with the ultralow velocity zones (ULVZs) which locates beneath the south Pacific and Atlantic Ocean (e.g. Bull et al., 2009; French and Romanowicz, 2015).

The geochemical heterogeneity for these Pacific and Atlantic hotspot volcanoes also suggested the plume hypothesis (Hofmann and White, 1982). Many geochemists insisted that the source of intraplate basalts contain various types of recycled crustal components and lithospheric mantle components which were transported by subduction process and undegassed lower mantle materials (Kellogg et al., 1999; Zindler and Hart, 1986). The subducted materials can be a major source of ULVZs, which can also be a major reservoir of the intraplate basalts.

The tectonic-controlled hypothesis indicated that the hotspot volcanoes have formed by the stress and cracks of the lithosphere (Anderson, 1998; Turcotte and Oxburgh, 1973). The small-scale flow driven by a discontinuity in the thickness of the lithosphere can be a heat source of the hotspot magma (King and Anderson, 1998). Anderson, 1998 explained that the chemical heterogeneity of intraplate basalts can be derived from the near surface sources although the source materials was not practically indicated.

1.2. West African passive margin intraplate basalts (WAPM-IB)

West African passive margin (WAPM, Fig. 1-1) is one of the major intraplate basalt localities on the Earth (Halliday et al., 1992). The major volcanic provinces of WAPM are Madeira Islands, Canary Islands, Cape Verde Islands, and Cameroon volcanic line

(CVL) from north to south, and their closely related continental region: Atlas Mountains, continental sector of CVL, and Benue trough. In this area, CVL, Canary Islands, and Cape Verde Islands form volcanic chains. The recent tomographic image also suggests that they are connected to the deep mantle derived plume (French and Romanowicz, 2015). However, the volcanic chains do not show clear age-progressive trend, these magmas are marked by absence of high-degree melts, and no flood basalts was formed. These signatures disagree with the plume hypothesis. Although continental and oceanic intraplate magmas show considerable variation in trace element abundances, they are typically more enriched in incompatible trace elements than basalts erupted at subduction zones and mid-ocean ridges (MORs). Trace element modeling for the petrogenesis of intraplate magmas invariably requires their derivation from a mantle source that is chemically distinct from the upper-mantle magma source that produces the MORBs (Weaver, 1991). Radiogenic isotopic compositions of the WAPM intraplate basalts (WAPM-IB) show heterogeneous compositions which can be explained by the involvement of recycled materials (Halliday et al., 1992). Therefore, geochemists insisted that the parental magna of the WAPM-IB involves plume components which have derived from the recycled crust or lithosphere.

Geographically, WAPM-IB are located both in the oceanic and continental setting. However, the seismic tomography and the magnetic anomaly images reveal that remnants of cratonic lithospheric fragments are widespread beneath these regions (Begg et al., 2009; O'Reilly et al., 2009) (Fig. 1-1). The evidence for the presence of Archaean to Proterozoic African sub-continental lithospheric mantle (SCLM) beneath this region was also proved by the peridotite xenolith in Cape Verde Islands (Coltorti et al., 2010). Because detached depleted cratonic SCLM is buoyant relative to the convecting mantle, it is likely that they are widespread beneath the Atlantic Ocean after its opening (Coltorti et al., 2010).

The development of small-scale convection in the upper mantle beneath the transition of thick cratonic lithosphere and thin oceanic lithosphere has been demonstrated by numerical models (King et al.,2000). These models explain the presence of relatively high seismic shear wave velocities (cold down wellings) in the mantle transition zone beneath the western margin of African cratons and the eastern margin of South American cratons.

Thus, small scale, edge-driven convection was proposed to be an alternative to plumes for explaining intraplate African and South American hot spot volcanism (King et al.,2000).

1.3. Volcanic occurrences of WAPM-IB

Cameroon Volcanic Line

Among the well-known examples of intraplate volcanism, the Cameroon volcanic line (CVL) forms ~ 1600 km linear chain of volcanic centers. Unique to other intraplate rift related volcanoes, the CVL consists of a chain of Cenozoic volcanoes developed on both the Atlantic Ocean floor and the continental crust of the African plate (Fig. 1-2). It exhibits no evidence of systematic age progression as observed in a typical hot spot settings such as the Hawaii-Emperor chain making a simple hot spot model an unlikely explanation for its formation.(e.g., Hedberg, 1969; Grant et al., 1972; Grunau et al., 1975; Dunlop and Fitton, 1979; Cornen and Maury, 1980;Dunlop, 1983; Fitton and Dunlop, 1985; Lee et al., 1994; Ngounouno et al., 1997; Marzoli et al., 1999, 2000;Ngounouno et al., 2001, 2003; Njilah et al., 2004; Ngounouno et al., 2005, 2006; Aka et al., 2009; Dongmo et al.,2010; Kamgang et al., 2010). The complex features (The linear alignment of the volcanoes but lack of a consistent time-space migration) of the CVL have caused much contention over its geodynamic origin.

Canary Islands

The Canary Islands is located 90 to 500 km west of northwest Africa, comprising seven major volcanic islands: Lanzarote, Fuerteventura, Gran Canaria, Tenerife, La Gomera, La Palma, and El Hierro from east to west. They are situated on Jurassic oceanic crust between 156 and 175 Ma (Roeser 1982; Klitgord and Schouten 1986; Schmincke et al. 1998). The subaerial shield stage volcanism for the Canary Islands show age-progressive trend from east (15 Ma for Lanzarote and 23 Ma for Fuerteventura) to west (1.1 for El HIerro and 1.7 Ma for La Palma) (Figs. 1-3), which has been interpreted as a fixed plume model beneath the moving plate (e.g., Morgan 1972; Holik et al. 1991; Hoernle et al. 1991; Hoernle and Schmincke 1993b; Anguita and Hernán 2000). Later, this model was minor revised as a combination of fixed mantle plume with edge-driven convection to explain the long duration of volcanism in a single volcanic centers

(Geldmacher et al., 2005). However, the seamounts in the Canary Island provinces vary from 142 Ma to 0.2 Ma (Fig. 1-4) and do not show any age-progressive trend, which is irreconcilable with the fixed plume model (van den Bogaard, 2013). van den Bogard (2013) proposed that this, the most long-lived hotspot track on the Earth with no-age progressive trend, should be formed by the plate-bound shallow mantle convection.

Madeira Islands

The Madeira Archipelago is located in the eastern North Atlantic at the end of a slightly curved northeast-southwest oriented chain of islands and seamounts (Fig. 1-3). The Madeira Archipelago is located on 140 Ma old oceanic crust and ascends from more than 4000 m water depths to an elevation of 1862 m above sea level (Pico Ruivo, Madeira Island) (Geldmacher et al.,2000). The volcanic activity has occurred in five islands at three different periods: (1) Madeira (0-5 Ma), (2) Desertas Islands (Ilheu Chao, Deserta Grande and Bugio; 3.2-3.6 Ma), situated on a submarine ridge extending more than 60 km SSE from the eastern tip of Madeira and (3) Porto Santo (11-14 Ma) (Geldmacher et al.,2000). Madeira and the Desertas Islands form a single volcanic system consisting of two rift arms: The E-W oriented Madeira Rift Arm and the NNW-SSE oriented Desertas Rift Arm. The subaerial evolution of the Madeira/Desertas volcanic complex can be divided into two stages: (1) shield stage (>4.6-0.7 Ma) consisting of the Early Madeira Rift Phase (> 4.6-3.9 Ma), Desertas Rift Phase (3.6-3.2 Ma) and Late Madeira Rift Phase (3-0.7 Ma) and (2) post-erosional stage (< 0.7 Ma) (Geldmacher et al.,2000). Although the Madeira Islands do not form the long volcanic chain, the NE-SW trending seamount show age-progressive volcanic chain, which is interpreted as the fixed plume model (Geldmacher et al., 2005; Geldmacher et al., 2001). On the other hand, the geological studies suggested that the tectonic lineament could play the important role for volcanism (Fonseca et al., 1998).

Cape Verde Islands

The Cape Verde archipelago (Fig. 1-5) is a group of 15 volcanic islands situated in the Atlantic Ocean 500-800 Km off the coast of Senegal and 1500 km east of the Atlantic MOR between latitude 14° and 17° N and longitudes 22° and 25° W (Duprat et al.,2007). The archipelago is formed on a topographical anomaly approximately 1000 km in

diameter that stands about 2 Km above this swell (Hayes and Rabinowitz,1975). The Caper Verde archipelago consists mainly of a northerly east-west extending island chain consisting of Santo Antao, Sao Vicente and Sao Nicolau and a Southerly chain of Sal, Boa Vista, Maio, Santiago, Fogo and Brava. The crust underlying the Cape Verde archipelago is oceanic. This interpreted from seismic investigations (Dash et al., 1976) and deducted from the presence of the magnetic quit zone boundary landwards of the islands (Hayes and Rabnowitz, 1975). Tholeiitic MOR basalts of Jurassic age on the island of Miao are believed to be the uplifted remnants of this oceanic floor (Klerkx and De Paepe, 1977; Stillman et al., 1982; Mitchell et al., 1983). These basalts are overlain by a relatively thin cover of pelagic sediments (Davies et al., 1989). The MORBs and pelagic sediments constitute the base upon which the Cape Verde magmas are extruded and intruded (Duprat et al.,2007). The close position of the rotation pole of the African plate since 6 Ma was modelled by Pollitz (1991) to be 19°N/16° W and the movement of the African plate was slow. Moho beneath the Cape Verde Islands is at depths of 16-17 Km, midway between crustal thickness typical for continental and oceanic crust (Dash et al., 1976).

Atlas Mountains

The Atlas Mountains (Fig. 1-6) are one of the most prominent topographic features in the northwestern Africa, spanning more than 2000 km and attaining elevations to 4 km. The Atlas Mountains have been traditionally considered as intercontinental in nature, distinguished from interpolate mountain belts (e.g the Alpine belts) by their distance from the collisional zone and their lack of nappe structures, ophiolites, regional metamorphism, and granitoid intrusions (Gomez et al.,2000). The Atlas Mountains are typically divided into the High Atlas and Middle Atlas of Morocco and the Saharan Atlas of Algeria. Two large crustal blocks that underwent little Cenozoic deformation are located north of the High and Saharan Atlas: the Moroccan Meseta to the west and the High Plateau to the east. South of the Moroccan Atlas are the upwarped Anti Atlas Mountains, exposing the Hercynian fold belt, and the stable Saharan platform (Gomez et al.,2000). The present-day Atlas Mountains comprise a system of failed rift associated with the early Mesozoic opening of the central Atlantic and Neo-Tethys oceans (e.g. Brede et al., 1992) (Fig. 1-7).

1.4. Cameroon Volcanic Line (CVL) as a representative WAPM-IB

The west African passive margin intraplate basalts (WAPM-IB) are characterized by the large distribution of highly alkaline volcanics including carbonatite and the long duration of volcanic activities in the same volcanic region. These highly alkaline magmas should be formed by relatively low degree of melting, which is inconsistent to have generated by the upwelling mantle plume. The heterogeneous elemental and isotopic compositions of the WAPM-IB have been generally explained by the mixing of the upwelling mantle plume that contains lower mantle material and recycled ancient crustal or lithospheric mantle materials; depleted MORB source mantle; and the delaminated SCLM. However, absence of clear age propagation of the hot-spot tracks despite their extended eruptive activity in each archipelago, suggesting the difficulty to explain their magma genesis by a model involving a simple long-lived upwelling mantle plume. Thus, the WAPM-IB defy common dynamic models of melt generation and volcanic activity on Earth. The complex tectono-magmatic history, geochemical characteristics and activities of the WAPM-IB have generated debates on issues like their origin, heat source and melt generation mechanism. Thus, the genesis of WAPM-IB remains poorly understood.

Among the WAPM-IB, CVL shows unique feature that forms a linear volcanic line that straddles from oceanic to the continental region along the Congo craton. Its unique tectonic setting, in which both oceanic and continental alkali basalts were erupted, offers a rare opportunity to constrain models for the chemical and thermal structure of both the sub-oceanic and sub-continental lithospheric mantle at the WAPM. Numerous numbers of geological (Grunau et al., 1975; Gorini and Bryan, 1976; Freeth, 1978; Sibuet and Mascle, 1978; Fitton,1980; Morgan, 1983; Burke, 2001), geochemical (Fitton and Dunlop, 1985; Deruelle et al., 1991; Lee et al., 1994; Njonfang et al., 2011), structural (Moreau et al., 1987; King and Anderson,1995), geophysical (Fairhead, 1988; Fairhead and Binks, 1991;Meyers et al., 1998; King and Ritsema, 2000; Reusch et al., 2010;Milelli et al., 2012) and geochronological (Dunlop and Fitton,1979; Aka et al., 2004) studies have developed the complementary models to explain the origin of the CVL. These models are: (1) melting of fossil plume (e.g. Halliday et al., 1988, 1990), (2) hot mantle plume model (Lee et al., 1994), (3) decompression melting beneath the reactivated shear

zones in the lithospheric mantle (e.g. Freeth, 1979), (4) lithospheric instabilities at the edge of a continent which could develop over long timescales, leading to small rates of upwelling and decompression melting along linear zones (Milelli et al., 2012; Fourel et al., 2013), and (5) edge-driven convection at the boundary between thick craton and thinner oceanic lithosphere (e.g. King and Anderson, 1995, Adams et al., 2015; King, 2000; Reusch et al., 2010).

Geochemical studies emphasized the mantle heterogeneity evidenced by the presence of large isotopic variation of CVL should be caused by involvements of recycled materials, delaminated sub continental lithospheric mantle (SCLM) in the depleted asthenospheric mantle. Geophysical studies, on the contrary, prefer to explain by tectonic controlled melting models such as lithospheric instability or edge-driven convection based on the seismic data obtained for the CVL (e.g Adams et al., 2015; Reusch et al.2010). The seismic tomography images suggested both the plume (French and Romanowicz, 2015) and non-plume (Ritsema and Allen, 2003) models. As an aspect of the NE-SW alignment of the CVL, Meyers et al. (1998b) argued this linear distribution is a consequence of the surface expression of cylindrical, longitudinal convective rolls in the upper mantle. They referred this convection axis to as 'hotline', which corresponds to regional asthenospheric upwelling, but the mechanism to produce such dynamic mantle flow was unclear. As shown here, there has been no single model that can sufficiently explain all the geochemical, geological, geophysical data to explain the genesis of CVL magmatism. Since most of the geochemical studies in this area had been done till the 1990s, it is important to revisit to analyze CVL volcanics using recently-developed highly precise and accurate geochemical and isotopic analytical method.

1.5. Objectives of this thesis

In my PhD research, I present a comprehensive geochemical data, i.e. major and trace elements and Sr, Nd, Hf, and Pb isotopic compositions, of mafic samples collected from five volcanic centers (Annobon, Sao Tome, Principe, Bioko, and Etinde) in the CVL. Based on these data, I will identify the source materials of the CVL magmas. Then, the petrological, chemical, and thermal structure of the mantle which formed the CVL magma will be interpreted. Based on the obtained data and interpretations from CVL, I will

examine the source components of other WAPM-IB (Canary Islands, Madeira Islands, Cape Verde Islands, Mount Atlas, and continental sector of CVL) using the so far published datasets. Finally, I will propose the general model for the genesis and evolution of the WAPM-IB magmatism.

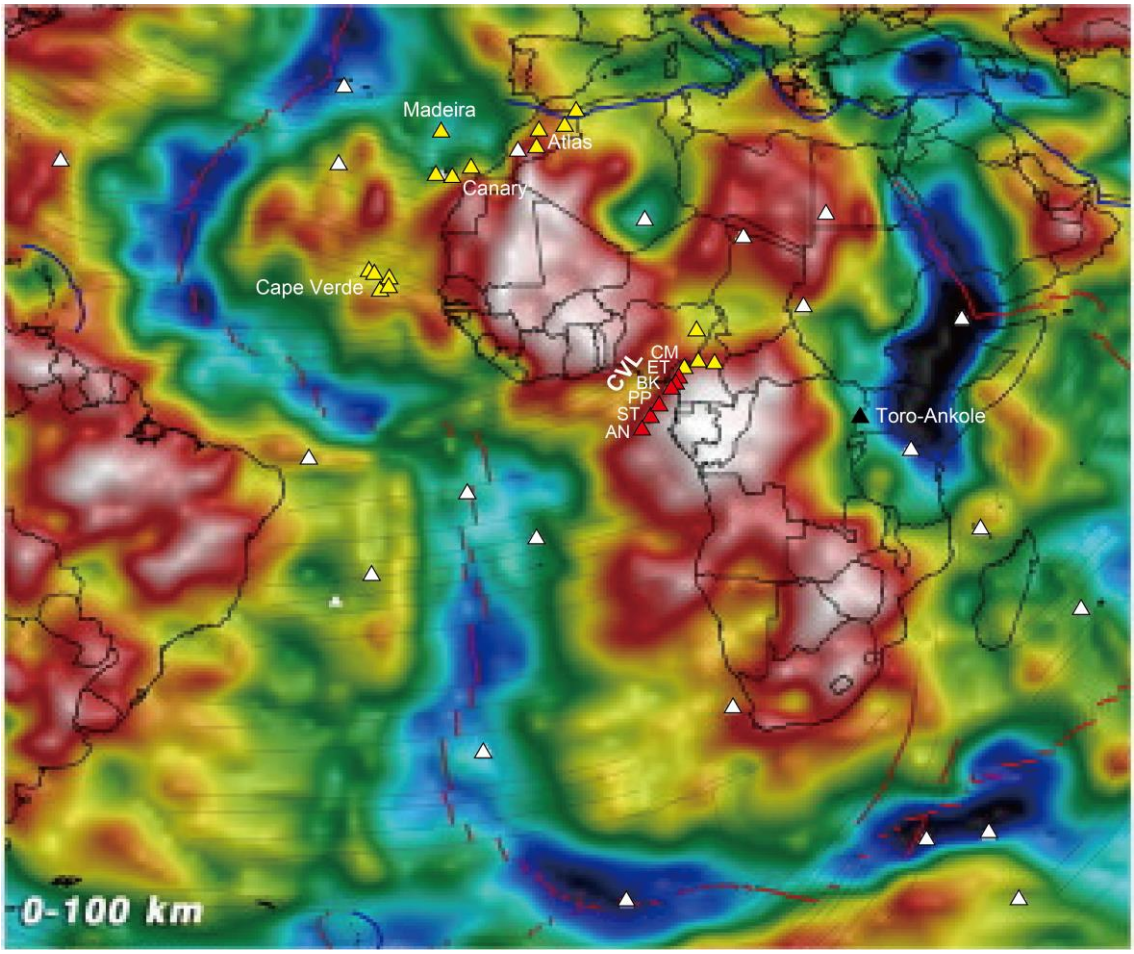

- **Figure 1-1 | Tomographic model images at the depth of 0-100km for the African continent and Atlantic Ocean and the location of volcanoes (O'Reilly et al., 2009).** Red triangles are Cameroon Volcanic Line (CVL) volcanoes studied in our laboratory (this study and Yokoyama et al., 2007). Yellow triangles are WAPM-IB volcanoes which will be examined in this study. Black triangle is Toro-Ankole region where the pyroxenite xenolith in the SCLM is obtained. AN: Annobon, ST: Sao Tome, PP: Principe, BK: Bioko, ET: Etinde, and CM: Mt. Cameroon. White triangles indicate other active volcanoes around Atlantic and African continent.

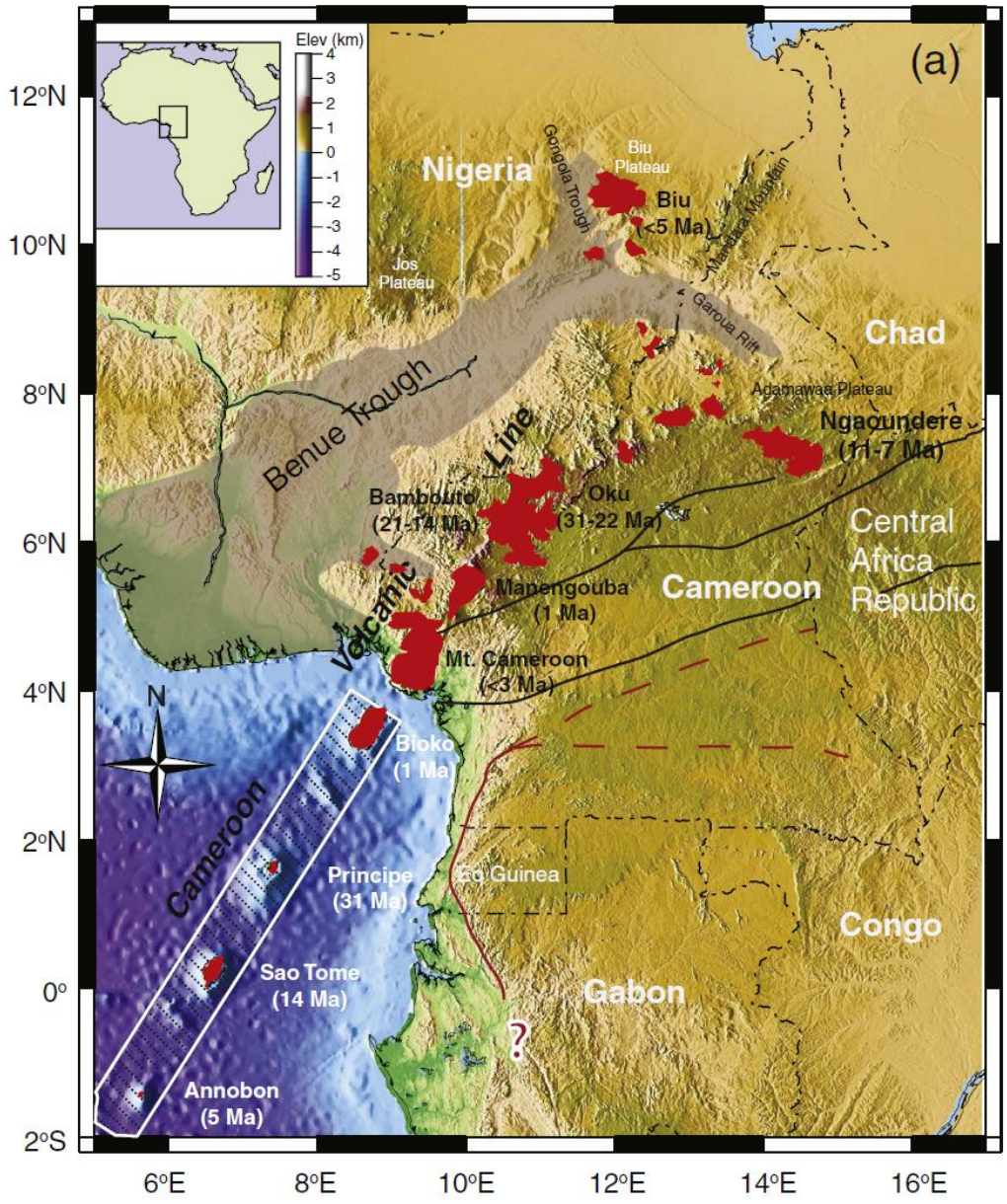

Figure 1-2 | Map showing distribution of Cenozoic volcanic rocks (red) in CVL chain and Cretaceous Sedimentary rocks (grey) of the Benue trough (Liu et al., 2016).

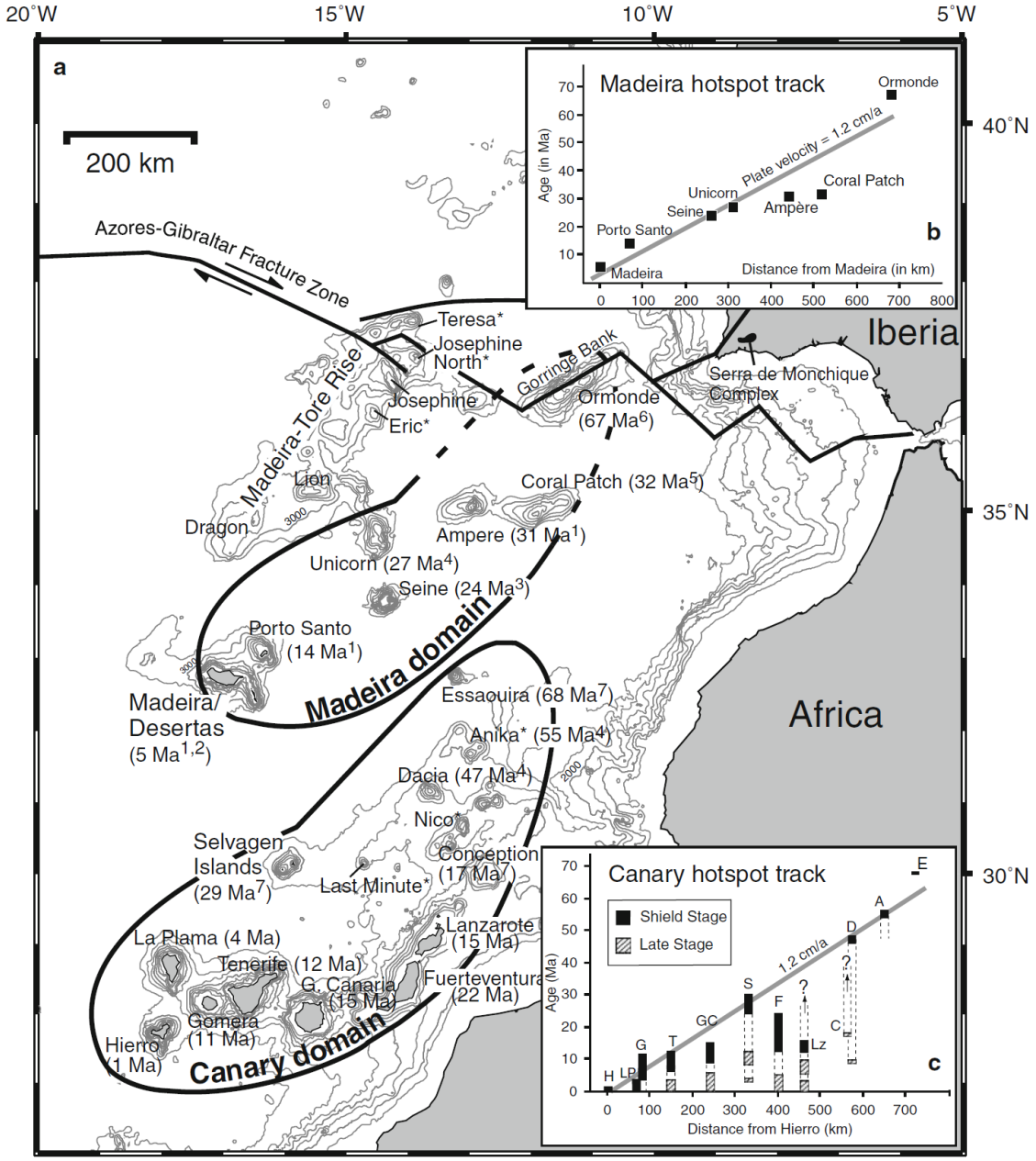

Figure 1-3 | Bathymetric map of the central northeast Atlantic and the oldest available ages from each localities (Geldmacher et al., 2011).

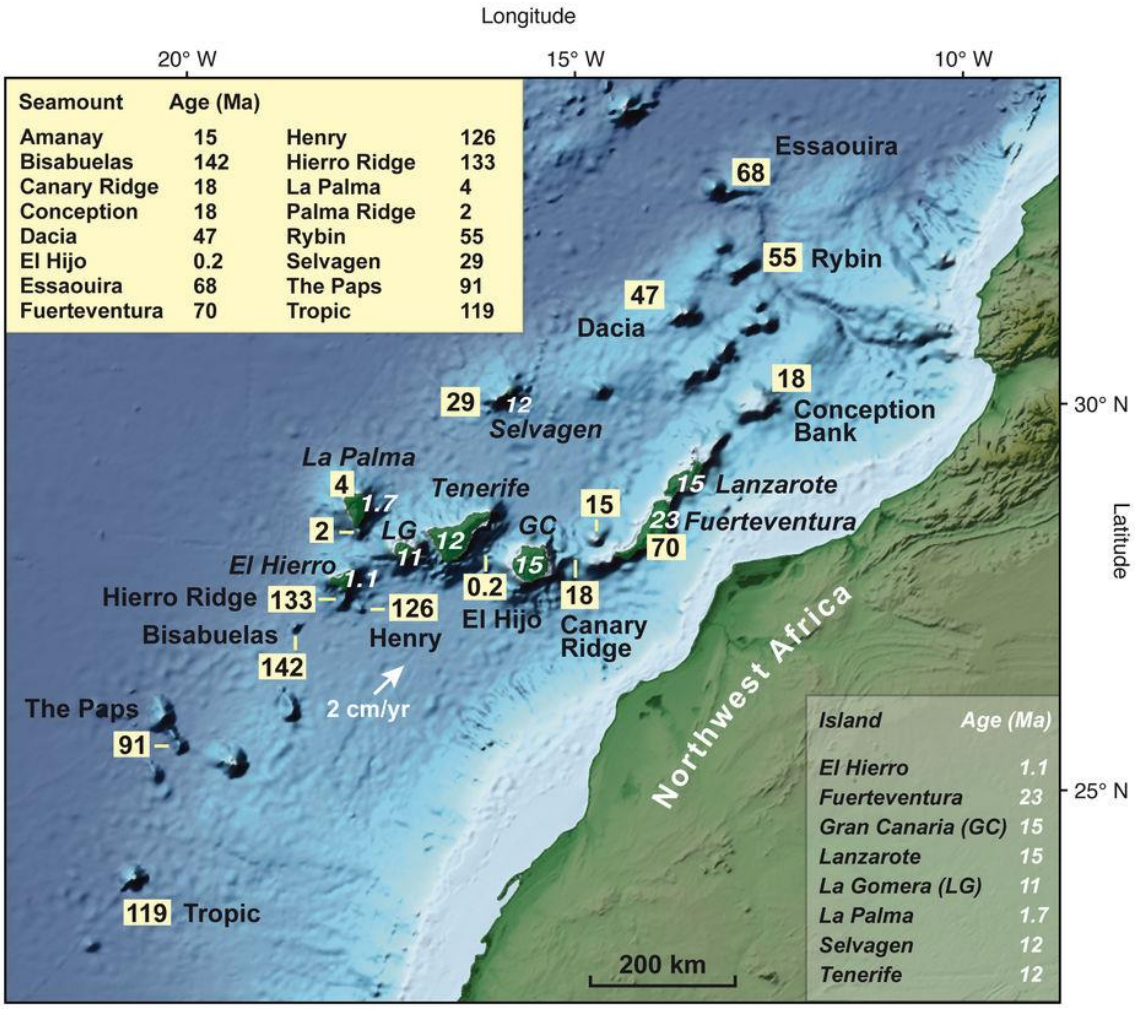

Figure 1-4 | Topographic map of the NW African continental margin and age distribution in the Canary Island Sea Mount Province (van den Bogaard, 2013). Numbers with black and white are the oldest ages for seamounts and islands, respectively.

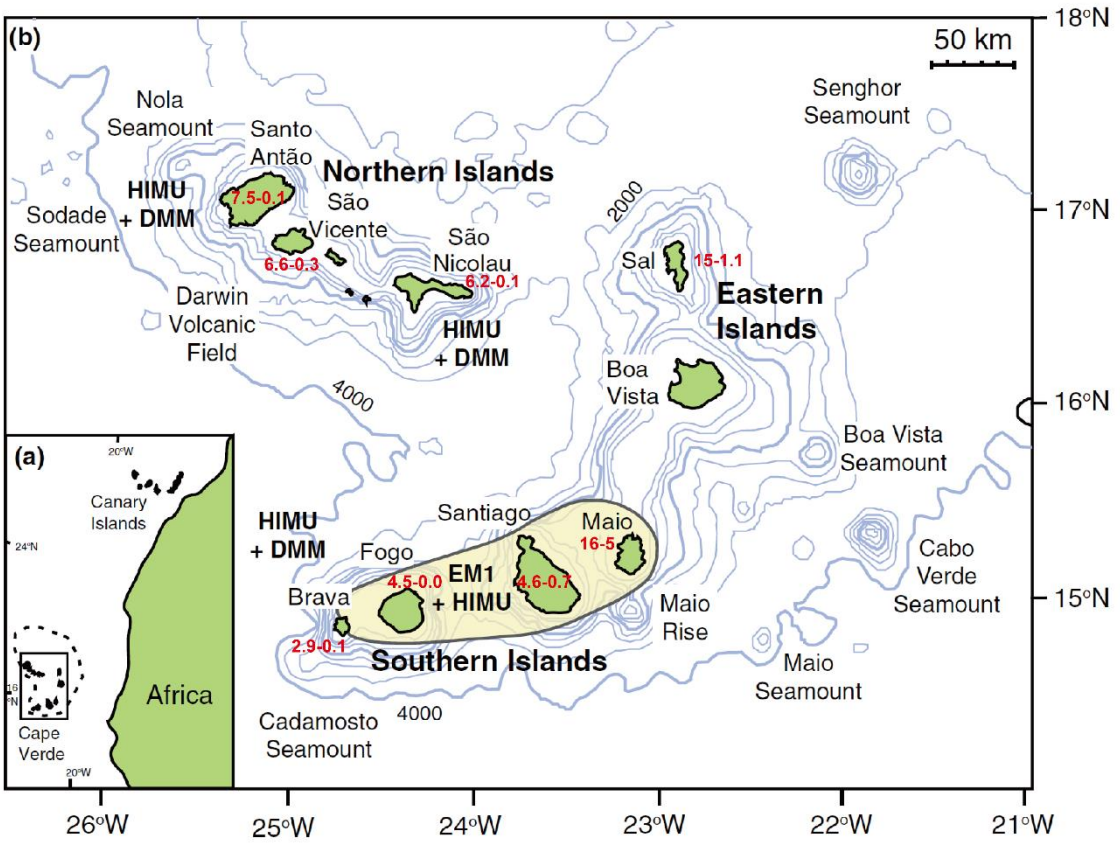

Figure 1-5 | Location map of the Cape Verde archipelago (modified after Barker et al., 2014). a, location of Cape Verde oceanic plateau, approximately 500 km west of Africa. b, The Cape Islands consist of northern, eastern, and southern Islands. Red numbers show ages obtained for volcanic rocks in Ma compiled by Liu and Zhao (2014).

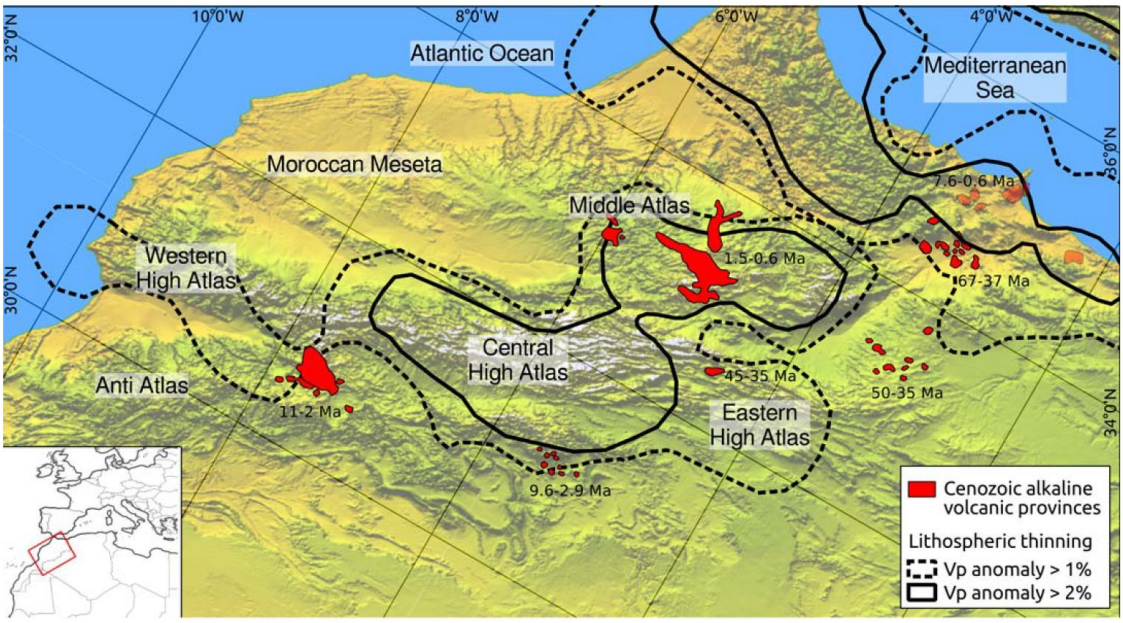

Figure 1-6 | The topography of the Moroccan Atlas mountains (Kaislaniemi and van Hunen, 2014).

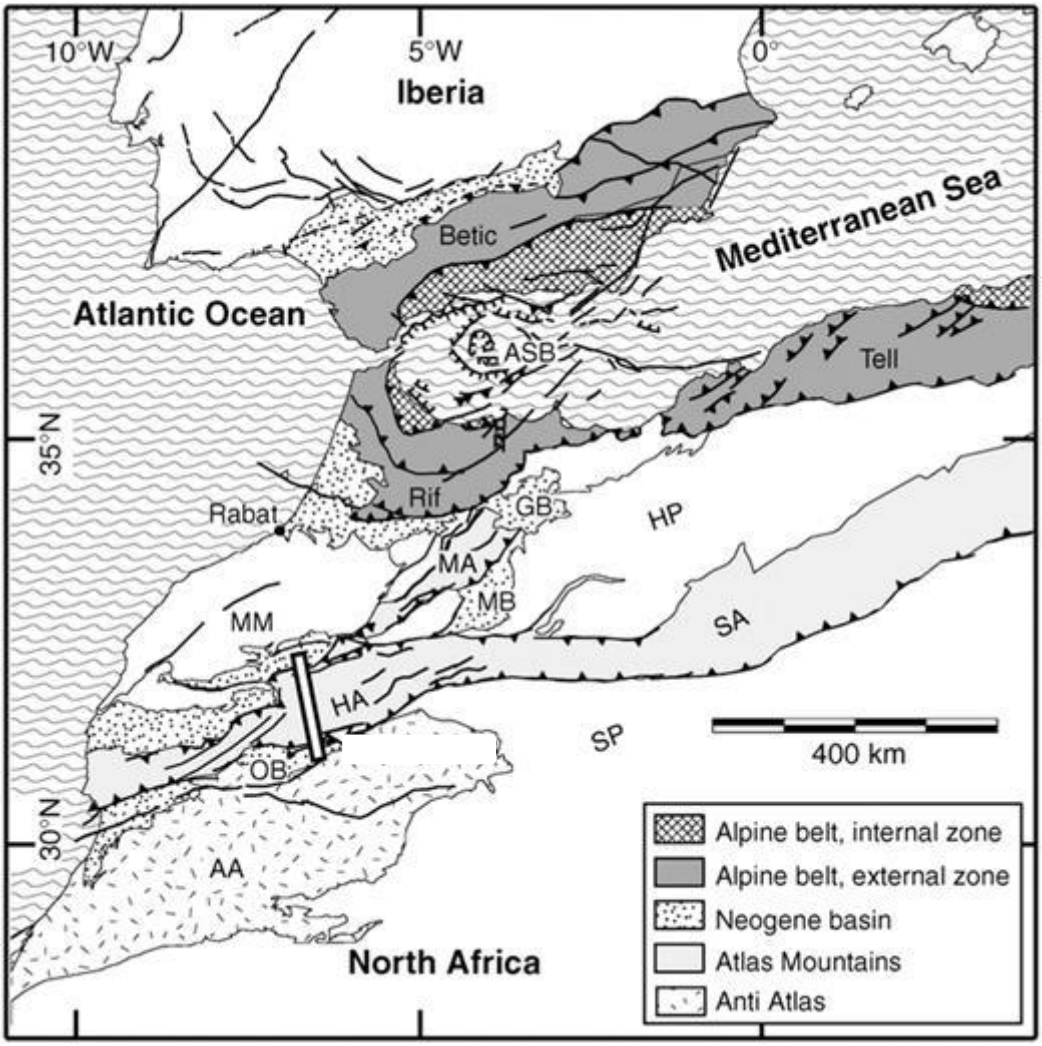

Figure 1-7 | Simplified tectonic Map of Western Mediterranean (Gomez et al., 2000). Abbreviations: HA=High Atlas, MA= Middle Atlas, SA= Saharan Atlas, AA= Anti Atlas, MM= Moroccan Meseta, HP=High Plateau, SP= Saharan platform GB= Guercif Basin, OB=Ouarzazte Basin, MB= Missour Basin, ASB= Alboran Sea Basin.

CHAPTER 2: GEOLOGICAL, GEOPHYSICAL, PETROLOGICAL, AND GEOCHEMICAL OVERVIEW OF THE CAMEROON VOLCANIC LINE

2.1. Geological background of the CVL

The CVL forms a 1600 km-long intraplate linear volcanic chain, mainly composed of Cenozoic alkaline basaltic volcanoes (Fitton and Dunlop, 1985). It extends from Annobòn (Pagalú) island in the Gulf of Guinea to the Biu Plateau in the continent interior of West Africa (Fig. 2-1). The CVL is oriented N30°E and segmented by N70°E shear zones that developed during Pan-African age (Deruelle et al., 2007), which is particularly developed in the continental sector. The chain has been divided into three geographical zones: the oceanic sector (Annobòn, São Tomé, and Principe), continent-ocean boundary (COB: Bioko, Etínde, and Mt. Cameroon) and the continental sector (Manengouba, Bambouto, Oku, Ngaoundere Plateau, Mandara Mountains, and Biu Plateau). The summarized age data of CVL (Deruelle et al., 2007) is shown in Figure 2-2.

Alkaline mafic to intermediate rocks (basalts, basanites, trachytes, and phonolites) are predominant along the CVL. In the continental sector, orogenic plutonic complexes and volcanic constructs of varying sizes and shapes are also developed (Deruelle et al., 2007). Continental CVL magmas intruded into the overlying Proterozoic meta-sedimentary, meta-granitic, and granitic rocks. These basement rocks are either of Precambrian age (Geze, 1943; Gouhier et al., 1974; Le Marechal, 1976; Lasserre, 1978; Dunlop, 1983) or Neo-Proterozoic age (Annor and Freeth, 1985; Toteu et al., 2004).

The oceanic sector volcanoes include three volcanoes: **Annobon** (813 m a.s.l.), **Sao Tome** (2024 m a.s.l.) and **Principe** (984 ma.s.l.). They are stratovolcanoes (Annobon and Sao Tome) and lava flows (Principe). These volcanic islands are made up of volcanic rocks ranging from nephelinite, basanite and basalt to trachyte and phonolite (Piper and Richardson, 1972; Dunlop and Fitton, 1979; Cornen and Maury, 1980; Fitton and Dunlop, 1985; Fitton, 1987; Halliday et al., 1988, 1990; Deruelle et al., 1991; Lee et al., 1994).

Bioko (a lava flow of 2872 m a.s.l), Mt. Etinde, and Mt. Cameroon volcanic centers are located close to the seismically-defined “continent-ocean boundary” (COB) zone (Emery and Uchupi, 1984). The **Bioko Island** (3008 m a.s.l) is the largest (700km^2) of the four Islands of the Gulf of Guinea located in the presently more active zone of the CVL. It is composed essentially of alkaline basalts and hawaiites, and lesser mugearites. The rocks show microlitic porphyritic texture with phenocrysts of Olivine (83% <Fo<

87%) and clinopyroxene in matrix of plagioclase, clinopyroxene and oxides (Yamgouot et al., 2016). **Mt. Etinde** is a small densely forested and highly dissected volcano located on the SW flank of Mt. Cameroon. It rises to a height of 1713 m a.s.l and is made up almost entirely of nephelinitic lavas rich in euhedral (3-7 mm) highly zoned clinopyroxene phenocrysts (Nkoumbou et al., 1995). **Mt. Cameroon** is the highest (4095 ma.s. l) volcano in west Africa occupying a surface area of about 1300 km^2. This volcano is the only presently active volcanic center of the CVL with seven eruptions recorded in the last 100 years, i.e., 1909, 1922, 1954, 1959, 1982, 1999, and 2000 (Geze, 1943; Fitton et al., 1983; Suh et al., 2003). It is a composite volcano made of alkaline basanitic and basaltic flows interbedded with small amounts of pyroclastic materials and numerous cinder cones (Suh et al., 2003, 2008; Yokoyama et al., 2007).

Major volcanic centers of continental sector volcanoes are Mounts Manengouba, Bambouto, and Oku and two main plateaus: Ngaoundere and Biu (Fitton,1987; Halliday et al.,1988; Marzoli et al.,1999; Marzoli et al., 2000; Ngounouno et al.,2000; Nono et al.,2004; Rankenburg et al.,2005). **Mt. Manengouba** (2411 m a.s.l) is a well preserved central volcano whose summit hosts two concentric calderas (Elengoum and Eboga). Eruptives consist of basalts, trachytes, quartz trachytes, and rare rhyolites lavas (Fitton, 1987; Kagou et al., 2010). **Mt. Bambouto** (2700 m a.s.l.) and **Mt. Oku** (3011 m a.s.l) are Oligocene to Quaternary stratovolcanoes with lava successions comprising a strongly bimodal basalt-trachyte-rhyolite suite (Marzoli et al., 2000; Njilah et al., 2004, 2007; Kamganget al., 2010, 2013; Tchouankoue et al., 2012). The **Ngaoundere Plateau**, in the northeastern part of the CVL, consists of alkaline basalts and basanites capped by trachytes and phonolitic flows. The most recent volcanism in this area consists of cinder cones aligned in a WNW- ESE direction, sometimes producing small lava flows (Fitton, 1987; Nono et al., 2004). The **Biu Plateau**, which is located in the northern part of the Ngaoundere Plateau, consists of basaltic flows with a maximum thickness of 250 m. This plateau is composed of basanite to transitional basalts (Rankenburg et al., 2005). Mt. Bambouto, the Oku volcanic group (Assah et al., 2015), and the Ngaounderé Plateau, produced chemically more evolved lavas than others. They are dominantly polygenetic, and alternate with less evolved monogenetic grabens (Sato et al., 1990; Nkouathio et al., 2008).

2.2. Tectonic history of west African passive margin

The tectonic history of the CVL has been described in elsewhere (Grunau et al., 1975; Gorini and Bryan, 1976; Fitton et al., 1983; Moreau et al., 1987; Ngako et al., 2006). The most relevant regional tectonic events of the CVL are (i) the breakup of Gondwana at ~125 Ma following which the South Atlantic opened to form the passive continental margin of West Africa, and (ii) the movement of the African Plate at 80- 65Ma relative to the underlying asthenosphere.

The rifting of Gondwana in this region started in the early Cretaceous at the South Atlantic, Benue trough, and Gulf of Guinea triple junction. Continental separation was established during the early Cretaceous and thinning of the lithosphere under the Benue trough lasted until the late Cretaceous, though it did not rift (Grant, 1971). The break-up is generally thought to have started in response to the build-up of intraplate stresses, augmented by the St. Helena hot spot, then located beneath the Equatorial plate boundary which may have played a part in weakening the lithosphere during extension (Guiraud et al.,1992; Wilson and Guiraud, 1992). The geometry of the triple junction influenced the separation of West Africa from Brazil required relative lateral movements of the two continents, accommodated by transform faults in the oceanic lithosphere and by shearing at the margin. The separation unzipped the continents from south to north, with Africa rotating anticlockwise (Lawrence et al., 2002).

Duration and thermal evolution of the rifted margins differ from the shear margins (Clift and Lorenzo, 1999), including earlier formation of oceanic crust at orthogonal margins. Shearing may induce internal strain in the African plate and may have dilated oceanic transform faults, encouraging volcanic activities. In the Gulf of Guinea, an interim phase of volcanic activity lasted up to 20 Ma in the shearing regions, prior to true oceanic crust formation (Lawrence et al., 2002). Several few hundred km to the west of the triple junction at the Ivory Coast to Ghana margin, however, heat conduction from the oceanic plate drove transient uplift of over 1 km without significant volcanism (Clift and Lorenzo, 1999). Remnant structures of this tectonic event before the opening of the South Atlantic have been identified in West Africa and may have a bearing on the CVL.

Begg et al. (2009) proposed the lithospheric architecture of Africa based on detail

seismic tomography. According to their velocity model, the oceanic sector of the CVL distributed along with a margin of the high Vs zone in the 0–100 km depth slice, which could be considered to the edge of lithospheric mantle of the Congo Craton (Fig. 2-3). They also argued the coincidence of cratonic margin and the focus of basaltic and carbonatitic magmatisms in Africa, such as Canary Islands and Hoggar Swell (Algeria) in the NW and NE edges of West African Craton (Allègre et al., 1981; Beccaluva et al., 2007). In the sight of mantle structure beneath the CVL, therefore, the traditionally defined oceanic sector of the CVL (Annobon, Saô Tomé, and Principe) should be reconsidered, that is, these volcanoes are also located on the continent-ocean boundary in terms of structure of the lithospheric mantle.

2.3. Tectono-magmatic activities of CVL

The tectono-magmatic activities in the CVL and adjacent Jos Plateau and the Benue Trough can be classified into four key events with a general age progression from the northwest to southeast. (1) After the cessation of Jos plateau activity, the initial phase of magmatic activity and the emplacement of an orogenic granite ring complexes occurred at ~150 Ma in the Benue Trough (Coulon et al., 1996). (2) The second stages of magmatic activity in the Benue Trough and the contemporaneous opening of the Equatorial Atlantic Ocean occurred at ~100 Ma (Wilson, 1992; Wilson and Guiraud, 1992). (3) The latest magmatic activity in the Benue Trough and the initial phase of intrusive activity of the continental sector of the CVL occurred at 70-30 Ma (Lasserre, 1966); and (4) the CVL volcanic activity occurred from 45 Ma to present (Fitton and Dunlop, 1985; Marzoli et al., 2000; Aka et al., 2004).

Gravity analyses revealed that oceanic sector of the CVL was underlain by middle Cretaceous oceanic crust (110–90 Ma). The topographic expression of CVL islands and seamounts is attributed to crustal uplift rather than thickening of the igneous oceanic crust (Meyers et al., 1998a). The basement of continental sector forms part of a mobile belt between West African and Congo cratons, composed dominantly of Pan-Africa granitic rocks with middle Proterozoic age (Marzoli, 2000). These granitoids are cross-cut by an active fault belt, Central African Shear Zone (Ibrahim et al., 1996). This strike-slip structure was developed by continental breakup of Gondwanaland during 120–130 Ma,

which was propagated from the Early Cretaceous opening of the South Atlantic via Benue Trough (Fairhead, 1988). Most volcanic centers in the CVL have been active in the past million years. Only the Mt. Cameroon at the center of the line recorded historically eruptions (Fitton et al., 1983; Suh et al., 2003; Déruelle et al., 2007). Sporadic activities have continued to present time in both tectonic regimes (Meyers and Rosendahl, 1991). The detail geology, tectonic model and petrology of the CVL have been reviewed elsewhere. (e.g Deruelle et al.,1991).

The NE-SW alignment of the CVL is known as a major geological feature in central Africa. It is also considered as a Pan-African lineament more or less permanently re-juvenated from the late Precambrian to the present (Moreau et al., 1987). The Cameroon line has also been explained as a Y-shaped zone (Fitton 1980, 1983) with trunk represented by a line from Annobon to Oku and the branches by the Adamawa and the Biu plateau. Thus, it has suggested that that the origin of the CVL is attributed to the reactivating of basement fractures. However, these structural hypotheses are not explicit on how reactivation generated the CVL magmas (Gorini and Bryan, 1976; Fairhead, 1988; Moreau et al., 1987; Deruelle et al., 1991).

Based on the size and shape similarities between the CVL and the adjacent Benue Trough, a continental rift related to the opening of the equatorial domain of the South Atlantic which was initiated in Late Jurassic-Early cretaceous times, which can be superimposed by rotating one with respect to the other about a pole in Sudan. Fitton (1983) postulated that the CVL resulted from the displacement of the African Lithosphere at ~80-65 Ma relative to the asthenosphere. The hot asthenospheric wedge which should have underlain the Benue trough was displaced to beneath Mt. Cameroon and Gulf of Guinea. Magmas destined for the Benue Trough then reach to the surface as the CVL instead.

2.4. Structure of the crust and lithospheric mantle beneath CVL

The lithospheric seismic structure of Cameroon has been determined by continent-scale surface-wave studies (e.g., Pasyanos and Nyblade, 2007; Priestley et al., 2008; Fishwick, 2010). They indicate that the CVL is underlain by mantle characterized by slow seismic wave speeds and that the lithosphere-asthenosphere boundary beneath the Congo

Craton is at a depth of ~ 250km. In contrast, the lithosphere is < 100 km thick beneath the CVL (Fishwick, 2010). Perez-Gussinye et al. (2009) constrain effective elastic plate thickness (a proxy for lithospheric strength) across Africa using coherence analysis of topography and Bouguer anomaly data. The weakest lithosphere is found in Ethiopia and is attributed both to the low wave speed, hot mantle beneath the region, and the large degree of extension in that part of the East African rift system. Channels of relatively weak lithosphere extend across the African continent from this region to the CVL, where the effective elastic plate thickness is also relatively low compared to the surrounding areas. Perez-Gussinye et al. (2009) proposed that flow of buoyant asthenosphere beneath continental lithosphere thinned extensively during Mesozoic rifting may now be contributing to volcanism along the CVL based on the model of Ebinger and Sleep (1998).

Dorbath et al. (1986) analyzed teleseismic P-wave travel-time residuals recorded by a 300 km-long profile of 40 short period seismograph stations across the Adamawa Plateau. They identified upper-mantle wave speed contrasts of < 2.5% across the Plateau, an observation they cite as evidence for the presence of a mantle thermal anomaly. Plomerova et al. (1993) analyzed data from the same seismic array and found evidence for ~ 70 km lithospheric thinning beneath the Adamawa Plateau in the region where it is crosscut by the Central African Shear Zone (CASZ). In support of these teleseismic studies, gravity studies by Poudjom Djomani et al. (1997) and Nnange et al. (2001) also found evidence for localized low-density mantle beneath the region. Later, Reusch et al. (2010) used body wave tomography to image the mantle seismic structure beneath Cameroon using data from the 2005–2007 CBSE network. They found that a continuous low velocity zone (δV_S= - 2 to -3%) underlies the entire CVL to a depth of at least 300 km and attributed this to a thermal anomaly of at least 280K.

Gravity maps have often been used to delineate tectonic subdivisions of CVL inaccessible by traditional field geology due to younger sediment cover (e.g., Fairhead and Okereke, 1987; Poudjom Djomani et al., 1992, 1995, 1997; Toteuetal.,2004; Tadjou et al., 2009; Shandini et al., 2010; Basseka et al., 2011). A steep gradient in the Bouguer gravity field at ~ 4°N and ~ 10°E within the Yaounde domain has been interpreted as the sediment-covered edge of the Congo Craton. The earliest seismological constraints on crustal thickness in Cameroon came from Stuart et al. (1985), who used direct as well as

reflected and refracted waves from quarry blasts to determine a crustal thickness of ~ 33 km beneath the Adamawa Plateau, which has an upper-mantle P-wave velocity of ~ 8 km/s. They also show that the crustal thickness in the Garoua Rift is ~ 23km with an upper mantle P-wave velocity of ~7.8 km/s. More recently, Tokam et al. (2010) conducted a joint receiver function and surface-wave study of crustal structure across Cameroon using data from the CBSE network. Average shear wave velocity across Cameroon was found to be ~3.7 km/s and mean crustal thickness ~36km. Beneath the Garoua Rift and toward the coast, the crust was found to be significantly thinner at 26–31 km.

In contrast, the Congo Craton in Cameroon has thicker crust (43–48 km) and elevated mean crustal seismic velocities (3.9 km/s). The CVL and Oubanguides belt are characterized by crustal thicknesses of 35–39 km. Thickened crust and ~ 25 km-thick high velocity lower-crustal layer beneath the northern margin of the Congo Craton was attributed to the collisional tectonic processes that characterized the formation of Gondwana. Tokam et al. (2010) also suggested that thin bodies of mafic material exist in the top 10–15 km of the crust throughout Cameroon. Cameroon is relatively aseismic compared to magmatically active regions such as Ethiopia (Keir et al., 2009; Ebinger et al., 2010) in East Africa. However, studies of seismicity around Mt. Cameroon, site of the most recent eruption along the CVL (e.g., Ateba et al., 2009), show that earth quakes occur at depths as great as 55–60 km in the subcontinental lithospheric mantle (Tabod et al., 1992; Ateba and Ntepe, 1997). Review of recent seismological studies can be found elsewhere (Fishwick and Bastow, 2011).

2.5. Geochemistry of CVL volcanics

Lack of age propagation along the CVL (Fig. 2-2) is against a simple hot spot model for the source of the CVL (Aka et al., 2004; Fitton and Dunlop, 1985; Marzoli et al., 2000). Fitton and Dunlop (1985) found geochemical similarity in trace elements and Sr isotopes for basalts from both the oceanic and continental sectors, and suggested that these magmas are derived from sub-lithospheric depths without further interaction with the overlying lithosphere. One of the notable areas of the CVL is COB, because anomalously high $^{206}Pb/^{204}Pb$ compositions were reported from volcanoes in this area (Halliday et al., 1990, 1988; Lee et al., 1994; Yokoyama et al., 2007). Halliday et al.,

(1988; 1990) reported anomalously high HIMU-type $^{206}Pb/^{204}Pb$ ratios (up to 20.5) for the COB volcanoes and a systematic decrease of $^{206}Pb/^{204}Pb$ with distance towards the oceanic and continental sectors. With the combination of other geochemical tracers such as Sr, Nd and O isotopes, Halliday et al. (1990) proposed that such a high $^{206}Pb/^{204}Pb$ signature was attributed to the re-melting and U/Pb fractionation during melt migration in the St. Helena fossil plume head as it cooled after emplacement at 125 Ma. The study concluded that Cameroon line magmas are currently derived from a zone in the upper portions of the fossil plume in the lithospheric mantle. This model implies that the observed Pb isotope anomaly did not derive from the heterogeneity of asthenospheric mantle but the metasomatized lithosphere by the previous plume activity. The $^{3}He/^{4}He$ in olivine grains also shows HIMU-like low values in the COB and MORB-like values both for the oceanic and the continental sectors (Aka et al., 2004). Lee et al. (1994) revised this model as the "hot zone" model to explain this distinct isotopic feature in the COB. They attribute the CVL to result from pulses of mantle plumes with HIMU source periodically emplaced, heated, and re-fertilized the base of lithosphere which moves laterally. The magmatism is not only confined beneath the plume center, but also occurs at the plume periphery where the emplacement of magma is controlled tectonically. Yokoyama et al. (2007) also suggested HIMU-like and ubiquitous FOZO components involved in magma genesis of recent Mt. Cameroon lava. They considered this HIMU-like reservoir to originate from the sub-continental lithospheric mantle (SCLM), which had been metasomatized by the ancient St. Helena plume. A summary of previous suggested models is shown in Fig 2-4.

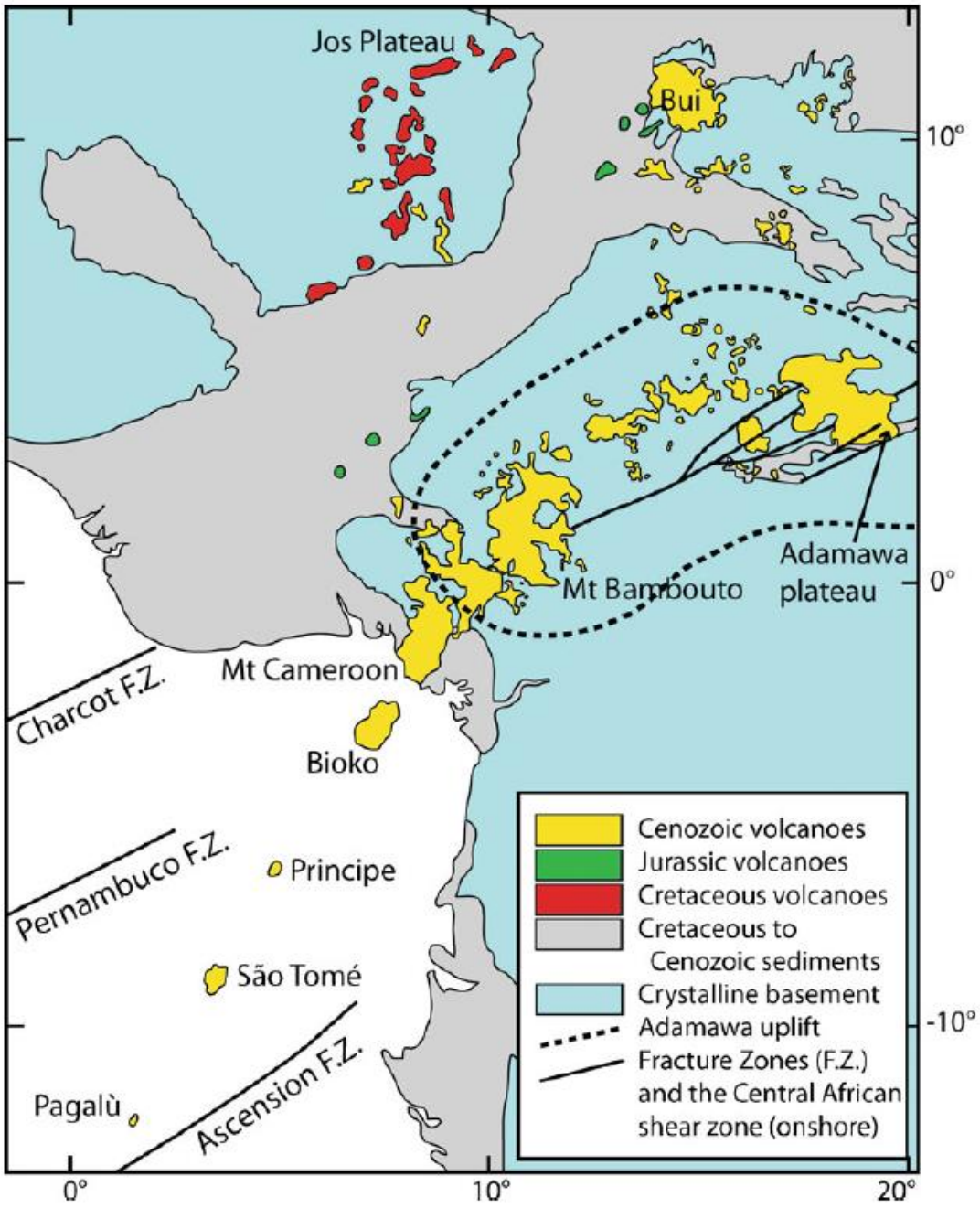

Figure 2-1 | Geological map of Mesozoic to Cenozoic volcanism in the Cameroon Volcanic Line (Matheu et al., 2011). Volcanoes with in the vicinity of the CVL are also included. Note that Pagalu is the other local name of the southernmost volcanic island- Annobon.

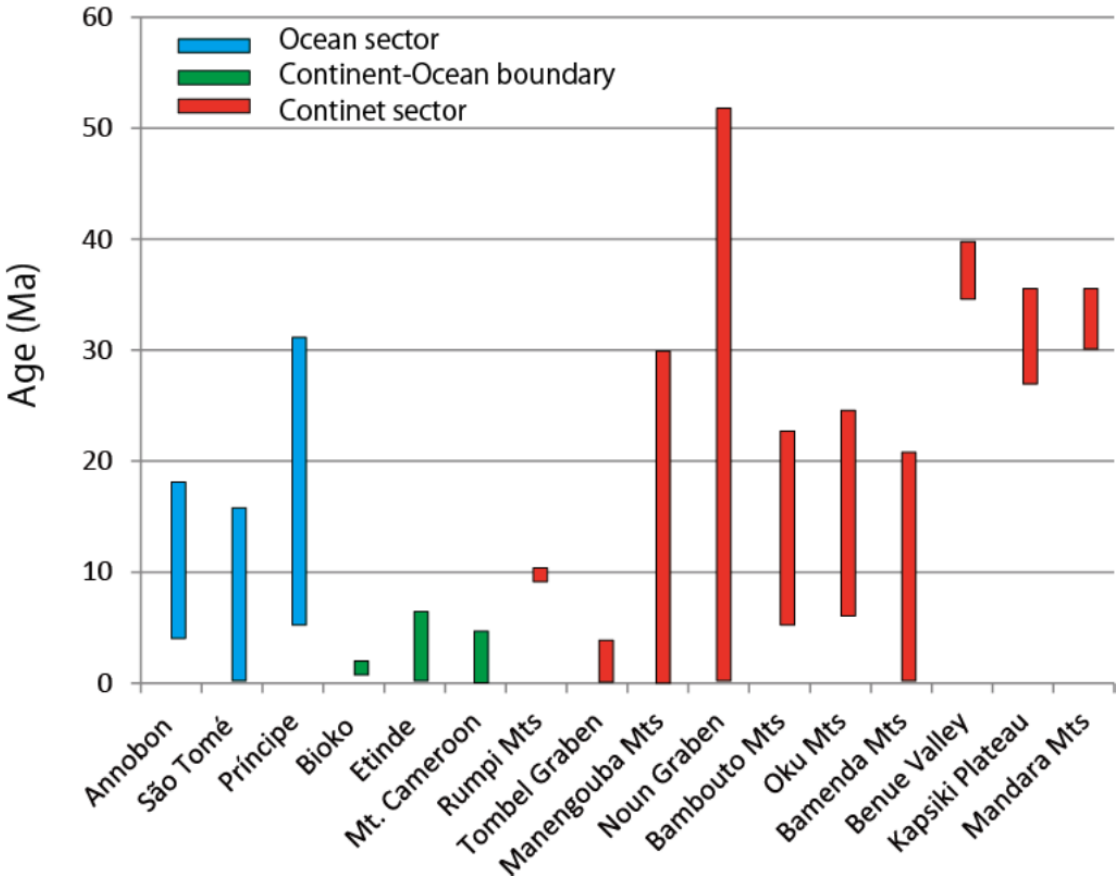

Figure 2-2 | Summarized plot of published age data of the CVL from previous studies (Deruelle et al., 2007 and references therein). Note that there is no systematic progression of ages either continent ward or ocean ward along the CVL. The maximum and minimum age for each volcano are plotted.

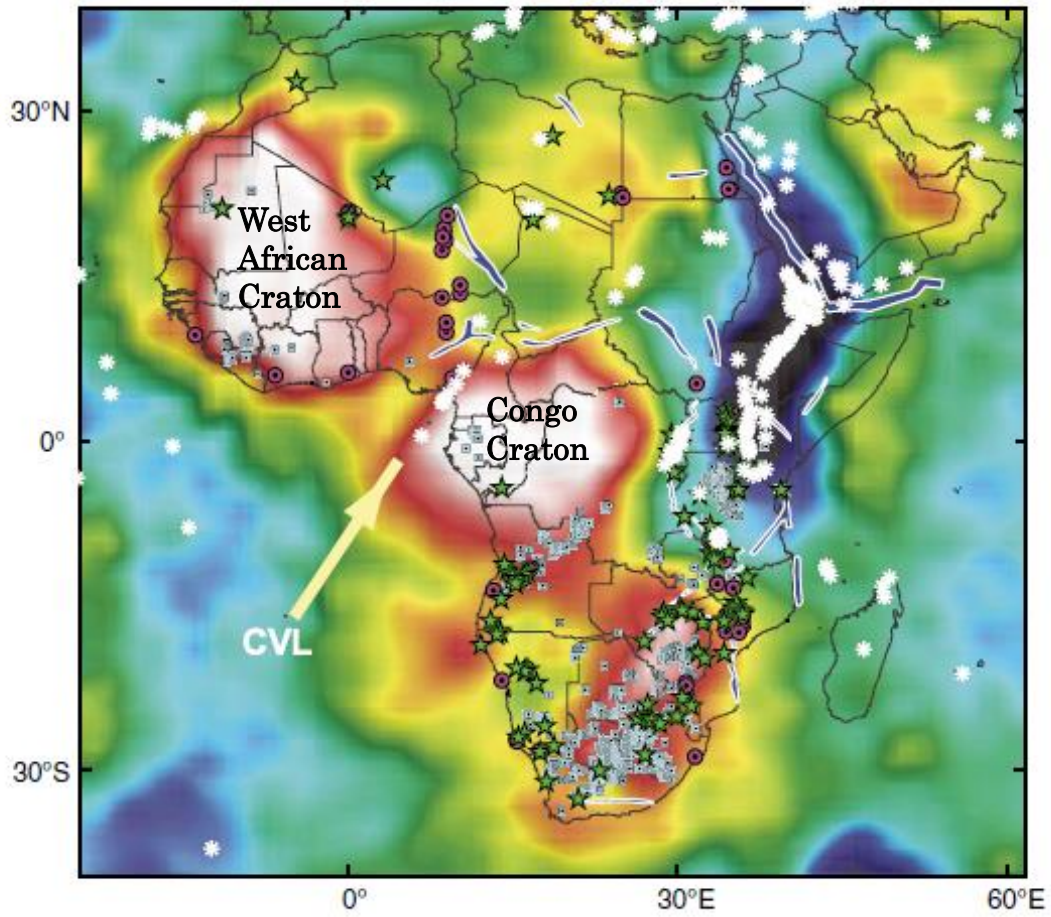

Figure 2-3 | Map illustrating tomographic image of Africa and distribution of low-volume melts (alkaline rocks, carbonatites, and kimberlites) and Mesozoic to Cenozoic rifts relative to the velocity structure and cratonic blocks of Africa (Begg et al., 2009). Note the coincidence of the CVL volcanoes with the NW edge of the Congo Craton (after Begg et al., 2009). Blue polygons—rifts; white asterisks—volcanoes; green stars—carbonatites; pink circles—nepheline syenites; white squares—kimberlites; CVL—Cameroon Volcanic Line. S-wave velocity (Vs) image is 100- to 175-km depth slice.

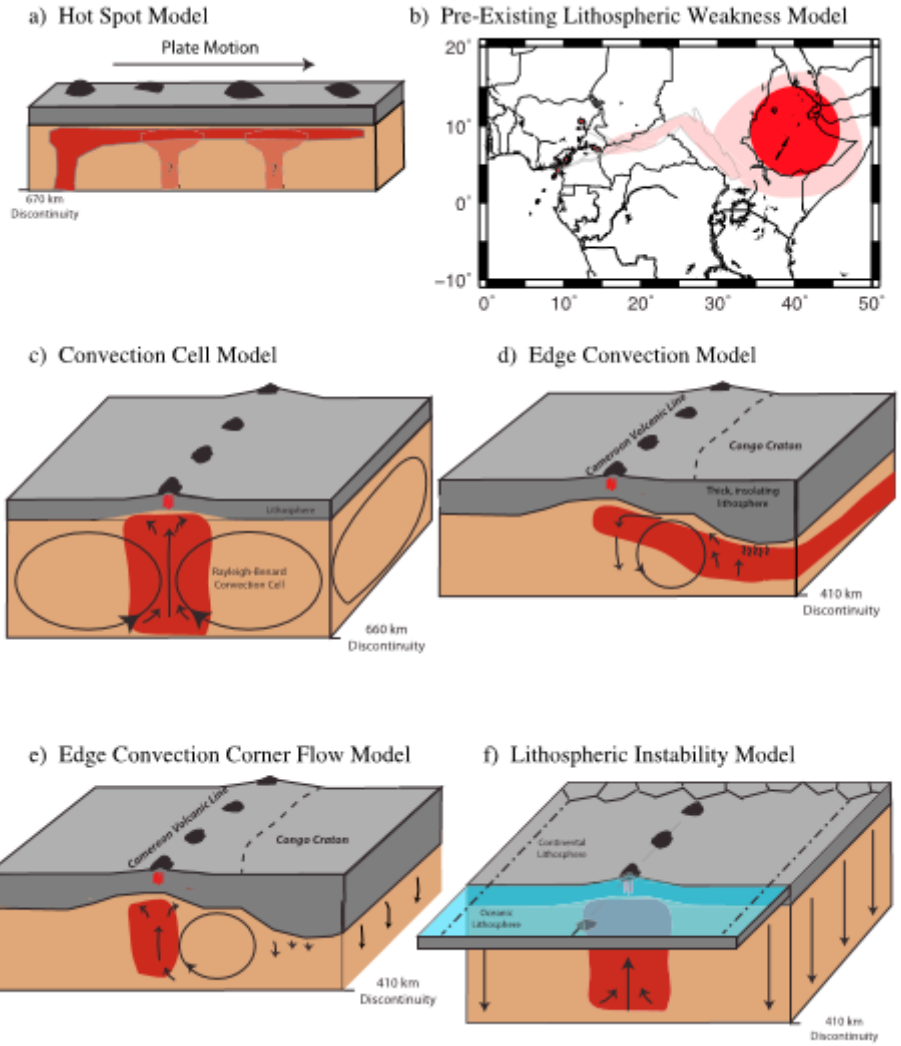

Figure 2-4 |Potential geodynamic models for the formation of the CVL (Adams et al.,2015). (a)Hot spot or multiple hotspot model. (b)Pre-existing weakness model, with possible transport of material from the Afar hot spot [from Reusch et al., 2010; after Ebinger and Sleep, 1998]. (c) Rayleigh-Baynard convection cell model [after Meyers et al., 1998]. (d) Edge convection model with lateral flow of warm material from beneath the Congo Craton [King and Anderson, 1995]. (e) Corner-flow eddy model [King and Anderson, 1998; King and Ritsema, 2000]. (f) Lithospheric instability along continental margin [Milelli et al., 2012].

CHAPTER 3: SAMPLES AND ANALYTICAL METHODS

3.1. Samples

A total of 104 samples collected from the oceanic sector volcanoes (Annobon, Saô Tomé and Principe) and the geographically defined continent ocean boundary (c.o.b) volcanoes (Bioko and Etinde) of the CVL were measured for major elements. All samples were collected by Dr. Festus T. Aka (Institute of Mining and Geological Research, Center for Volcanological and Geophysical Research, Cameroon). Among them, all mafic samples having SiO_2 < 53 wt.% (N=90) were measured for trace elements and Sr-Nd-Hf-Pb isotopic compositions. Trace elements and isotopic measurements were carried out under clean condition better than class 1000 at the Pheasant Memorial Laboratory (PML), Institute for Planetary Materials (IPM), Okayama University (Nakamura et al., 2003). Workflow of the sample preparation and analytical procedures is shown in Figure 3-1.

3.2. Sample preparation

From all samples, thin sections were prepared. Phenocryst mineral assemblages and modal abundances were examined by the optical-microscopic observation. For the bulk rock chemical analyses, the powdered samples were prepared as follows. The rock specimens were crushed by a jaw crusher to coarse chips of 3-5 mm in diameter, and then the chips without weathered parts were carefully hand-picked. The secondary minerals filled in vesicles and veins were also carefully removed from sample chips. Subsequently, the chips were rinsed with deionized water in an ultrasonic bath for several times until the supernatants of water become clear. The chips were then dried in an oven at 100°C for an overnight. The dried chips were pulverized using an alumina ceramic puck mill to make fine powder.

3.3. Reagents and rock reference materials

Purification procedures for all the reagents were described in Nakamura et al. (2003).

3.3.1. Reagents

Water: Three types of water, MilliQ water, USQ (Ultra Super Milli-Q) water and B-USQ (Boron-free USQ) were used in this study. MilliQ water (≥18.2 MΩ cm) was prepared by deionizing with a mixed-bed resin and filters (MILLIPORE). The USQ water was

prepared by passing the Milli-Q water through a Q-Pak cartridge equipped with 0.22μm final filter (MILLIPORE). The B-USQ is same as USQ, but its low boron blank was confirmed.

Hydrofluoric acid: Two types of concentrated HF solutions: 2D HF (twice distilled HF) and B-HF (Boron free concentrated HF) were used. The both HF reagents were prepared by the Analytical grade 46% HF (Wako). The 2D HF was distilled at 80ºC using the using a two-bottle Teflon apparatus. The B-HF was prepared by adding the 1g/L of mannitol, then distilled at 80ºC using a two-bottle Teflon apparatus.

Hydrochloric acid: EL grade (highly purified chemicals for the electronic industry) 36% HCl (Kanto Chemical) was diluted to 6M with MilliQ water, then distilled using a two-bottle Teflon apparatus at 110ºC.

Nitric Acid: EL grade 69% HNO_3 (Kanto Chemical) was diluted using a two-bottle Teflon apparatus, making a 16M 1D HNO_3.

Hydrobromic acid: Analytical grade 47~49% HBr (Kanto Chemical) (8M) was diluted using a two-bottle Teflon apparatus twice, makeing 2D HBr.

Perchloric acid: Highly purified 70% (7M) $HClO_4$ (TEMAPURE-AA-100) was used.

Mannitol solution: Analytical grade mannitol powder (Merck) was dissolved in ~ 0.01M HF to obtain a 0.1% solution.

Aluminum Solution: 1% of Al solution dissolved in HCl (Johnson Matthey) was used without purification.

Pyridine: Analytical grade pyridine (Merck) and 1 time distilled and diluted to USQ to make 25% (V/V) pyridine.

D.P.E (0.06M DCTA in 0.5M pyridine): DCTA was dissolved in pyridine and diluted with Milli-Q, resulting in a 0.06M DCTA in a 0.5M pyridine solution. The solution was then passed twice through a cation resin bed (Bio-Rad X 12).

HIBA (α-hydroxyisobutyric acid): 208 g of analytical grade HIBA (Tokyo Kasei) was dissolved in 1L of 1D H_2O, and the solution was passed through 0.45 μm and 0.2 μm

filters. The solution was subsequently purified by passing it once through cation exchange resin (Muromac AG 50WX12), resulting in a 2M solution. 2M HIBA was further diluted into appropriate concentrations (0.5M or 0.2M) by adding 1D H_2O and aqueous ammonia with adjusting pH to be approximately 5.

3.3.2. Rock Reference materials

A GSJ basaltic rock reference sample JB-2 was used as a standard for Sr and Nd isotope analysis. For major elements, JA-2, JA-3, JB-1b, JB-2, JB-3, JG-1a, JG-2, JGb-1, JGb-2, JH-1, JP-1, JR-1, JR-2, and JR-3 were used for calibration. For the trace elements and, Pb and Hf isotope analysis, a GSJ basaltic reference sample JB-3 was used. In addition, in-house rock standard MYK-1 was used as bracketing during trace element analyses. To minimize sample heterogeneity, JB-2 and JB-3 was further pulverized using an alumina ceramic swing mill.

3.4. Major-element analysis

3.4.1. XRF analysis

Whole rock major element compositions, including Cr and Ni contents were determined by a Philips PW 2400 X-ray Fluorescence Spectrometer (XRF). All the analyses were duplicated. Before making the fused glass, the lithium tetraborate flux was pre-dried at 600°C to eliminate the absorbed water. Approximately 0.5 g of the powdered sample was mixed with 10 times of lithium tetraborate flux, then fused in a Pt crucible (95% Pt + 5% Au) by a frequency-induced heating furnace by stepwise heating procedure (Takei, 2002). Peridotitic to rhyolitic reference materials issued from Geological Survey of Japan were used for making calibration curves. Analytical errors (1δ) for major element analysis was < 1%.

3.4.2. Loss on ignition

The loss on ignition was determined using an electric muffle furnace. The samples previously dried at 110°C were heated at 1100°C, then the loss/gain of the weight were gravimetrically determined. Each analysis was duplicated. All analyses were duplicated, and the average value of loss on ignition (LOI) for each sample was shown here.

3.4.3. FeO and H_2O^+ determination

A determination of ferrous iron was performed by titration following the Yokoyama and Nakamura (2002). In this method, excess V^{5+} and Fe^{2+} were added to the sample before and after sample decomposition, respectively. Then Fe^{2+} was determined by titrating the mix solution of decomposed sample and excess Fe^{2+} using $K_2Cr_2O_7$ (~0.04 M) as titrant. The H_2O^+ was then calculated based on the LOI, FeO, and total Fe_2O_3 compositions.

3.5. Trace element analysis

Trace element abundances of 29 elements (Li, Be, B, Rb, Sr, Y, Zr, Nb, Cs, Ba, La, Ce, Pr, Nd, Sm, Eu, Gd, Tb, Dy, Ho, Er, Tm, Yb, Lu, Hf, Ta, Pb, Th, and U) were analyzed using a Q-pole type inductively coupled plasma mass spectrometer (Q-ICP-MS, Agilent 7500 CS, Yokogawa Analytical Systems, Japan). The analysis of these elements was performed in three groups (insoluble fluoride forming, aquaphile, and oxophile elements, fluorophile elements, and B; definition is after Makishima et al., 2009) as detailed below. All analysis of trace elements was done in duplicate samples. Typical analytical errors of < 5% were obtained for all the analysis of trace elements.

3.5.1. Insoluble fluoride forming, aquaphile, and oxophile elements (Li, Be, Rb, Sr, Cs, Ba, Pb, Th, U and REE)

Analysis of trace element abundance was performed following Makishima and Nakamura (2006). Approximately 20 mg of sample powder was weighed in a Teflon beaker. A ^{149}Sm-enriched spike solution was subsequently added to the sample to achieve the best desired isotopic ratio ($^{149}Sm/^{147}Sm \sim 8$) to obtain the minimum error. The sample was subsequently decomposed with 1 ml of 7M $HClO_4$, 0.2 ml of 1D 16M HNO_3 and 1 ml of 2D 30M HF. All the samples have been agitated in ultrasonic bath for an overnight then heated at 120°C. To effectively decompose the fluoride minerals, stepwise drying of sample solutions at 120, 165, and 195°C was performed following Yokoyama et al. (1999). Approximately 1ml of 7M $HClO_4$ and an equivalent amount of USQ was again added into the dried sample, then agitated by ultra-sonic bath for 30 minutes and then stepwisely dried. Subsequently, 1 ml of 6M HCl was added, agitated and dried at 120°C. Finally, the samples have been dissolved in 0.5M HNO_3 to make dilution factor (DF;

defined as the total solution volume in ml divided by the mass of the sample in g) of 250. This sample solution was agitated by ultra-sonic bath to dissolve perfectly and further diluted to achieve DF ~1000 with 0.5M HNO_3 in a 1.5 mL micro tube, then the solution was used for the Q-ICP-MS analysis.

The mass resolution power of Q-ICP-MS is not enough to separate ^{157}Gd from $^{141}Pr^{16}O$, therefore, interference correction for ^{157}Gd intensities was performed by subtracting the $^{141}Pr^{16}O$. To estimate the contribution of Pr-oxide, a yield of oxide was determined by analyzing the Cs tuning solution in each analytical session. The range of the oxide-yield during the analysis was from 0.55 to 0.88 %.

3.5.2. Fluorophile elements (Zr, Hf, Nb and Ta)

Approximately 20 mg of sample powder was weighed and mixed with 0.2ml of 0.1% mannitol solution in an 8-ml propylene beaker. To suppress the coprecipitation of the analyzing elements, an Al solution was added to samples with (Al/(Ca+ Al) molar ratio (denoted as Al#) less than 0.6 following the method developed by Tanaka et al. (2003). Appropriate amount of Zr-Hf spike solutions was then added to the weighed samples.

The samples were subsequently decomposed with 1 ml 1D 30M B-HF in an ultrasonic bath for more than one day. The decomposed samples were dried at < 80°C. The dried samples were diluted by adding 5 ml of 0.5M HF and then agitated for 30 minutes in an ultra-sonic bath and centrifuged to settle the fluoride precipitates. The final sample solution for analysis was prepared by diluting the supernatant from the centrifuged sample solution by 0.5M HF-MT (HF with mannitol) solutions. Dilution factor of ~ 1000 was obtained.

3.5.3. Boron

Determination of concentration of boron was done by weighing ~ 20 mg of sample powder in an 8-mL propylene beaker. Approximately 0.2ml of 0.1% mannitol solution was added to the beaker before sample weighing to avoid vaporization of B. Boron spike was subsequently added. 1ml of B-HF was added to decompose the samples. All the

samples were put inside ultrasonic bath for agitation for two days and then drying at < 80ºC was done in a boron free evaporator. Finally, the dried sample was diluted by 0.5M HF and centrifuged. For analysis by ICP-MS Q pole the sample solution has been diluted further by 0.5 M HF-MT (HF with mannitol) solutions to make dilution factor of ~ 1000.

3.6. Isotope composition analyses

3.6.1. Pb isotope analysis

Pb isotopic analyses were performed by double-spike method using a thermal ionization mass spectrometry in static multicollection mode using Thermo TRITON after Kuritani and Nakamura (2002, 2003). Approximately ~ 300mg of the weighted powdered sample in a Teflon beaker was first leached with 6 M HCl at 90°C for 9 hours to remove potential contaminant. After rinsing with USQ water for three times, the residual powder was dissolved with 2.5 mL 2D HBr and 2.5 mL 2D HF in an ultrasonic bath for an overnight, followed by on a heating plate set at 110 ºC for an overnight. Then, the sample solution was centrifuged for 30 minutes at 3000 rpm. Subsequently the supernatant solution separated from the fluorides was transferred to another Teflon beaker, then dried at 110 ºC. The dried sample was then dissolved with 3ml 0.5M HBr and centrifuging at 3000rpm for 30 minutes, which is used for the ion-exchange separation.

The procedures of chemical separation of Pb were essentially followed after Kuritani and Nakamura (2002) consisting of two column steps. The volumes of columns were 100µl and 10µl for the first and second columns respectively. An anion exchange resin, Bio-Rad AG-1X8, was charged into a polyethylene column at the first column chromatography. The resin bed was cleaned by flushing the column with 1.5 ml of 0.5 M HNO_3, followed by 1.5 ml of water. The resin was then conditioned with 0.1 ml of 2D 0.5 M HBr. After loading the sample solution on the resin, 0.8 ml of 0.25 M HBr – 0.5 M HNO_3 mix acid was then introduced to remove the elements other than Pb. Using the HBr–HNO_3 mixture is more efficient than to use HBr alone with respect to the separation of Zn from Pb (Strelow, 1978; Lugmair and Galer, 1992). The Pb was then eluted with 0.8 ml of 1D 6M HCl and dried at 90 ºC. In the second column, 0.01 ml of anion-exchange resin, Bio-Rad AG-1X8, was charged into the column, and the resin bed was cleaned by

flushing the column with 1.5 ml of 0.5 M HNO_3 and 1.5 ml of water. The resin was then conditioned with 0.1 ml of 0.5 M HBr. The dried sample collected from the first column was dissolved in 0.2 ml of 0.5 M HBr, and loaded onto the resin. To remove contaminants in the samples from the first column, 0.3 ml of 0.5 M HBr was introduced. Subsequently, 0.6 ml of 1D titrated 0.5M HNO_3 was added to the column as a Pb elution.

Prior to analysis by TIMS, the recovery of Pb after purification process was checked by Q-ICP-MS. The samples yielding > 30ng Pb were divided for the unspiked (~ 30 ng) and spiked (5 ng) runs. For the spiked batch, ^{207}Pb-^{204}Pb spike solution was added. Then, 2 drops of 0.015M H_3PO_4 and 1D HNO_3 were added in both solutions. The both solutions were dried at ~70 ºC for > 8 hours. To minimize the contamination, the samples yielding < 30 ng Pb were dried in a MUKADE closed system evaporator. Further addition of 3 drops of $HClO_4$ prior to 1D HNO_3 was employed to avoid effect of organic materials on Pb isotope analysis. The dried Pb sample was dissolved in the emitter consisting of silicic acid and diluted phosphoric acid (Gerstenberger and Haase, 1997). The dissolved sample was loaded onto the top of trapezoid-shaped rhenium filament (Koide and Nakamura, 1990).

During analysis, the NBS981 standard yielded the average of 16.9430 ± 0.0042 for $^{206}Pb/^{204}Pb$, 15.5003 ± 0.0045 for $^{207}Pb/^{204}Pb$, and 36.730 ± 0.013 for $^{208}Pb/^{204}Pb$ (n= 34, quoted uncertainty in 2δ), which are consistent with that obtained in Kuritani and Nakamura (2003) and are comparable to those from other studies (Baker et al., 2004). The rock standard JB-3 yields $^{206}Pb/^{204}Pb$ = 18.2975 ± 0.0020, $^{207}Pb/^{204}Pb$ = 15.5393 ± 0.0021, and $^{208}Pb/^{204}Pb$ = 38.2570 ± 0.0047 (n = 2, the error is relative difference over the average), which are also consistent with that reported in Kuritani and Nakamura (2003). Typical analytical reproducibility during analysis was 300 ppm. Total blank was typically ~ 20 pg and is considered to be negligible with respect to the amount of element in the dissolved sample (>100 ng).

The factors applied for age correction is larger than the analytical error, and thus we have used the age corrected Pb isotope data throughout. The ages assigned to the samples are derived from published K-Ar ages compiled by Mbowou et al. (2012) and analyzed in this study.

3.6.2. Hf isotope analysis

Hf isotope analyses were done by multi collector inductively coupled plasma magnetic sector field mass spectrometer (MC-ICP-MS, Neptune, Thermo Electron Corp., Germany) following the method developed by Lu et al. (2007b). Approximately 100 mg sample powder was weighed. The sample powder was soaked in 0.2ml of 0.1% mannitol solution. Addition of ~ 1.5 ml of 1D 30M B-HF was subsequently employed. The sample solution was then agitated in an ultrasonic bath for two days for complete decomposition. The decomposed samples have been dried at < 80°C in boron free evaporator. The dried sample was prepared for loading by dissolving in 4ml of 0.4M HCl–0.5M HF solution. The sample solution was agitated in an ultrasonic bath for one night and then centrifuged for 15 minutes at 3000 rpm.

Purification of Hf was performed using two steps of ion-exchange chromatography. The first chromatography uses 0.3 mL of anion exchange resin (AG1X8) to remove most of the major cations. The anion-exchange resin was washed by 3 ml of 6 M HCl–0.5 M HF mix acid, then conditioned with 1 ml of 0.4 M HCl–0.5 M HF mix acid. After loading the 2ml of sample solution onto the resin, major elements in the cation-form were washed out by 2 ml of the 0.4 M HCl–0.5 M HF mix acid. Finally, Hf together with Zr and Ti, was recovered by adding the 2 ml of the 6 M HCl–0.5 M HF mix acid into a 7 ml Teflon beaker. After adding three drops of $HClO_4$, the Hf-enriched solution was dried at 120°C. After drying, three drops of $HClO_4$ and one drop of concentrated HF were added and solution was heated for 5 hours at 115ºC to remove F^-. If still white precipitates (TiO_2 in this case) remain, addition of $HClO_4$ and HF and drying were repeated. This is because TiO_2 can incorporate Hf, resulting poor Hf yield. The sample solution was then dissolved in one drop of 30% H_2O_2 and 1 ml of 9 M HNO_3 and put into ultrasonic bath for ~ 20 minutes.

In the second column, a two-layered resin bed was used.0.15 ml of pre-filter resin was packed at the bottom of a polyethylene column to absorb organic compounds released from 0.15ml UTEVA which was packed in the upper layer. The two-layered resin bed was washed with 3 ml 0.5 M HNO_3 and conditioned with 1 ml 9 M HNO_3. Then the sample solution was loaded onto the column. Addition of 4 ml of 9 M HNO_3 was subsequently

done to wash out the Ti and other elements. Then Hf was collected by 6 ml of 4M HNO_3. The solution was evaporated and finally dissolved in 0.5 to 1 mL of 0.5 M HF for analyses by MC-ICP-MS.

During analysis, the $^{176}Hf/^{177}Hf$ of JMC 14374 standard yielded the average of 0.282178± 0.000005 (n= 72, uncertainty in 2s). The rock standard JB-3 yields 0.283229 ± 0.000007 (n=14, 2s). Total blank average results 4 pg (n=7).

3.6.3. Sr and Nd isotope analysis

Approximately 100 mg sample powder was weighed in a Teflon beaker. The samples were then leached using 6 M HCl at 90 ˚C for 5 hours to minimize the altered materials. Sample decomposition was subsequently done by adding 1 mL of 7M $HClO_4$, 1ml of 2D HF and 1D 6M HNO_3. All the samples have been agitated in an ultrasonic bath for an overnight. Stepwise drying of sample solutions was performed following Yokoyama et al. (1999). The dried sample was finally dissolved in 1.5 mL of 4M HCl and agitated in an ultrasonic bath for 20 minutes, then transferred into a 1.5 mL micro tube and centrifuged for 7 minutes at 3000 rpm. The recoveries of Sr and Nd were monitored by Q-ICP-MS using a 0.1ml of sample aliquot, after drying and dissolved in 5ml of 0.5M HNO_3.

The chemical separation of Sr and Nd was done in two steps. The first column employs a cation resin bed BioRad 50W “X10”. After washing the resin by addition 6M El HCl and MilliQ and USQ and conditioned with 1 ml of 4 M HCl, 1mL of sample solution was loaded onto the resin. Then, Rb-Sr rich fraction and REE-rich fraction were separated using 2.8 M HCl and followed by addition of 2.5ml of 2.8M HCl to wash the major elements. Finally, collection of Rb and Sr elutes and Sm and Nd elutes was separately done by addition 4M HCl and 6M HCl, respectively. After drying each fraction, Sr and Nd were purified using 0.5 mL of 50W-X10 and 0.3 mL of 50W-X8 cation exchange resins, respectively.

Sr and Nd isotope analyses were performed by thermal ionization mass spectrometry in static multicollection mode using a Thermo TRITON, following the methods by Yoshikawa and Nakamura (1993) for Sr and Nakamura et al. (2003) for Nd

isotope analysis. Sr and Nd isotope ratios were normalized to $^{86}Sr/^{88}Sr$=0.1194 and $^{146}Nd/^{144}Nd$=0.7219, respectively. During analysis $^{87}Sr/^{86}Sr$ of NIST987 yielded an average of 0.710279 ± 0.000018 for (n=15, uncertainty in 2s) and of JB-2 yielded 0.703705 ± 0.000011 (n=5, 2SD). In house standard PMLNd standard yielded 0.511749 ± 0.000017 for $^{143}Nd/^{144}Nd$ (n=17, 2SD), which corresponds to 0.511885 for La Jolla standard. The rock standard JB-2 yielded 0.513124± 0.000017 (n=7, 2SD). The average values of total procedural blanks for Sr and Nd were 259 pg (n=5) and 7pg (n=5), respectively.

3.7. K-Ar geochronology

The K-Ar age dating was done following the method of Nagao et al. (1996). Fresh samples without any altered materials were selected by the microscope observation. After crushing the sample and sieving between 0.18 and 0.25mm, groundmass fraction was separated magnetically using the Frantz isodynamic separator. All the K and Ar analyses were duplicated.

3.7.1. Potassium analysis

Samples for K analysis were grounded in a Si_3N_4 mortar to obtain fine powders. Approximately 20 mg sample powder was weighed in Teflon beakers and decomposed with HF and $HClO_4$ following the method described by Yokoyama et al., (1999). The decomposed samples were re-dissolved into 0.1M HCl with Cs buffer. Abundance of K was determined by flame photometry using a Shimadzu AA-6200. Calibration was performed using multi standard solutions (0, 0.5, 1, 1.5 and 2 ppm) K standard solutions.

3.7.2 Argon analysis

The radiogenic ^{40}Ar abundance was determined by isotope dilution mass spectrometry using noble gas mass spectrometer (VG5400, Micromass, Uk). Samples for Ar analysis were weighed at 500 mg in aluminum capsules and fused at 1500°C in a Mo crucible in a vacuumed cell. The extracted Ar was mixed with ^{38}Ar-enriched spike in a cryogenic charcoal, then the mixed Ar was purified with Ti-V-Fe and Al-Fe getters, prior to the admission into mass spectrometer.

3.7.3. K-Ar age for reference materials

During the course of K-Ar analysis, the reference standard rocks and minerals were analyzed along with samples; LP-6, 128.6 ± 0.2 Ma (n=5); Bern 4B, 17.47 ± 0.11 Ma (n=5); Bern 4M, 17.78 ± 0.30 Ma (n=7); 80901-2, 2.91 ± 0.06 Ma (n=8); 80908-5, 2.99 ± 0.01 Ma (n=4); 80811-3, 3.03 ± 0.09 Ma (n=5). Results show good agreement with reported ages (Nagao et al., 1996) providing confirmation to the reliability of the results.

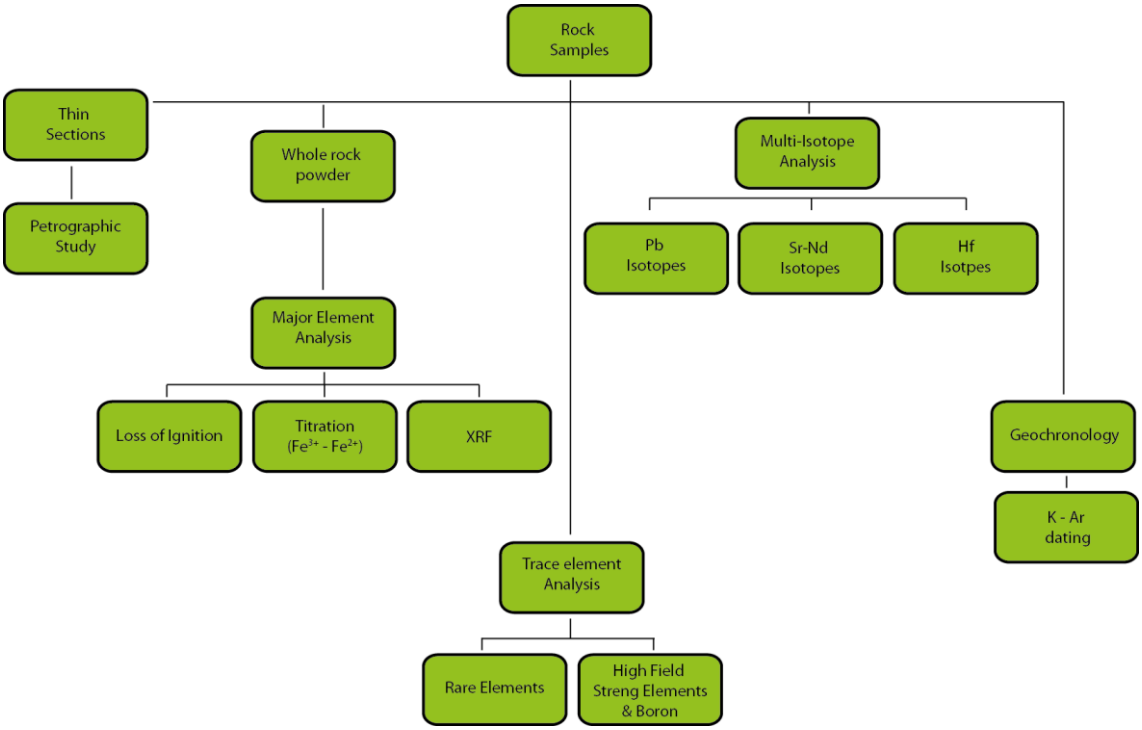

Figure 3-1 | Analytical Workflow

CHAPTER 4: RESULTS

4.1. Petrography

4.1.1. General petrographic feature of the CVL samples

In this section, I will describe the petrographic features of the studied volcanic rocks. Photomicrographs of representative thin sections are shown in Figure 4-1. Lavas from oceanic sector volcanoes of the CVL are mainly porphyritic alkaline basalts and basanites. Phenocryst assemblages of the basalts and basanites are dominated in olivine, clinopyroxene, and plagioclase. Olivine phenocrysts are rarely altered to iddingsite. Clinopyroxene and plagioclase sometimes occur as micro- phenocrysts (< 0.5mm). In some samples, amphiboles and biotites exits as minor constituent phenocrysts. Deformed clinopyroxenes occur as xenocrysts in some lavas. Abundant peridotite xenoliths or mafic aggregates occur in samples from all the volcanic centres. Magma mixing is inferred from reaction rims on olivine and reverse zoning of clinopyroxene. The groundmass of most lavas consists of glass, Fe-Ti oxides, clinopyroxene, and plagioclase. As documented in Yokoyama et al. (2007), Mt. Cameroon samples range from porphyritic to aphyric basanites. The major phenocrysts of the porphyritic samples are olivine and clinopyroxene (~15 vol.%) and a small amount of plagioclase (1-2 vol.%). A summary of petrography characteristics of all the studied lavas samples and the modal abundance of the representative samples are presented in Table 1 and Table 2, respectively.

4.1.2. Microscopic description

Annobon

Samples collected from Annobon, the south-western terminal of the CVL, are dominantly composed by porphyritic basalts and basanites with minor amounts of trachy-basalts and picro-basalts (Fig. 4-1A). Phenocryst mineral assemblages are olivine, clinopyroxene, and plagioclase. Microphenocrysts of olivine and plagioclase are also observed. The mineral phases are often characterized by euhedral and subhedral crystal habits. Plagioclase phenocrysts and microphenocrysts sometimes show columnar habit. The groudmass comprises clinopyroxene, plagioclase, titano-magnetite, and glass. The olivine phenocrysts in basalts and basanites often show deformation and dissolution textures.

Sao Tome

Samples collected from Sao Tome, located at the oceanic sector of the CVL, are composed by aphyric to porphyritic basalt, basanite, picrobasalt, trachy-andesite, phono-tephrite, tephri-phonolite, and phonolite (Fig. 4-1E). Phenocryst mineral assemblages are olivine, clinopyroxene, plagioclase, and rarely amphiboles. The phenocrysts are euhedral, subhedral, anhedral, tabular and acicular habits in texture. Olivine phenocrysts commonly occur as dissolved olivine and rarely deformed. Clinopyroxene phenocrysts show zoning textures. The basalts and basanites samples often contain clinopyroxene and olivine xenocrysts. The ground mass comprises clinopyroxene, titano-magnetite, olivine, and glass. Hydrous phases occur in the matrix of some basanites.

Principe

Samples collected from Principe, located at the oceanic sector of the CVL, are composed by aphyric to porphyritic basalt, basanite, picrobasalt, trachy-basalt, trachy-andesite, trachy-dacite, phono-tephrite, tephri-phonolite, phonolite, and nephelinite (Fig. 4-1C). Phenocryst mineral assemblages are mostly euhedral to anhedral olivine, clinopyroxene, and plagioclase. In the nephelinite samples, nepheline, amphibole and sphene phases occur as phenocrysts. Most of the olivine and clinopyroxene phases are euhedral and subhedral. The plagioclase is often marked by columnar habit and nepheline display a tabular habit. The groundmass comprises clinopyroxene, plagioclase, titano-magnetite, and glass. Olivine phenocrysts often show dissolved texture and rim of the most of the olivine are altered to iddingsite. Zoning texture is common in the clinopyroxene phases. Peridotite xenolith occurs in some samples.

Bioko

Samples collected from Bioko, located at the COB sector of the CVL, are composed by aphanitic to porphyritic basalts and basanites (Fig. 4-1B, F). One sample (BK01) is porphyritic basaltic andesite. The phenocryst mineral assemblages are euhedral and subhedral olivine, clinopyroxene, and plagioclase. The olivine and clinopyroxenes often display euhedral and subhedral habits. Plagioclase is shows columnar habit. The ground mass comprises clinopyroxene, plagioclase, titano-magnetite, and glass. The

clinopyroxene commonly shows zoning texture. Olivine phenocrysts often show deformed and dissolved texture, and most of olivines rim are altered to iddingsite in most of the samples. Reaction rims are also abundant in olivine phenoscrusts. Peridotite xenoliths are commonly observed in some samples.

Etinde

Samples collected from Etinde, at the COB sector of the CVL, are composed by porphyritic nephelinite (Fig. 4-1D). Phenocryst mineral assemblages are euhedral clinopyroxene and nepheline. The groundmass comprises clinopyroxene, titano-magnetite, nepheline, and glass. The clinopyroxene phenocrysts show zoning texture. Peridotite xenoliths occur in all the samples.

4.2 K-Ar dating

Most of the studied samples were dated by Aka et al. (2004). K-Ar age data for eight representative samples analyzed in this study are shown in Table 3.

Annobon samples yield ages ranging from 1.63 to 4.7 Ma. One sample from Sao Tome records an age of 2.12 Ma. Principe samples indicate ages from 5.8 to 6.53 Ma. Bioko lavas yield ages from 0.17 to 0.18 Ma. A sample from Etinde shows an age of 0.43 Ma. The obtained data sets demonstrate the absence of age progression along the CVL which is in agreement with previous geochronological studies.

4.3 Whole rock chemical and isotopic compositions

We report high-precision major and trace element data and the Sr, Nd, Hf, and Pb isotopic compositions of 90 oceanic sector and ocean-continent boundary CVL lavas: Etinde, Bioko, Principe, Sao Tome, and Annobon (Table 4, 5, and 6). The data from Mt. Cameroon samples which were analyzed previously in the same laboratory (N = 26) (Yokoyama et al., 2007) are also used here.

4.3.1 Major element compositions

Whole rock major element data and CIPW norm composition are presented in Table 4. Classification of the lavas based on the CIPW norm compositions indicates that

most of the samples are nepheline normative (Fig. 4-2). The total-alkalis silica (TAS) classification (Le Maitre et al.,1989) of the samples (Fig. 4-3) demonstrates that alkaline mafic rocks (basalts, basanites, and nephelinites) predominate the volcanism along the CVL. Here I show the exhibited major element characteristics of each volcano.

Samples from Annobon are plotted in the field of basalts, picro-basalts, and trachy-basalts with alkaline affinity (Fig. 4-3). These samples have SiO_2 and MgO concentrations ranging from 41.6–47.8 wt.% and 4.9–18.5 wt.%, respectively (Fig. 4-4), suggesting that they have undergone a variable degree of fractionation. Their Mg# (100[MgO/(MgO+FeO)]) range from 0.4-0.6 indicating that they have been modified by differentiation processes.

Samples from Sao Tome have alkaline affinity and plotted in the field of picrobasalt, basanite, basalt, phono-tephrite, tephri phonolite, trachy-andesite, trachy-dacite and phonolite (Fig. 4-3). They display a range of SiO_2 content from 40.8–58.5 wt.% and MgO content range from 0.2–11.8 wt. % (Fig. 4-4). Their Mg# ranges from 0.2–0.5.

Samples from Principe are characterized by strongly alkaline nephelinites, picrobasalt, basanites, phono-tephrite, and phonolite (Fig. 4-3). One basalt sample displays tholeiite affinity (Figs. 4-2 and 4-3). The SiO_2 and MgO contents range from 37.8-63.3 wt.% and 0.2–13.3 wt. % respectively (Fig. 4-4). They display Mg# ranging from 0.1–0.6.

Samples from Bioko are basalts, basanites, trachy basalts and basaltic andesite (Fig. 4-3). The basalts are dominantly alkaline and rarely tholeiites. One sample plots on the dividing line between alkaline and tholeiite suits (Fig. 4-3). The SiO_2 and MgO range from 42.9–53 wt. % and 3.6–13 wt. % respectively (Fig. 4-4). Their Mg# ranges from 0.3–0.6.

Samples from Etinde are characterized by alkaline nephelinites (Fig. 4-3). They display narrow ranges of SiO_2 and MgO contents from 39.3–41.5 and 3.8–5.0 wt.% respectively (Fig. 4-4). These samples are characterized by Mg# ranging from 0.3–0.4.

As shown in the major element variation diagram (Fig. 4-4), the main features observed are: (1) Ca, Cr, and Ni decreases monotonously with a decrease in MgO; (2)

TiO_2, Fe_2O_3, and P_2O_5 also decreased with decreasing MgO, especially among more evolved rocks; (3) Al abundance increases with decreasing MgO. Such features ascribe to fractionation of olivine, spinel, and clinopyroxene in the earlier stage, and apatite and Fe-Ti oxide in the later stage of magnetic differentiation. The plagioclase was a minor role during the differentiation. Among the CVL lavas, the Etinde lavas show striking characteristics: lower SiO_2 and higher MnO for a given MgO than the other CVL lavas (Fig. 4-4).

4.3.2 Trace element compositions

Whole rock trace element data are presented in the Table 5. The primitive mantle normalized trace element pattern of CVL samples illustrate a high enrichment in incompatible elements and most of the samples show negative anomalies of K, Pb, P, Zr, Hf, and Ti (Fig. 4-5), which is distinct from the MORB or OIB except for HIMU basalts (Willbold and Stracke, 2006). Trace element ratios among the volcanic centres were compared (Fig. 4-6). The ratios for other typical OIB having HIMU, EM1, and EM2 affinities (Willbold and Stracke, 2006) are also compared in Figure 4.6. The average values of Rb/Nb, Ba/Nb, Ba/Th, K/La, and Ba/La show systematic decrease from SW to NE volcanic centres (Fig. 4-6). The trace element ratios of Etinde and Mt. Cameroon are identical to the HIMU basalts while the Annobon tend shows similarity with EM1 or EM2 lavas. These systematic trends suggest the contribution of distinct source materials which may be related with the location.

4.3.3 Sr, Nd, Hf, and Pb isotopic compositions

The Sr-Nd-Hf-Pb isotopic compositions of the studied lavas are presented in the Table 6. The lavas define a considerable range of Sr-Nd-Hf-Pb isotopic compositions: $^{87}Sr/^{86}Sr = 0.702926 - 0.704279$, $\varepsilon Nd = 3.05\text{-}7.22$, $\varepsilon Hf = 1.68\text{-}8.12$ and $^{206}Pb/^{204}Pb = 19.14\text{-}20.99$ (Fig. 4-7). The isotopic compositions clearly indicate the heterogeneous nature of the mantle, presumably due to the presence of different source components beneath the CVL.

The $^{206}Pb/^{204}Pb$ show systematic trend correlated with the location, the lowest value for the Annobon (19.14 - 19.37) and the values increased towards the NE volcanoes

Mt. Cameroon and Etinde (20.38 – 20.60) that resembles to HIMU basalts. This trend is consistent with that observed in trace element ratios (Fig. 4-6). Compared to the other volcanic suites, Annobon lavas display large variation in $^{207}Pb/^{204}Pb$ (15.6-15.68), $^{176}Hf/^{177}Hf$ (0.282800-0.283015), $^{87}Sr/^{86}Sr$ (0.703204-0.704279) and $^{143}Nd/^{144}Nd$ (0.512878-0.512988). Samples from Saô Tomé and Principe have more radiogenic Pb isotopic composition and show larger variation in $^{206}Pb/^{204}Pb$ (19.74-20.99). Among the samples, one sample from Principe (PP26) show exceptional unique characteristics, which is the most radiogenic $^{206}Pb/^{204}Pb$ (~21.0), and remarkably more radiogenic in the $^{208}Pb/^{204}Pb$ (~40.6) against the $^{207}Pb/^{204}Pb$ (~15.7), and is slightly offset to the extent of the main trend of Principe. The Bioko samples show larger variation in $^{206}Pb/^{204}Pb$ (19.84-20.56) with a fairly uniform $^{207}Pb/^{204}Pb$ (15.67-15.69), and the trend extending to compositions found in Etinde is oblique to the trends of Saô Tomé and Principe. In contrast to the Pb isotope variation of the four islands, Etinde and Mt. Cameroon samples show relatively homogeneous Pb isotopic composition. The Pb isotope signature of the Etinde lavas show more radiogenic Pb compositions than Mt. Cameroon.

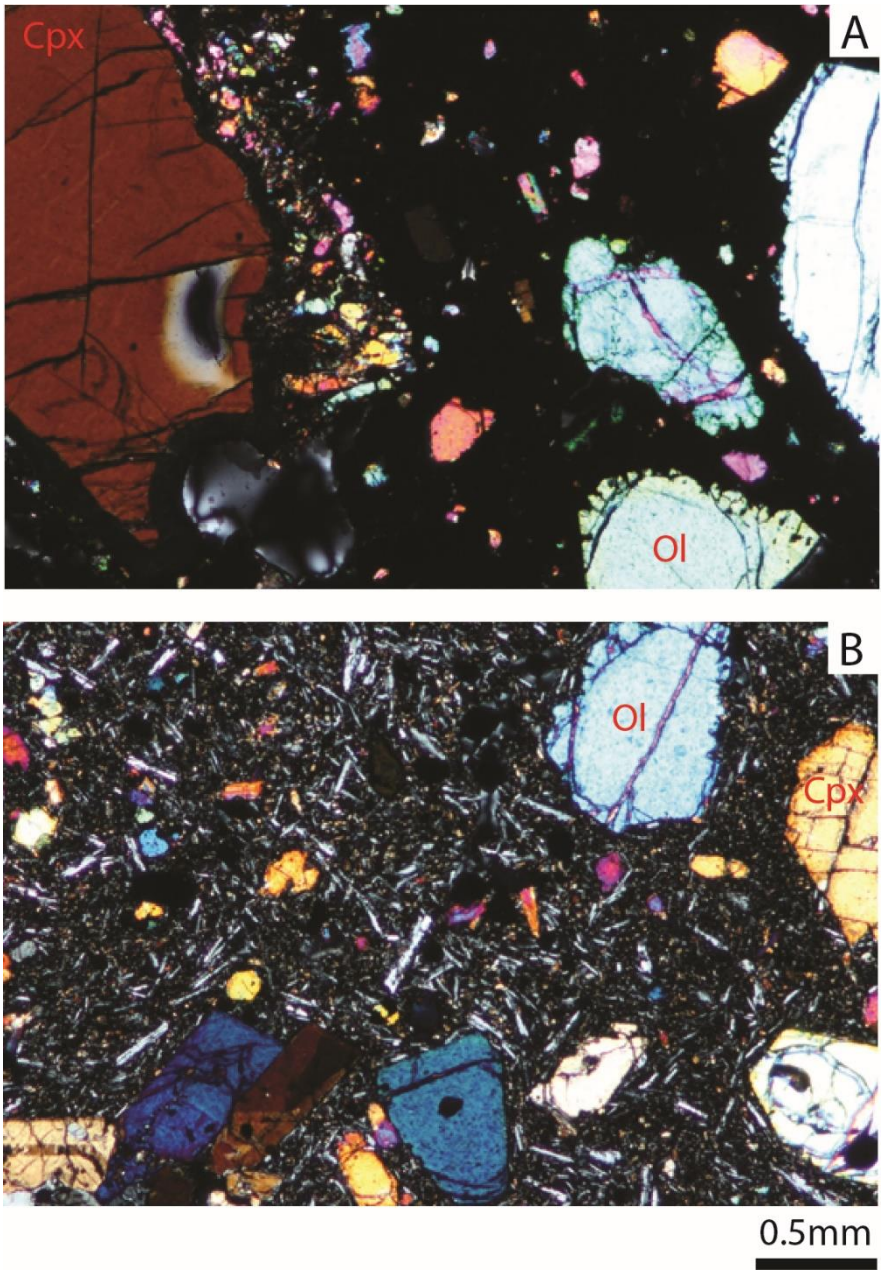

Figure 4-1 | A, Photomicrographs of Annobon (basanite); B, Bioko (basaltic andesite); C, Principe (basalt); D, Etinde (nephelinite); E, Sao Tome (basanite), and F, Bioko (tholeiite basalt). Abbreviations: Ol = Olivine; Cpx = Clinopyroxene; Plag = Plagioclase; Neph = Nepheline; Amph = Amphibole.

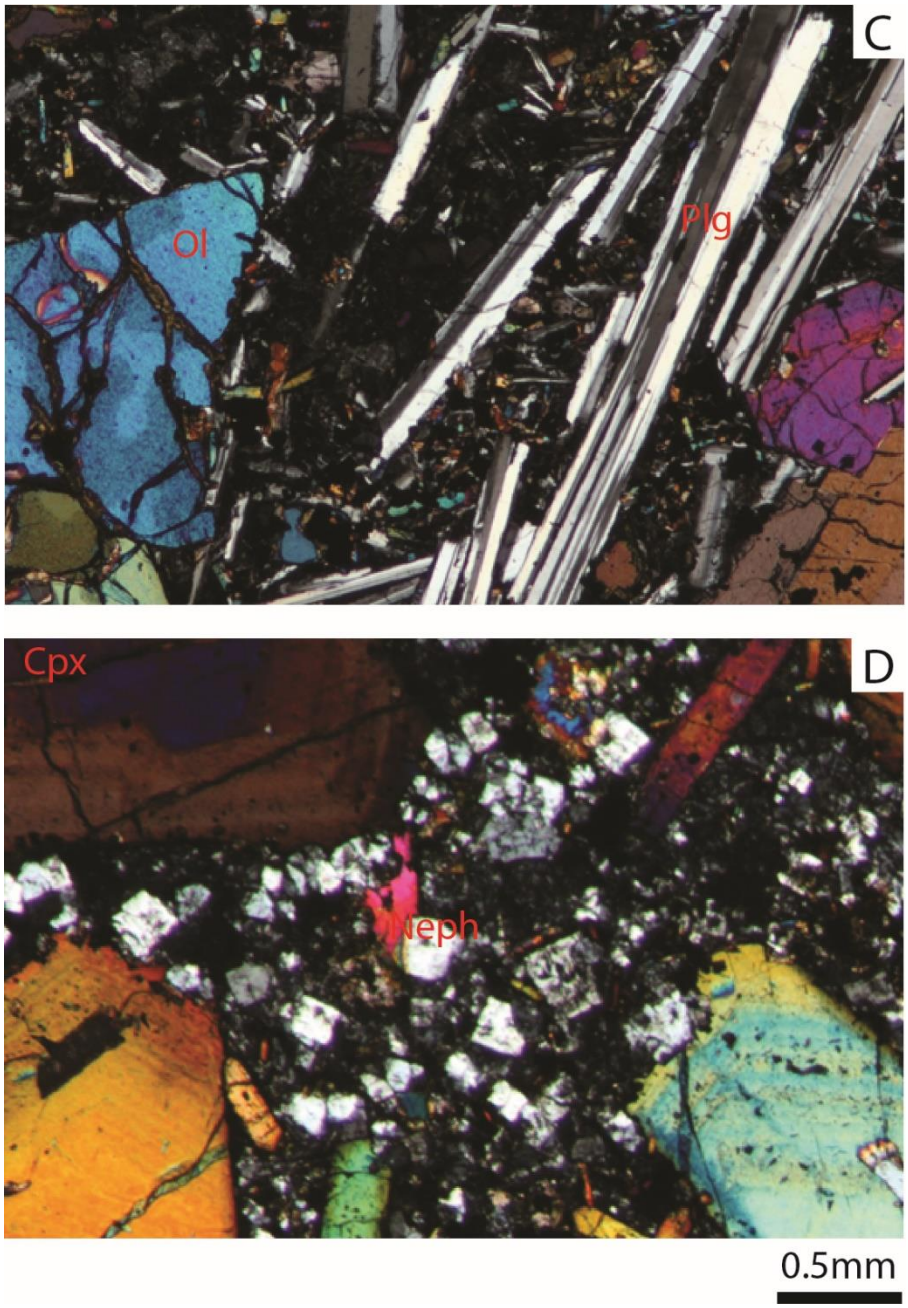

Figure 4-1| ***(continued)***

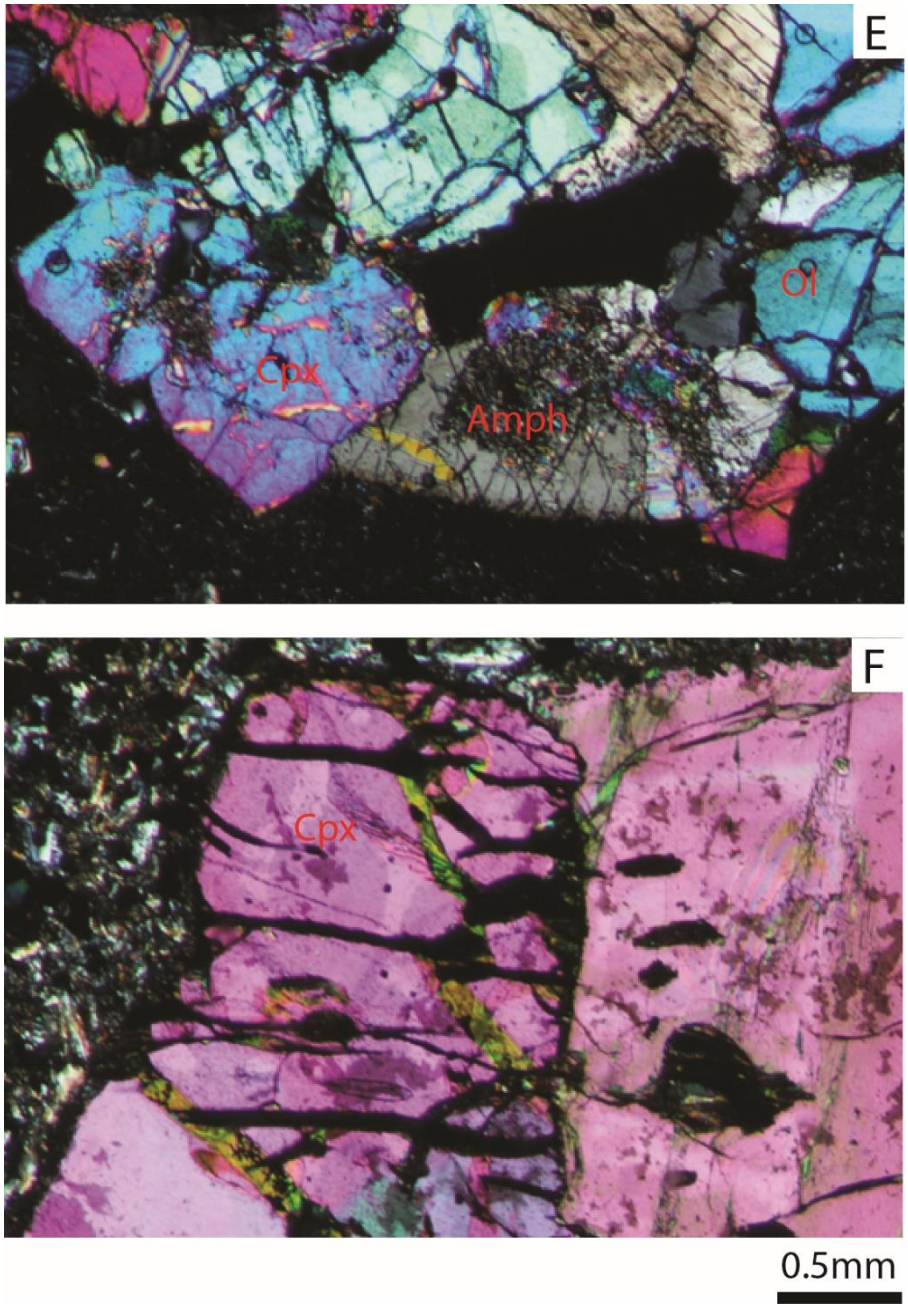

Figure 4-1| ***(continued)***

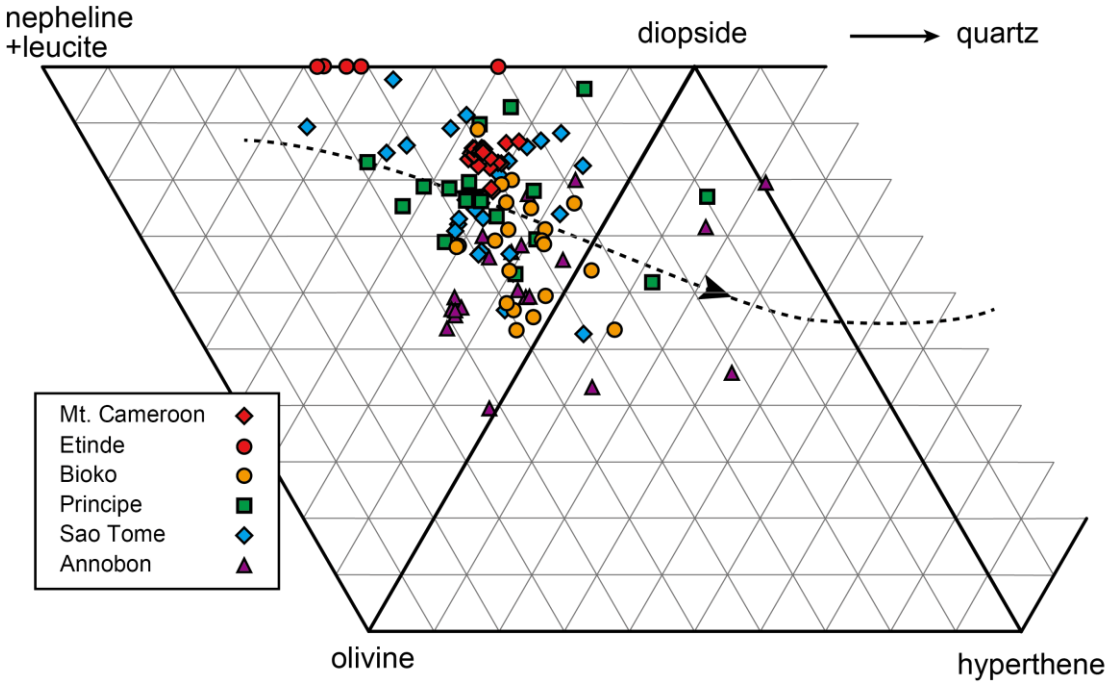

Figure 4-2 | CIPW normative compositions of the CVL samples. The diagram is after Thompson (1984). Broken line indicates a cotectic curve at 1 atm (Thompson et al., 2001).

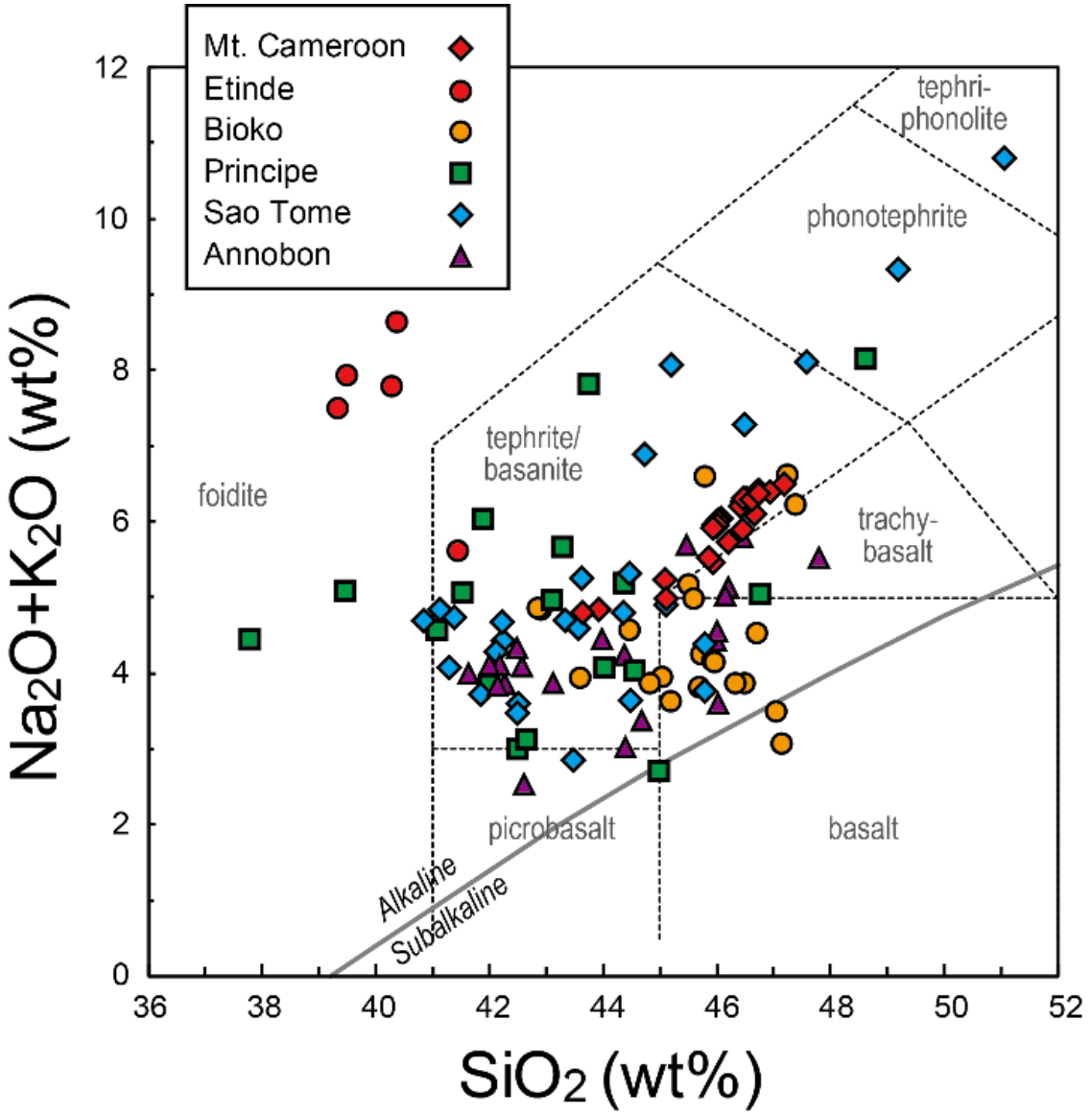

Figure 4-3 | Total alkali-silica (TAS) classification for volcanic rocks of oceanic and continent-ocean boundary of the Cameroon volcanic line. The classification diagram is after Le Maitre et al. (1989). The alkaline-sub-alkaline dividing line is from Irvine and Baragar (1971).

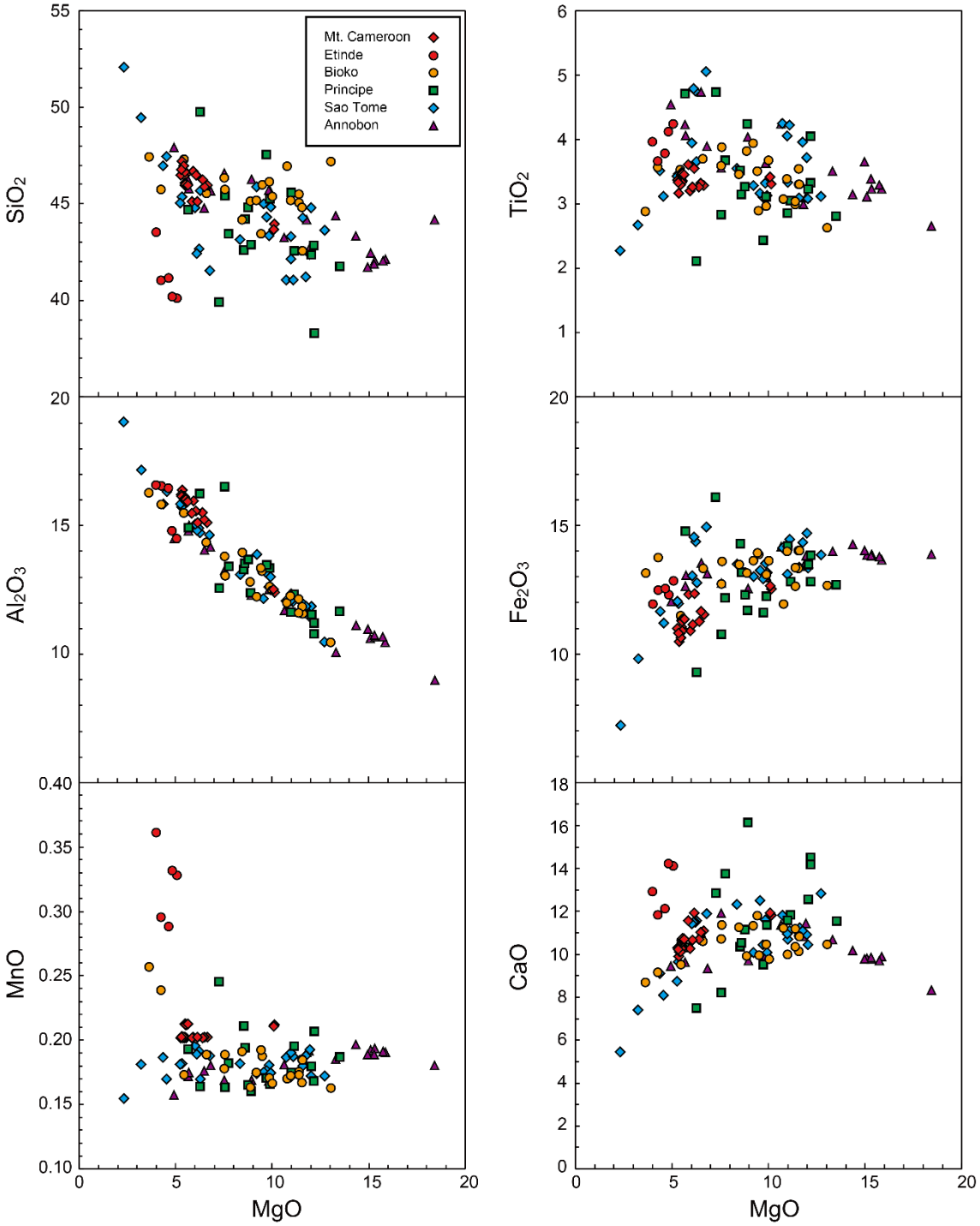

Figure 4-4 | Whole-rock major elements variation diagrams of major element oxides in CVL lavas (units are in wt. %).

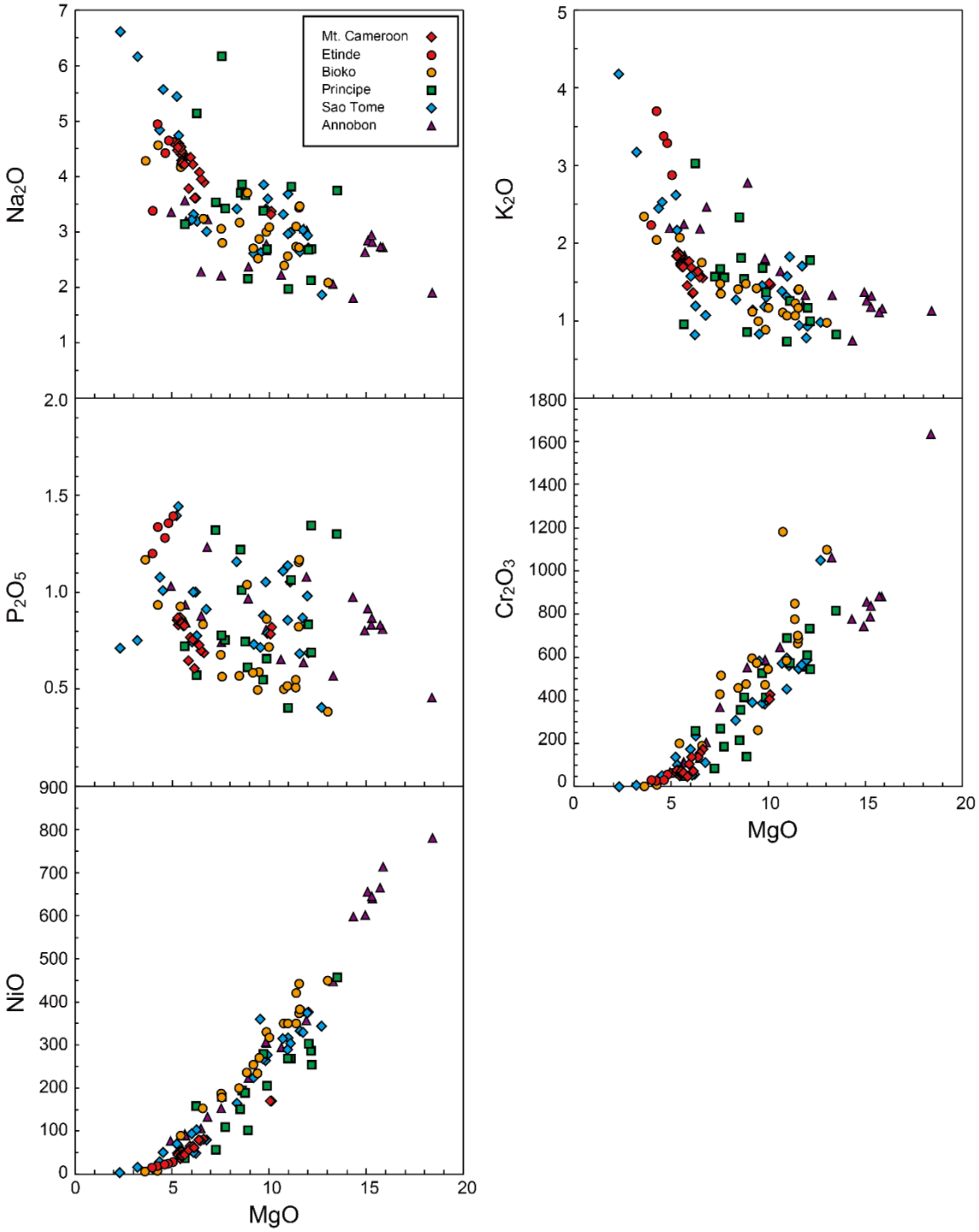

Figure 4-4| (*continued*)

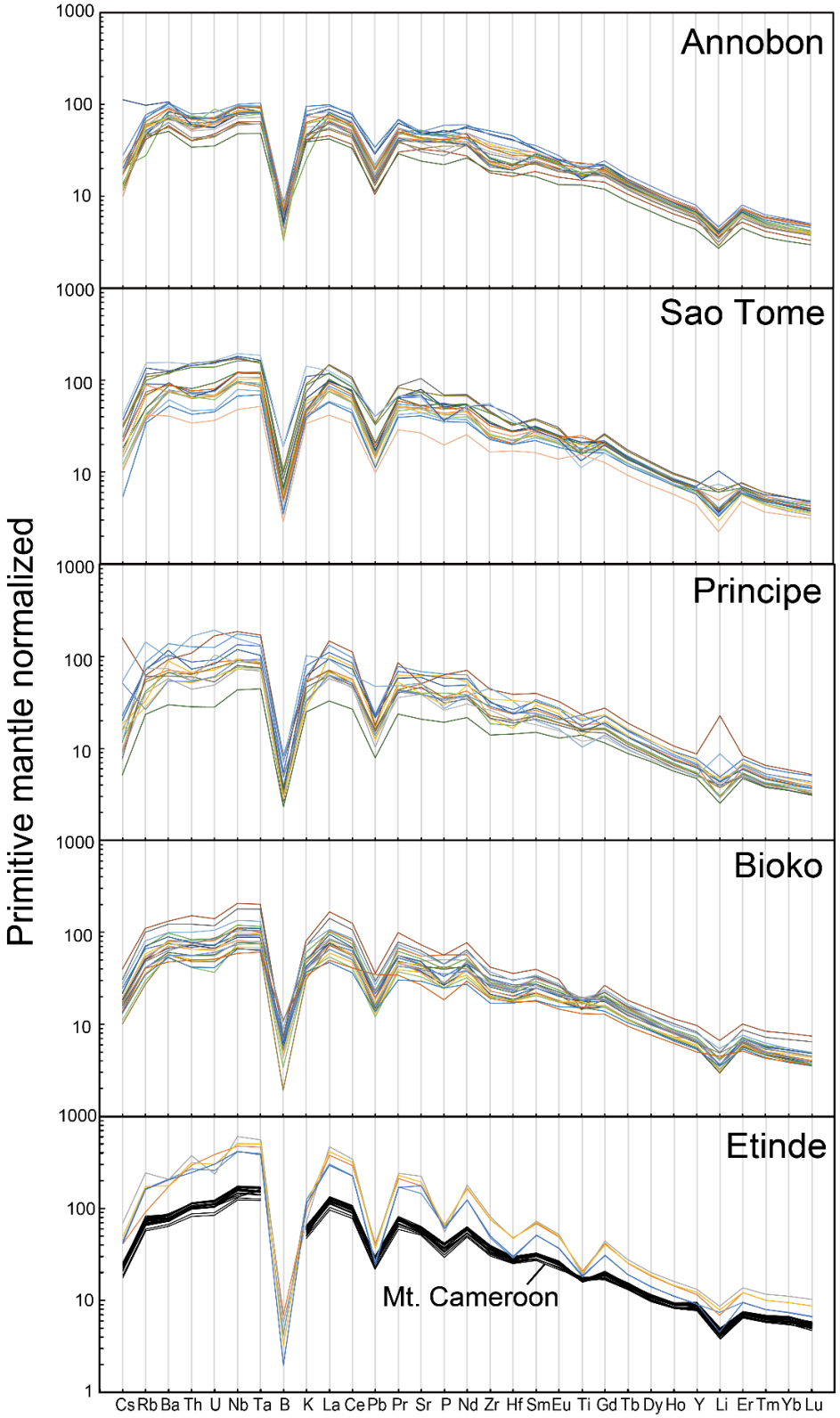

Figure 4-5 | Primitive Mantle normalized trace element patterns of the CVL lavas. The normalizing values of the primitive mantle values are from McDonough and Sun (1995).

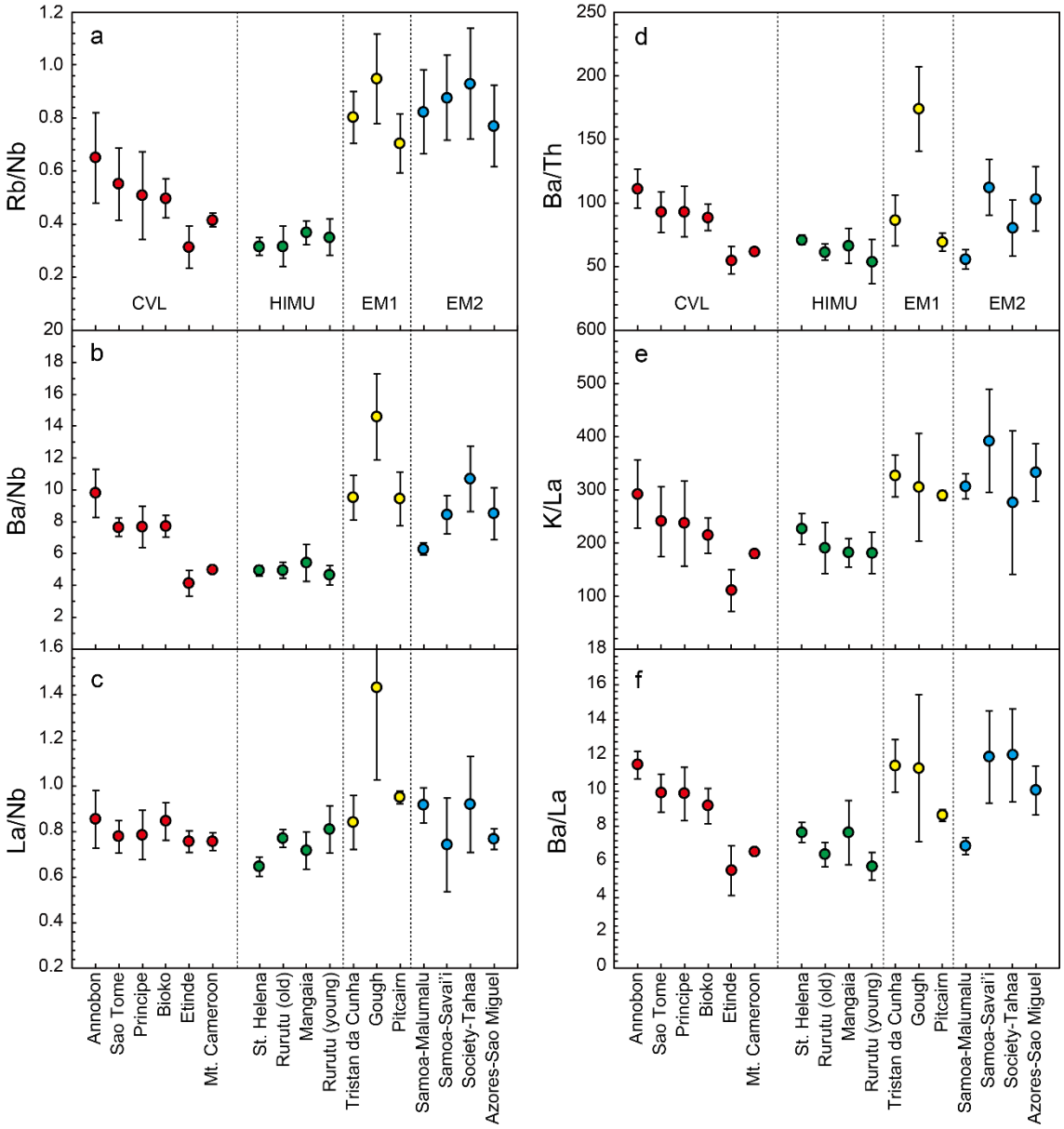

Figure 4-6 | Comparison of trace element ratios for the CVL lavas and global Oceanic Islands. The compiled data for HIMU, EM1, and EM2 are after Willbold and Stracke (2006). Average values are plotted with 1 standard deviation**.**

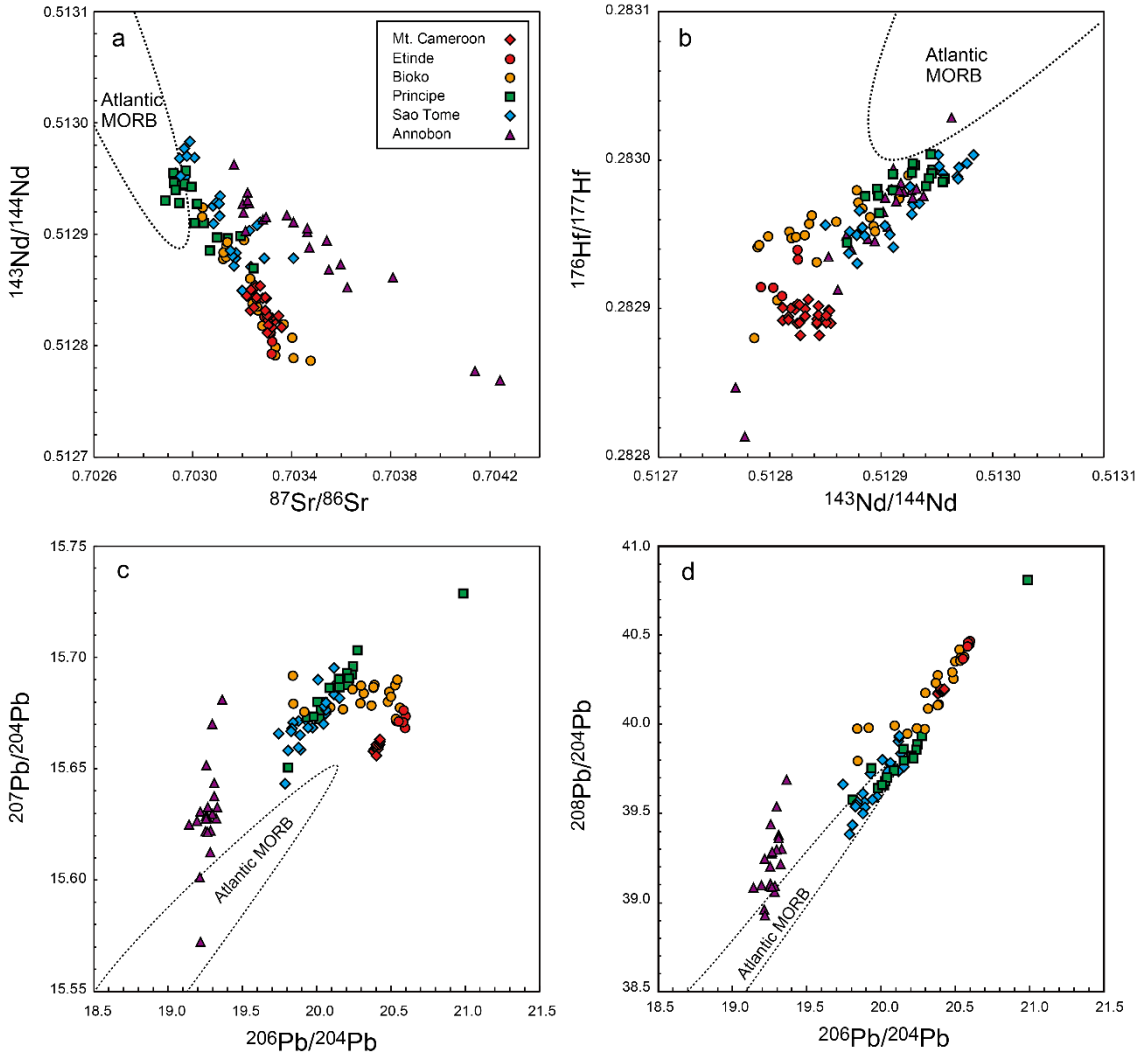

Figure 4-7 | a, $^{87}Sr/^{86}Sr$ vs. $^{143}Nd/^{144}Nd$; b, $^{143}Nd/^{144}Nd$ vs. $^{176}Hf/^{177}Hf$; c, $^{206}Pb/^{204}Pb$ vs. $^{207}Pb/^{204}Pb$; and d, $^{206}Pb/^{204}Pb$ vs. $^{208}Pb/^{204}Pb$ diagrams for CVL samples. Atlantic MORB between 30° N and 30° S is compiled data (Supplementary Table 1).

Table 1 | Petrographical descriptions of the CVL samples

Sample name	Rock name	locality	Phenocryst minerals					Phenocryst textures					Ground Mass minerals						Other textures							
			Ol	Cpx	Pl	Nph	Amp	euhedral	subhedral	anhederal	Rod/ tabular	aphanitic	Ol	Cpx	Gl	Ti-Mag	Plag	Neph	Ol deformed	Cpx zoning	reaction rims	ol/cpx dissol.	Xenocryst	Xenoliths	secondary minerals	iddingsite
Annobon																										
AN01	Basanite	San Antonio	✓	✓					✓					✓		✓			✓	✓	✓	✓	✓			±
AN02	Basanite	San Antonio	✓	✓					✓		✓			✓	✓	✓			✓	✓	✓	✓		✓		
AN04-3	Trachy-basalt	Lake Masafin	✓		✓				✓		✓	✓		✓	✓	✓										✓
AN05	Basanite	Lake Masafin	✓	✓				✓	✓					✓	✓	✓	✓				✓			✓		±
AN06	Basanite	Lake Masafin	✓	✓	✓			✓	✓			✓		✓	✓	✓						✓				±
AN07	Basanite	Lake	✓	✓				✓	✓		✓			✓	✓	✓			✓		✓	✓				
AN08	Basanite	Ridge	✓	✓					✓					✓	✓	✓			✓		✓	✓				
AN10-3	Basanite	Santa Cruz	✓	✓	✓			✓	✓			✓		✓	✓	✓										±
AN11	Basanite	Santa Cruz	✓	✓				✓	✓					✓	✓	✓	✓							✓		±
AN12	Basalt	San Antonio	✓	✓	✓			✓	✓					✓	✓	✓				✓						
AN13	Basanite	San Antonio	✓	✓	✓			✓	✓					✓	✓	✓					✓	✓	✓	✓		±
AN14	Basalt	River Dashim	✓	✓	✓			✓	✓					✓	✓	✓	✓			✓						
AN15	Basanite	River Dashim	✓	✓	✓			✓	✓					✓	✓	✓	✓			✓				✓		±
AN16	Basanite	San Antonio	✓	✓				✓	✓					✓	✓	✓	✓					✓				
AN17	Trachy-basalt	San Pedro	✓	✓	✓				✓			✓		✓	✓	✓				✓	✓					✓
AN18	Basanite	San Pedro	✓	✓				✓	✓					✓	✓	✓	✓			✓						±
AN19	Basalt	San Pedro	✓	✓				✓	✓						✓	✓				✓				✓		
AN20	Basanite	Tortuga	✓	✓				✓	✓					✓	✓	✓			✓			✓				✓
AN22	Basanite	San Antonio	✓	✓				✓	✓		✓			✓	✓	✓			✓		✓	✓		✓		
AN23	Basanite	San Antonio	✓	✓					✓					✓	✓	✓			✓					✓		±
AN24	Picro-basalt	San Antonio	✓	✓				✓	✓					✓	✓	✓			✓		✓	✓				
Sao Tome																										
ST01	Basanite	Palmar	✓	✓					✓		✓			✓	✓	✓	✓				✓	✓				
ST02	Basanite	Boa Morte	✓	✓					✓		✓			✓	✓	✓					✓	✓				
ST03	Basanite	Diogo Nunes	✓	✓	✓			✓	✓		✓			✓	✓	✓				✓		✓		✓		
ST04	Basanite	Diogo Nunes	✓	✓				✓	✓			✓								✓		✓		✓		
ST05	Basanite	Diogo Nunes	✓	✓				✓	✓		✓			✓	✓	✓	✓			✓		✓				
ST06	Basanite	Milla Grosa	✓	✓	✓			✓	✓			✓										✓			✓	
ST08	Basanite	Santa Adelaida	✓	✓					✓		✓			✓	✓	✓				✓		✓			✓	✓
ST09	Basanite	Milla Grosa	✓	✓					✓		✓			✓	✓	✓			✓			✓		✓		
ST10	Basalt	Ribera funda	✓	✓	✓			✓	✓		✓			✓	✓	✓	✓			✓		✓		✓		✓
ST11	Basanite	River Provez	✓	✓				✓	✓								✓			✓	✓		✓			
ST13	Basanite	River Provez	✓	✓	✓			✓	✓		✓			✓	✓	✓	✓			✓	✓	✓			✓	
ST14	Phono-tephrite	River Provez																								
ST16	Basanite	Annobon	✓	✓	✓			✓	✓								✓			✓		✓				
ST17	Basanite	Annobon	✓	✓	✓			✓	✓								✓			✓		✓				
ST20	Basanite	Trindade	✓	✓				✓	✓								✓									
ST21	Basanite	Trindade	✓	✓					✓			✓		✓	✓	✓	✓			✓		✓	✓			
ST23E	Basanite	Praia das Pombas	✓	✓	✓			✓	✓		✓			✓	✓	✓	✓			✓		✓	✓		✓	
ST24	Basanite	Praia das Pombas	✓	✓	✓		✓	✓	✓	✓				✓	✓	✓	✓			✓					✓	
ST26	Basanite	Praia das Pombas	✓	✓				✓	✓					✓	✓	✓	✓		✓	✓		✓		✓	✓	
ST27	Basanite	Praia das Pombas	✓	✓	✓				✓		✓			✓	✓	✓	✓								✓	
ST29	Basalt	Praia Morrao	✓	✓	✓			✓	✓		✓			✓	✓	✓	✓			✓	✓	✓				±
ST30	Basanite	Aqua Joao		✓					✓			✓	✓	✓	✓	✓	✓			✓					✓	±
ST31	Basanite	Aqua Joao		✓					✓		✓	✓	✓	✓	✓	✓	✓			✓		✓				±
ST34	Tephri-phonolite	Rio Caue		✓	✓			✓	✓	✓				✓	✓	✓	✓			✓						
ST35	Basanite	Rio Caue	✓					✓	✓						✓	✓	✓					✓				±
ST36	Picro-basalt	Rio Caue	✓	✓	✓			✓	✓					✓	✓	✓	✓			✓	✓					

Table 1 | *(continued)*

Sample name	Rock name	locality	Phenocryst minerals					Phenocryst textures					Ground Mass minerals						Other textures							
			Ol	Cpx	Pl	Nph	Amp	euhedral	subhedral	anhederal	Rod/ tabular	aphanitic	Ol	Cpx	Gl	Ti-Mag	Plag	Neph	Ol deformed	Cpx zoning	reaction rims	ol/cpx dissol.	Xenocryst	Xenoliths	secondary minerals	iddingsite
Principe																										
PP01	Basanite	Porto Real	✓	✓				✓	✓		✓			✓	✓	✓	✓			✓		✓		✓		
PP03	Basanite	Okiponte	✓	✓	✓			✓	✓		✓			✓	✓	✓	✓			✓		✓				±
PP04	Basanite	Principe	✓	✓	✓			✓	✓		✓			✓	✓	✓				✓						±
PP05	Basanite	Bom Bom Is	✓		✓				✓	✓		✓		✓	✓	✓	✓									✓
PP07	Basanite	Campanha	✓	✓					✓					✓	✓	✓						✓		✓		
PP09	Basalt	Ponte Banana	✓	✓	✓			✓	✓					✓	✓	✓	✓			✓						±
PP10	Basanite	Ponte Banana	✓	✓	✓				✓		✓	✓		✓	✓	✓	✓					✓				
PP11	Phonotephrite	Praia Seca																								±
PP13	Basanite	Praia Seca																							✓	
PP18	Basalt	Praia Abelha	✓	✓	✓			✓	✓		✓			✓	✓	✓	✓			✓		✓		✓		
PP19	Basanite	Lapa	✓	✓				✓	✓		✓				✓	✓						✓			✓	
PP20	Trachy-basalt	Lapa	✓	✓	✓			✓	✓								✓			✓	✓	✓		✓		±
PP21	Picro-basalt	Lapa	✓	✓	✓			✓	✓		✓			✓	✓	✓	✓			✓		✓				
PP23	Nephelinite	Lapa	✓	✓	✓	✓	✓	✓	✓		✓			✓	✓	✓	✓									
PP24	Basanite	Praia Sundy	✓	✓	✓			✓	✓		✓			✓	✓	✓	✓			✓						
PP25	Basanite	Santo Antonio	✓	✓	✓			✓	✓		✓			✓	✓	✓	✓			✓		✓		✓		
PP26	Nephelinite	Santo Antonio	✓	✓					✓		✓				✓	✓	✓									±
Bioko																										
BK02	Basalt	Baney	✓	✓	✓			✓	✓		✓			✓	✓	✓	✓		✓	✓	✓	✓				
BK03	Basalt	Bao Basoala	✓	✓					✓						✓	✓					✓	✓		✓		
BK04	Basalt	Ruiche	✓	✓				✓	✓					✓	✓	✓				✓	✓	✓		✓		
BK06	Basalt	Luba	✓	✓	✓			✓	✓		✓			✓	✓	✓	✓			✓				✓		
BK07	Basanite	B. Cristol	✓	✓				✓	✓			✓		✓	✓	✓	✓		✓	✓	✓	✓		✓		
BK08	Basalt	B. Cristol	✓	✓	✓			✓	✓		✓			✓	✓	✓	✓			✓			✓			
BK09	Basalt	B. Cristol	✓	✓	✓			✓	✓		✓			✓	✓	✓	✓			✓	✓	✓		✓		
BK10	Basalt	B. Cristol	✓	✓	✓			✓	✓		✓			✓	✓	✓	✓					✓		✓		
BK11	Basalt	Luba	✓	✓	✓			✓	✓		✓			✓	✓	✓	✓			✓	✓	✓				
BK12	Basalt	Luba-Batete	✓	✓				✓	✓			✓		✓	✓	✓	✓			✓		✓		✓		
BK13	Basanite	Luba-Batete	✓	✓				✓	✓					✓	✓	✓				✓	✓	✓				
BK14	Basanite	Batete	✓	✓	✓			✓	✓						✓	✓				✓		✓		✓		
BK15	Basanite	Moca		✓	✓				✓		✓	✓		✓	✓	✓				✓		✓				
BK16	Basanite	Moca		✓	✓			✓	✓			✓		✓	✓	✓				✓		✓				
BK17	Basanite	Pico Basile	✓	✓				✓	✓			✓		✓	✓	✓					✓	✓				
BK18	Basanite	Pico Basile	✓	✓				✓	✓					✓	✓	✓					✓			✓		
BK19	Basanite	Mt Basile	✓	✓				✓	✓					✓	✓	✓	✓			✓	✓	✓		✓		
BK20	Basalt	Bososo	✓	✓	✓			✓	✓					✓	✓	✓	✓		✓	✓		✓				
BK21	Basanite	Barioba	✓	✓	✓				✓		✓	✓		✓	✓	✓						✓				
BK22	Basalt	Bakake	✓	✓	✓			✓	✓		✓			✓	✓	✓	✓			✓	✓					
BK23	Basalt	Riaba	✓	✓				✓	✓					✓	✓	✓				✓	✓	✓				±
Etinde																										
2208A	Nephelinite	Mt Etinde		✓		✓		✓			✓			✓	✓	✓		✓			✓				✓		
2208B	Nephelinite	Mt Etinde		✓		✓		✓			✓			✓	✓	✓		✓			✓				✓		
2208C	Nephelinite	Mt Etinde		✓		✓		✓			✓			✓	✓	✓		✓			✓				✓		
2208D	Nephelinite	Mt Etinde		✓		✓		✓			✓			✓	✓	✓		✓			✓				✓		
CA062	Nephelinite	Batoke																								

Table 2 | Mineral modal compositions for representative CVL samples

Sample No.	Rock name	Modal abundance (volume fraction)								GM minerals
		Ol	Cpx	Pl	Nph	Amp	Bt	GM	others	
Annobon										
AN01	basanite	0.2	0.18					0.6	0.02	Gl+Ti-Mag+Pl
AN02	basanite	0.03	0.16					0.81		Gl+Ti-Mag+Cpx
AN04	trachy-basalt	0.03	0.02	0.05				0.9		Gl+Ti-Mag
AN05	basanite	0.38						0.62		Gl+Cpx+Ti-Mag+Pl
AN10	basanite	0.07	0.03	0.35				0.55		Gl+Ti-Mag+Cpx
AN11	basanite	0.1	0.25	0.05				0.6		Gl+Cpx+Ti-Mag+Pl
AN13	basanite	0.19	0.08					0.73		Gl+Ti-Mag+Cpx
AN16	basanite	0.09	0.01					0.9		Gl+Cpx+Ti-Mag+Pl
AN19	basalt	0.1						0.9		Gl+Ti-Mag
AN24	picro-basalt	0.03	0.14					0.83		Gl+Ti-Mag+Cpx
Principe										
PP11	phonotephrite	0.05	0.1	0.33		0.02		0.5		Pl+Ti-Mag
PP23	nephelinite	0.05	0.1	0.05		0.1	0.15	0.55		Pl+Ti-Mag+ Gl
PP24	basanite	0.1	0.15	0.1				0.65		Cpx+Ti-Mag
Sao Tome										
ST01	basanite	0.2	0.05					0.75		Gl+Ti-Mag
ST06	basanite	0.02	0.05	0.01				0.9	0.02	Gl+Cpx+Ti-Mag
ST14	phono-tephrite	0.03	0.05	0.02		0.05		0.85		Pl+Ti-Mag+ Gl
ST20	basanite	0.3		0.03				0.67		Pl+Ti-Mag

Abbreviations: Ol, olivine; Cpx, clinopyroxene; Pl, plagioclase; Nph, nepheline; Amp, amphibole; Bt, biotite; GM, groundmass; others, secondary minerals or undefined accessory minerals.

Table 2 | *(continued)*

Sample No.	Rock name	Modal abundance (volume fraction)								GM minerals
		Ol	Cpx	Pl	Nph	Amp	Bt	GM	others	
Bioko										
BK04	basalt	0.19	0.2	0.01				0.6		Ol +Ti-Mag+Gl
BK06	basalt	0.1	0.1	0.3				0.5		Ol +Pl+Ti-Mag
Bk11	basalt	0.2	0.2	0.1				0.5		Cpx+Pl+Ti-Mag
Etinde										
2208A	nephelinite		0.2		0.2			0.6		Gl+Cpx+Ti-Mag
2208B	nephelinite		0.2		0.3			0.5		Nph+Ti-Mag+Cpx
2208C	nephelinite		0.25		0.25			0.5		Nph+Ti-Mag+Cpx

Table 3 | K-Ar age data for selected CVL samples

Sample ID	*Unit*	*[K] (wt%)*	*[^{36}Ar] counts (nccSTP/g)*	*^{40}Ar/^{36}Ar*	*[^{40}Ar] counts (nccSTP/g)*	*f (%) (air fraction)*	*age (Ma)*
AN15	Annobon	2.62	0.680±0.018	971.5±2.8	679±17	29.6	4.69±0.26
			0.689±0.019	968.5±2.9	685±18	29.8	4.72±0.27
						Mean	**4.70±0.37**
AN22	Annobon	1.06	0.578±0.016	404.7±0.9	236±6	72.3	1.59±0.09
			0.595±0.016	406.8±0.8	244±7	72.0	1.66±0.09
						Mean	**1.63±0.13**
ST09	Sao Tome	1.42	0.982±0.026	414.4±0.7	119±3	70.9	2.16±0.12
			0.931±0.025	415.5±0.8	114±3	70.6	2.07±0.12
						Mean	**2.12±0.17**
PP23	Principe	1.33	1.73±0.05	473.4±0.3	312±8	62.2	6.02±0.34
			1.76±0.05	457.6±2.5	290±8	64.3	5.61±0.32
						Mean	**5.80±0.47**
PP26	Principe	1.53	1.86±0.05	502.5±0.7	390±10	58.6	6.55±0.37
			2.04±0.05	484.1±0.9	388±10	60.8	6.52±0.36
						Mean	**6.53±0.52**
BK02	Bioko	1.59	0.515±0.008	324.9±0.8	15.0±0.4	90.3	0.243±0.008
			0.521±0.008	312.4±0.8	8.6±0.4	94.8	0.139±0.007
			0.572±0.016	307.6±0.7	6.6±0.4	96.2	0.108±0.008
			0.511±0.014	316.4±0.7	10.4±0.4	93.6	0.17±0.01
						Mean	**0.17±0.03**
BK06	Bioko	1.06	0.497±0.014	309.7±0.4	6.8±0.3	95.6	0.17±0.01
			0.484±0.013	311.2±0.6	7.4±0.3	95.1	0.18±0.01
						Mean	**0.18±0.01**
2208A	Etinde	3.15	1.86±0.03	324.0±0.5	52.1±1.1	91.4	0.43±0.01
			1.73±0.03	331.6±1.2	62.0±2.0	89.3	0.51±0.02
			2.99±0.08	309.9±0.5	41.5±1.5	95.5	0.34±0.02
			4.02±0.10	309.5±0.5	54.2±2.3	95.6	0.44±0.03
						Mean	**0.43±0.04**

Table 4 | Major element compositions and CIPW norm compositions of CVL samples

unit	Annobon	Annobon	Annobon	Annobon	Annobon	Annobon	Annobon
sample name	AN01	AN02	AN08	AN16	AN22	AN23	AN24
locality	San Antonio	San Antonio	Ridge	San Antonio	San Antonio	San Antonio	San Antonio
age (Ma)	*0.20*	*1.50*	*1.50*	*1.50*	*1.63*	*1.50*	*1.50*
type	1	1	1	1	1	1	1
Major elements							
SiO_2 (wt. %)	42.00	42.13	42.57	42.47	42.27	42.17	42.60
TiO_2	3.41	3.30	3.12	3.09	3.25	3.24	3.10
Al_2O_3	10.76	10.70	10.64	11.54	10.50	10.71	10.94
Fe_2O_3	4.67	2.92	4.54	4.73	3.65	3.93	5.13
FeO	8.27	9.79	8.42	8.12	9.06	8.98	8.00
MnO	0.19	0.19	0.19	0.19	0.19	0.19	0.19
MgO	15.35	15.79	15.16	11.91	15.94	15.39	14.12
CaO	9.85	9.70	9.80	11.37	9.87	9.78	9.96
Na_2O	2.95	2.75	2.85	3.02	2.73	2.82	1.77
K_2O	1.17	1.10	1.25	1.32	1.15	1.31	0.73
P_2O_5	0.83	0.83	0.92	1.07	0.81	0.86	0.96
H_2O^+	0.84	1.22	0.98	1.06	1.07	0.75	2.28
Total	100.3	100.4	100.4	99.9	100.5	100.1	99.8
Fe_2O_3T	13.85	13.79	13.89	13.74	13.70	13.90	14.00
Cr_2O_3 (μg/g)	788	882	855	554	880	839	775
NiO	643	664	655	356	713	638	596
CIPW norm							
Quartz							
Orthoclase	6.94	6.52	7.41	7.80	6.80	7.75	4.29
Albite	7.71	6.81	9.18	8.18	6.91	6.69	14.98
Anorthite	12.67	13.61	12.54	14.05	13.00	12.69	19.76
Nepheline	9.33	8.90	8.09	9.40	8.77	9.31	
Diopside	24.36	23.25	23.89	28.13	24.43	24.03	18.55
Hypersthene							5.47
Olivine	23.32	27.72	23.77	16.11	26.22	25.11	18.94
Magnetite	6.77	4.24	6.58	6.85	5.29	5.70	7.43
Ilmenite	6.47	6.28	5.93	5.87	6.17	6.16	5.89
Apatite	1.93	1.92	2.12	2.49	1.88	2.00	2.22
Leucite							
CaDiSilicate							
Wollastonite							
Hematite							
Titanite							
Total	99.5	99.3	99.5	98.9	99.5	99.4	97.5

Table 4 | *(continued)*

unit	Annobon	Annobon	Annobon	Annobon	Annobon	Annobon	Annobon
sample name	AN04-3	AN05	AN06	AN07	AN10-3	AN11	AN12
locality	Lake Masafin	Lake Masafin	Lake Masafin	Lake	Santa Cruz	Santa Cruz	San Antonio
age (Ma)	*4.50*	*1.50*	*4.50*	*1.50*	*1.50*	*1.50*	*4.50*
type	2	2	2	2	2	2	2
Major elements							
SiO_2 (wt. %)	47.80	44.40	46.46	41.63	43.98	43.11	45.98
TiO_2	4.54	2.67	4.25	3.64	4.66	4.24	3.65
Al_2O_3	14.48	9.04	14.88	10.96	13.81	11.68	12.59
Fe_2O_3	6.01	4.16	3.96	4.16		3.42	2.96
FeO	5.40	8.81	7.86	8.84		9.64	9.13
MnO	0.16	0.18	0.17	0.19	0.17	0.18	0.17
MgO	4.94	18.53	5.71	14.94	6.40	10.62	9.94
CaO	9.40	8.33	9.65	9.72	10.78	11.30	9.95
Na_2O	3.34	1.91	3.58	2.63	2.24	2.22	2.68
K_2O	2.18	1.13	2.24	1.36	2.14	1.63	1.78
P_2O_5	1.03	0.45	0.94	0.80	0.86	0.65	0.81
H_2O^+	1.21	0.57	0.75	1.04		1.66	0.80
Total	100.5	100.2	100.5	99.9	98.3	100.3	100.4
Fe_2O_3T	12.01	13.94	12.69	13.98	13.30	14.12	13.10
Cr_2O_3 (µg/g)	66.0	1634	114	745	132	645	585
NiO	76.3	780	91.5	600	104	293	304
CIPW norm							
Quartz	0.14						
Orthoclase	12.87	6.66	13.26	8.05	12.62	9.63	10.50
Albite	28.26	14.81	22.27	6.75	18.97	9.08	18.52
Anorthite	18.09	12.78	17.89	14.06	21.31	17.08	17.08
Nepheline		0.71	4.35	8.41		5.25	2.25
Diopside	17.05	20.30	19.10	23.01	8.61	27.83	21.71
Hypersthene	4.42				6.20		
Olivine		32.22	6.86	23.83	4.04	15.34	16.51
Magnetite	4.77	6.04	5.75	6.04		4.96	4.30
Ilmenite	8.62	5.06	8.08	6.92	0.37	8.05	6.94
Apatite	2.38	1.05	2.18	1.85	1.99	1.50	1.88
Leucite							
CaDiSilicate							
Wollastonite							
Hematite	2.72						
Titanite					10.96		
Total	99.3	99.6	99.7	98.9	85.1	98.7	99.7

Table 4 | *(continued)*

unit	Annobon	Annobon	Annobon	Annobon	Annobon	Annobon	Annobon
sample name	AN13	AN14	AN15	AN17	AN18	AN19	AN20
locality	San Antonio	River Dashim	River Dashim	San Pedro	San Pedro	San Pedro	Tortuga
age (Ma)	*4.50*	*4.50*	*4.70*	*4.50*	*1.50*	*4.50*	*1.50*
type	2	2	2	2	2	2	2
Major elements							
SiO_2 (wt. %)	45.46	46.00	46.20	46.15	44.68	46.02	44.38
TiO_2	3.88	3.66	4.04	4.10	3.54	3.52	3.01
Al_2O_3	14.11	12.62	12.29	15.15	10.15	13.11	11.85
Fe_2O_3	4.14	2.82	4.05	5.02	3.36	4.07	3.47
FeO	8.04	9.21	7.63	7.32	9.65	7.67	9.01
MnO	0.18	0.17	0.17	0.18	0.19	0.17	0.19
MgO	6.81	9.93	8.94	5.76	13.42	7.47	11.87
CaO	9.29	9.95	9.67	10.48	10.73	11.74	10.85
Na_2O	3.22	2.79	2.37	3.22	2.07	2.19	3.07
K_2O	2.45	1.80	2.77	1.85	1.33	1.37	1.20
P_2O_5	1.22	0.81	0.96	0.85	0.57	0.73	0.64
H_2O^+	1.53	0.71	1.24	1.07	0.55	2.46	0.61
Total	100.3	100.5	100.3	101.1	100.2	100.5	100.1
Fe_2O_3T	13.06	13.04	12.52	13.15	14.07	12.59	13.47
Cr_2O_3 (µg/g)	204	588	551	109	1062	369	560
NiO	131	305	223	87.5	447	151	377
CIPW norm							
Quartz							
Orthoclase	14.47	10.65	16.35	10.91	7.88	8.10	7.10
Albite	20.57	17.90	18.05	22.98	12.68	18.49	11.34
Anorthite	16.82	16.59	14.74	21.44	14.46	21.92	15.02
Nepheline	3.60	3.08	1.08	2.30	2.62		7.92
Diopside	17.04	22.11	21.43	19.90	28.05	25.25	27.78
Hypersthene						5.66	
Olivine	10.11	16.54	11.72	5.56	21.13	4.40	18.21
Magnetite	6.00	4.09	5.87	7.28	4.87	5.91	5.03
Ilmenite	7.38	6.96	7.68	7.78	6.72	6.68	5.71
Apatite	2.84	1.88	2.23	1.96	1.32	1.69	1.47
Leucite							
CaDiSilicate							
Wollastonite							
Hematite							
Titanite							
Total	98.8	99.8	99.1	100.1	99.7	98.1	99.6

Table 4 | *(continued)*

unit	Saô Tomé	Saô Tomé	Saô Tomé	Saô Tomé	Saô Tomé	Saô Tomé	Saô Tomé
sample name	ST01	ST02	ST04	ST05	ST16	ST17	ST20
locality	Palmar	Boa Morte	Diogo Nunes	Diogo Nunes	Annobon	Annobon	Trindade
age (Ma)	*3.00*	*3.00*	*3.00*	*3.00*	*3.00*	*3.00*	*1.38*
type	1	1	1	1	1	1	1
Major elements							
SiO_2 (wt. %)	40.84	41.14	43.33	43.57	44.73	45.19	43.62
TiO_2	4.24	4.24	3.57	3.35	3.42	3.45	3.37
Al_2O_3	12.03	12.10	13.18	12.70	15.53	15.89	12.45
Fe_2O_3	4.29	4.34	4.20	3.57	6.31	4.00	3.96
FeO	8.80	9.15	8.42	9.02	4.95	7.29	8.32
MnO	0.19	0.19	0.18	0.18	0.18	0.18	0.17
MgO	10.67	11.12	8.38	9.88	5.25	5.26	11.06
CaO	11.75	11.09	12.38	11.65	9.50	8.77	10.76
Na_2O	3.30	3.01	3.44	3.43	4.67	5.47	3.71
K_2O	1.38	1.83	1.28	1.19	2.13	2.63	1.58
P_2O_5	1.10	1.05	1.16	1.06	1.42	1.40	0.86
H_2O^+	1.85	1.17	1.03	0.80	1.92	0.70	0.58
Total	100.4	100.4	100.5	100.4	100.0	100.2	100.5
Fe_2O_3T	14.05	14.49	13.54	13.59	11.81	12.09	13.19
Cr_2O_3 (µg/g)	572	563	309	383	102	141	452
NiO	315	304	164	263	67.0	69.7	317
CIPW norm							
Quartz							
Orthoclase	8.14	10.82	7.54	7.03	12.60	15.52	9.36
Albite	3.92	3.01	10.51	10.68	21.19	15.72	8.15
Anorthite	13.93	14.07	16.76	15.71	15.12	11.07	12.64
Nepheline	13.00	12.18	10.07	9.96	9.94	16.55	12.59
Diopside	29.61	27.17	29.68	28.24	17.72	18.76	28.02
Hypersthene							
Olivine	13.21	15.27	9.43	14.03	3.42	6.36	15.02
Magnetite	6.21	6.29	6.09	5.18	6.62	5.80	5.74
Ilmenite	8.05	8.06	6.79	6.37	6.50	6.56	6.41
Apatite	2.56	2.44	2.70	2.45	3.30	3.24	2.00
Leucite							
CaDiSilicate							
Wollastonite							
Hematite					1.75		
Titanite							
Total	98.6	99.3	99.6	99.7	98.2	99.6	99.9

Table 4 | *(continued)*

unit	Saô Tomé	Saô Tomé	Saô Tomé	Saô Tomé	Saô Tomé	Saô Tomé	Saô Tomé
sample name	ST23E*	ST24*	ST26*	ST27*	ST35	ST03	ST06*
locality	Praia das Pombas	Praia das Pombas	Praia das Pombas	Praia das Pombas	Rio Caue	Diogo Nunes	Milla Grosa
age (Ma)	*3.00*	*3.00*	*3.00*	*3.00*	*3.00*	*0.17*	*3.00*
type	1	1	1	1	1	2	2
Major elements							
SiO_2 (wt. %)	42.51	44.48	44.46	42.49	42.12	45.11	46.49
TiO_2	2.98	3.07	3.12	3.00	4.07	3.16	3.49
Al_2O_3	11.52	11.79	13.22	11.51	12.09	13.12	15.70
Fe_2O_3	3.21	2.68	4.93	3.51	4.22	3.58	4.83
FeO	8.69	9.54	7.23	8.11	8.97	8.72	6.05
MnO	0.17	0.17	0.18	0.17	0.19	0.18	0.18
MgO	11.13	11.95	9.74	9.02	10.96	9.99	4.32
CaO	10.78	10.35	10.47	11.79	10.93	10.12	8.99
Na_2O	2.55	2.70	3.88	2.49	2.97	3.63	4.79
K_2O	0.90	0.92	1.45	0.79	1.31	1.31	2.42
P_2O_5	0.66	0.68	0.88	0.68	1.14	0.79	1.06
H_2O^+	4.38	2.02	0.95	6.66	1.43	0.60	2.22
Total	99.5	100.4	100.5	100.2	100.4	100.3	100.5
Fe_2O_3T	12.86	13.26	12.96	12.51	14.18	13.26	11.54
Cr_2O_3 (µg/g)	549	586	389	582	598	402	36.5
NiO	333	376	268	359	290	277	27.8
CIPW norm							
Quartz							
Orthoclase	5.32	5.44	8.58	4.64	7.74	7.76	14.28
Albite	13.18	16.05	14.46	14.85	10.47	16.28	23.16
Anorthite	17.33	17.32	14.40	17.92	15.77	15.63	14.18
Nepheline	4.54	3.69	9.94	3.37	7.96	7.83	9.43
Diopside	25.55	23.75	25.21	29.01	24.75	23.60	18.59
Hypersthene							
Olivine	17.39	20.83	11.91	11.46	15.84	15.63	2.63
Magnetite	4.66	3.88	7.15	5.09	6.12	5.19	7.00
Ilmenite	5.66	5.83	5.92	5.69	7.72	6.00	6.63
Apatite	1.52	1.58	2.05	1.56	2.63	1.84	2.47
Leucite							
CaDiSilicate							
Wollastonite							
Hematite							
Titanite							
Total	95.1	98.4	99.6	93.6	99.0	99.8	98.4

Table 4 | *(continued)*

unit	Saô Tomé	Saô Tomé	Saô Tomé	Saô Tomé	Saô Tomé	Saô Tomé	Saô Tomé
sample name	ST08*	ST09	ST10	ST11	ST13*	ST14	ST21
locality	Santa Adelaida	Milla Grosa	Ribera funda	River Provez	River Provez	River Provez	Trindade
age (Ma)	*3.00*	*2.12*	*3.00*	*3.00*	*3.00*	*3.00*	*3.00*
type	2	2	2	2	2	2	2
Major elements							
SiO_2 (wt. %)	41.85	41.39	45.79	41.29	44.35	49.19	47.59
TiO_2	3.69	3.99	3.68	5.04	3.92	2.66	3.14
Al_2O_3	11.33	11.91	14.78	14.58	14.93	17.10	16.40
Fe_2O_3	6.00	3.81	4.79	7.00	5.65	4.39	4.03
FeO	7.67	9.54	7.22	7.08	6.54	4.85	6.50
MnO	0.19	0.19	0.17	0.19	0.19	0.18	0.17
MgO	11.83	11.79	6.29	6.74	5.96	3.21	4.55
CaO	10.77	11.13	11.59	11.81	11.29	7.35	8.10
Na_2O	2.91	3.05	3.20	2.99	3.20	6.13	5.59
K_2O	0.76	1.71	1.19	1.06	1.56	3.15	2.54
P_2O_5	0.97	0.87	0.78	0.90	0.74	0.75	1.01
H_2O^+	2.17	0.95	1.01	1.47	1.67	1.02	0.78
Total	100.1	100.3	100.5	100.1	100.0	100.0	100.4
Fe_2O_3T	14.52	14.39	12.80	14.86	12.91	9.77	11.25
Cr_2O_3 (µg/g)	589	565	238	115	177	7.60	51.5
NiO	374	330	103	78.7	92.9	15.30	51.1
CIPW norm							
Quartz							
Orthoclase	4.52	10.11	7.05	6.26	9.21	18.63	14.99
Albite	14.74	1.66	22.06	14.93	18.60	24.59	23.14
Anorthite	15.59	13.78	22.46	23.21	21.80	9.84	12.14
Nepheline	5.37	13.07	2.72	5.63	4.58	14.78	13.11
Diopside	24.85	28.58	23.89	22.98	23.13	17.22	17.18
Hypersthene							
Olivine	15.01	17.11	5.64	4.31	3.71	0.78	4.93
Magnetite	8.70	5.52	6.94	8.83	8.20	6.37	5.85
Ilmenite	7.00	7.58	6.99	9.57	7.45	5.06	5.96
Apatite	2.25	2.02	1.80	2.10	1.71	1.73	2.35
Leucite							
CaDiSilicate							
Wollastonite							
Hematite				0.91			
Titanite							
Total	98.0	99.4	99.5	98.7	98.4	99.0	99.7

Table 4 | *(continued)*

unit	Saô Tomé	Saô Tomé	Saô Tomé	Saô Tomé	Saô Tomé	Principe	Principe
sample name	ST29	ST30*	ST31	ST34	ST36	PP01	PP03
locality	Praia Morrao	Aqua Joao	Aqua Joao	Rio Caue	Rio Caue	Porto Real	Okiponte
age (Ma)	*3.00*	*3.00*	*3.00*	*3.00*	*5.20*	*5.50*	*5.50*
type	2	2	2	2	2	1	1
Major elements							
SiO_2 (wt. %)	45.79	42.24	42.23	51.06	43.48	43.29	43.09
TiO_2	3.29	4.71	4.78	2.24	3.12	3.08	3.65
Al_2O_3	13.89	14.76	14.77	18.68	10.46	13.26	13.31
Fe_2O_3	3.70	5.77	4.89	2.00	3.62	4.27	4.33
FeO	8.39	7.61	8.64	4.57	9.18	7.77	6.98
MnO	0.17	0.19	0.19	0.15	0.17	0.19	0.18
MgO	9.20	6.16	6.08	2.27	12.68	8.44	7.70
CaO	10.06	11.38	11.42	5.34	12.77	10.31	13.62
Na_2O	2.61	3.58	3.30	6.48	1.86	3.79	3.40
K_2O	1.14	0.81	1.34	4.10	0.98	1.76	1.54
P_2O_5	0.73	0.99	1.00	0.70	0.40	0.99	0.74
H_2O^+	1.47	2.02	1.81	2.66	1.78	2.67	2.00
Total	100.4	100.2	100.5	100.3	100.5	99.8	100.5
Fe_2O_3T	13.01	14.22	14.49	7.08	13.81	12.90	12.07
Cr_2O_3 (µg/g)	392	58.4	56.9	BDL	1050	355	186
NiO	225	48.9	49.6	3.0	343	193	108
CIPW norm							
Quartz							
Orthoclase	6.75	4.80	7.95	24.22	5.76	10.41	9.08
Albite	22.09	18.88	14.41	26.60	6.73	12.13	4.32
Anorthite	22.80	21.83	21.49	9.75	17.29	13.98	16.51
Nepheline		6.17	7.34	15.31	4.90	10.78	13.24
Diopside	17.89	22.22	22.91	9.94	34.75	24.57	36.67
Hypersthene	2.29						
Olivine	13.87	4.74	6.10	3.02	17.25	10.97	3.86
Magnetite	5.36	8.36	7.10	2.90	5.25	6.20	6.27
Ilmenite	6.24	8.95	9.07	4.25	5.93	5.85	6.93
Apatite	1.69	2.29	2.31	1.62	0.94	2.28	1.73
Leucite							
CaDiSilicate							
Wollastonite							
Hematite							
Titanite							
Total	99.0	98.3	98.7	97.6	98.8	97.2	98.6

Table 4 | *(continued)*

unit	Principe	Principe	Principe	Principe	Principe	Principe	Principe
sample name	PP04	PP07	PP10	PP23	PP24	PP26	PP05
locality	Principe	Campanha	Ponte Banana	Lapa	Praia Sundy	Santo Antonio	Bom Bom Is
age (Ma)	*5.50*	*5.85*	*5.50*	*5.80*	*5.50*	*6.53*	*5.50*
type	1	1	1	1	1	1	2
Major elements							
SiO_2 (wt. %)	42.65	41.07	41.89	39.47	41.99	37.78	44.01
TiO_2	3.32	2.77	3.47	4.69	3.20	4.00	4.65
Al_2O_3	10.74	11.49	13.10	12.45	11.45	11.05	14.72
Fe_2O_3	3.75	3.84	5.43	5.62	4.21	4.88	6.67
FeO	8.11	7.78	7.78	9.26	8.24	7.89	7.10
MnO	0.17	0.18	0.21	0.24	0.18	0.20	0.19
MgO	12.14	13.30	8.41	7.19	11.95	12.04	5.59
CaO	14.10	11.33	10.18	12.68	12.43	14.30	10.15
Na_2O	2.12	3.69	3.65	3.49	2.66	2.65	3.09
K_2O	0.98	0.81	2.29	1.55	1.15	1.75	0.93
P_2O_5	0.68	1.28	1.20	1.31	0.83	1.32	0.71
H_2O^+	1.68	2.41	2.26	2.31	2.16	2.59	2.07
Total	100.4	99.9	99.9	100.3	100.4	100.5	99.9
Fe_2O_3T	12.75	12.48	14.06	15.90	13.36	13.63	14.56
Cr_2O_3 (µg/g)	733	817	216	84.0	610	543	50.2
NiO	286	456	149	55.9	301	253	36.1
CIPW norm							
Quartz							
Orthoclase	5.82	4.77	13.55	9.16	6.81		5.51
Albite	2.58	5.46	7.79	2.50	4.47		26.14
Anorthite	16.88	12.41	12.59	13.72	15.90	13.11	23.54
Nepheline	8.31	13.94	12.49	14.65	9.76	12.15	
Diopside	38.68	28.21	23.94	32.54	32.15	26.62	17.32
Hypersthene							3.05
Olivine	13.22	19.01	10.04	5.35	15.15	15.40	2.14
Magnetite	5.43	5.57	7.87	8.16	6.11	7.07	9.68
Ilmenite	6.30	5.26	6.59	8.91	6.08	7.60	8.83
Apatite	1.58	2.96	2.78	3.03	1.91	3.07	1.64
Leucite						8.09	
CaDiSilicate						4.81	
Wollastonite							
Hematite							
Titanite							
Total	98.8	97.6	97.6	98.0	98.3	97.9	97.9

Table 4 | *(continued)*

unit	Principe	Principe	Principe	Principe	Principe	Principe	Principe
sample name	PP09	PP11	PP013*	PP18	PP19*	PP20	PP21
locality	Ponte Banana	Praia Seca	Praia Seca	Praia Abelha	Lapa	Lapa	Lapa
age (Ma)	*5.50*	*5.50*	*5.50*	*5.50*	*5.50*	*5.50*	*5.50*
type	2	2	2	2	2	2	2
Major elements							
SiO_2 (wt. %)	44.98	48.61	43.75	44.55	41.53	46.76	42.49
TiO_2	2.82	2.07	2.73	3.06	2.99	2.40	4.21
Al_2O_3	11.48	15.89	15.94	13.14	12.04	13.25	12.27
Fe_2O_3	4.90	3.76	5.69	4.06	5.45	3.61	4.84
FeO	8.20	4.78	4.22	7.21	6.35	7.04	6.08
MnO	0.17	0.16	0.16	0.16	0.19	0.17	0.16
MgO	10.86	6.14	7.30	9.75	10.89	9.57	8.84
CaO	11.40	7.31	7.90	11.18	11.54	9.35	15.98
Na_2O	1.95	5.02	5.94	2.64	3.72	3.32	2.14
K_2O	0.72	2.95	1.60	1.34	1.22	1.65	0.84
P_2O_5	0.40	0.56	0.75	0.65	1.04	0.54	0.61
H_2O^+	1.87	1.88	4.95	2.15	2.73	2.15	2.02
Total	99.7	99.1	100.9	99.9	99.7	99.8	100.5
Fe_2O_3T	14.00	9.07	10.38	12.06	12.50	11.42	11.59
Cr_2O_3 (µg/g)	689	259	268	416	572	528	139
NiO	267	157	179	203	268	278	102
CIPW norm							
Quartz							
Orthoclase	4.26	17.42	9.46	7.92	7.22	9.72	4.96
Albite	16.50	23.04	17.99	15.47	7.04	21.41	3.72
Anorthite	20.44	12.12	12.09	20.04	12.55	16.39	21.41
Nepheline		10.53	17.48	3.74	13.24	3.62	7.78
Diopside	26.75	16.26	17.33	24.83	29.87	21.14	42.17
Hypersthene	5.50						
Olivine	11.09	7.23	7.11	12.60	11.11	14.37	2.08
Magnetite	7.10	5.46	6.19	5.88	7.90	5.23	7.02
Ilmenite	5.36	3.93	5.19	5.82	5.67	4.56	7.99
Apatite	0.92	1.29	1.73	1.50	2.40	1.24	1.40
Leucite							
CaDiSilicate							
Wollastonite							
Hematite			1.42				
Titanite							
Total	97.9	97.3	96.0	97.8	97.0	97.7	98.5

Table 4 | *(continued)*

unit	Principe	Bioko	Bioko	Bioko	Bioko	Bioko	Bioko
sample name	PP25	BK02	BK04	BK06	BK07	BK08	BK12
locality	Santo Antonio	Baney	Ruiche	Luba	B. Cristol	B. Cristol	Luba-Batete
age (Ma)	*5.50*	*0.14*	*1.00*	*0.17*	*0.82*	*1.00*	*1.00*
type	2	1	1	1	1	1	1
Major elements							
SiO_2 (wt. %)	44.37	46.33	45.05	46.49	45.51	46.70	45.59
TiO_2	3.24	2.98	3.00	2.93	3.86	3.62	3.72
Al_2O_3	13.57	12.70	12.15	13.39	12.91	13.92	14.37
Fe_2O_3	3.12	3.57	5.75	2.34	3.62	2.64	3.90
FeO	8.16	8.60	6.20	10.53	8.68	9.17	8.50
MnO	0.16	0.17	0.18	0.19	0.16	0.18	0.19
MgO	8.70	9.93	11.41	9.61	8.95	7.61	6.62
CaO	11.01	10.49	11.18	10.02	9.97	10.78	10.59
Na_2O	3.63	3.01	2.73	2.91	3.73	3.09	3.25
K_2O	1.51	0.88	1.22	1.00	1.49	1.49	1.75
P_2O_5	0.73	0.87	0.55	0.59	1.05	0.68	0.83
H_2O^+	1.74	0.73	0.80	0.54	0.63	0.57	1.02
Total	100.0	100.3	100.2	100.5	100.6	100.4	100.3
Fe_2O_3T	12.18	13.12	12.63	14.02	13.26	12.81	13.33
Cr_2O_3 (µg/g)	414	473	847	263	477	427	191
NiO	187	329	418	269	235	186	152
CIPW norm							
Quartz							
Orthoclase	8.95	5.21	7.23	5.93	8.79	8.79	10.34
Albite	11.95	23.57	16.22	21.45	19.64	20.25	19.19
Anorthite	16.25	18.52	17.27	20.51	14.08	19.74	19.44
Nepheline	10.17	1.05	3.74	1.72	6.47	3.17	4.51
Diopside	26.97	22.38	27.20	20.59	22.89	23.72	22.27
Hypersthene							
Olivine	11.60	15.99	12.51	19.51	13.10	11.95	8.94
Magnetite	4.53	5.18	8.33	3.39	5.25	3.82	5.65
Ilmenite	6.15	5.67	5.69	5.56	7.33	6.88	7.06
Apatite	1.70	2.01	1.27	1.38	2.42	1.58	1.93
Leucite							
CaDiSilicate							
Wollastonite							
Hematite							
Titanite							
Total	98.3	99.58	99.45	100.03	99.98	99.90	99.34

Table 4 | *(continued)*

unit	Bioko	Bioko	Bioko	Bioko	Bioko	Bioko	Bioko
sample name	BK14	BK15	BK16	BK17	BK18	BK19	BK21
locality	Batete	Moca	Moca	Pico Basile	Pico Basile	Mt Basile	Barioba
age (Ma)	*1.00*	*0.05*	*1.00*	*1.00*	*1.00*	*0.32*	*1.00*
type	1	1	1	1	1	1	1
Major elements							
SiO_2 (wt. %)	44.46	47.24	45.79	42.91	42.86	44.83	47.38
TiO_2	3.48	2.88	3.57	3.34	3.33	3.56	3.54
Al_2O_3	14.05	16.24	15.86	11.68	11.68	11.86	15.53
Fe_2O_3	4.49	5.55	5.98	3.44	3.35	3.14	3.58
FeO	8.17	6.80	7.00	9.63	9.70	9.19	7.12
MnO	0.19	0.26	0.24	0.19	0.19	0.17	0.17
MgO	8.54	3.63	4.28	11.66	11.69	11.57	5.47
CaO	11.31	8.61	9.16	10.94	10.89	10.13	9.49
Na_2O	3.19	4.27	4.56	3.47	3.49	2.72	4.17
K_2O	1.41	2.33	2.04	1.41	1.41	1.16	2.07
P_2O_5	0.57	1.16	0.93	1.16	1.18	0.82	0.92
H_2O^+	0.67	1.26	0.86	0.62	0.58	1.03	0.91
Total	100.5	100.2	100.3	100.4	100.3	100.2	100.4
Fe_2O_3T	13.56	13.09	13.75	14.13	14.12	13.34	11.49
Cr_2O_3 (µg/g)	456	2	11	662	684	699	201
NiO	199	4	7	372	381	441	87.6
CIPW norm							
Quartz							
Orthoclase	8.35	13.74	12.07	8.31	8.35	6.84	12.22
Albite	13.18	28.75	23.58	7.62	7.43	17.81	24.12
Anorthite	19.85	18.29	16.76	12.15	12.03	16.73	17.53
Nepheline	7.47	3.98	8.15	11.77	11.97	2.81	6.07
Diopside	26.02	13.59	18.01	27.68	27.56	22.57	18.89
Hypersthene							
Olivine	10.58	4.42	3.27	18.31	18.56	19.21	6.59
Magnetite	6.52	8.04	8.67	4.99	4.86	4.56	5.19
Ilmenite	6.62	5.46	6.79	6.34	6.32	6.76	6.73
Apatite	1.32	2.69	2.16	2.70	2.72	1.90	2.14
Leucite							
CaDiSilicate							
Wollastonite							
Hematite							
Titanite							
Total	99.92	98.98	99.46	99.86	99.80	99.18	99.49

Table 4 | *(continued)*

unit	Bioko	Bioko	Bioko	Bioko	Bioko	Bioko	Bioko
sample name	BK23	BK03	BK09	BK10	BK11	BK13	BK20
locality	Riaba	Bao Basoala	B. Cristol	B. Cristol	Luba	Luba-Batete	Bososo
age (Ma)	*1.00*	*1*	*1.00*	*0.15*	*1.00*	*1.00*	*1.00*
type	1	2	2	2	2	2	2
Major elements							
SiO_2 (wt. %)	47.04	45.74	45.70	45.93	47.16	43.61	45.19
TiO_2	3.08	3.71	3.99	3.07	2.63	3.52	3.39
Al_2O_3	12.03	12.59	12.39	11.72	10.47	13.41	12.28
Fe_2O_3	3.37	2.48	2.51	3.16	2.74	3.46	3.76
FeO	7.73	10.13	10.15	9.30	8.93	9.47	9.22
MnO	0.17	0.17	0.18	0.17	0.16	0.19	0.17
MgO	10.81	10.11	9.31	11.52	13.05	9.47	10.99
CaO	11.22	9.83	11.43	10.44	10.43	11.81	9.98
Na_2O	2.40	3.11	2.74	3.13	2.09	2.52	2.57
K_2O	1.10	1.17	1.12	1.07	0.97	1.42	1.06
P_2O_5	0.50	0.72	0.59	0.51	0.38	0.50	0.52
H_2O^+	0.85	0.62	0.54	0.53	1.45	1.33	1.24
Total	100.3	100.4	100.6	100.5	100.4	100.7	100.4
Fe_2O_3T	11.95	13.72	13.78	13.49	12.65	13.98	13.99
Cr_2O_3 (µg/g)	1183	545	595	776	1097	573	584
NiO	349	316	253	348	448	233	348
CIPW norm							
Quartz							
Orthoclase	6.51	6.94	6.63	6.30	5.74	8.40	6.27
Albite	20.32	19.93	16.84	16.77	17.68	8.62	19.71
Anorthite	18.79	16.95	18.18	14.78	16.31	21.06	18.86
Nepheline		3.45	3.44	5.25		6.90	1.08
Diopside	26.82	21.90	28.03	27.04	26.39	27.61	21.87
Hypersthene	0.96				5.48		
Olivine	14.21	18.32	14.44	18.31	17.59	13.98	18.28
Magnetite	4.89	3.59	3.64	4.59	3.97	5.02	5.44
Ilmenite	5.85	7.04	7.58	5.83	5.00	6.69	6.45
Apatite	1.15	1.67	1.37	1.19	0.88	1.15	1.19
Leucite							
CaDiSilicate							
Wollastonite							
Hematite							
Titanite							
Total	99.50	99.79	100.15	100.06	99.04	99.43	99.16

Table 4 | *(continued)*

unit	Bioko	Etinde	Etinde	Etinde	Etinde	Etinde
sample name	BK22	2208A	2208B	2208C	2208D	CA062
locality	Bakake	Mt Etinde	Mt Etinde	Mt Etinde	Mt Etinde	Batoke
age (Ma)	*1.33*	*0.27*	*0.50*	*0.50*	*0.50*	*0.43*
type	2	1	1	1	1	1
Major elements						
SiO_2 (wt. %)	45.97	40.37	39.34	41.46	39.49	40.29
TiO_2	3.90	3.61	4.17	3.79	4.05	3.71
Al_2O_3	13.13	16.29	14.25	15.81	14.55	16.12
Fe_2O_3	3.76	5.50	6.61	5.79	5.79	5.68
FeO	8.92	6.11	5.40	5.03	5.66	5.94
MnO	0.19	0.29	0.32	0.34	0.33	0.28
MgO	7.63	4.21	4.99	3.82	4.75	4.55
CaO	11.41	11.61	13.84	12.29	13.96	11.85
Na_2O	2.82	4.86	4.54	3.22	4.57	4.33
K_2O	1.35	3.63	2.81	2.12	3.22	3.30
P_2O_5	0.56	1.31	1.36	1.14	1.33	1.25
H_2O^+	0.48	2.07	2.37	4.72	2.47	2.03
Total	100.1	99.8	100.0	99.5	100.2	99.3
Fe_2O_3T	13.66	12.27	12.60	11.37	12.07	12.26
Cr_2O_3 (μg/g)	515	27	63	32	56	31
NiO	176	18	26	14	22	21
CIPW norm						
Quartz						
Orthoclase	7.98	7.78	3.83	12.54	0.77	10.56
Albite	19.21			10.90		
Anorthite	19.19	11.90	10.21	22.41	9.64	14.83
Nepheline	2.52	22.28	20.79	8.86	20.96	19.83
Diopside	27.14	24.99	26.85	20.58	25.57	25.65
Hypersthene						
Olivine	9.49					
Magnetite	5.45	7.97	6.36	6.34	7.56	8.23
Ilmenite	7.42	6.86	7.91	7.20	7.69	7.04
Apatite	1.31	3.04	3.16	2.64	3.09	2.90
Leucite		10.73	10.03		14.33	7.00
CaDiSilicate						
Wollastonite		2.28	6.31	1.97	7.56	1.30
Hematite			2.22	1.42	0.58	
Titanite						
Total	99.69	97.83	97.68	94.86	97.76	97.34

*: Slightly altered sample which contain secondary minerals.; n.d.: no data.; The CIPW norm calculation scheme is after Kelsey (1965) and calculated using Excel spread sheet distributed by Jake Lowenstern (https://volcanoes.usgs.gov/observatories/yvo/jlowenstern/other/NormCalc_JBL.xls). The CIPW normative composition of AN10-3 was calculated at $Fe_2O_3/Fe_2O_3T = 0.3$.; See footnote of Table 5 for the definition of Type 1 and Type 2.

Table 5 | Trace element compositions of mafic CVL samples (μg/g)

unit	Annobon	Annobon	Annobon	Annobon	Annobon	Annobon	Annobon
sample name	AN01	AN02	AN08	AN16	AN22	AN23	AN24
locality	San Antonio	San Antonio	Ridge	San Antonio	San Antonio	San Antonio	San Antonio
age (Ma)	*0.20*	*1.50*	*1.50*	*1.50*	*1.63*	*1.50*	*1.50*
type	1	1	1	1	1	1	1
Li	5.73	5.94	6.64	6.50	5.90	6.01	6.55
Be	1.56	1.56	1.84	1.66	1.54	1.66	1.83
B	2.30	1.93	2.31	1.89	1.63	1.90	1.66
Rb	35.7	31.1	29.2	27.5	28.5	34.1	16.6
Sr	766	783	937	928	810	814	1041
Y	27.0	27.6	28.5	29.0	26.2	28.1	30.3
Zr	240	232	278	269	237	249	279
Nb	55.8	54.9	63.2	60.6	52.7	56.6	62.4
Cs	0.391	0.368	0.275	0.382	0.376	0.486	0.431
Ba	453	466	505	555	477	490	544
Hf	5.51	5.44	6.27	6.06	5.48	5.75	6.34
Ta	3.06	3.05	3.46	3.11	2.92	3.11	3.36
La	40.2	41.6	46.4	53.0	41.6	43.1	51.0
Ce	80.9	84.6	93.7	105	79.3	86.9	98.0
Pr	10.3	10.8	12.1	13.6	10.4	11.0	12.7
Nd	44.5	45.9	52.3	58.9	45.8	48.6	54.3
Sm	9.46	9.67	10.7	11.7	9.44	10.0	11.2
Eu	2.95	3.04	3.33	3.66	2.99	3.11	3.54
Gd	9.34	9.65	10.3	11.5	9.53	10.1	11.0
Tb	1.24	1.30	1.38	1.47	1.24	1.32	1.44
Dy	6.67	6.84	7.24	7.47	6.58	6.93	7.56
Ho	1.13	1.17	1.21	1.26	1.13	1.19	1.29
Er	2.76	2.79	2.87	2.94	2.66	2.86	3.04
Tm	0.336	0.338	0.348	0.348	0.325	0.346	0.361
Yb	1.89	1.98	2.00	1.96	1.91	2.00	2.10
Lu	0.261	0.268	0.271	0.268	0.255	0.276	0.283
Pb	2.09	2.24	2.45	2.90	2.08	2.36	2.61
Th	4.79	4.83	5.52	5.72	4.30	5.04	5.93
U	1.23	1.31	1.31	1.42	1.28	1.28	1.42
$(Hf/Sm)_N$	0.83	0.81	0.84	0.74	0.83	0.83	0.81
$(Ti/Gd)_N$	0.99	0.93	0.82	0.73	0.92	0.87	0.76

Table 5 | *(continued)*

unit	Annobon	Annobon	Annobon	Annobon	Annobon	Annobon	Annobon
sample name	AN04-3	AN05	AN06	AN07	AN10-3	AN11	AN12
locality	Lake Masafin	Lake Masafin	Lake Masafin	Lake	Santa Cruz	Santa Cruz	San Antonio
age (Ma)	*4.50*	*1.50*	*4.50*	*1.50*	*1.50*	*1.50*	*4.50*
type	2	2	2	2	2	2	2
Li	6.19	4.31	7.46	5.56	5.94	5.42	5.94
Be	2.22	1.11	2.21	1.59	1.87	1.63	1.82
B	1.57	1.45	2.47	2.08	1.10	2.01	0.97
Rb	58.5	26.7	46.2	36.2	34.7	29.9	33.4
Sr	974	481	932	782	830	756	830
Y	31.7	18.7	31.1	27.3	31.7	25.5	27.8
Zr	501	199	409	221	367	320	387
Nb	51.1	31.6	64.2	54.7	52.0	46.5	54.7
Cs	2.35	0.287	0.383	0.388	0.210	0.383	0.264
Ba	706	336	629	460	593	484	483
Hf	11.8	5.10	9.61	5.45	9.00	7.56	8.89
Ta	3.00	1.79	3.55	3.02	2.97	2.68	3.14
La	57.2	27.2	53.7	39.9	46.6	39.3	44.9
Ce	119	55.8	107.2	80.3	103	84.7	94.9
Pr	16.0	7.39	14.1	10.3	13.9	11.2	12.5
Nd	69.4	32.6	61.1	44.9	60.9	49.5	54.2
Sm	13.1	6.65	12.1	9.54	12.1	9.83	10.9
Eu	3.85	2.06	3.74	3.03	3.70	2.94	3.36
Gd	11.9	6.47	11.6	9.61	11.3	9.26	10.4
Tb	1.53	0.870	1.50	1.27	1.51	1.22	1.34
Dy	7.92	4.64	7.74	6.75	7.80	6.45	6.92
Ho	1.36	0.797	1.35	1.16	1.35	1.13	1.19
Er	3.27	1.96	3.28	2.74	3.26	2.72	2.77
Tm	0.406	0.243	0.395	0.342	0.401	0.332	0.337
Yb	2.43	1.42	2.38	1.94	2.37	1.92	2.00
Lu	0.334	0.200	0.331	0.266	0.327	0.268	0.268
Pb	4.33	1.68	3.27	2.11	3.06	2.60	2.96
Th	4.78	2.71	5.48	4.58	4.21	4.05	4.61
U	1.14	0.714	1.47	1.14	1.23	1.09	1.39
$(Hf/Sm)_N$	1.29	1.10	1.14	0.82	1.06	1.10	1.17
$(Ti/Gd)_N$	1.03	1.12	0.99	1.03	1.11	1.24	0.95

Table 5 | *(continued)*

unit	Annobon	Annobon	Annobon	Annobon	Annobon	Annobon	Annobon
sample name	AN13	AN14	AN15	AN17	AN18	AN19	AN20
locality	San Antonio	River Dashim	River Dashim	San Pedro	San Pedro	San Pedro	Tortuga
age (Ma)	*4.50*	*4.50*	*4.70*	*4.50*	*1.50*	*4.50*	*1.50*
type	2	2	2	2	2	2	2
Li	7.34	6.31	6.26	6.85	5.02	4.61	5.84
Be	2.45	1.84	2.69	1.92	1.40	1.34	1.31
B	1.34	0.98	1.98	2.06	1.82	2.10	2.59
Rb	46.3	36.3	42.9	39.2	26.3	27.8	24.8
Sr	1003	844	939	867	604	659	649
Y	34.4	28.1	30.6	30.2	24.5	25.0	22.6
Zr	491	349	543	350	302	254	189
Nb	65.8	48.4	53.0	61.1	39.3	40.9	42.2
Cs	0.586	0.271	0.424	0.363	0.241	0.369	0.262
Ba	686	484	676	600	423	372	389
Hf	11.5	8.41	12.9	7.92	7.19	6.17	4.66
Ta	3.82	2.93	3.02	3.47	2.29	2.26	2.41
La	62.5	45.3	64.6	49.6	35.9	34.4	29.5
Ce	134	95.5	129	97.6	75.7	72.9	61.3
Pr	17.5	12.6	17.2	12.8	10.2	9.79	7.68
Nd	75.1	55.0	72.3	55.3	45.0	44.0	34.4
Sm	14.5	11.1	13.3	11.1	9.25	9.08	7.58
Eu	4.26	3.35	3.81	3.42	2.87	2.83	2.48
Gd	13.2	10.4	11.9	10.7	9.14	8.95	7.77
Tb	1.69	1.35	1.45	1.38	1.17	1.18	1.04
Dy	8.76	7.03	7.47	7.42	6.07	6.15	5.53
Ho	1.48	1.19	1.28	1.30	1.06	1.06	0.962
Er	3.52	2.84	3.05	3.15	2.52	2.54	2.29
Tm	0.427	0.342	0.376	0.395	0.308	0.314	0.282
Yb	2.49	1.99	2.20	2.30	1.80	1.84	1.63
Lu	0.339	0.278	0.311	0.324	0.252	0.252	0.223
Pb	4.44	3.01	5.13	2.91	2.29	1.96	1.57
Th	6.27	4.67	5.58	5.46	3.43	3.20	3.21
U	1.66	1.81	1.42	1.44	0.921	0.901	0.966
$(Hf/Sm)_N$	1.13	1.08	1.40	1.03	1.12	0.97	0.88
$(Ti/Gd)_N$	0.80	0.95	0.92	1.04	1.05	1.06	1.05

Table 5 | *(continued)*

unit	Saô Tomé	Saô Tomé	Saô Tomé	Saô Tomé	Saô Tomé	Saô Tomé	Saô Tomé
sample name	ST01	ST02	ST04	ST05	ST16	ST17	ST20
locality	Palmar	Boa Morte	Diogo Nunes	Diogo Nunes	Annobon	Annobon	Trindade
age (Ma)	*3.00*	*3.00*	*3.00*	*3.00*	*3.00*	*3.00*	*1.38*
type	1	1	1	1	1	1	1
Li	5.76	5.91	6.49	6.17	9.62	10.25	5.55
Be	1.79	1.76	1.63	1.51	3.22	3.20	1.67
B	1.90	2.01	1.48	1.45	2.49	3.10	1.52
Rb	54.4	41.3	24.8	23.3	70.3	64.9	30.3
Sr	1299	1582	1039	984	2074	1482	1010
Y	28.9	27.8	29.9	28.3	34.7	33.7	24.8
Zr	355	357	255	249	489	470	272
Nb	79.9	79.2	63.7	61.4	116	112	71.2
Cs	0.458	0.344	0.256	0.220	0.510	0.675	0.306
Ba	595	617	516	509	815	778	510
Hf	7.91	7.87	5.84	5.78	9.22	9.06	6.18
Ta	4.37	4.38	3.28	3.14	5.64	5.66	3.94
La	62.8	63.6	55.8	52.9	96.2	94.8	52.6
Ce	130	130	112	105	181	173	97.9
Pr	16.3	16.4	14.0	13.2	22.0	21.1	12.6
Nd	69.1	68.0	61.0	56.9	87.6	84.3	52.4
Sm	12.8	12.6	11.9	11.2	15.5	15.0	10.2
Eu	3.90	3.84	3.82	3.56	4.73	4.51	3.16
Gd	11.9	11.5	11.3	10.6	14.2	13.8	9.80
Tb	1.47	1.43	1.48	1.37	1.73	1.66	1.24
Dy	7.37	7.16	7.61	7.07	8.78	8.51	6.49
Ho	1.21	1.19	1.28	1.18	1.45	1.41	1.06
Er	2.81	2.75	2.97	2.74	3.35	3.31	2.49
Tm	0.336	0.327	0.352	0.331	0.409	0.407	0.299
Yb	1.90	1.87	2.02	1.89	2.36	2.32	1.66
Lu	0.262	0.254	0.273	0.252	0.316	0.316	0.227
Pb	2.58	2.57	2.48	2.26	5.13	5.18	2.42
Th	5.78	5.18	5.65	5.04	12.2	12.2	5.75
U	1.54	1.59	1.37	1.35	3.27	3.18	1.39
$(Hf/Sm)_N$	0.88	0.90	0.70	0.74	0.86	0.87	0.87
$(Ti/Gd)_N$	0.97	1.00	0.85	0.86	0.65	0.68	0.93

Table 5 | *(continued)*

unit	Saô Tomé	Saô Tomé	Saô Tomé	Saô Tomé	Saô Tomé	Saô Tomé	Saô Tomé
sample name	ST23E*	ST24*	ST26*	ST27*	ST35	ST03	ST06*
locality	Praia das Pombas	Praia das Pombas	Praia das Pombas	Praia das Pombas	Rio Caue	Diogo Nunes	Milla Grosa
age (Ma)	*3.00*	*3.00*	*3.00*	*3.00*	*3.00*	*0.17*	*3.00*
type	1	1	1	1	1	2	2
Li	3.93	4.36	8.42	4.20	6.26	6.10	9.87
Be	1.15	1.26	1.98	1.22	1.99	1.66	3.03
B	3.26	2.15	4.05	3.84	2.04	1.78	3.40
Rb	15.4	18.4	29.8	18.6	30.0	25.8	59.0
Sr	802	786	1074	895	1054	975	1197
Y	22.6	23.8	27.4	22.5	27.0	26.1	30.2
Zr	196	205	295	202	373	271	515
Nb	41.3	43.4	75.5	42.6	80.5	62.8	105.8
Cs	0.097	0.154	0.268	0.178	0.385	0.255	0.587
Ba	432	395	571	412	578	487	664
Hf	4.79	5.02	6.59	4.94	7.79	6.33	11.0
Ta	2.31	2.45	3.92	2.42	4.41	3.45	5.79
La	36.1	38.4	58.3	37.3	66.4	48.6	72.0
Ce	70.8	75.2	107	72.5	126	95.4	139
Pr	9.25	9.88	13.6	9.73	16.3	11.8	16.7
Nd	40.8	42.8	56.3	41.1	66.4	50.0	67.8
Sm	8.35	8.70	10.7	8.26	12.1	10.0	12.4
Eu	2.66	2.83	3.37	2.66	3.70	3.13	3.87
Gd	8.19	8.54	10.5	8.24	11.3	9.62	11.4
Tb	1.07	1.12	1.33	1.07	1.40	1.24	1.46
Dy	5.71	5.89	6.75	5.61	7.17	6.48	7.53
Ho	0.959	1.01	1.14	0.967	1.21	1.09	1.26
Er	2.28	2.35	2.68	2.29	2.83	2.54	2.99
Tm	0.275	0.289	0.326	0.276	0.343	0.309	0.364
Yb	1.59	1.63	1.83	1.60	1.92	1.79	2.10
Lu	0.219	0.225	0.252	0.219	0.266	0.245	0.286
Pb	1.45	1.57	2.82	1.52	3.10	2.33	4.79
Th	3.08	3.26	6.33	3.22	6.45	5.23	9.58
U	0.838	0.915	1.23	0.827	1.90	1.24	2.78
$(Hf/Sm)_N$	0.82	0.83	0.88	0.86	0.92	0.91	1.27
$(Ti/Gd)_N$	0.98	0.97	0.81	0.98	0.97	0.89	0.83

Table 5 | *(continued)*

unit	Saô Tomé	Saô Tomé	Saô Tomé	Saô Tomé	Saô Tomé	Saô Tomé	Saô Tomé
sample name	ST08*	ST09	ST10	ST11	ST13*	ST14	ST21
locality	Santa Adelaida	Milla Grosa	Ribera funda	River Provez	River Provez	River Provez	Trindade
age (Ma)	*3.00*	*2.12*	*3.00*	*3.00*	*3.00*	*3.00*	*3.00*
type	2	2	2	2	2	2	2
Li	5.41	4.66	5.41	7.85	5.00	16.39	9.68
Be	1.53	1.42	1.48	1.62	1.75	4.09	2.97
B	1.31	1.70	1.16	1.39	1.56	5.67	2.92
Rb	32.6	40.5	22.3	53.2	36.1	81.4	59.6
Sr	919	886	877	965	977	1381	1467
Y	25.9	25.2	26.6	28.3	27.8	29.8	28.6
Zr	248	261	237	295	325	560	459
Nb	62.4	67.3	51.9	70.6	70.8	120	107
Cs	0.337	0.338	0.228	0.708	0.388	0.780	0.649
Ba	483	605	405	489	469	827	803
Hf	6.03	6.32	5.61	6.93	7.19	11.8	9.61
Ta	3.57	3.81	2.82	4.01	3.94	6.08	5.97
La	47.6	51.6	38.2	49.6	49.7	76.6	77.8
Ce	100	105	80.3	97.6	98.5	141	143
Pr	13.0	13.4	10.7	13.3	13.0	17.0	17.0
Nd	54.0	55.9	46.3	57.8	55.1	65.2	67.5
Sm	10.4	10.3	9.63	11.4	10.7	11.5	12.3
Eu	3.23	3.26	3.15	3.51	3.35	3.51	3.82
Gd	9.63	9.68	9.35	10.7	10.1	10.7	11.4
Tb	1.24	1.24	1.22	1.38	1.32	1.36	1.40
Dy	6.45	6.37	6.62	7.28	6.93	7.15	7.33
Ho	1.09	1.05	1.12	1.26	1.20	1.24	1.21
Er	2.56	2.48	2.65	2.99	2.87	3.04	2.92
Tm	0.308	0.300	0.327	0.370	0.364	0.385	0.356
Yb	1.79	1.72	1.92	2.15	2.15	2.33	2.07
Lu	0.246	0.237	0.262	0.299	0.295	0.326	0.287
Pb	1.82	1.68	1.71	2.13	2.51	6.07	4.88
Th	4.09	5.12	3.69	5.12	5.62	11.5	11.0
U	1.08	1.40	0.968	1.35	1.56	3.10	2.83
$(Hf/Sm)_N$	0.83	0.88	0.84	0.87	0.96	1.48	1.12
$(Ti/Gd)_N$	1.04	1.11	1.07	1.27	1.05	0.67	0.74

Table 5 | *(continued)*

unit	Saô Tomé	Saô Tomé	Saô Tomé	Saô Tomé	Saô Tomé	Principe	Principe
sample name	ST29	ST30*	ST31	ST34	ST36	PP01	PP03
locality	Praia Morrao	Aqua Joao	Aqua Joao	Rio Caue	Rio Caue	Porto Real	Okiponte
age (Ma)	*3.00*	*3.00*	*3.00*	*3.00*	*5.20*	*5.50*	*5.50*
type	2	2	2	2	2	1	1
Li	5.23	6.19	6.15	11.80	3.57	6.93	4.72
Be	1.38	1.89	1.92	3.16	0.986	1.88	1.73
B	1.04	2.10	1.52	5.71	0.85	1.09	0.97
Rb	20.6	49.2	44.7	92.7	25.0	42.3	33.6
Sr	814	1056	1053	1309	528	1179	891
Y	24.8	28.2	27.5	28.1	19.3	26.6	27.5
Zr	238	331	338	586	174	339	288
Nb	44.0	78.5	79.4	128.2	31.6	78.6	60.2
Cs	0.115	0.470	0.456	0.882	0.225	0.422	0.197
Ba	346	592	587	1025	267	773	471
Hf	5.64	7.51	7.71	10.14	4.80	6.70	6.67
Ta	2.57	4.44	4.52	6.91	1.91	3.81	3.03
La	37.0	60.6	60.6	81.9	26.9	61.2	46.4
Ce	74.1	118	117	153	57.1	121	95.1
Pr	10.0	15.1	15.0	17.1	7.31	14.7	12.2
Nd	43.4	64.0	63.0	64.4	31.8	60.8	52.8
Sm	8.92	12.1	12.0	10.7	6.61	11.2	10.6
Eu	2.85	3.72	3.73	3.33	2.12	3.41	3.27
Gd	8.78	11.5	11.2	8.8	6.93	10.3	10.2
Tb	1.16	1.43	1.41	1.22	0.913	1.30	1.30
Dy	6.17	7.41	7.27	6.31	4.85	6.66	6.87
Ho	1.08	1.23	1.21	1.10	0.856	1.11	1.15
Er	2.56	2.87	2.77	2.72	2.09	2.60	2.69
Tm	0.321	0.347	0.338	0.352	0.250	0.316	0.326
Yb	1.90	1.98	1.93	2.16	1.49	1.82	1.88
Lu	0.265	0.264	0.264	0.310	0.210	0.251	0.264
Pb	1.67	2.93	2.84	6.11	1.48	3.23	2.26
Th	3.36	6.06	6.06	11.88	2.71	5.79	5.23
U	0.916	1.59	1.63	3.33	0.740	1.68	1.75
$(Hf/Sm)_N$	0.91	0.89	0.93	1.35	1.04	0.86	0.90
$(Ti/Gd)_N$	1.01	1.11	1.16	0.69	1.22	0.81	0.97

Table 5 | *(continued)*

unit	Principe	Principe	Principe	Principe	Principe	Principe	Principe
sample name	PP04	PP07	PP10	PP23	PP24	PP26	PP05
locality	Principe	Campanha	Ponte Banana	Lapa	Praia Sundy	Santo Antonio	Bom Bom Is
age (Ma)	*5.50*	*5.85*	*5.50*	*5.80*	*5.50*	*6.53*	*5.50*
type	1	1	1	1	1	1	2
Li	4.67	7.56	7.86	36.25	4.89	7.03	5.97
Be	1.34	1.54	2.23	2.59	1.34	1.97	1.73
B	0.80	1.53	1.63	2.15	1.16	2.47	1.45
Rb	23.7	19.8	44.1	37.4	25.1	51.3	15.8
Sr	765	1231	1262	1008	788	1365	773
Y	23.7	26.6	33.1	37.3	23.3	29.3	28.4
Zr	219	223	329	457	196	301	300
Nb	47.9	61.7	88.2	122	50.5	115.1	59.3
Cs	0.189	0.386	0.475	3.33	0.252	0.245	1.08
Ba	380	589	685	613	446	907	357
Hf	5.64	4.65	7.52	11.0	5.01	6.75	6.95
Ta	2.58	3.21	4.80	6.30	2.75	6.00	3.47
La	37.4	65.9	71.6	95.5	44.4	86.0	40.6
Ce	77.8	130	142	187	85.0	162	85.6
Pr	10.4	16.0	17.5	21.8	11.1	19.8	10.8
Nd	46.0	66.5	71.3	88.4	48.0	79.0	47.1
Sm	9.46	12.1	13.2	16.1	9.38	13.8	9.74
Eu	2.94	3.65	4.06	4.96	2.91	4.23	3.15
Gd	9.12	10.8	12.2	14.9	8.98	12.7	9.65
Tb	1.15	1.35	1.55	1.86	1.15	1.51	1.31
Dy	6.06	6.76	8.16	9.53	5.99	7.70	7.07
Ho	0.994	1.12	1.38	1.58	1.03	1.27	1.22
Er	2.27	2.58	3.34	3.66	2.37	2.83	2.94
Tm	0.272	0.312	0.415	0.446	0.287	0.341	0.359
Yb	1.55	1.79	2.41	2.57	1.66	1.93	2.12
Lu	0.214	0.244	0.340	0.352	0.231	0.260	0.293
Pb	1.55	2.58	3.41	2.68	1.90	3.52	2.10
Th	3.51	5.32	6.91	8.64	4.33	10.1	4.25
U	0.988	1.45	1.86	3.41	1.20	2.54	1.23
$(Hf/Sm)_N$	0.86	0.55	0.82	0.98	0.77	0.70	1.02
$(Ti/Gd)_N$	0.98	0.69	0.77	0.85	0.96	0.85	1.30

Table 5 | *(continued)*

unit	Principe	Principe	Principe	Principe	Principe	Principe	Principe
sample name	PP09	PP11	PP013*	PP18	PP19*	PP20	PP21
locality	Ponte Banana	Praia Seca	Praia Seca	Praia Abelha	Lapa	Lapa	Lapa
age (Ma)	*5.50*	*5.50*	*5.50*	*5.50*	*5.50*	*5.50*	*5.50*
type	2	2	2	2	2	2	2
Li	4.06	14.06	44.14	6.41	50.61	6.76	5.87
Be	0.929	3.52	3.53	1.73	4.72	1.42	1.65
B	0.69	2.12	6.49	0.79	3.06	0.84	0.85
Rb	14.1	86.1	40.1	36.3	63.3	44.2	17.0
Sr	413	1028	658	926	737	767	792
Y	20.3	21.7	22.3	21.6	28.4	21.1	31.1
Zr	146	475	345	225	385	274	359
Nb	28.5	103	79.0	52.8	75.4	56.9	48.1
Cs	0.107	1.11	0.678	0.163	5.00	0.312	0.328
Ba	197	641	434	403	483	489	362
Hf	4.06	9.29	7.41	5.37	7.57	5.79	9.35
Ta	1.65	4.93	4.12	2.77	3.66	3.35	2.66
La	21.3	60.2	54.3	40.0	61.2	39.5	43.4
Ce	44.5	105	103	81.3	117	75.6	90.9
Pr	5.99	12.2	12.2	10.2	14.0	9.08	13.3
Nd	27.1	46.7	48.6	43.4	58.1	38.0	60.4
Sm	6.07	8.16	8.80	8.44	11.0	7.34	12.9
Eu	1.99	2.49	2.69	2.74	3.43	2.38	4.03
Gd	6.23	7.63	7.92	7.98	10.1	7.13	12.7
Tb	0.872	0.967	1.03	1.03	1.29	0.947	1.60
Dy	4.86	5.12	5.28	5.48	6.63	5.11	8.23
Ho	0.844	0.904	0.919	0.920	1.15	0.900	1.35
Er	2.06	2.24	2.14	2.15	2.79	2.20	3.10
Tm	0.256	0.290	0.267	0.261	0.341	0.269	0.362
Yb	1.53	1.73	1.57	1.54	2.02	1.62	2.06
Lu	0.212	0.246	0.217	0.208	0.281	0.230	0.279
Pb	1.18	7.05	8.12	2.34	4.91	1.89	1.82
Th	2.25	13.3	8.21	4.78	9.45	4.35	4.12
U	0.572	3.92	3.60	1.08	6.50	2.10	1.22
$(Hf/Sm)_N$	0.96	1.63	1.21	0.91	0.99	1.13	1.04
$(Ti/Gd)_N$	1.22	0.73	0.93	1.04	0.80	0.91	0.90

Table 5 | *(continued)*

unit	Principe	Bioko	Bioko	Bioko	Bioko	Bioko	Bioko
sample name	PP25	BK02	BK04	BK06	BK07	BK08	BK12
locality	Santo Antonio	Baney	Ruiche	Luba	B. Cristol	B. Cristol	Luba-Batete
age (Ma)	*5.50*	*0.14*	*1.00*	*0.17*	*0.82*	*1.00*	*1.00*
type	2	1	1	1	1	1	1
Li	5.93	5.84	4.76	4.66	6.50	5.69	6.72
Be	1.86	1.25	1.31	1.16	1.82	1.54	1.77
B	0.96	0.57	1.90	1.40	2.06	1.99	1.29
Rb	31.6	16.2	30.4	21.3	32.7	39.5	41.5
Sr	1001	802	751	729	973	887	1019
Y	22.7	28.9	23.8	25.3	29.9	29.2	31.2
Zr	238	213	222	214	301	325	298
Nb	57.6	44.3	57.8	45.2	59.9	61.8	78.7
Cs	0.330	0.211	0.388	0.286	0.415	0.520	0.464
Ba	440	376	444	384	496	502	648
Hf	5.75	5.08	5.27	5.03	7.24	7.58	6.97
Ta	3.13	2.32	3.25	2.55	3.32	3.46	4.30
La	45.6	46.8	49.5	38.6	55.5	49.1	65.5
Ce	84.9	93.0	96.6	78.6	112	105	125
Pr	11.1	11.6	11.8	10.0	14.3	13.3	15.8
Nd	46.5	50.5	47.7	42.7	61.8	56.8	64.7
Sm	9.05	10.1	8.88	8.33	12.6	11.1	11.9
Eu	2.91	3.22	2.75	2.67	3.95	3.43	3.63
Gd	8.69	10.0	8.41	8.26	12.1	10.3	11.2
Tb	1.09	1.32	1.10	1.09	1.54	1.38	1.43
Dy	5.74	6.92	5.84	5.88	7.78	7.20	7.54
Ho	0.976	1.19	1.01	1.04	1.27	1.26	1.31
Er	2.31	2.79	2.50	2.58	2.86	3.06	3.18
Tm	0.279	0.343	0.310	0.319	0.339	0.389	0.400
Yb	1.64	1.97	1.88	1.89	1.91	2.29	2.40
Lu	0.220	0.273	0.264	0.267	0.250	0.324	0.334
Pb	2.43	2.06	2.44	1.96	2.80	3.22	3.50
Th	5.05	3.82	5.74	3.99	5.79	5.45	6.65
U	1.52	0.970	1.37	0.977	1.49	1.49	1.72
$(Hf/Sm)_N$	0.91	0.73	0.85	0.87	0.82	0.98	0.84
$(Ti/Gd)_N$	1.01	0.80	0.96	0.96	0.86	0.95	0.90

Table 5 | *(continued)*

unit	Bioko	Bioko	Bioko	Bioko	Bioko	Bioko	Bioko
sample name	BK14	BK15	BK16	BK17	BK18	BK19	BK21
locality	Batete	Moca	Moca	Pico Basile	Pico Basile	Mt Basile	Barioba
age (Ma)	*1.00*	*0.05*	*1.00*	*1.00*	*1.00*	*0.32*	*1.00*
type	1	1	1	1	1	1	1
Li	5.78	10.61	7.88	6.61	6.66	5.81	8.68
Be	1.55	2.73	2.14	1.66	1.67	1.49	2.14
B	1.56	2.18	2.17	1.93	2.00	1.78	2.60
Rb	42.4	65.9	60.2	29.9	30.8	24.4	48.4
Sr	950	1463	1255	1096	1095	860	1173
Y	28.6	41.8	35.3	28.7	28.2	27.3	34.2
Zr	241	437	363	284	291	267	391
Nb	73.5	136	118	71.4	73.3	50.8	89.0
Cs	0.451	0.838	0.641	0.354	0.366	0.334	0.577
Ba	592	870	809	538	528	401	657
Hf	5.72	10.1	8.58	6.69	6.43	6.20	8.42
Ta	4.06	7.45	6.63	3.77	3.69	2.80	4.87
La	61.8	109	91.7	68.3	67.9	47.7	69.8
Ce	114	210	178	137	135	92.7	143
Pr	14.2	25.1	20.0	17.3	17.0	12.3	18.6
Nd	56.7	96.3	80.2	71.1	71.0	53.4	75.9
Sm	10.0	16.1	13.5	13.1	12.9	11.1	13.9
Eu	3.10	4.72	4.02	4.02	3.98	3.44	4.20
Gd	9.62	14.4	12.0	12.2	12.2	10.8	12.9
Tb	1.24	1.81	1.55	1.50	1.49	1.37	1.63
Dy	6.74	9.76	8.46	7.49	7.44	6.99	8.43
Ho	1.19	1.71	1.51	1.22	1.21	1.18	1.42
Er	2.95	4.39	3.79	2.79	2.72	2.69	3.35
Tm	0.380	0.571	0.494	0.329	0.322	0.320	0.423
Yb	2.32	3.51	3.00	1.84	1.81	1.81	2.40
Lu	0.324	0.500	0.436	0.251	0.243	0.247	0.331
Pb	2.86	5.36	4.41	2.89	2.89	2.23	4.02
Th	6.13	12.1	9.76	6.54	6.18	4.45	7.96
U	1.45	2.85	2.39	1.71	1.65	1.15	2.15
$(Hf/Sm)_N$	0.82	0.90	0.92	0.73	0.72	0.80	0.87
$(Ti/Gd)_N$	0.98	0.54	0.81	0.74	0.74	0.89	0.74

Table 5 | *(continued)*

unit	Bioko	Bioko	Bioko	Bioko	Bioko	Bioko	Bioko
sample name	BK23	BK03	BK09	BK10	BK11	BK13	BK20
locality	Riaba	Bao Basoala	B. Cristol	B. Cristol	Luba	Luba-Batete	Bososo
age (Ma)	*1.00*	*1*	*1.00*	*0.15*	*1.00*	*1.00*	*1.00*
type	1	2	2	2	2	2	2
Li	5.20	5.84	5.05	5.63	7.16	4.87	5.18
Be	1.51	1.51	1.34	1.27	1.07	1.28	1.24
B	1.30	2.00	1.32	1.77	3.31	1.44	1.01
Rb	28.6	24.9	24.9	20.6	24.3	34.8	17.9
Sr	724	779	782	585	535	883	649
Y	29.3	28.4	29.3	23.1	21.4	25.5	24.1
Zr	242	278	291	177	201	213	206
Nb	53.7	48.9	51.9	43.4	38.9	64.8	49.0
Cs	0.347	0.313	0.292	0.276	0.286	0.412	0.233
Ba	469	374	366	352	313	514	357
Hf	5.65	6.51	6.90	4.82	4.93	5.18	5.20
Ta	2.92	2.79	2.96	2.39	2.24	3.57	2.76
La	48.0	42.4	41.9	30.4	32.1	51.6	35.0
Ce	93.9	84.0	87.7	60.6	68.6	94.8	68.6
Pr	12.0	10.9	11.6	7.71	8.66	11.9	9.44
Nd	49.9	47.4	50.2	34.1	36.9	48.5	40.3
Sm	9.00	10.1	10.6	7.38	7.23	8.70	8.34
Eu	2.80	3.20	3.28	2.38	2.25	2.71	2.68
Gd	8.73	10.0	10.3	7.55	6.98	8.45	8.36
Tb	1.14	1.35	1.38	1.04	0.947	1.10	1.12
Dy	5.99	6.93	7.28	5.70	5.13	5.95	5.91
Ho	1.09	1.18	1.25	0.979	0.919	1.08	1.03
Er	2.63	2.73	3.01	2.36	2.25	2.66	2.44
Tm	0.323	0.337	0.371	0.296	0.289	0.345	0.310
Yb	1.90	1.92	2.15	1.70	1.72	2.08	1.75
Lu	0.276	0.263	0.296	0.238	0.243	0.293	0.247
Pb	2.83	2.30	2.37	2.06	5.22	2.54	1.82
Th	5.22	4.47	4.38	3.31	3.99	5.21	3.28
U	1.34	1.23	1.12	0.838	1.03	1.29	0.741
$(Hf/Sm)_N$	0.90	0.93	0.93	0.94	0.98	0.85	0.89
$(Ti/Gd)_N$	0.95	1.00	1.05	1.10	1.02	1.13	1.10

Table 5 | *(continued)*

unit	Bioko	Etinde	Etinde	Etinde	Etinde	Etinde
sample name	BK22	2208A	2208B	2208C	2208D	CA062
locality	Bakake	Mt Etinde	Mt Etinde	Mt Etinde	Mt Etinde	Batoke
age (Ma)	*1.33*	*0.27*	*0.50*	*0.50*	*0.50*	*0.43*
type	2	1	1	1	1	1
Li	7.77	11.8	11.0	13.7	12.6	7.23
Be	1.58	3.81	3.80	4.41	3.50	3.78
B	3.20	1.25	2.08	1.70	0.96	0.59
Rb	28.7	98.4	54.8	145	103	96.5
Sr	896	2891	3514	4434	3838	3489
Y	26.8	39.0	49.6	56.6	52.9	39.2
Zr	316	497	792	847	802	525
Nb	68.1	272	311	397	331	274
Cs	0.363	0.928	0.861	1.45	1.04	0.883
Ba	419	1376	1151	1368	1156	1351
Hf	7.28	8.17	13.6	13.3	13.4	8.54
Ta	3.92	14.5	17.1	20.5	18.5	14.1
La	53.5	197	246	304	267	190
Ce	111	379	488	571	529	374
Pr	14.2	43.5	53.3	60.9	57.8	42.7
Nd	60.2	155	204	225	209	154
Sm	11.0	20.8	27.8	29.5	28.6	20.7
Eu	3.23	5.58	7.49	7.98	7.65	5.69
Gd	9.80	16.8	22.7	24.1	21.9	16.8
Tb	1.26	1.90	2.52	2.76	2.53	1.90
Dy	6.60	9.41	12.4	13.5	12.6	9.49
Ho	1.17	1.67	2.16	2.40	2.18	1.66
Er	2.86	4.15	5.31	6.00	5.31	4.12
Tm	0.364	0.538	0.683	0.789	0.683	0.542
Yb	2.20	3.25	4.17	4.87	4.15	3.22
Lu	0.305	0.453	0.590	0.690	0.587	0.448
Pb	3.48	3.93	6.16	5.79	5.49	3.64
Th	5.94	21.4	23.4	29.7	25.1	19.5
U	1.77	5.21	7.85	4.79	6.09	6.13
$(Hf/Sm)_N$	0.95	0.56	0.70	0.64	0.67	0.59
$(Ti/Gd)_N$	1.08	0.58	0.50	0.43	0.50	0.60

*: Slightly altered sample which contain secondary minerals.; $(Hf/Sm)_N$ and $(Ti/Gd)_N$ are primitive mantle normalized ratio. The trace element composition of primitive mantle is after McDonough and Sun (1995). The samples with $(Hf/Sm)_N<1$ and $(Ti/Gd)_N<1$ are classified as Type 1 and others Type 2.

Table 6 | Sr, Nd, Hf, and Pb isotopic compositions of mafic CVL samples

unit	Annobon	Annobon	Annobon	Annobon	Annobon	Annobon	Annobon
sample name	AN01	AN02	AN08	AN16	AN22	AN23	AN24
age (Ma)	0.20	1.50	1.50	1.50	1.63	1.50	1.50
type	1	1	1	1	1	1	1
$^{87}Sr/^{86}Sr$	0.703202	0.703212	0.703226	0.703295	0.703219	0.703220	0.703283
±2SE	0.000006	0.000006	0.000007	0.000006	0.000007	0.000006	0.000006
$^{143}Nd/^{144}Nd$	0.512920	0.512903	0.512928	0.512916	0.512931	0.512938	0.512913
±2SE	0.000006	0.000009	0.000007	0.000008	0.000007	0.000006	0.000005
$^{176}Hf/^{177}Hf$	0.282979	0.282975	0.282975	0.282980	0.282981	0.282976	0.282972
±2SE	0.000007	0.000004	0.000003	0.000004	0.000003	0.000005	0.000003
$^{206}Pb/^{204}Pb$	19.2824	19.2642	19.2509	19.1399	19.2172	19.2536	19.1924
$^{207}Pb/^{204}Pb$	15.6225	15.6218	15.6222	15.6250	15.5725	15.6277	15.6267
$^{208}Pb/^{204}Pb$	39.0946	39.0914	39.0966	39.0844	38.9315	39.1061	39.0996
initial value							
$(^{87}Sr/^{86}Sr)_i$	0.703202	0.703210	0.703224	0.703293	0.703217	0.703217	0.703282
$(^{143}Nd/^{144}Nd)_i$	0.512920	0.512902	0.512927	0.512915	0.512930	0.512937	0.512912
$(^{176}Hf/^{177}Hf)_i$	0.282979	0.282975	0.282975	0.282979	0.282981	0.282976	0.282972
$(^{206}Pb/^{204}Pb)_i$	19.281	19.255	19.243	19.132	19.207	19.245	19.184
$(^{207}Pb/^{204}Pb)_i$	15.622	15.621	15.622	15.625	15.572	15.627	15.626
$(^{208}Pb/^{204}Pb)_i$	39.093	39.081	39.085	39.075	38.920	39.095	39.088
εNd_T	5.66	5.34	5.83	5.59	5.89	6.02	5.54
εHf_T	6.85	6.74	6.74	6.91	6.95	6.78	6.65

Table 6 | *(continued)*

unit	Annobon	Annobon	Annobon	Annobon	Annobon	Annobon	Annobon
sample name	AN04-3	AN05	AN06	AN07	AN10-3	AN11	AN12
age (Ma)	4.50	1.50	4.50	1.50	1.50	1.50	4.50
type	2	2	2	2	2	2	2
$^{87}Sr/^{86}Sr$	0.704240	0.703549	0.703462	0.703200	0.703597	0.703624	0.703470
±2SE	0.000007	0.000006	0.000007	0.000006	0.000008	0.000007	0.000007
$^{143}Nd/^{144}Nd$	0.512769	0.512868	0.512902	0.512927	0.512873	0.512853	0.512888
±2SE	0.000007	0.000008	0.000007	0.000007	0.000007	0.000007	0.000006
$^{176}Hf/^{177}Hf$	0.282847	0.282949	0.282965	0.282979	0.282940	0.282935	0.282947
±2SE	0.000004	0.000004	0.000004	0.000003	0.000004	0.000004	0.000005
$^{206}Pb/^{204}Pb$	19.2971	19.3300	19.2986	19.2849	19.2152	19.3114	19.2627
$^{207}Pb/^{204}Pb$	15.6701	15.6328	15.6298	15.6126	15.6308	15.6436	15.6284
$^{208}Pb/^{204}Pb$	39.5401	39.3025	39.2963	39.0600	39.2438	39.3786	39.2748
initial value							
$(^{87}Sr/^{86}Sr)_i$	0.704229	0.703546	0.703453	0.703198	0.703595	0.703622	0.703463
$(^{143}Nd/^{144}Nd)_i$	0.512766	0.512867	0.512898	0.512926	0.512872	0.512851	0.512884
$(^{176}Hf/^{177}Hf)_i$	0.282846	0.282949	0.282965	0.282979	0.282939	0.282935	0.282947
$(^{206}Pb/^{204}Pb)_i$	19.285	19.324	19.278	19.277	19.209	19.305	19.241
$(^{207}Pb/^{204}Pb)_i$	15.670	15.633	15.629	15.612	15.631	15.643	15.627
$(^{208}Pb/^{204}Pb)_i$	39.524	39.294	39.271	39.049	39.237	39.371	39.252
εNd_T	2.76	4.67	5.34	5.81	4.76	4.36	5.08
εHf_T	2.27	5.83	6.46	6.90	5.50	5.33	5.81

Table 6 | *(continued)*

unit	Annobon	Annobon	Annobon	Annobon	Annobon	Annobon	Annobon
sample name	AN13	AN14	AN15	AN17	AN18	AN19	AN20
age (Ma)	4.50	4.50	4.70	4.50	1.50	4.50	1.50
type	2	2	2	2	2	2	2
$^{87}Sr/^{86}Sr$	0.703808	0.703463	0.704140	0.703380	0.703541	0.703407	0.703165
±2SE	0.000006	0.000007	0.000006	0.000007	0.000007	0.000005	0.000007
$^{143}Nd/^{144}Nd$	0.512861	0.512906	0.512778	0.512917	0.512894	0.512911	0.512963
±2SE	0.000008	0.000006	0.000005	0.000007	0.000007	0.000007	0.000008
$^{176}Hf/^{177}Hf$	0.282913	0.282955	0.282814	0.282984	0.282945	0.282994	0.283029
±2SE	0.000006	0.000005	0.000004	0.000004	0.000003	0.000005	0.000003
$^{206}Pb/^{204}Pb$	19.2560	19.2679	19.3654	19.2548	19.3117	19.3231	19.2124
$^{207}Pb/^{204}Pb$	15.6516	15.6327	15.6811	15.6286	15.6377	15.6278	15.6013
$^{208}Pb/^{204}Pb$	39.4407	39.2859	39.6877	39.2039	39.3632	39.2159	38.9602
initial value							
$(^{87}Sr/^{86}Sr)_i$	0.703800	0.703455	0.704132	0.703372	0.703538	0.703399	0.703163
$(^{143}Nd/^{144}Nd)_i$	0.512858	0.512902	0.512774	0.512914	0.512893	0.512907	0.512962
$(^{176}Hf/^{177}Hf)_i$	0.282912	0.282955	0.282813	0.282984	0.282945	0.282994	0.283028
$(^{206}Pb/^{204}Pb)_i$	19.239	19.241	19.352	19.232	19.306	19.302	19.203
$(^{207}Pb/^{204}Pb)_i$	15.651	15.631	15.681	15.628	15.637	15.627	15.601
$(^{208}Pb/^{204}Pb)_i$	39.420	39.263	39.671	39.176	39.356	39.191	38.950
εNd_T	4.55	5.42	2.93	5.65	5.17	5.52	6.51
εHf_T	4.60	6.10	1.11	7.13	5.69	7.47	8.64

Table 6 | *(continued)*

unit	Saô Tomé	Saô Tomé	Saô Tomé	Saô Tomé	Saô Tomé	Saô Tomé	Saô Tomé
sample name	ST01	ST02	ST04	ST05	ST16	ST17	ST20
age (Ma)	3.00	3.00	3.00	3.00	3.00	3.00	1.38
type	1	1	1	1	1	1	1
$^{87}Sr/^{86}Sr$	0.703271	0.703260	0.702987	0.702976	0.703110	0.703107	0.702966
±2SE	0.000007	0.000006	0.000006	0.000007	0.000006	0.000007	0.000006
$^{143}Nd/^{144}Nd$	0.512911	0.512908	0.512983	0.512970	0.512934	0.512927	0.512977
±2SE	0.000007	0.000006	0.000005	0.000006	0.000006	0.000007	0.000008
$^{176}Hf/^{177}Hf$	0.282941	0.282950	0.283004	0.282995	0.282971	0.282963	0.282998
±2SE	0.000004	0.000003	0.000004	0.000005	0.000002	0.000004	0.000008
$^{206}Pb/^{204}Pb$	20.0618	20.0450	19.7866	19.8095	20.0627	20.0503	19.8769
$^{207}Pb/^{204}Pb$	15.6765	15.6701	15.6431	15.6582	15.6764	15.6780	15.6595
$^{208}Pb/^{204}Pb$	39.7752	39.7364	39.3817	39.4368	39.7392	39.7300	39.5002
initial value							
$(^{87}Sr/^{86}Sr)_i$	0.703266	0.703257	0.702984	0.702973	0.703106	0.703101	0.702964
$(^{143}Nd/^{144}Nd)_i$	0.512909	0.512906	0.512981	0.512968	0.512932	0.512925	0.512976
$(^{176}Hf/^{177}Hf)_i$	0.282941	0.282949	0.283003	0.282994	0.282970	0.282963	0.282998
$(^{206}Pb/^{204}Pb)_i$	20.043	20.026	19.770	19.791	20.043	20.031	19.869
$(^{207}Pb/^{204}Pb)_i$	15.676	15.669	15.642	15.657	15.676	15.677	15.659
$(^{208}Pb/^{204}Pb)_i$	39.752	39.716	39.359	39.414	39.715	39.706	39.489
εNd_T	5.51	5.45	6.92	6.66	5.97	5.83	6.78
εHf_T	5.58	5.88	7.78	7.47	6.62	6.37	7.55

Table 6 | *(continued)*

unit	Saô Tomé	Saô Tomé	Saô Tomé	Saô Tomé	Saô Tomé	Saô Tomé	Saô Tomé
sample name	ST23E*	ST24*	ST26*	ST27*	ST35	ST03	ST06*
age (Ma)	3.00	3.00	3.00	3.00	3.00	0.17	3.00
type	1	1	1	1	1	2	2
$^{87}Sr/^{86}Sr$	0.703175	0.703160	0.702951	0.703153	0.703229	0.702969	0.702929
±2SE	0.000007	0.000006	0.000007	0.000007	0.000006	0.000007	0.000006
$^{143}Nd/^{144}Nd$	0.512883	0.512880	0.512952	0.512885	0.512903	0.512951	0.512955
±2SE	0.000006	0.000008	0.000006	0.000004	0.000008	0.000008	0.000008
$^{176}Hf/^{177}Hf$	0.282955	0.282966	0.282996	0.282949	0.282956	0.283003	0.282991
±2SE	0.000004	0.000004	0.000004	0.000006	0.000006	0.000007	0.000005
$^{206}Pb/^{204}Pb$	19.8403	19.8352	19.9412	19.8278	20.0640	19.9710	20.1175
$^{207}Pb/^{204}Pb$	15.6709	15.6683	15.6686	15.6669	15.6796	15.6686	15.6835
$^{208}Pb/^{204}Pb$	39.5647	39.5480	39.5770	39.5385	39.7840	39.5927	39.7374
initial value							
$(^{87}Sr/^{86}Sr)_i$	0.703173	0.703158	0.702947	0.703150	0.703225	0.702969	0.702923
$(^{143}Nd/^{144}Nd)_i$	0.512881	0.512878	0.512950	0.512883	0.512901	0.512951	0.512953
$(^{176}Hf/^{177}Hf)_i$	0.282954	0.282966	0.282995	0.282949	0.282956	0.283003	0.282991
$(^{206}Pb/^{204}Pb)_i$	19.823	19.817	19.928	19.811	20.045	19.970	20.100
$(^{207}Pb/^{204}Pb)_i$	15.670	15.667	15.668	15.666	15.679	15.669	15.683
$(^{208}Pb/^{204}Pb)_i$	39.543	39.527	39.554	39.517	39.763	39.591	39.717
εNd_T	4.96	4.91	6.31	5.01	5.36	6.27	6.38
εHf_T	6.05	6.46	7.51	5.86	6.10	7.72	7.33

Table 6 | *(continued)*

unit	Saô Tomé	Saô Tomé	Saô Tomé	Saô Tomé	Saô Tomé	Saô Tomé	Saô Tomé
sample name	ST08*	ST09	ST10	ST11	ST13*	ST14	ST21
age (Ma)	3.00	2.12	3.00	3.00	3.00	3.00	3.00
type	2	2	2	2	2	2	2
$^{87}Sr/^{86}Sr$	0.703200	0.703407	0.703080	0.703107	0.703083	0.702946	0.703006
±2SE	0.000008	0.000006	0.000009	0.000006	0.000006	0.000008	0.000007
$^{143}Nd/^{144}Nd$	0.512850	0.512878	0.512926	0.512916	0.512909	0.512968	0.512969
±2SE	0.000005	0.000008	0.000006	0.000006	0.000005	0.000007	0.000008
$^{176}Hf/^{177}Hf$	0.282956	0.282930	0.282982	0.282975	0.282980	0.282989	0.282987
±2SE	0.000007	0.000004	0.000004	0.000004	0.000003	0.000003	0.000003
$^{206}Pb/^{204}Pb$	19.8791	20.1185	19.8873	20.1350	20.0585	20.1532	19.8936
$^{207}Pb/^{204}Pb$	15.6716	15.6953	15.6651	15.6856	15.6747	15.6816	15.6584
$^{208}Pb/^{204}Pb$	39.6115	39.9052	39.5640	39.8361	39.7511	39.7621	39.5353
initial value							
$(^{87}Sr/^{86}Sr)_i$	0.703196	0.703403	0.703077	0.703101	0.703079	0.702939	0.703001
$(^{143}Nd/^{144}Nd)_i$	0.512848	0.512877	0.512923	0.512914	0.512907	0.512966	0.512967
$(^{176}Hf/^{177}Hf)_i$	0.282956	0.282930	0.282982	0.282975	0.282980	0.282989	0.282987
$(^{206}Pb/^{204}Pb)_i$	19.861	20.100	19.870	20.115	20.039	20.137	19.876
$(^{207}Pb/^{204}Pb)_i$	15.671	15.694	15.664	15.685	15.674	15.681	15.658
$(^{208}Pb/^{204}Pb)_i$	39.589	39.883	39.542	39.812	39.728	39.743	39.513
εNd_T	4.32	4.87	5.80	5.62	5.48	6.63	6.64
εHf_T	6.10	5.17	7.02	6.78	6.95	7.27	7.21

Table 6 | *(continued)*

unit	Saô Tomé	Saô Tomé	Saô Tomé	Saô Tomé	Saô Tomé	Principe	Principe
sample name	ST29	ST30*	ST31	ST34	ST36	PP01	PP03
age (Ma)	3.00	3.00	3.00	3.00	5.20	5.50	5.50
type	2	2	2	2	2	1	1
$^{87}Sr/^{86}Sr$	0.703096	0.703167	0.703172	0.703235	0.703288	0.703245	0.702965
±2SE	0.000007	0.000006	0.000007	0.000006	0.000008	0.000006	0.000006
$^{143}Nd/^{144}Nd$	0.512929	0.512872	0.512878	0.512871	0.512878	0.512869	0.512945
±2SE	0.000009	0.000006	0.000008	0.000006	0.000006	0.000004	0.000007
$^{176}Hf/^{177}Hf$	0.282970	0.282952	0.282950	0.282937	0.282950	0.282945	0.282991
±2SE	0.000004	0.000003	0.000003	0.000002	0.000003	0.000007	0.000004
$^{206}Pb/^{204}Pb$	19.7444	20.1221	20.1253	20.0100	19.9274	20.1507	20.0884
$^{207}Pb/^{204}Pb$	15.6659	15.6869	15.6876	15.6900	15.6717	15.6903	15.6862
$^{208}Pb/^{204}Pb$	39.6614	39.9262	39.9341	39.8000	39.7226	39.8638	39.7395
initial value							
$(^{87}Sr/^{86}Sr)_i$	0.703093	0.703161	0.703167	0.703227	0.703279	0.703237	0.702957
$(^{143}Nd/^{144}Nd)_i$	0.512926	0.512869	0.512876	0.512869	0.512874	0.512865	0.512941
$(^{176}Hf/^{177}Hf)_i$	0.282970	0.282952	0.282950	0.282937	0.282949	0.282944	0.282990
$(^{206}Pb/^{204}Pb)_i$	19.728	20.105	20.108	19.993	19.901	20.121	20.045
$(^{207}Pb/^{204}Pb)_i$	15.665	15.686	15.687	15.689	15.670	15.689	15.684
$(^{208}Pb/^{204}Pb)_i$	39.641	39.905	39.912	39.780	39.691	39.830	39.697
εNd_T	5.85	4.75	4.88	4.74	4.89	4.73	6.20
εHf_T	6.60	5.96	5.90	5.43	5.91	5.75	7.38

Table 6 | *(continued)*

unit	Principe	Principe	Principe	Principe	Principe	Principe	Principe
sample name	PP04	PP07	PP10	PP23	PP24	PP26	PP05
age (Ma)	5.50	5.85	5.50	5.80	5.50	6.53	5.50
type	1	1	1	1	1	1	2
$^{87}Sr/^{86}Sr$	0.703006	0.703017	0.702944	0.702922	0.702995	0.703193	0.703069
±2SE	0.000007	0.000006	0.000007	0.000007	0.000006	0.000007	0.000007
$^{143}Nd/^{144}Nd$	0.512911	0.512928	0.512928	0.512955	0.512943	0.512898	0.512886
±2SE	0.000007	0.000006	0.000006	0.000009	0.000007	0.000007	0.000008
$^{176}Hf/^{177}Hf$	0.282990	0.282991	0.282998	0.282985	0.282988	0.282964	0.282976
±2SE	0.000006	0.000004	0.000005	0.000003	0.000006	0.000004	0.000004
$^{206}Pb/^{204}Pb$	19.9784	20.0390	20.2165	20.2742	20.0066	20.9870	19.9347
$^{207}Pb/^{204}Pb$	15.6733	15.6801	15.6907	15.7032	15.6799	15.7289	15.6731
$^{208}Pb/^{204}Pb$	39.6414	39.7032	39.8121	39.9340	39.6612	40.8100	39.7521
initial value							
$(^{87}Sr/^{86}Sr)_i$	0.702999	0.703014	0.702936	0.702913	0.702988	0.703183	0.703065
$(^{143}Nd/^{144}Nd)_i$	0.512906	0.512923	0.512924	0.512951	0.512939	0.512894	0.512881
$(^{176}Hf/^{177}Hf)_i$	0.282990	0.282990	0.282997	0.282985	0.282987	0.282964	0.282975
$(^{206}Pb/^{204}Pb)_i$	19.942	20.005	20.186	20.198	19.971	20.937	19.902
$(^{207}Pb/^{204}Pb)_i$	15.672	15.678	15.689	15.700	15.678	15.727	15.672
$(^{208}Pb/^{204}Pb)_i$	39.599	39.662	39.774	39.870	39.619	40.745	39.715
εNd_T	5.52	5.87	5.88	6.41	6.16	5.31	5.04
εHf_T	7.36	7.39	7.62	7.20	7.26	6.46	6.84

Table 6 | *(continued)*

unit	Principe	Principe	Principe	Principe	Principe	Principe	Principe
sample name	PP09	PP11	PP013*	PP18	PP19*	PP20	PP21
age (Ma)	5.50	5.50	5.50	5.50	5.50	5.50	5.50
type	2	2	2	2	2	2	2
$^{87}Sr/^{86}Sr$	0.703142	0.702970	0.702930	0.702888	0.702954	0.703097	0.703045
±2SE	0.000007	0.000006	0.000005	0.000006	0.000007	0.000006	0.000006
$^{143}Nd/^{144}Nd$	0.512896	0.512957	0.512940	0.512930	0.512944	0.512897	0.512911
±2SE	0.000004	0.000007	0.000005	0.000006	0.000007	0.000006	0.000007
$^{176}Hf/^{177}Hf$	0.282981	0.282987	0.282982	0.282997	0.283004	0.282976	0.282980
±2SE	0.000005	0.000003	0.000003	0.000006	0.000005	0.000004	0.000005
$^{206}Pb/^{204}Pb$	19.8070	20.2445	20.2383	20.0196	20.2125	20.2044	20.1524
$^{207}Pb/^{204}Pb$	15.6506	15.6958	15.6923	15.6723	15.6875	15.6930	15.6867
$^{208}Pb/^{204}Pb$	39.5758	39.8882	39.8575	39.6593	39.8215	39.8222	39.7978
initial value							
$(^{87}Sr/^{86}Sr)_i$	0.703135	0.702952	0.702916	0.702879	0.702935	0.703084	0.703040
$(^{143}Nd/^{144}Nd)_i$	0.512892	0.512954	0.512936	0.512926	0.512940	0.512893	0.512906
$(^{176}Hf/^{177}Hf)_i$	0.282980	0.282987	0.282982	0.282996	0.283004	0.282976	0.282979
$(^{206}Pb/^{204}Pb)_i$	19.780	20.213	20.213	19.994	20.138	20.142	20.115
$(^{207}Pb/^{204}Pb)_i$	15.649	15.694	15.691	15.671	15.684	15.690	15.685
$(^{208}Pb/^{204}Pb)_i$	39.541	39.853	39.839	39.621	39.786	39.779	39.756
εNd_T	5.24	6.45	6.11	5.91	6.19	5.27	5.52
εHf_T	7.01	7.26	7.09	7.59	7.85	6.86	6.99

Table 6 | *(continued)*

unit	Principe	Bioko	Bioko	Bioko	Bioko	Bioko	Bioko
sample name	PP25	BK02	BK04	BK06	BK07	BK08	BK12
age (Ma)	5.50	0.14	1.00	0.17	0.82	1.00	1.00
type	2	1	1	1	1	1	1
$^{87}Sr/^{86}Sr$	0.702925	0.703123	0.703319	0.703264	0.703038	0.703240	0.703281
±2SE	0.000007	0.000008	0.000006	0.000007	0.000006	0.000006	0.000007
$^{143}Nd/^{144}Nd$	0.512946	0.512878	0.512823	0.512831	0.512916	0.512838	0.512818
±2SE	0.000006	0.000005	0.000008	0.000007	0.000007	0.000007	0.000007
$^{176}Hf/^{177}Hf$	0.282993	0.282980	0.282948	0.282949	0.282974	0.282963	0.282952
±2SE	0.000002	0.000010	0.000004	0.000003	0.000004	0.000004	0.000005
$^{206}Pb/^{204}Pb$	20.0288	20.1771	20.3829	20.5422	20.2956	20.4813	20.5007
$^{207}Pb/^{204}Pb$	15.6765	15.6767	15.6868	15.6898	15.6794	15.6802	15.6823
$^{208}Pb/^{204}Pb$	39.6789	39.9498	40.2771	40.3741	39.9745	40.2925	40.3525
initial value							
$(^{87}Sr/^{86}Sr)_i$	0.702918	0.703123	0.703317	0.703264	0.703037	0.703238	0.703279
$(^{143}Nd/^{144}Nd)_i$	0.512942	0.512878	0.512823	0.512831	0.512915	0.512837	0.512817
$(^{176}Hf/^{177}Hf)_i$	0.282993	0.282980	0.282948	0.282949	0.282974	0.282963	0.282952
$(^{206}Pb/^{204}Pb)_i$	19.994	20.176	20.377	20.541	20.291	20.477	20.496
$(^{207}Pb/^{204}Pb)_i$	15.675	15.677	15.687	15.690	15.679	15.680	15.682
$(^{208}Pb/^{204}Pb)_i$	39.640	39.949	40.269	40.373	39.969	40.287	40.346
εNd_T	6.22	4.84	3.78	3.93	5.59	4.07	3.67
εHf_T	7.48	6.89	5.79	5.82	6.70	6.30	5.92

Table 6 | *(continued)*

unit	Bioko	Bioko	Bioko	Bioko	Bioko	Bioko	Bioko
sample name	BK14	BK15	BK16	BK17	BK18	BK19	BK21
age (Ma)	1.00	0.05	1.00	1.00	1.00	0.32	1.00
type	1	1	1	1	1	1	1
$^{87}Sr/^{86}Sr$	0.703333	0.703367	0.703407	0.703136	0.703140	0.703040	0.703259
±2SE	0.000008	0.000007	0.000007	0.000007	0.000006	0.000006	0.000006
$^{143}Nd/^{144}Nd$	0.512799	0.512820	0.512789	0.512890	0.512893	0.512924	0.512835
±2SE	0.000006	0.000006	0.000008	0.000006	0.000008	0.000008	0.000007
$^{176}Hf/^{177}Hf$	0.282948	0.282947	0.282941	0.282961	0.282955	0.282990	0.282957
±2SE	0.000006	0.000004	0.000003	0.000003	0.000004	0.000005	0.000003
$^{206}Pb/^{204}Pb$	20.5371	20.5593	20.5339	20.3903	20.3839	20.2415	20.3698
$^{207}Pb/^{204}Pb$	15.6713	15.6774	15.6723	15.6876	15.6863	15.6857	15.6783
$^{208}Pb/^{204}Pb$	40.3750	40.3793	40.3591	40.1135	40.1060	39.9760	40.2305
initial value							
$(^{87}Sr/^{86}Sr)_i$	0.703331	0.703367	0.703405	0.703135	0.703139	0.703040	0.703258
$(^{143}Nd/^{144}Nd)_i$	0.512798	0.512820	0.512788	0.512889	0.512892	0.512924	0.512835
$(^{176}Hf/^{177}Hf)_i$	0.282948	0.282947	0.282941	0.282961	0.282955	0.282990	0.282957
$(^{206}Pb/^{204}Pb)_i$	20.532	20.559	20.528	20.384	20.378	20.240	20.364
$(^{207}Pb/^{204}Pb)_i$	15.671	15.677	15.672	15.687	15.686	15.686	15.678
$(^{208}Pb/^{204}Pb)_i$	40.368	40.379	40.351	40.106	40.099	39.974	40.224
εNd_T	3.30	3.70	3.11	5.08	5.14	5.74	4.02
εHf_T	5.80	5.74	5.55	6.26	6.04	7.25	6.10

Table 6 | *(continued)*

unit	Bioko	Bioko	Bioko	Bioko	Bioko	Bioko	Bioko
sample name	BK23	BK03	BK09	BK10	BK11	BK13	BK20
age (Ma)	1.00	1	1.00	0.15	1.00	1.00	1.00
type	1	2	2	2	2	2	2
$^{87}Sr/^{86}Sr$	0.703258	0.703124	0.703135	0.703208	0.703403	0.703333	0.703232
±2SE	0.000006	0.000006	0.000007	0.000006	0.000006	0.000007	0.000006
$^{143}Nd/^{144}Nd$	0.512842	0.512883	0.512880	0.512895	0.512807	0.512791	0.512860
±2SE	0.000006	0.000006	0.000008	0.000007	0.000006	0.000007	0.000007
$^{176}Hf/^{177}Hf$	0.282931	0.282967	0.282971	0.282952	0.282906	0.282943	0.282958
±2SE	0.000003	0.000005	0.000004	0.000004	0.000003	0.000004	0.000003
$^{206}Pb/^{204}Pb$	20.2996	20.3170	20.4899	19.8444	19.8405	20.5307	20.0927
$^{207}Pb/^{204}Pb$	15.6874	15.6836	15.6842	15.6791	15.6916	15.6875	15.6772
$^{208}Pb/^{204}Pb$	40.1766	40.0856	40.2530	39.7947	39.9717	40.4180	39.9901
initial value							
$(^{87}Sr/^{86}Sr)_i$	0.703257	0.703123	0.703134	0.703208	0.703401	0.703332	0.703231
$(^{143}Nd/^{144}Nd)_i$	0.512841	0.512882	0.512879	0.512895	0.512806	0.512790	0.512859
$(^{176}Hf/^{177}Hf)_i$	0.282931	0.282967	0.282971	0.282952	0.282905	0.282942	0.282958
$(^{206}Pb/^{204}Pb)_i$	20.295	20.312	20.485	19.844	19.838	20.525	20.088
$(^{207}Pb/^{204}Pb)_i$	15.687	15.683	15.684	15.679	15.691	15.687	15.677
$(^{208}Pb/^{204}Pb)_i$	40.170	40.079	40.247	39.794	39.969	40.411	39.984
εNd_T	4.15	4.95	4.88	5.17	3.46	3.15	4.49
εHf_T	5.19	6.46	6.60	5.90	4.28	5.59	6.15

Table 6 | *(continued)*

unit	Bioko	Etinde	Etinde	Etinde	Etinde	Etinde
sample name	BK22	2208A	2208B	2208C	2208D	CA062
age (Ma)	1.33	0.27	0.50	0.50	0.50	0.43
type	2	1	1	1	1	1
$^{87}Sr/^{86}Sr$	0.703476	0.703291	0.703320	0.703316	0.703322	0.703301
±2SE	0.000007	0.000007	0.000006	0.000007	0.000007	0.000006
$^{143}Nd/^{144}Nd$	0.512786	0.512825	0.512792	0.512811	0.512803	0.512825
±2SE	0.000009	0.000008	0.000008	0.000007	0.000007	0.000007
$^{176}Hf/^{177}Hf$	0.282880	0.282939	0.282914	0.282908	0.282914	0.282933
±2SE	0.000003	0.000004	0.000005	0.000004	0.000005	0.000004
$^{206}Pb/^{204}Pb$	19.9181	20.5972	20.5994	20.5875	20.5824	20.5553
$^{207}Pb/^{204}Pb$	15.6755	15.6681	15.6734	15.6761	15.6708	15.6712
$^{208}Pb/^{204}Pb$	39.9765	40.4492	40.4668	40.4555	40.4343	40.3664
initial value						
$(^{87}Sr/^{86}Sr)_i$	0.703474	0.703290	0.703320	0.703315	0.703321	0.703301
$(^{143}Nd/^{144}Nd)_i$	0.512785	0.512825	0.512792	0.512811	0.512803	0.512825
$(^{176}Hf/^{177}Hf)_i$	0.282880	0.282939	0.282914	0.282908	0.282914	0.282933
$(^{206}Pb/^{204}Pb)_i$	19.911	20.593	20.593	20.583	20.577	20.548
$(^{207}Pb/^{204}Pb)_i$	15.675	15.668	15.673	15.676	15.671	15.671
$(^{208}Pb/^{204}Pb)_i$	39.969	40.444	40.460	40.447	40.426	40.358
εNd_T	3.06	3.81	3.17	3.54	3.39	3.82
εHf_T	3.38	5.46	4.57	4.36	4.56	5.23

CHAPTER 5: DISCUSSION

5.1 Classification of source components of the CVL parental magma

In order to evaluate the source materials for the CVL, I first classify the samples based on the trace element compositions. Most of the CVL samples show unique trace element patterns having negative anomalies of K, Pb, P, Zr, Hf, and Ti (Figure 4-5) along with the general enrichment of the highly enriched incompatible elements, which is distinct from the MORB or OIB except for HIMU basalts (Willbold and Stracke, 2006). The negative anomalies of Zr, Hf, and Ti indicate the influence of melt derived from the carbonatite-metasomatized SCLM or CO_2-rich melt formed at the garnet-peridotite stability condition because of their high partition coefficients relative to REE between carbonatite and garnet (Dasgupta et al., 2009).

To evaluate the influence of carbonatitic melt in the source, the CVL samples are classified into Type 1 and Type 2 based on the Hf/Sm and Ti/Gd (Fig. 5-1). Type 1 is defined for the samples having both the Hf/Sm_N and Ti/Gd_N are <1, where the ratio with $_N$ is the primitive mantle normalized ratio. Type 1 show negative anomalies of K, Pb, Sr, P, Zr, Hf, and Ti (Figs. 5-2 and 5-3), most of which resemble to Group 1 kimberlite and the Siberian High-Mg high-density fluids (HDFs) in the diamond xenocryst in kimberlite (Fig. 5-4). Among the Type 1 samples, those from SW volcanos (Annobon, Sao Tome, and Principe) shows relatively flat pattern for P and positive anomaly for Ba, while those for NE volcanoes (Etinde and Mt. Cameroon) show negative anomalies of P and Ba (Fig. 5-3). The Bioko, located in between those volcanoes, show intermediate patterns (Fig. 5-3). Type 1 samples show positive correlation between Ba/Th and P/Nd (Fig. 5-5). The NE volcanoes and lower P/Nd Bioko data show positive correlation between K/La and P/Nd while others do not show clear correlation (Fig. 5-5). Phosphorous content of the mantle-derived melt is primarily controlled by accessory phosphate minerals and secondary by garnet (Konzett et al., 2012). Garnet has the highest partition coefficient for P among the constituent minerals in peridotite, and it increases with increasing pressure (Konzett et al., 2012). However, the NE and SW samples do not show negative correlation on the plot of P/Nd vs. Gd/Lu (Fig. 5-5), suggesting that variation of P/Nd between NE and SW magmas was not controlled by the melt-garnet partitioning. Thus, depletion of P along with K and Ba for NE volcanoes could be presence of the complex K-Ba-phosphate phase which is

stable near-solidus phase at 4-7Ga (Mitchell, 1995) or the remaining of mixture of phosphate (e.g. apatite) and K-rich rich phase (e.g. K-richterite) as a residual phase.

The Pb isotopic composition of the Type 1 NE and SW samples consistently show distinct isotopic trends (Fig. 5-6). The distinct $^{207}Pb/^{204}Pb$ at a given $^{206}Pb/^{204}Pb$ among the NE and SW volcanoes reveals that they are formed from the different source materials either by distinct age or $^{238}U/^{204}Pb$. Bioko forms mixing trend between the NE and SW data, and this relationship consistently observed in the plot of $^{206}Pb/^{204}Pb$ vs. $[P/Nd]_N$ (Fig. 5-5). This mixing trend is also observed for other isotopic compositions (Fig. 5-7).

Type 2 samples are mostly from SW volcanoes and Bioko. Only two samples from Mt. Cameroon can be classified as Type 2 from NE volcanos, although they show nearly the boundary of classification definition. Thus, it can be regarded that the Type 2 samples are basically coexisted only with the Type 1 SW magma. On the plot of $^{206}Pb/^{204}Pb$ vs. $^{207}Pb/^{204}Pb$ and $^{206}Pb/^{204}Pb$ vs. $^{208}Pb/^{204}Pb$, those of Type 2 samples tend to extend toward the common composition: higher $^{208}Pb/^{204}Pb$ for Annobon and Sao Tome and lower $^{206}Pb/^{204}Pb$ for Bioko relative to the Type 1 (Fig. 5-6). These Type 2 samples also show the higher $^{87}Sr/^{86}Sr$ and lower $^{143}Nd/^{144}Nd$ and $^{176}Hf/^{177}Hf$ (Fig. 5-7). These isotopic signatures decipher that the variation of Type 2 samples must be controlled by the mixing of the component which extend the above-mentioned trends.

5.2. Estimation of source components

Geophysical data revealed that the CVL are located along the NW edge of the Congo craton (Fig. 1-1). The continental rift model also demonstrated the wide distribution of African SCLM beneath the Atlantic Ocean (Beaumont and Ings, 2012; Huismans and Beaumont, 2011). Thus, it is plausible that these SCLM is a common source for the CVL. Here I will evaluate the possible source materials for the parental magmas of Type 1 NE, Type 1 SW, and Type 2 lavas by the plausible source materials that can exist in the SCLM without considering the recycled components such as EM1, EM2, and HIMU. Since Pb isotopic composition is more sensitive to identify the different source materials, the evaluation is basically performed by Pb isotopic systematics. Then the consistency will be evaluated by other isotopes.

5.2.1. Contamination of the continental upper and lower crusts

Mantle-derived magma may have experienced the crustal contamination during its ascend in the crustal region. Thus, contamination of upper and crustal material will be evaluated first. Low Ce/Pb ratio is regarded as one of the diagnostic features for contamination of upper continental crust (UCC), due to the significantly higher concentration of Pb in the continental crust relative to mantle-derived magma (Miller et al., 1994). Hofmann et al. 1986 have shown that OIB and MORB mantles have high and relatively constant ratios (25+/-5), whereas the UCC has much lower ratios, 3.2 (Taylor et al., 1985). All the analyzed samples display high Ce/Pb between 13 and 103, suggesting insignificant UCC contamination (Fig. 5-8). The plot on Rb/Nb vs. Ba/Nb diagram (Willbold and Stracke, 2006) also suggests little effect of UCC contamination for the studies samples (Fig. 5-8). Although relatively higher SiO_2 for Type 2 Annobon than that for Type 1 Annobon suggest UCC contamination, the Pb isotopic trend from Type 1 to Type 2 Annobon is distinct from that for the UCC. Presence of mantle xenolith and mantle-derived xenocrysts in many samples suggests rapid magma ascend, avoiding significant contamination of upper crust. Previous studies also insisted insignificant crustal contamination not only for oceanic sector but also for continental sector CVL lavas based on the petrological and geochemical evidences (Aka et al., 2004; Ballentine et al., 1997; Halliday et al., 1988; Lee et al., 1996; Rankenburg et al., 2004). Thus, I do not consider the effect of upper crustal contamination in the following discussion.

The Rb/Nb vs. Ba/Nb diagram (Fig. 5-8) suggest the involvement of ~1% of average LCC component into the DM or HIMU source mantle component for the Type 2 Annobòn lavas. The Ba/Nb of Annobòn lavas show positive correlation $^{87}Sr/^{86}Sr$ (R^2=0.87) (Fig. 5-8) and negative correlation with $^{143}Nd/^{144}Nd$ (R^2=0.78) and $^{176}Hf/^{177}Hf$ (R^2=0.70) (not shown). Thus, it is likely that the variation of $^{207}Pb/^{204}Pb$ and $^{208}Pb/^{204}Pb$ against $^{206}Pb/^{204}Pb$ observed in Annobòn lavas were attributed to the involvement of LCC component into the less radiogenic Pb component. Although these trace element compositions indicate the involvement of LCC component for the Type 2 magma, the Pb isotopic composition of the LCC from African continent show much lower $^{207}Pb/^{204}Pb$ and $^{208}Pb/^{204}Pb$ than the Type 2 lavas (Fig. 5-9), thus it is unlikely that the Pb isotopic

trend that extend from Type 1 to Type 2 Annobon are caused by the contamination of LCC.

5.2.2. MORB-source asthenospheric mantle

The asthenospheric mantle which must reside beneath the oceanic and continental lithospheric mantle is defined by the compilation of Atlantic MORB between 30°N and 30°S (PetDB database, http://www.earthchem.org/petdb). All the compile data are shown in the Supplementary Table 1. The Sr, Nd, Hf, and Pb isotopic compositions of most of the CVL samples are distinct from the MORB. Therefore, the depleted MORB-type mantle source cannot be a major source for the CVL magmas.

5.2.3. Ancient asthenospheric mantle-derived melt

The isotopic compositions of the ancient asthenospheric mantle-derived melt which could have metasomatized the lithospheric mantle is calculated based on the elemental and isotopic composition of the MORB-source asthenospheric mantle compositions with various degrees of melting (Fig. 5-10). Calculation was performed under the garnet-peridotite condition at 7GPa (Walter, 1998) because (1) the thickness of cratonic lithosphere is estimated to ~200 km (Sleep, 2005), (2) the asthenospheric mantle-derived metasomatic agent can be expected as carbonatite or highly alkaline melt, and (3) the ^{238}U-^{230}Th data of the Mt. Cameroon lavas revealed the presence of garnet in the source (Yokoyama et al., 2007). The calculation was performed at the various ages: 600, 280, 130, and 30 Ma, which correspond for Pan African cycle (Djomani et al., 1995), Artinskian stage when shallow shelf was developed along the current coast line of west Africa (Torsvik and Cocks, 2011), opening of the south Atlantic (Fairhead, 1988), and the beginning of CVL volcanism, respectively (Fig. 5-11). The Sr, Nd, Hf, and Pb isotopic compositions of the asthenospheric mantle is estimated from the averaged values of the compiled Atlantic MORB between 30°N and 30°S (Supplementary Table 1) and the enriched end of the MORB-source mantle, which are denoted as DMM (depleted MORB source mantle) and E-DMM (enriched-DMM), respectively (Table 8). The used compositions of parent and daughter elements (Table 8) are after Workman and Hart (2005).

The trace element compositions of metasomatic agent (C_L) was calculated by non-modal batch melting equation (Shaw, 1970):

$$C_L = \frac{C_0}{D_0 + F(1-P)}$$

where C_0 is an initial concentration in the source (DMM and E-DMM in Table 8), D_0 is distribution coefficient at a start of melting, and F is fraction of melting. P is defined as $\sum p^i K_o^i$, where p^i and K_0 are fractional contribution of phase to the melt and partition coefficient of phase i. The compositions of parent and daughter elements was calculated both for silicate melt and carbonatite melt (parameters are shown in Table 9). Type 1 samples imply the involvement of carbonatitic melt and the common thickness of cratonic lithosphere is estimated to about 200 km (Sleep, 2005), modal composition and melting proportions were calculated for garnet-peridotite at 7 GPa and 17.7 wt%. melt-extracted fertile peridotite (Walter, 1998) for DMM and fertile peridotite (Walter, 1998) for E-DMM (Table 9). For the carbonatite melt model, calculation was performed only for E-DMM using the same modal composition and melting proportions for silicate melt model. Partition coefficient between mineral and silicate melt are after (Halliday et al., 1995; Kelemen et al., 2003; McKenzie and O'Nions, 1991; Wittig et al., 2010; Zindler and Jagoutz, 1988) and between mineral and carbonatite are after (Dasgupta et al., 2009), which are summarized in Table 9. The calculated result with various degree of melting are shown in Tables 10 and 11 and Figures 5-12 and 5-13).

The calculated results reveal that the ancient asthenospheric mantle-derived melt can be the source of the Type 1 NE parental magmas (Fig. 5-10). As the trace element pattern indicated, the source for Type 1 samples must be influenced by carbonatitic or ultra-low degree of melt. Thus, it is likely that the metasomatic agent to form the rejuvenated lithospheric mantle was initially fertile and isotopically enriched composition. The model calculation suggests that the Pb isotopic range of the Type 1 NE samples can be reproduced by the low degree of melt from the fertile asthenospheric mantle during the continental breakup at ~130Ma. The Sr and Nd isotopic composition also support this model. On the other hand, the Pb isotopic compositions of the Type 1 SW and Type 2 differ from these metasomatic compositions. The Type 1 NE component show high

$^{206}Pb/^{204}Pb$ up to 20.6, which are often referred as HIMU. However, it is distinct from the typical HIMU component which is characterized by the St. Helens samples (Fig. 5-10).

5.2.4. Lower part of SCLM

The lowermost part of the SCLM, which can be spread in this region (Beaumont and Ings, 2012; Huismans and Beaumont, 2011) can be a source of the CVL magma. Kimberlite has the potential to provide the nature and composition of deep part of SCLM close to the lithosphere-asthenosphere boundary (Fig. 5-14), which could be the most fertile portion of the SCLM with the lowest solidus temperature. To estimate the present isotopic compositions of the lowermost part of cratonic mantle (Kalahari, Congo, and West Africa cratons), the time-progressed isotopic compositions of the initial isotopic compositions of the published data were first calculated. The calculation was performed with various $^{238}U/^{204}Pb$ (μ) and $^{232}Th/^{238}U$ (κ) values. The current isotopic compositions of the SCLM calculated from Group 1 and Group 2 kimberlites are denoted as Group 1 SCLM and Group 2 SCLM, respectively. The data used are bulk kimberlite (Becker and le Roex, 2006; Davies et al., 2001; Donnelly et al., 2011; Hoal, 2003; Kramers, 1977; Nowell et al., 2004; Smith, 1983; Walker et al., 1989; Weis and Demaiffe, 1985; Wu et al., 2013); groundmass perovskite (Donnelly et al., 2012; Griffin et al., 2014; Kamenetsky et al., 2014; Wu et al., 2013); cpx megacryst (Sr & Nd) (de Bruin, 2005), cpx, garnet, ilmenite, zircon (Nowell et al., 2004), cpx and garnet (Davies et al., 2001). The calculated results are shown in Supplementary Table 4.

Since the isotopic variations of Sr and Nd for kimberlite are widely spreading for the ranges both for MORB and all CVL, they cannot be used to discriminate the source materials. The number of Hf isotopic data for kimberlite samples are limited and the re-calculated data is highly sensitive to the assumed Lu/Hf which can have variable values for the kimberlite source, so that the Nd-Hf isotope systematics will be only used for the supportive evidences. Thus, the calculation is initially done only for Pb isotopic composition. Major and trace element compositions of compiled African Kimberlite and carbonatitic melt inclusions are shown in Table 7.

As the trace element pattern revealed (Fig. 5-2), it is unlikely that the Group 2 SCLM as a source for Type 1 CVL magma because of their too low $^{206}Pb/^{204}Pb$, $^{143}Nd/^{144}Nd$, $^{176}Hf/^{177}Hf$ and too high $^{87}Sr/^{86}Sr$ compositions relative to CVL. Melting of the Group 1 SCLM can explain the Pb isotopic variation of Type 1 SW samples at the plausible $^{238}U/^{204}Pb$ (μ) and $^{232}Th/^{238}U$ (κ) values (Figs. 5-15 and 5-16). Most of the Nd and Hf isotopic compositions of the Type 1 SW samples also accord with the range of Group 1 SCLM. On the other hand, the $^{207}Pb/^{204}Pb$ of NE Type 1 samples are lower and the $^{208}Pb/^{204}Pb$ of Type 2 samples are higher than those range of Group 1 SCLM at a given $^{206}Pb/^{204}Pb$. Thus, it is impossible that the Group 1 SCLM can be a source of Type 1 NE and Type 2 parental magmas.

5.2.5. Type 2 component

The Type 2 component defined in this study resembles to the EM1 (enriched mantle 1) component (Zindler and Hart, 1986). Involvement of EM1 component into the Annobon and Sao Tome have already discussed elsewhere (Lee et al., 1994). Lee et al. (1994) predicted that oceanic CLV were formed by melting of upwelling mantle plume which was originally dominated in HIMU component, and the mixture of DM-EM1 component was entrained from the ambient mantle. The source of EM1 was estimated as either ancient pelagic sediments in the source or delaminated subcontinental lithosphere (Lee et al., 1994). These studies, however, do not show the actual material which can be a source for their EM1 component.

The Type 2 Annobon show higher SiO_2, Rb/Nb, Zr/Nb, Ba/Nb, La/Nb, K/La, Nd/Sr, Pb/Ce, $^{87}Sr/^{86}Sr$ and lower $^{143}Nd/^{144}Nd$ and $^{176}Hf/^{177}Hf$ relative to those of the Type 1 Annobon. As described before, the above-mentioned trace element ratios suggest the lower crust (i.e. granulite) for the EA component (Willbold and Stracke, 2006). However, the $^{208}Pb/^{204}Pb$ of lower crust obtained from African continent are too low to explain for Type 2 magma. All of these geochemical signature is also consistent to the characteristics of Group 2 kimberlite relative to Group 1 kimberlite (Becker and le Roex, 2006). However, the $^{207}Pb/^{204}Pb$ and $^{208}Pb/^{204}Pb$ of the current Group 2 kimberlite source SCLM (Group 2 SCLM) are again too low to explain the Pb isotopic trend of EA component. Among the lower crustal and mantle xenoliths compiled from cratonic and near cratonic

regions of Africa, only the pyroxenite xenolith collected from Toro-Ankole volcanic region, SW Uganda in the Western blanch of the East African Rift (Davies and Lloyd, 1989) show the elevated $^{207}Pb/^{204}Pb$ and $^{208}Pb/^{204}Pb$ values that can explain the Type 2 component (Fig. 5-9). The Tro-Ankole region is located in rifting zone of the continuous Congo and Tanzania cratons in Uganda (Globig et al., 2016; Rosenthal et al., 2009). These pyroxenite xenoliths and pyroxene xenoctysts in the Tro-Ankole region yielded an age of ~1.9 Ga, which are interpreted as derived from the layer of veins in the SCLM peridotite of Congo-Tanzania craton (Davies and Lloyd, 1989; Lloyd et al., 1999; Rosenthal et al., 2009). Thus, pyroxenite vein/layer in the cratonic SCLM which formed during Archaean or Proterozoic is the best candidate for the Type 2 component. The close relationship of Type 2 component coexisted only with Type 1 SW parental magmas which are estimated to have derived from lowermost part of SCLM is consistent to this result.

5.2.6. Summary for the source components of CVL

Figure 5-17 shows the summary of estimated source components of CVL. The systematic isotopic trend of the Type 1 samples from SW to NE indicates that the dominant melting region of the CVL parental magma changed from Group 1 SCLM to rejuvenated lithospheric mantle. Melting of pyroxenite vein/layer in the Group 1 SCLM may affect the isotopic variation from Type 1 SW to Type 2 samples. Since the Sr, Nd, Hf, and Pb isotopic variations of the CVL can be explained by these SCLM components, no recycled material nor deep mantle plume component are necessary for their genesis.

5.3 Origin of West African passive margin intraplate basalts

The CVL is the one of the example of intraplate basalts locating along the passive continental margin. There also exist several intraplate basalts at the western offshore of African continent: e.g. Madeira Islands, Canary Islands, Cape Verde Islands, and Cameroon volcanic line (CVL) from north to south, and their closely related continenal region: Atlas mountains, continental sector of CVL, and Benue trough (Fig. 1-1). The representative common characteristics of west African passive margin intraplate basalts (WAPM-IB) are the large distribution of highly alkaline volcanics including carbonatite and the long duration of volcanic activities in the same volcanic region: ~72 My for

Medeira Islands (Geldmacher et al., 2000), ~142 My for Canary Islands (van den Bogaard, 2013), 15-25 My for Cape Verde Islands (Mitchell et al., 1983), and ~30 My for CVL (Lee et al., 1994). The heterogeneous elemental and isotopic compositions of the WAPM-IB are explained by the mixing of the upwelling mantle plume that contains lower mantle material and recycled ancient crustal or lithospheric mantle materials; depleted MORB source mantle; and the delaminated SCLM. However, no clear age propagation of the hot-spot tracks despite their extended eruptive activity in each archipelago, suggest the difficulty to explain their magma genesis by a model involving a simple long-lived upwelling mantle plume.

Geographically, WAPM-IB are located both in the oceanic and continental setting. However, the seismic tomography image reveals that remnants of cratonic lithospheric fragments are widespread beneath these regions (Begg et al., 2009; O'Reilly et al., 2009) (Figs. 1-1 and 2-3). The evidence for the presence of Archaean to Proterozoic African sub-continental lithospheric mantle (SCLM) beneath this region was also proved by the peridotite xenolith in Cape Verde Islands (Coltorti et al., 2010). Because detached depleted cratonic SCLM is buoyant relative to the convecting mantle, it is likely that they are widespread beneath the Atlantic Ocean after its opening (Coltorti et al., 2010). The WAPM has been recognized as the type II margins which is characterized by the ultra-wide regions of the thin continental crust, which can be generated by the breakup of the lower lithosphere before the break up of upper lithosphere (Huismans and Beaumont, 2011). The widely distributed continental lithosphere beneath the western offshore of the African continents (Begg et al., 2009; O'Reilly et al., 2009) is consistent with this model. The presence of enriched mantle component (EM1 and EM2) in the WAPM-IB could be attributed to the interaction of continental remnant mixed into the plume and/or MORB-source mantle-derived magma (O'Reilly et al., 2009). The lavas in the WAPM show low $^{3}He/^{4}He$ except for several samples from the northern Island of Cape Verde (Doucelance et al., 2003). The short–lived ^{182}Hf-^{182}W system for Canary Island sample consistently shows normal $^{182}W/^{184}W$ value which is indistinguishable from normal mantle value (Mundl et al., 2017). Thus, even if these sources of the WAPM-IB are derived for large, low-shear-velocity provinces (LLSVPs), their characteristics is distinct from those of Hawaii, Iceland, and Samoa which have low $^{182}W/^{184}W$ and high $^{3}He/^{4}He$ values (Mundl

et al., 2017).

The result of this study demonstrates that all the source materials for the CVL volcanoes can be derived from the African SCLM without external 'plume' component. To investigate this model for other WAPM-IB, Sr, Nd, Hf, and Pb isotopic composition of Madeira Islands, Canary Islands, Atlas Mountains, Cape Verde Islands, and continental sector of CVL (Abratis et al., 2002; Aparicio et al., 2010; Asaah et al., 2015; Aulinas et al., 2010; Ballentine et al., 1997; Barker et al., 2009, 2010; Berger et al., 2014; Bosch et al., 2014; Christensen et al., 2001; Cousens et al., 1990; Davies et al., 1989; Day et al., 2010; Deegan et al., 2012; Del Moro et al., 2015; Doucelance et al., 2014; Doucelance et al., 2003; Doucelance et al., 2010; Duggen et al., 2005; El Azzouzi et al., 1999; Escrig et al., 2005; Geldmacher and Hoernle, 2000; Geldmacher et al., 2011; Geldmacher et al., 2006; Geldmacher et al., 2001; Gerlach et al., 1988; Gurenko et al., 2006; Gurenko et al., 2009; Halliday et al., 1990; Hildner et al., 2012; Hoernle et al., 1991; Holm et al., 2006; Johansen et al., 2005; Jørgensen and Holm, 2002; Marcantonio et al., 1995; Martins et al., 2010; Mata et al., 1998; Millet et al., 2008; Mourão et al., 2012; Natali et al., 2013; Nkouandou et al., 2008; Ovchinnikiva et al., 1995; Prægel and Holm, 2006; Rankenburg et al., 2005; Simonsen et al., 2000; Tchuimegnie Ngongang et al., 2015; Thirlwall et al., 1997; Thomas et al., 1999; Turner et al., 2015; Wagner et al., 2003; Whitehouse and Neumann, 1995; Wiesmaier et al., 2011) and Atlantic MORB (Agranier et al., 2005; Andres et al., 2004; Debaille et al., 2006; Dosso et al., 1991; Fontignie and Schilling, 1996; Haase et al., 2016; Hoernle et al., 2011; Moeller, 2002; Paulick et al., 2010; Schilling et al., 1994; Stroncik and Niedermann, 2016; Ulrich et al., 2012; White and Schilling, 1978; Wilson et al., 2013; Yu, 1993) are compared with CVL (this study) (Fig. 5-18). Sr, Nd, Hf, and Pb isotopic compositions of the compiled data were normalized to $^{87}Sr/^{86}Sr$ = 0.71024 for SRM 987, $^{143}Nd/^{144}Nd$ = 0.51186 for La Jolla, $^{176}Hf/^{177}Hf$ = 0.28216 for JMC-475, $^{206}Pb/^{204}Pb$ = 16.9424, $^{207}Pb/^{204}Pb$ = 15.5003, and $^{208}Pb/^{204}Pb$ = 36.7266 for SRM 981. All the Pb isotopic data plotted in $^{206}Pb/^{204}Pb$ vs. $^{207}Pb/^{204}Pb$ and $^{206}Pb/^{204}Pb$ vs. $^{208}Pb/^{204}Pb$ diagrams and principal component analysis was calculated (PCA, N = 707). All the samples except Madeira (because all the available Pb data for Madeira were analyzed by conventional method) were analyzed by double spike method and Tl-doped method. The $^{206}Pb/^{204}Pb$ data for Canary Islands and Cape Verde plotted

with $^{87}Sr/^{86}Sr$, $^{143}Nd/^{144}Nd$, $^{176}Hf/^{177}Hf$ include conventional data.

The Principal Component Analysis (PCA) result indicates that the Canary Islands, Atlas Mountains, continental sector of CVL, and most of the Cape Verde Islands data can be formed by the same source of CVL (Fig. 5-19). Only the part of Cape Verde Islands and Madeira may involve the difference source materials (Fig. 5-19). The Sr, Nd, Hf, and Pb isotopic compositions consistently show that most of WAPM-IB except Madeira and parts of Cape Verde are within the range of those of CVL (Figs. 5-18 and 5-20). The isotopic data of Madeira are close to or within the range of Atlantic MORB, but showing distinctly lower $^{207}Pb/^{204}Pb$ at a given $^{206}Pb/^{204}Pb$ than the MORB and CVL. The isotopic trend of Madeira on the plot of $^{206}Pb/^{204}Pb$ vs. $^{207}Pb/^{204}Pb$ suggests that the source of Madeira can be composed of mixture of asthenospheric-mantle-derived metasomatic agent at <~130 Ma and the current asthenospheric mantle. The geophysical data and numerical models (Beaumont and Ings, 2012; Begg et al., 2009; Huismans and Beaumont, 2011; O'Reilly et al., 2009) revealed that the these WAPM-IB except for Madeira are located on or near the edge of cratonic SCLM which is widely distributed beneath the Atlantic Ocean. The absence of SCLM beneath the Madeira Island (Fig. 1-1) is consistent with the isotope systematics. Figure 5-21 shows the reconstructed tectonic map of the Mesozoic African-South American continents and the rift axis. On the Fig. 5-21, current location of the WAPM-IB are traced. The location of the Canary Islands, Atlas Mountains, Cape Verde, and CVL are located on or near the Mesozoic rift axis where the continent broke-up. Therefore, it is feasible that the SCLM exists beneath these regions.

Among all WAPM-IB, only some basanites from Middle Atlas show similar Pb isotopic compositions with the Type 1 NE CVL samples. The Pb isotopic trend of these Atlas samples extend to the basanite lavas in Canary Islands ($^{206}Pb/^{204}Pb$ <20.27) (Day et al., 2010; Gurenko et al., 2006). Previous studies insisted that the high-$^{206}Pb/^{204}Pb$ components in the Canary-Atlas chain magma were derived from the HIMU-like components in the upwelling mantle plume (Day et al., 2010; Duggen et al., 2005; Duggen et al., 2009; Geldmacher et al., 2011; Gurenko et al., 2006; Gurenko et al., 2010; Gurenko et al., 2009; Hoernle et al., 1991). The common characteristics of these Atlas-Canary high $^{206}Pb/^{204}Pb$ samples (>20.1) is their silica undersaturated (basanite or

nephelinite) composition (Bosch et al., 2014; Day et al., 2010; Duggen et al., 2005; Gurenko et al., 2006). In other Canary Island samples, silica undersaturated mafic lavas tend to have the radiogenic Pb isotopic compositions (Hoernle et al., 1991). These studies indicated that the HIMU-like component in Canary-Atlas chain was derived from the ancient subducted/recycled oceanic crust in the plume. These explanations, however, cannot explain (1) why the plume-originated highest $^{206}Pb/^{204}Pb$ magmas were formed at the edge of the thick continental region both in CVL and Canary-Atlas regions, (2) why the most silica undersaturated magma were derived from the silica-enriched pyroxenite, eclogite, or pyroxenite-peridotite mixture source materials, and (3) why the more fertile source forms low-degree of highly alkaline melts. Moreover, it is not necessary to bring extra component to form the high $^{206}Pb/^{204}Pb$ Type 1 NE CVL and Canary-Atlas chain magmas as explained in this study.

The heavily acid-leached clinopyroxene separates in SCLM peridotite xenolith in the Middle Atlas Quaternary volcanoes which are estimated to have metasomatized by carbonatite melt also have Type 1 NE CVL-like Pb isotopic composition (Wittig et al., 2010). During the late Triassic and early Jurassic, the Moroccan microcontinent separated from the northwest African continent, forming the Atlas Rift, followed by the rift structure inverted during the Cenozoic, forming the current Atlas Mountains (Schettino and Turco, 2009). Thus, SCLM beneath the Atlas Mountains could have been metasomatized by the asthenospheric mantle-derived melt at ~200 Ma during the continental breakup, the same mechanism for the Type 1 NE CVL component. The lithospheric thinning beneath the Atlas Mountains at the NW edge of West African craton has been also observed by geophysical data (Schettino and Turco, 2009). These Pb isotopic systematics formed by Mt. Cameroon, Etinde, and highly alkaline Atlas Mountain samples are distinct from any other African and its vicinity volcanics (36ºN-38ºS and 25ºW-60ºE, GEOROC data base, http://georoc.mpch-mainz.gwdg.de/georoc/). We thus insist that this isotopic trend is a unique character for the lithospheric mantle rejuvenated during the Jurassic-Cretaceous continental breakup.

The isotope systematics of Cape Verde magmas can also be explained by the Group 1 SCLM, rejuvenated lithosphere, and pyroxenite vein/layer in the SCLM. The

Cape Verde Islands are located ~500km west of the African continents. Although it locates far from the African continental edge, tomographic image reveals that the SCLM extends around the Cape Verde Island chains (Fig. 1-1). The Sr, Nd, Pb, He, and Ar isotopic variation of the Cape Verde Islands have been explained by the mixing of variable mantle components including HIMU, EM1, and DM in the upwelling mantle plume (Christensen et al., 2001; Gerlach et al., 1988). Later studies, on the other hand, insisted that the involvement of the remnant of African SCLM fragments into the upwelling Cape Verde plume contribute to characterize the EM1 signature for these magmas (Doucelance et al., 2003; Escrig et al., 2005). The presence of the Archaean to Proterozoic SCLM remnant, the detached fragments of the African SCLM during opening the Atlantic Ocean, beneath the Cape Verde Islands has been also revealed by the petrological and isotopic characteristics of mantle xenolith in the Cape Verde lavas (Bonadiman et al., 2005; Coltorti et al., 2010). Thus, since the presence of African SCLM beneath the Cape Verde Islands is evident, it is likely that the isotopic variation of Cape Verde basalts was formed by the mixing of the proposed three components. Only the undegassed lower mantle component can be involved for the northern Cape Verde Islands which are characterized by high $^{3}He/^{4}He$ (Doucelance et al., 2003). Since the northern Cape Verde Islands are located off-rift zone of the Mesozoic rift axis, magma genesis of these islands can be affected by the different process relative to southern Islands. To solve this problem, further study should be necessary.

5.4. Heat source and melting process

Although the geochemical studies have insisted the significant involvement of the recycled components in CVL, the heat source and melting process were not clearly explained (Halliday et al., 1990; Halliday et al., 1988; Lee et al., 1994). In the Canary and Cape Verde Islands and Atlas Mountains, the heterogeneous geochemical components especially for the involvement of HIMU components has been explained by the plume hypothesis. Although the tomographic images do not show clear plume conduit from the core-mantle boundary to the WAPM-IB, influence of whole-mantle scale plume activities for the Canary and Cape Verde Islands has been inferred (French and Romanowicz, 2015).

On the other hand, tectonic-controlled small-scale convection of the

asthenospheric mantle either by the lithospheric instability or edge-driven convection model (Adams et al., 2015; Fourel et al., 2013; King, 2007; King and Anderson, 1998; Milelli et al., 2012; Reusch et al., 2010) has been proposed for the genesis of CVL magmatism. The numerical continental rift model for the passive continental margin (Beaumont and Ings, 2012; Huismans and Beaumont, 2011) also shows the edge-driven lateral flow of the asthenospheric mantle at the continent-oceanic boundary. In these models, tectonic-controlled mantle flow can be a heat source to melt the SCLM at the continent-oceanic lithospheric boundary. Since most of the erupted magma at the WAPM-IB are highly alkaline basalts and basanites, i.e. low degree of melt, significant thermal elevation is not necessary. Small thermal increase is enough to melt Carbonated peridotite which has much lower solidus temperature compared to dry Peridotite (Fig. 5-23).

The coincident distribution of CVL and Canary-Atlas chains at the NW edge of the cratonic lithospheric mantle where the mantle flow collide near the edge of the SCLM rather than at the front collision suggests that the heating of the SCLM by the edge-driven convection rather than the lithospheric instability can be the most effective process. The edge-driven convection can occur more than several tens Mys at the same location, forming the long duration of magmatism without showing the time-progressive linear hot spot track.

5.5. Summary

Finally, I propose the model for the magma genesis of WAPM-IB as follows (Fig. 5-22). During the initial stage of Mesozoic continental breakup, low-degree of partial melt formed by the upwelled asthenospheric mantle at the rift axis could metasomatize the lower part of the lithospheric mantle, forming the rejuvenated SCLM. After breaking up the SCLM at ridge axis, followed by forming MORB at >~40 My after the initial rifting, the lateral flow of asthenospheric mantle form edge-driven counter flow convection near the oceanic and continental boundary (King and Ritsema, 2000) (Missenard and Cadoux, 2012) (similar to the Model II-A in ref. (Huismans and Beaumont, 2011)). This edge-driven convection can elevate temperature in the SCLM beneath the Atlantic Ocean, melting the low solidus material at the lowermost part of the cratonic SCLM which had already metasomatized during Archaean to Proterozoic age.

Melt derived from the pyroxenite vein or layer that formed in the cratonic SCLM during Archaean or Proterozoic was also involved in the SCLM-derived melt. Current tomographic data reveal that the CVL, Canary Islands, and Cape Verde Islands are located along the edge of the continental lithospheric mantle. The reconstructed map of Pangea consistently shows that the location of Atlas, Canary, southern islands of Cape Verde, and CVL were located on or near the reconstructed rift zone during Jurassic to Cretaceous where the continental breakup initiated (Fig. 5-21). Thus, intraplate magmatism at the passive continental margin can be explained by melting of SCLM heated by the edge-driven mantle convection without considering the mantle plume. On the other hand, location of Madeira was off-rift axis during the continental breakup. This is consistent that the parental magma of Madeira can be explained by the large involvement of asthenospheric mantle and less involvement of SCLM. Although the whole mantle-scale tomographic image suggests the major distribution of hot spots at the Pacific and Atlantic Ocean should be closely connected ultralow velocity zone near the core-mantle boundary (French and Romanowicz, 2015), the intra-plate hot spot magmatism at the WAPM were not directly related to the whole-mantle scale mantle plume activity.

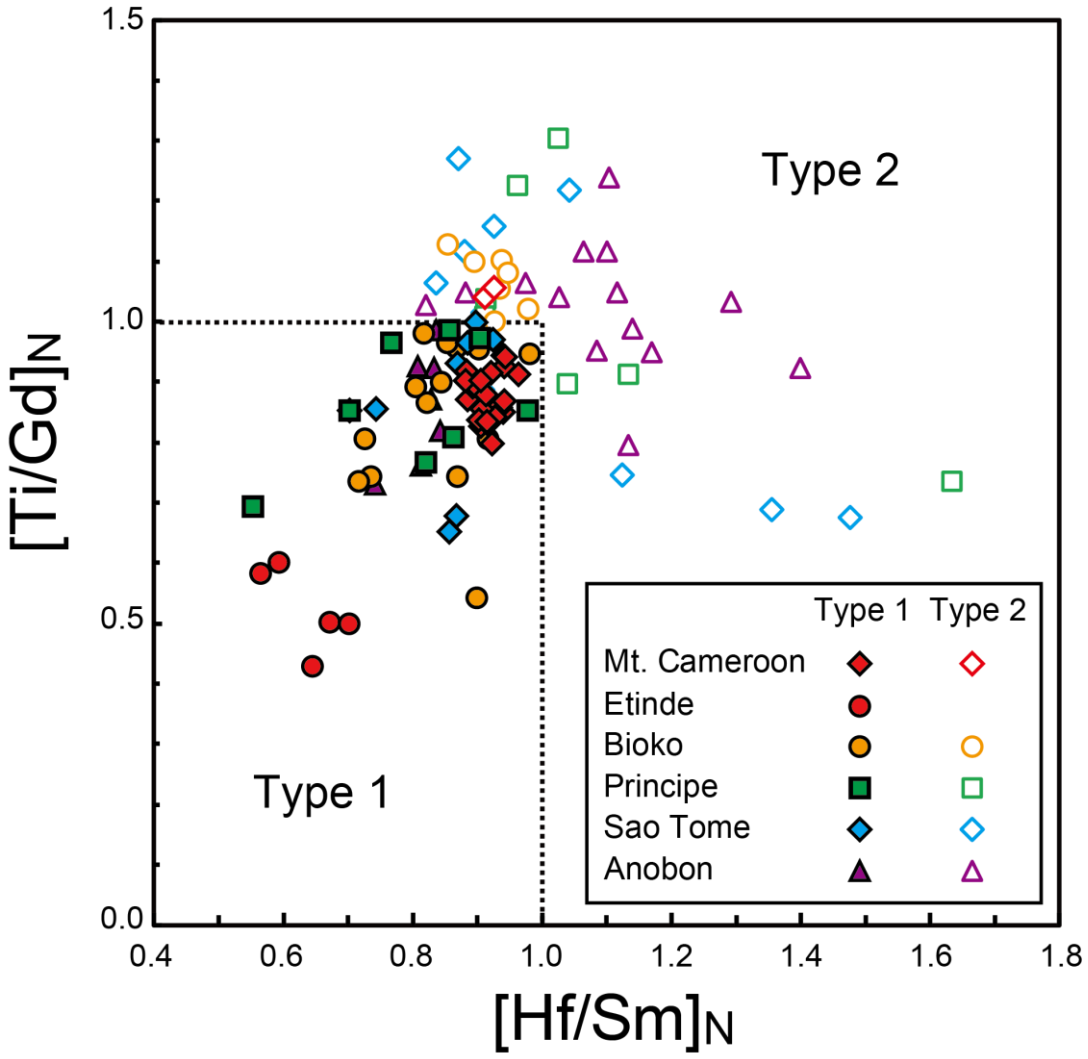

Figure 5-1 | Primitive mantle normalized Hf/Sm vs. Ti/Gd diagram for the CVL samples. Samples having $[Hf/Sm]_N<1$ and $[Ti/Gd]_N<1$ are classified as Type 1 and the others as Type 2. Primitive mantle compositions are after McDonough and Sun (1995).

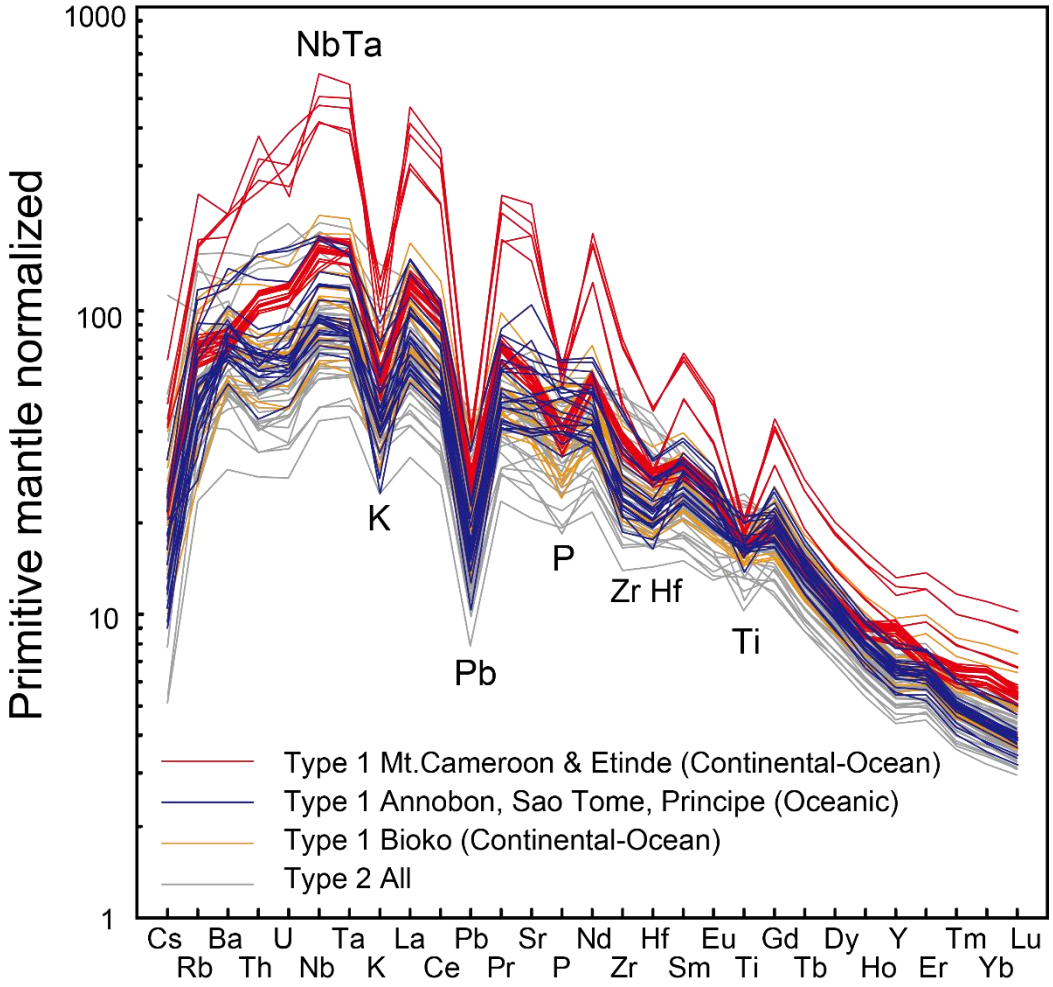

Figure 5-2 | Primitive mantle normalized incompatible element patterns of Type 1 and Type 2 samples from CVL. Primitive mantle compositions are after McDonough and Sun (1995).

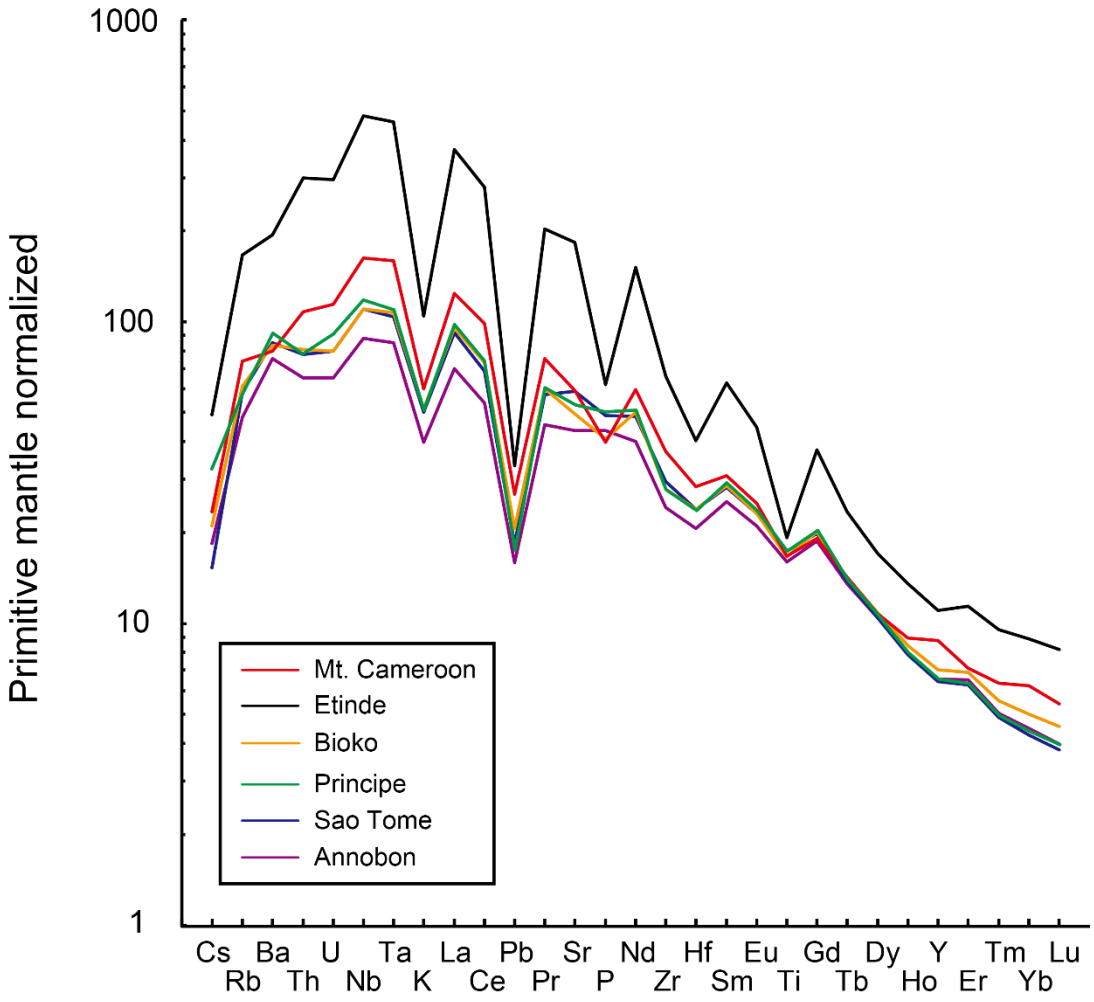

Figure 5-3 | Primitive mantle normalized incompatible element patterns for the Type 1 samples from CVL. Each line is average values of Type 1 samples for each volcanic region.

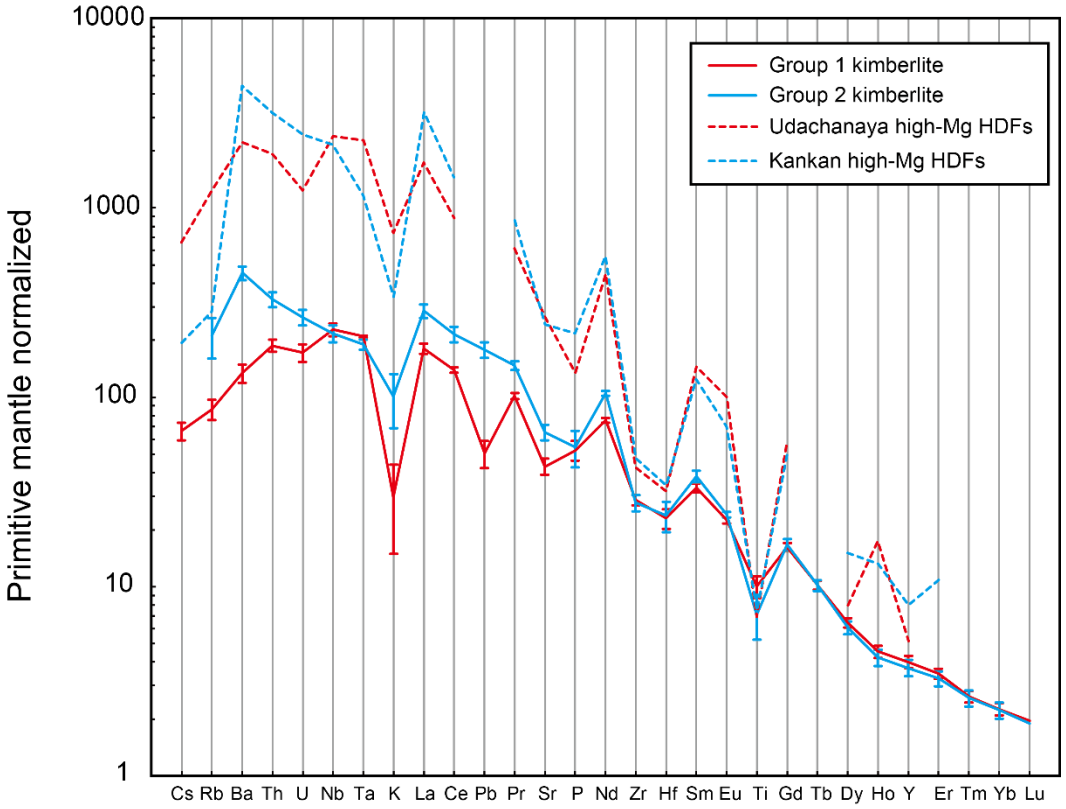

Figure 5-4 | Primitive mantle normalized trace patterns of the Group 1 and Group 2 kimberlites and high-Mg carbonatitic fluids from diamond inclusions. The average value of Group 1 and Group 2 kimberlite from Africa (Becker and le Roex, 2006; Becker et al., 2007; Coe et al., 2008; Donnelly et al., 2011; Galloway et al., 2009; Harris et al., 2004; Le Roex et al., 2003; Wu et al., 2013) and high-Mg carbonatitic high-density fluids (HDFs) from Udachanaya and Kankan (Weiss et al., 2011; Weiss et al., 2009). Error bars of the kimberlite values are 1 standard error. The average values plotted are shown in Table 7.

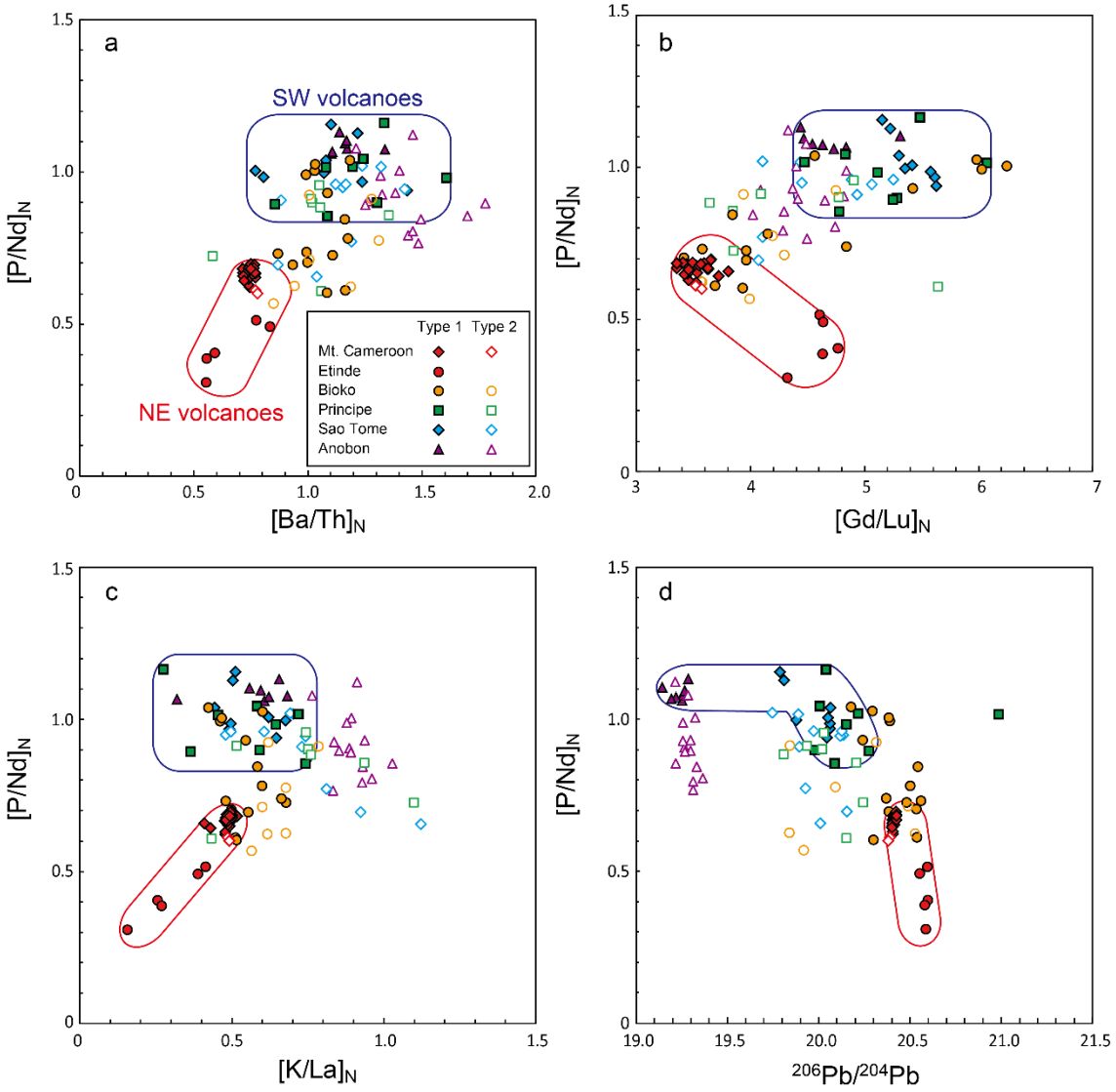

Figure 5-5 | a, $(Ba/Th)_N$ vs. $(P/Nd)_N$; b, $(Ga/Lu)_N$ vs. $(P/Nd)_N$; c, $(K/La)_N$ vs. $(P/Nd)_N$ and; d, $^{206}Pb/^{204}Pb$ vs. $(P/Nd)_N$ for the CVL samples. The range of NE volcanoes (Mt. Cameroon and Etinde) and Type 1 SW volcanoes (Annobon, Sao Tome, and Principe) are shown with red and blue lines, respectively.

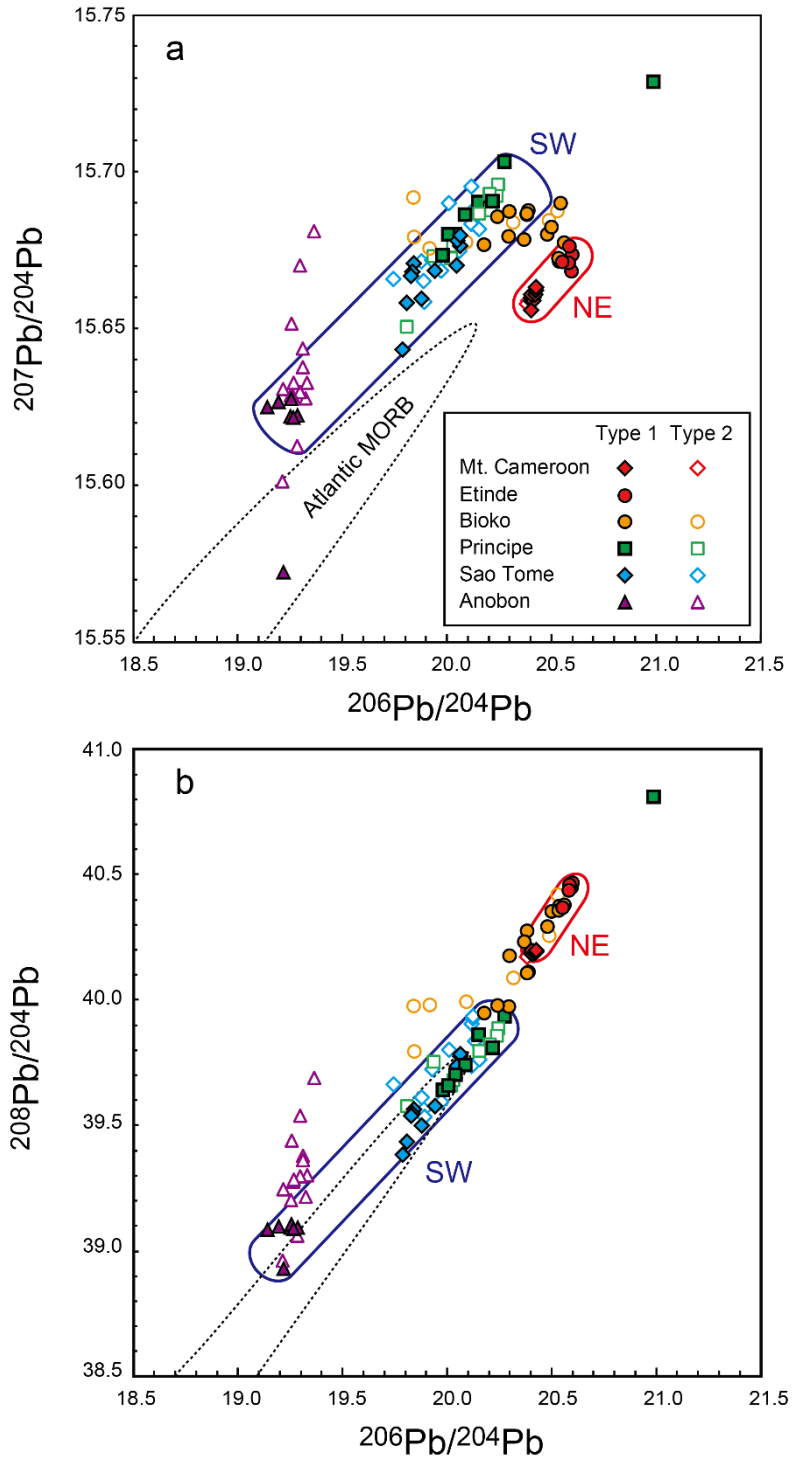

Figure 5-6 | a, $^{206}Pb/^{204}Pb$ vs. $^{207}Pb/^{204}Pb$ and b, $^{206}Pb/^{204}Pb$ vs. $^{208}Pb/^{204}Pb$ diagrams for CVL samples and the range of Type 1 NE and Type 1 SW volcanoes.

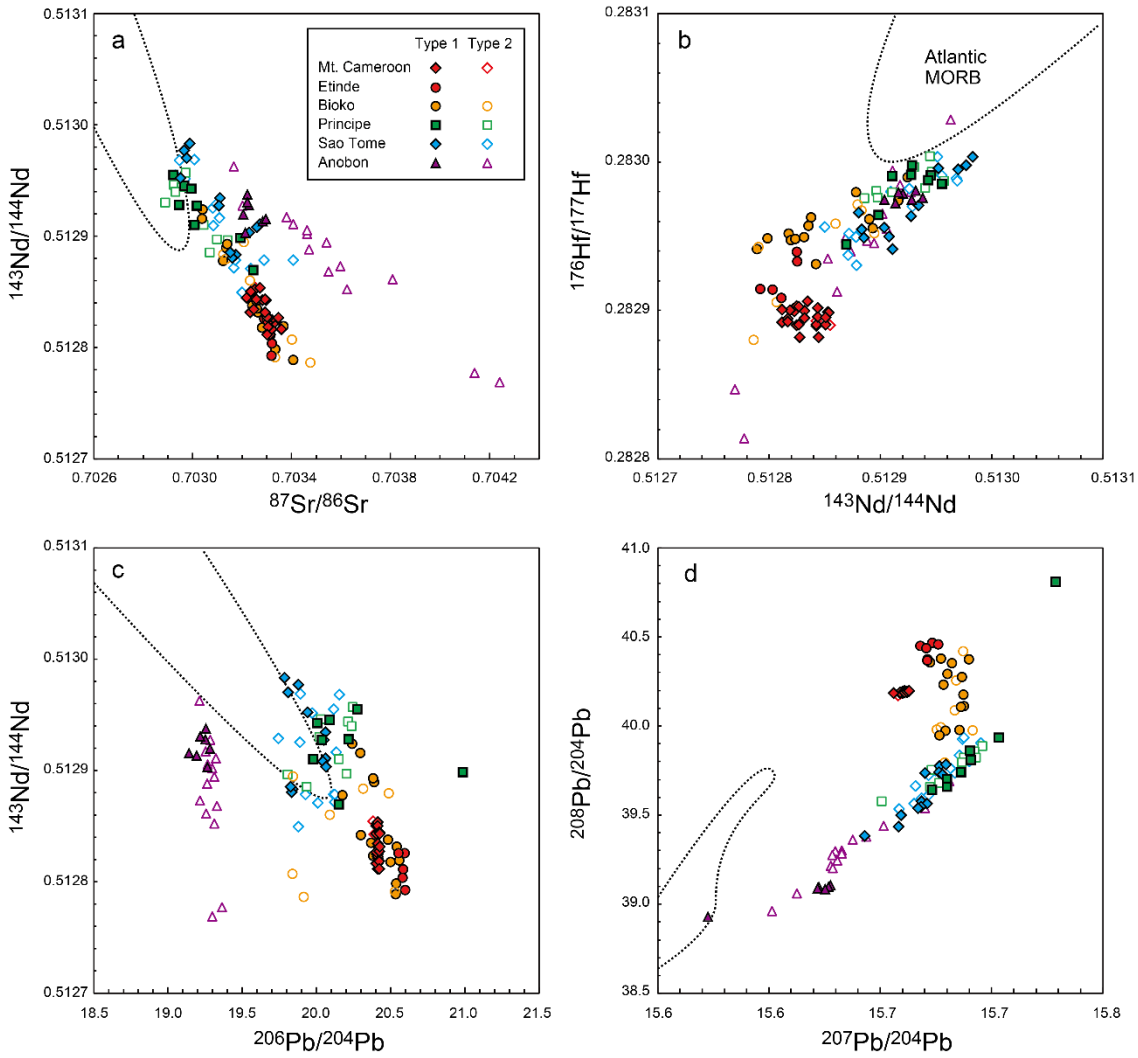

Figure 5-7 | a, $^{87}Sr/^{86}Sr$ vs. $^{143}Nd/^{144}Nd$; b, $^{143}Nd/^{144}Nd$ vs. $^{176}Hf/^{177}Hf$; c, $^{206}Pb/^{204}Pb$ vs. $^{143}Nd/^{144}Nd$; and d, $^{207}Pb/^{204}Pb$ vs. $^{208}Pb/^{204}Pb$ diagrams for CVL samples.

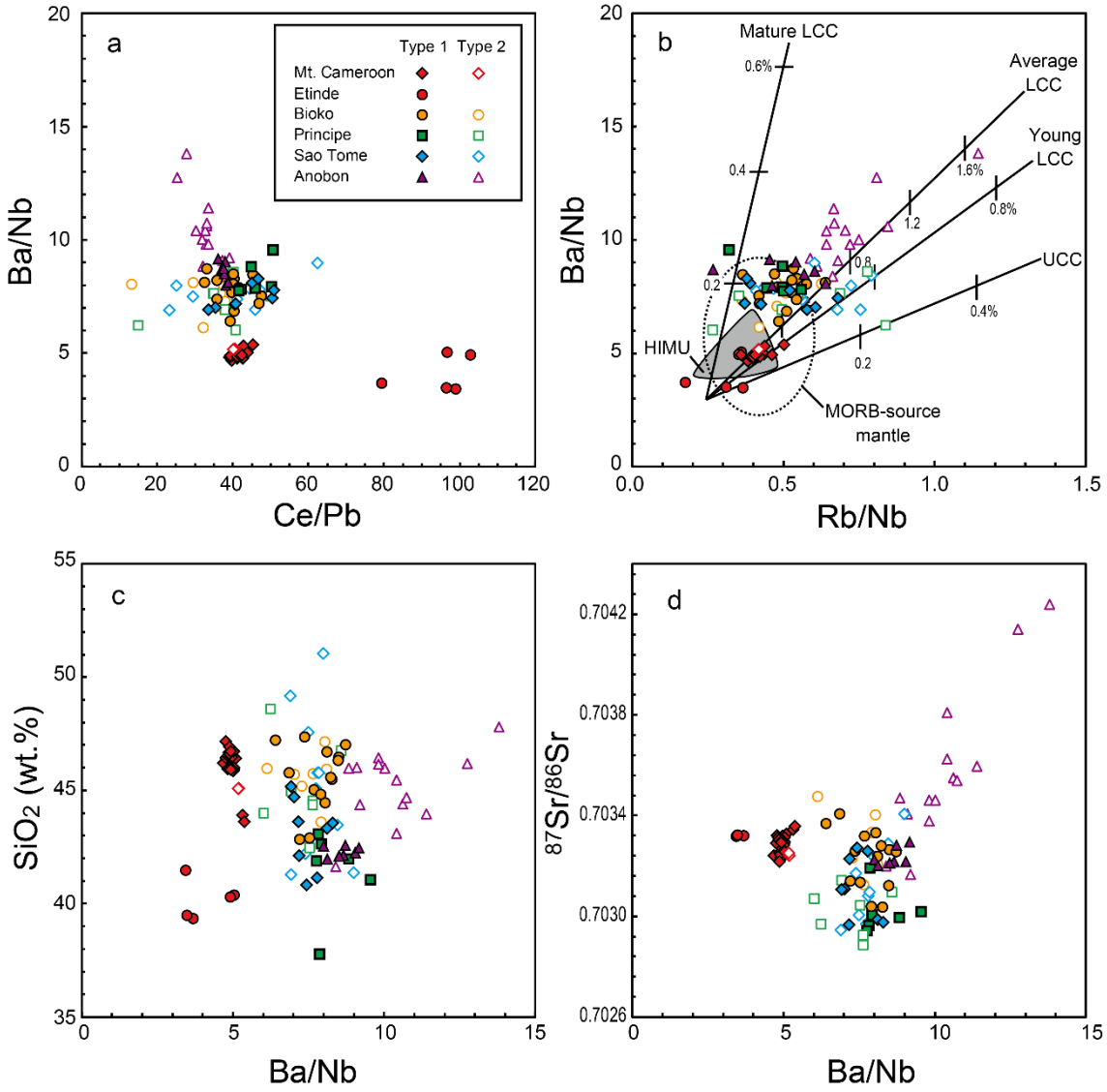

Figure 5-8 | a, Ce/Pb vs. Ba/Nb; b, Rb/Nb vs. Ba/Nb; c, Ba/Nb vs. SiO_2; and d, Ba/Nb vs. 87Sr/86Sr diagrams for CVL samples. The mixing line with upper continental crust (UCC) and lower continental crust (LCC) in b are after Willbold and Stracke (2006).

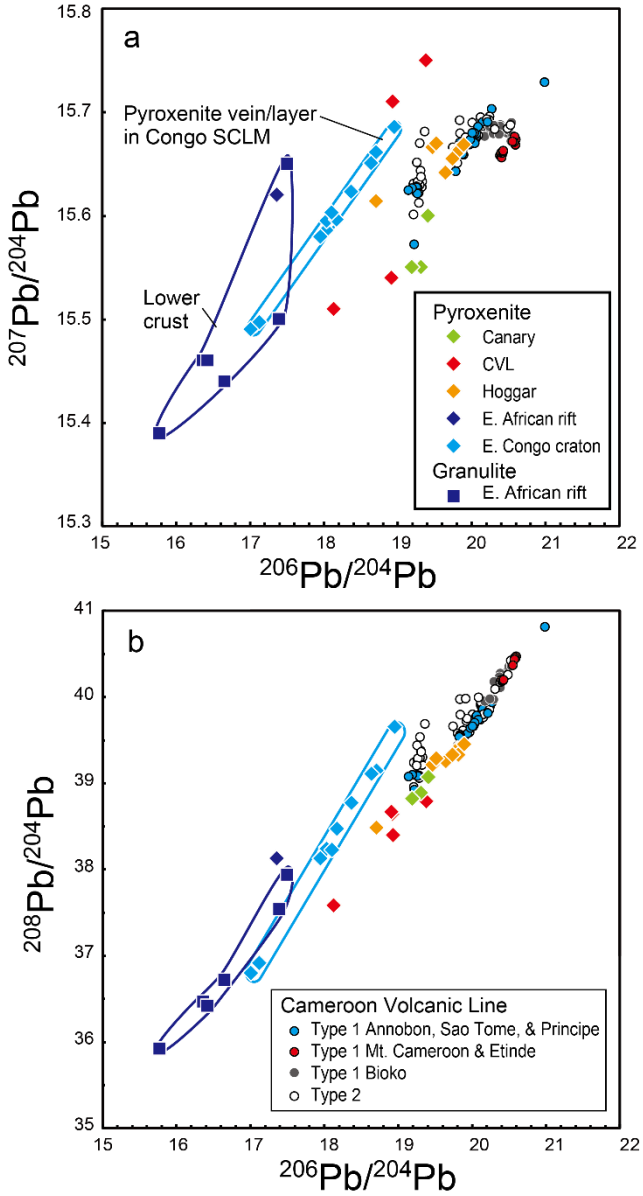

Figure 5-9 | a, $^{206}Pb/^{204}Pb$ vs $^{207}Pb/^{204}Pb$ and b, $^{206}Pb/^{204}Pb$ vs $^{208}Pb/^{204}Pb$ diagrams for granulite and pyroxenite xenoliths in African cratonic region and Canary Island plotted with CVL lavas. Data source are shown in Supplementary Table 3. : cpx, garnet, and amphibole in pyroxenite from the continental sector of CLV (Lee et al., 1996), whole rock of pyroxenite from Hogger swell (Beccaluva et al., 2007; Kaczmarek et al., 2016), whole rock of pyroxenite from Canary Islands (Whitehouse and Neumann, 1995), cpx in pyroxenite from western EAR (Davies and Lloyd, 1989), cpx in lherzolite and pyroxenite and whole rock of granulite from EAR (Bianchini et al., 2014; Cohen et al., 1984; Meshesha et al., 2011).

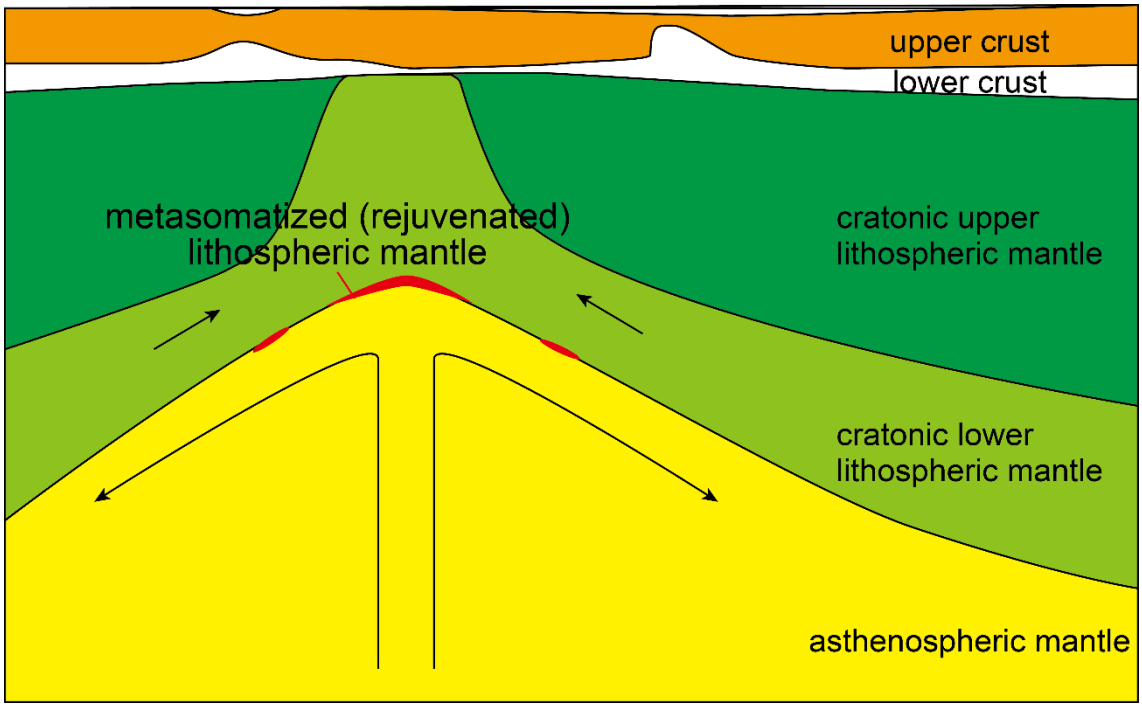

Figure 5-10 | Schematic illustration expressing the metasomatic process of the cratonic lower lithospheric mantle by the asthenospheric mantle derived melt during the continental breakup. The cross section of the rift system is based on the Huismans and Beaumount (2011).

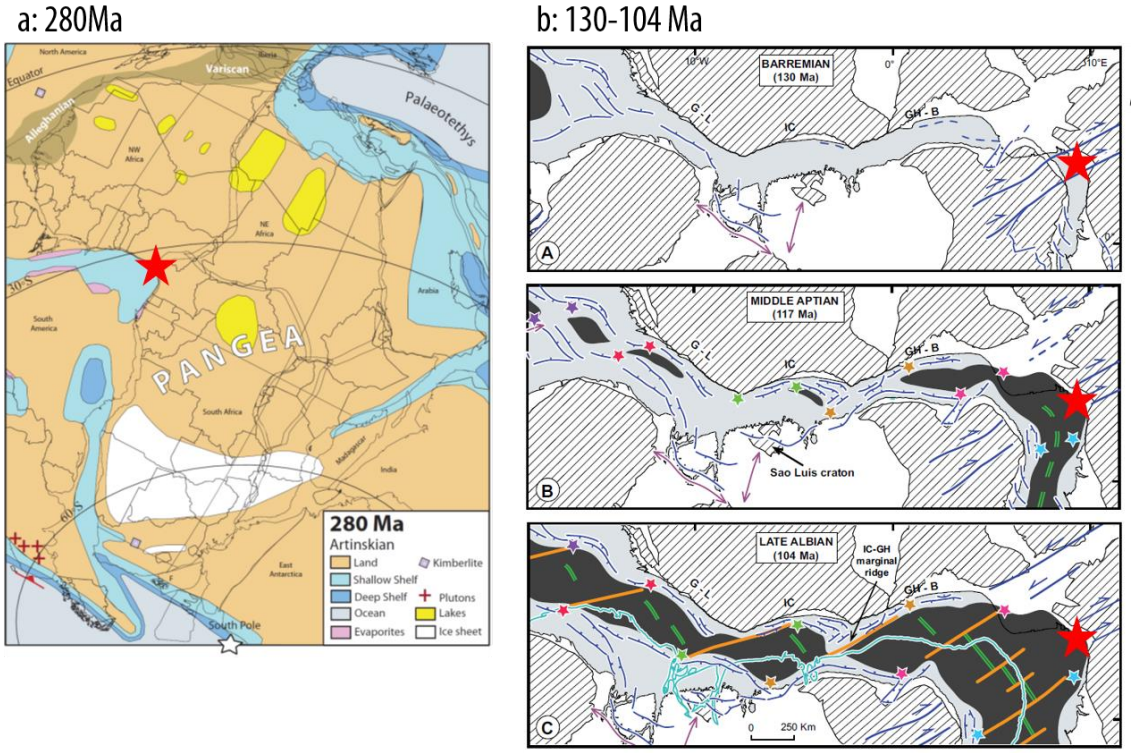

Figure 5-11 | Reconstructed configuration of the Pangea and Atlantic Ocean at 280Ma early Permian Artinskian stage (a) and Early Cretaceous (b). The figure a is Figure 12 of Torsvik and Cocks (2011) and b is Figure 15 of Ye et al. (2017).

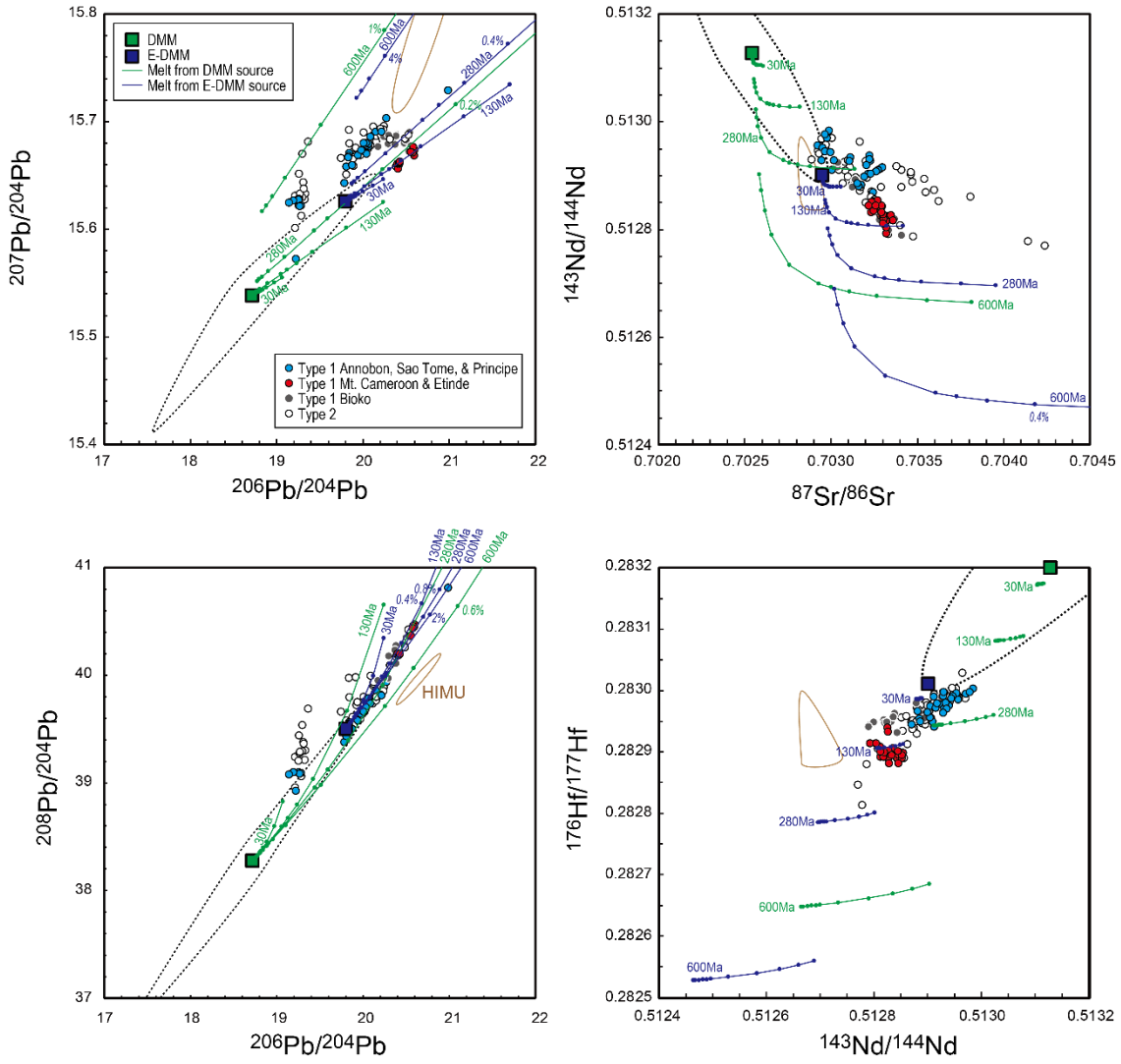

Figure 5-12 | The calculated Sr, Nd, Hf, and Pb isotopic evolution curves of the ancient asthenospheric mantle derived silicate melt at various age. Sticks in each curve is different degree of partial melting: 0.1, 0.2, 0.4, 0.6, 0.8, 1, 2, 4, 6, 8, and 10%. Range of HIMU is data from St. Helena after Strack (2012). All the calculated data are shown in Table 10.

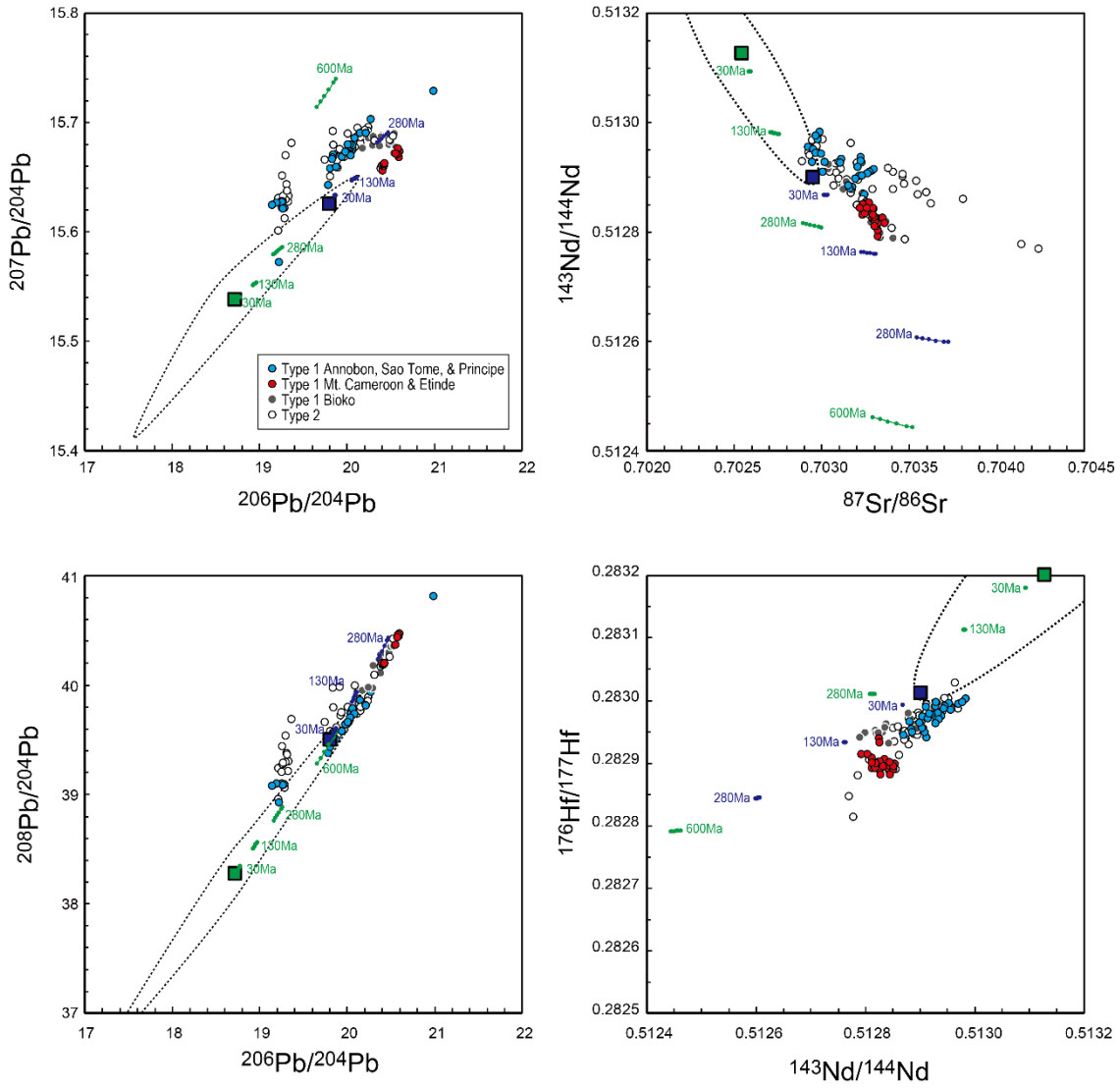

Figure 5-13 | The calculated Sr, Nd, Hf, and Pb isotopic evolution curves of the ancient asthenospheric mantle derived carbonatite melt at various age. Sticks in each curve is different degree of partial melting: 0.1, 0.2, 0.4, 0.6, 0.8, 1, 2, 4, 6, 8, and 10%. Range of HIMU is data from St. Helena after Strack (2012). All the calculated data are shown in Table 11.

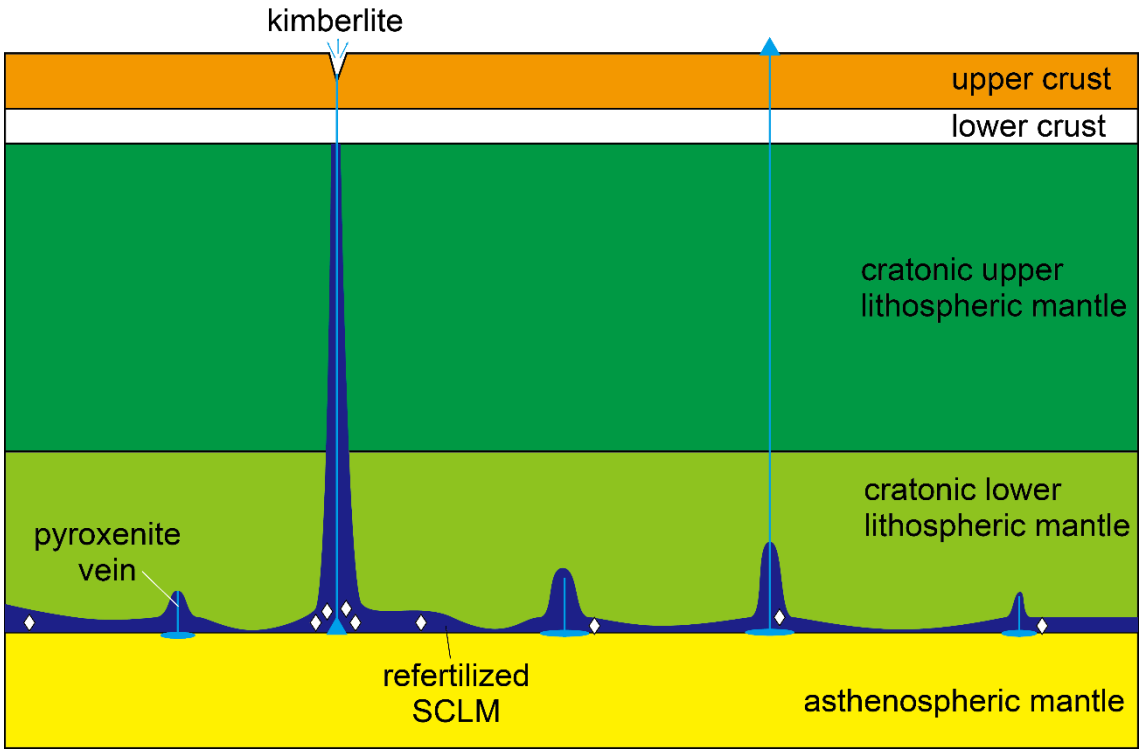

Figure 5-14 | Schematic illustration expressing the lower most part of the SCLM. The figure is modified after Griffin et al. (2013).

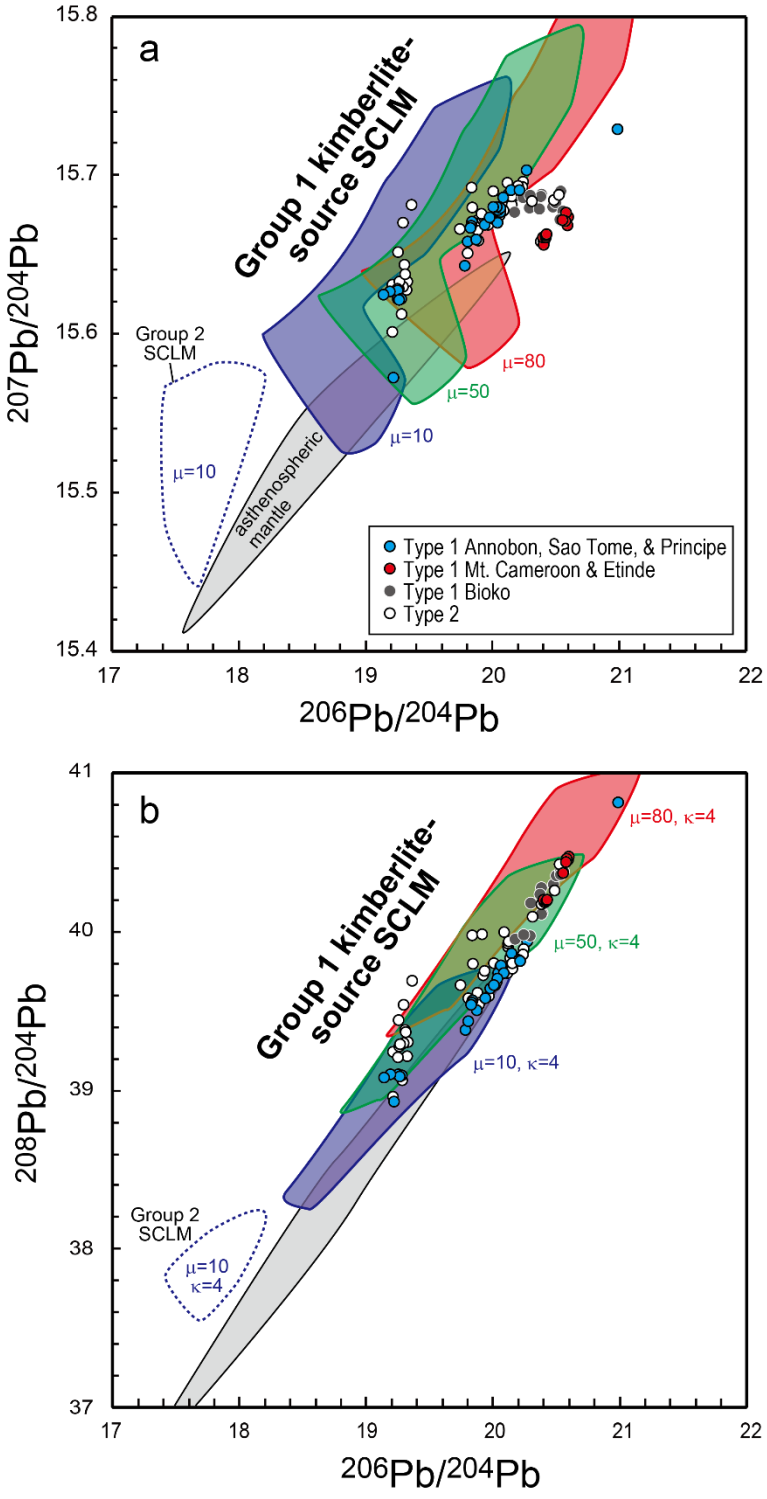

Figure 5-15 | Pb isotopic compositions of the calculated current lowermost part of SCLM. The detailed calculation method is written in the text.

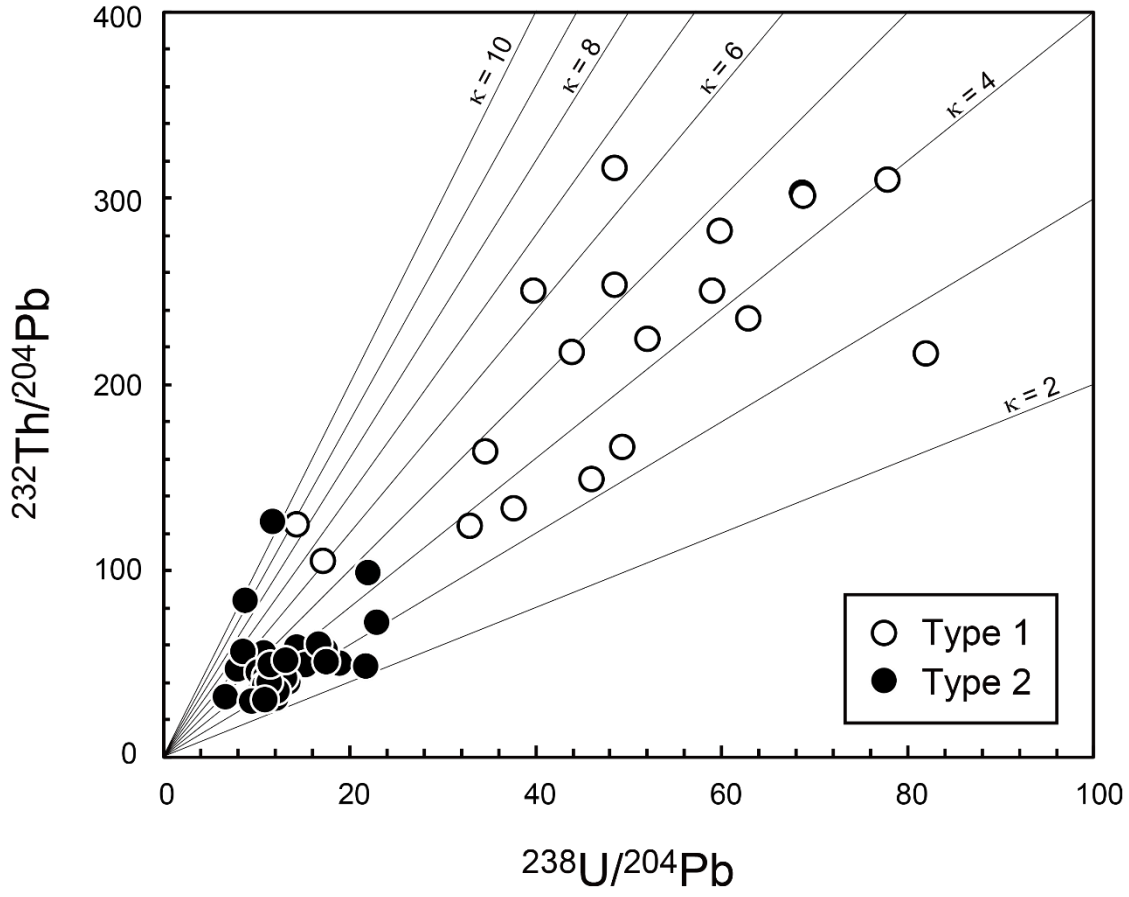

Figure 5-16 | The $^{238}U/^{204}Pb$ vs. $^{232}Th/^{204}Pb$ of Type 1 and Type 2 kimberlite. The data are compiled by GEOROC data base.

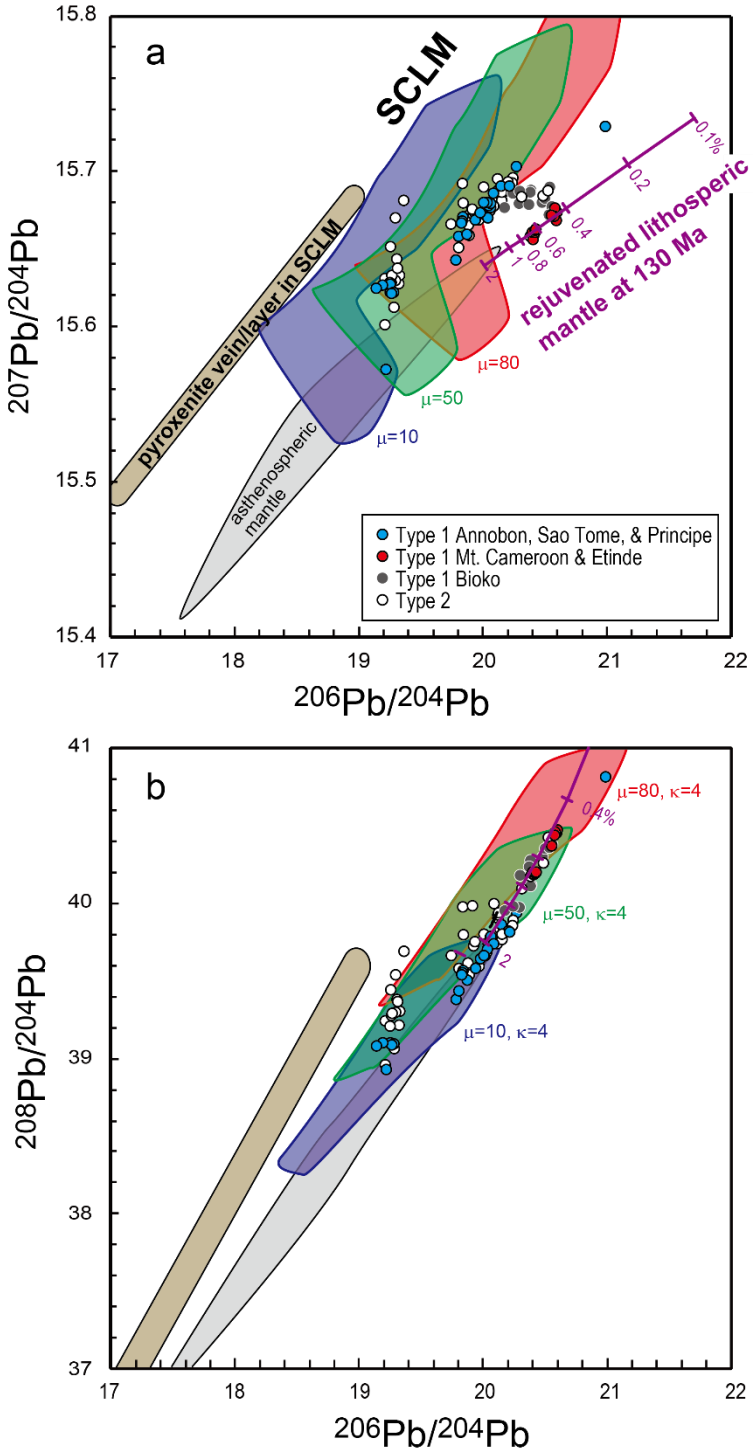

Figure 5-17 | Summary of estimated source components of the CVL magmas. The isotopic compositions of each source component are from Figures 5-9, 5-12, and 5-15.

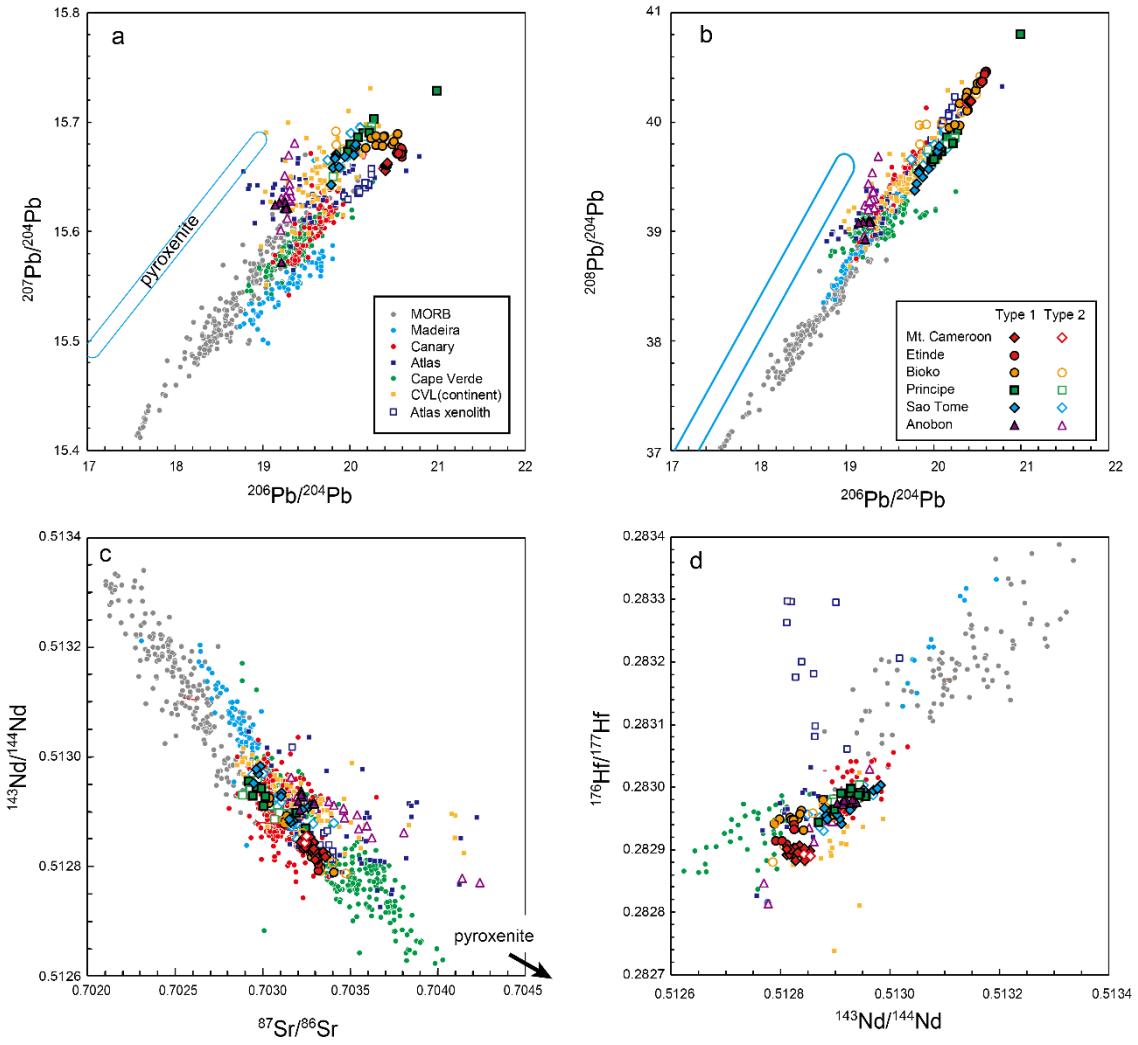

Figure 5-18 | a, $^{206}Pb/^{204}Pb$ vs. $^{207}Pb/^{204}Pb$; b, $^{206}Pb/^{204}Pb$ vs. $^{208}Pb/^{204}Pb$; c, $^{87}Sr/^{86}Sr$ vs. $^{143}Nd/^{144}Nd$; and d, $^{143}Nd/^{144}Nd$ vs. $^{176}Hf/^{177}Hf$ of WAPM-IB and Atlantic MORB. All the compiled data are shown in Supplementary Table 1 and 2.

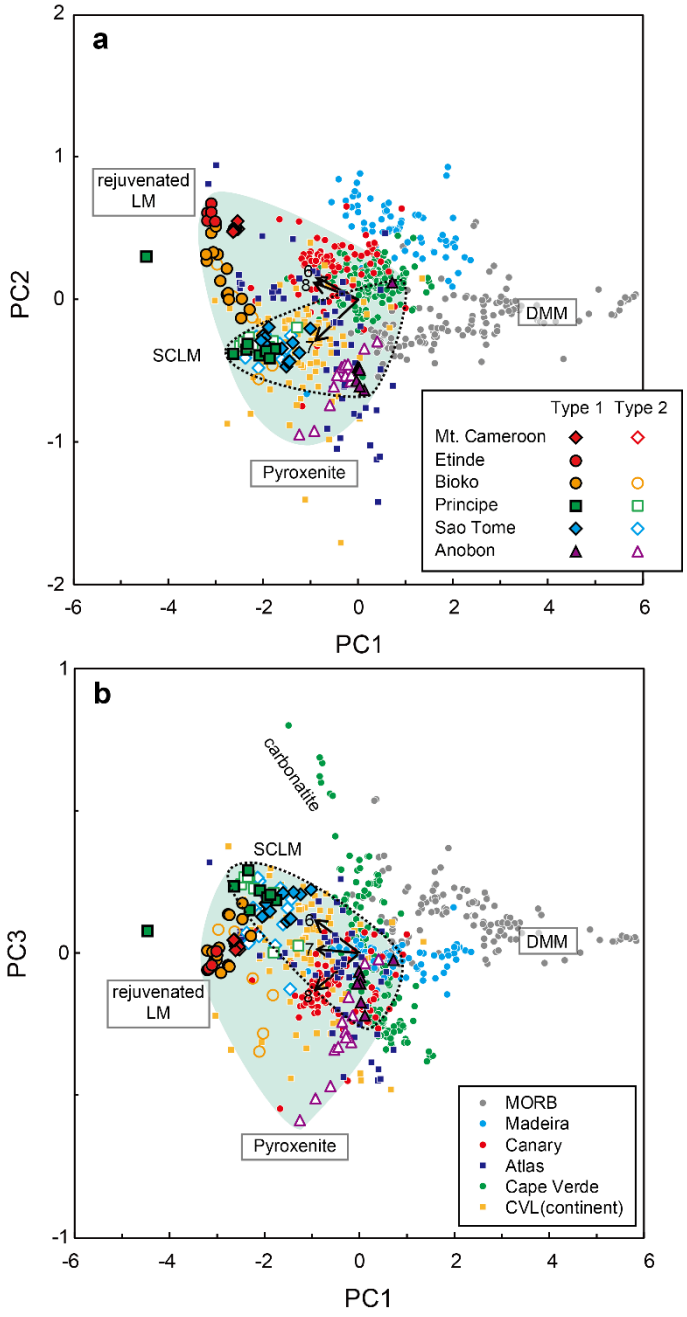

Figure 5-19 | Diagrams of principal component analysis of the Pb isotope data of the CVL and comped data from WAPM-OIB, Atlas Mountains, continental CVL, and Atlantic MORB. The first, second, and third principal component (PC1, PC2, and PC3) accounts for 94.3, 4.6, and 1.1% of the total variability of the data. The source of the compiled data is shown in Supplementary Tables 1 and 2. The light green area shows the range of CVL. DMM: depleted MORB mantle, SCLM: sub continental lithospheric mantle, rejuvenated LM: metasomatized lithospheric mantle1 (metasomatized by low degree of melt during or after the opening of Atlantic). Number of data is 707. CVL=116 (this study and Yokoyama et al. (Yokoyama et al., 2007)), MORB = 140, Medeira = 70, Salvagen= 16, Cape Verde = 153, Canary Islands=72, Atlas Mountain = 54, continental section of CVL and Benue trough = 86.

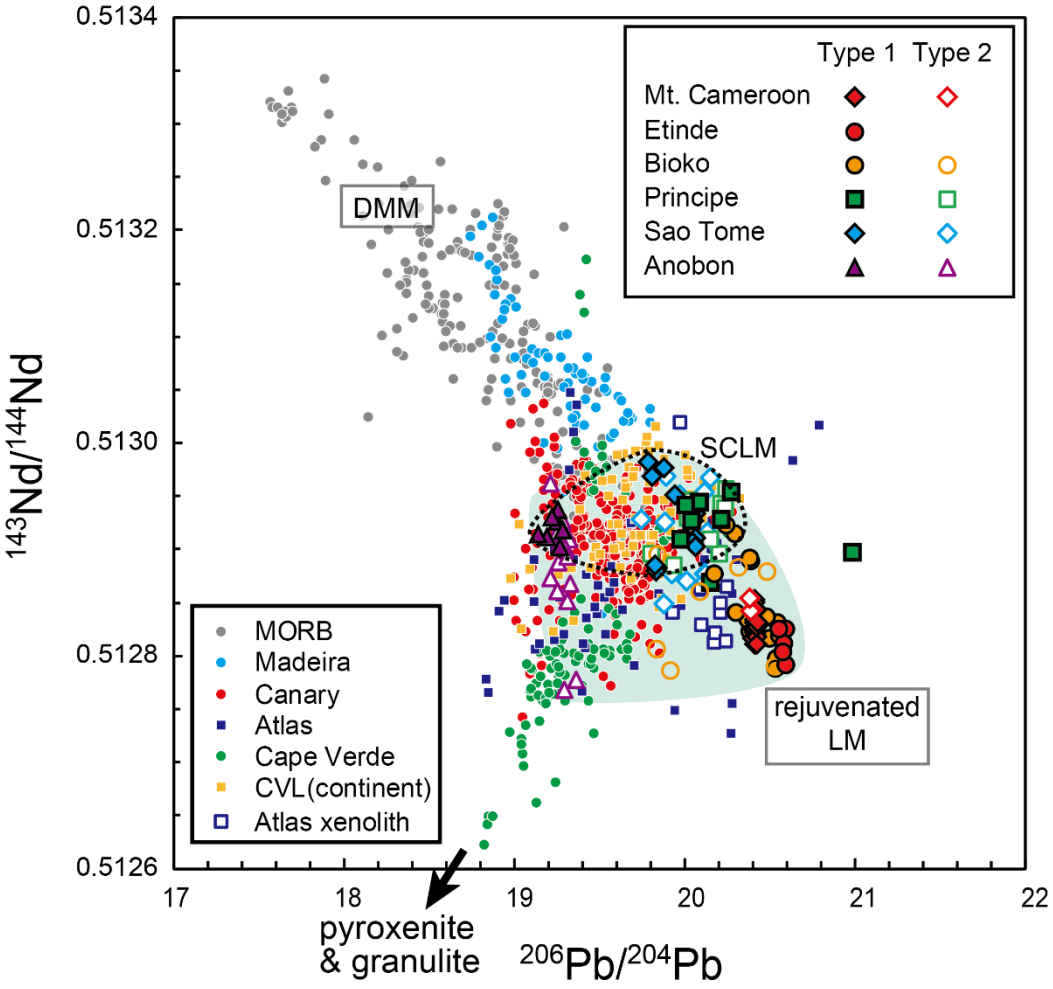

Figure 5-20 | $^{206}Pb/^{204}Pb$ vs. $^{143}Nd/^{144}Nd$ of the WAPM-IB and the estimated components for the CVL magmas. The light green area shows the range for CVL.

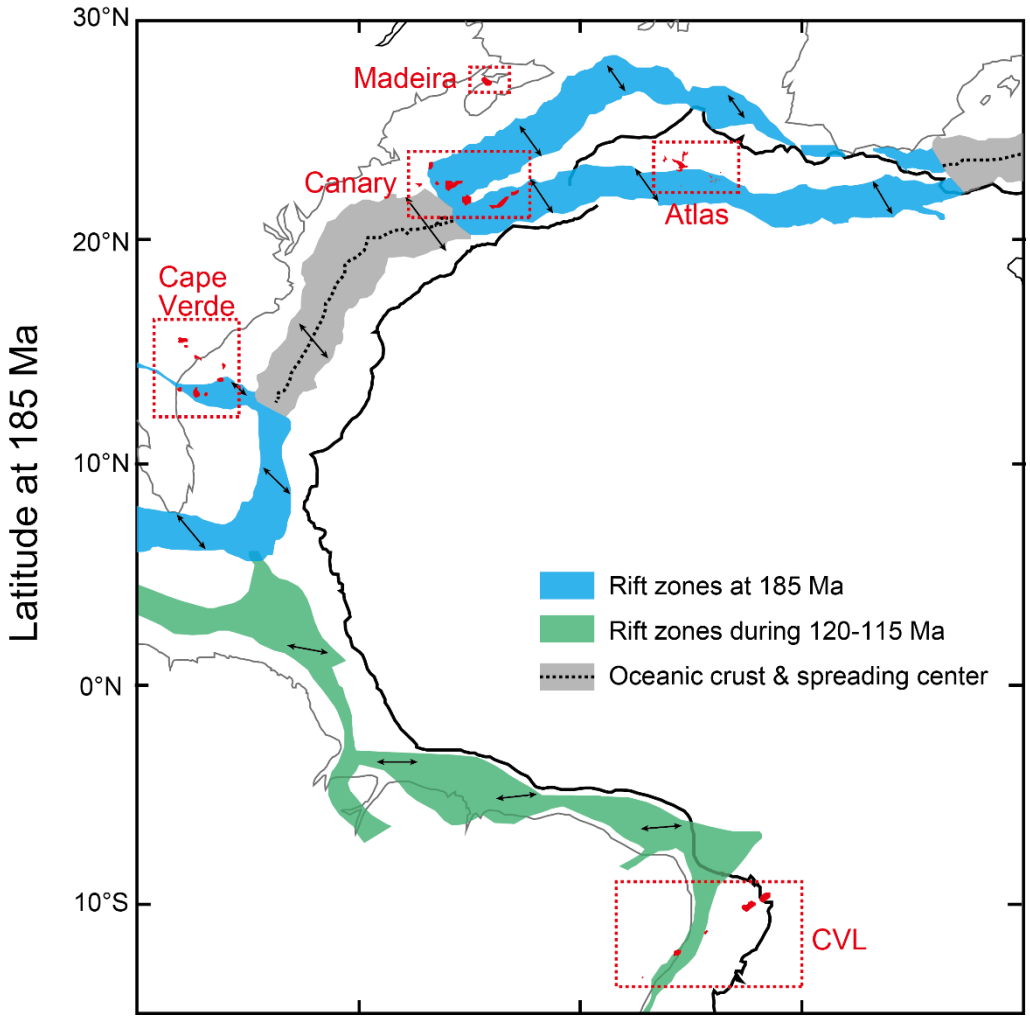

Figure 5-21 | The reconstructed Mesozoic rift zone of African and South American continents and Atlantic Ocean and location of WAPM-IB. The locations for the WAPM-IB (red) are illustrated from the current distance from the coastline of the African continent. The rift zone at 185 Ma and 120-115 Ma are after Schettino and Turco (2009) and Ye et al. (2017).

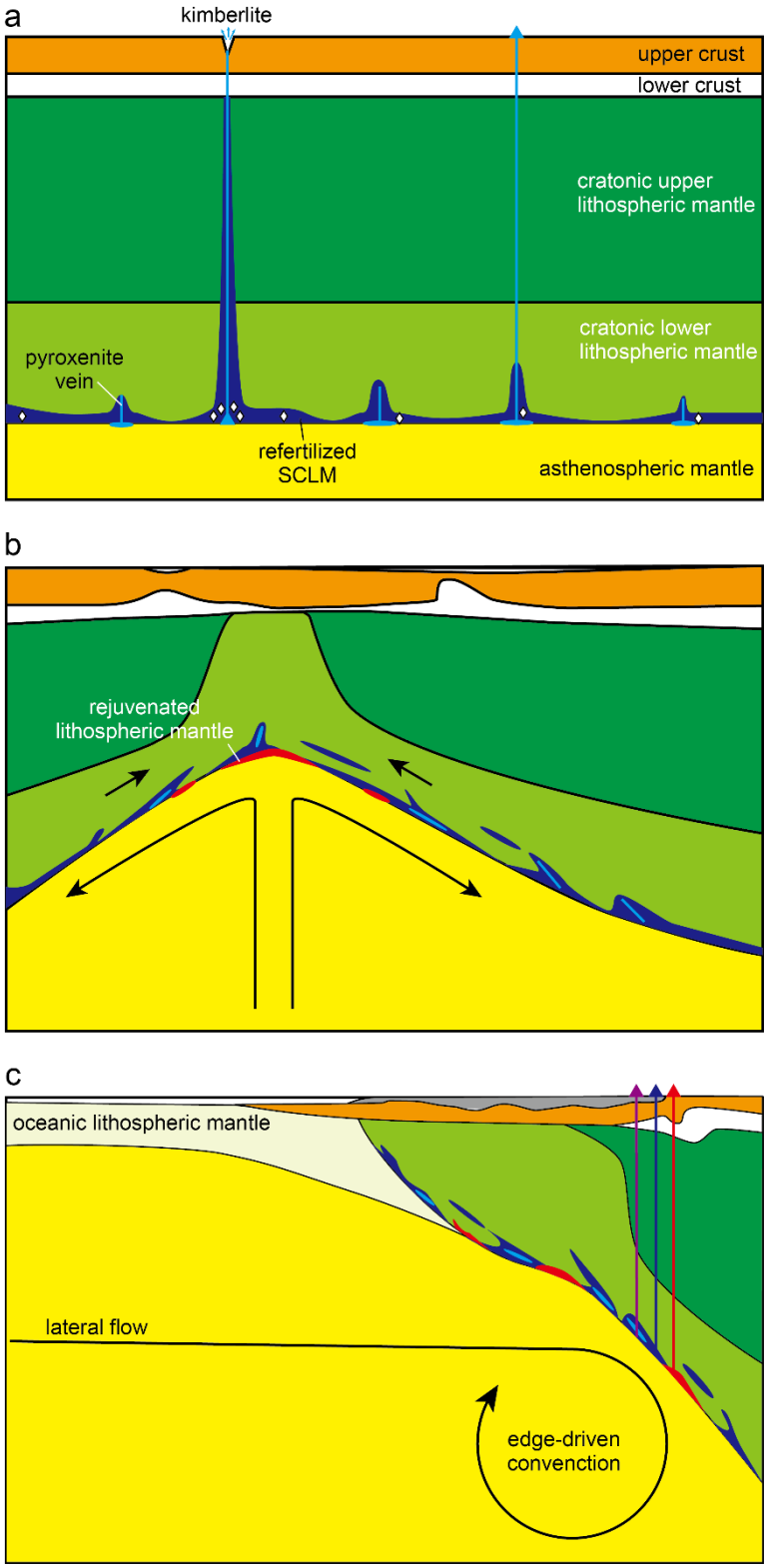

Figure 5-22| Schematic diagram of the melting process of WAPM magmatism by the edge-driven convection. Image of the SCLM was modified after Huismans and Beaumount (2011) and Griffin et al. Griffin et al. (2013).

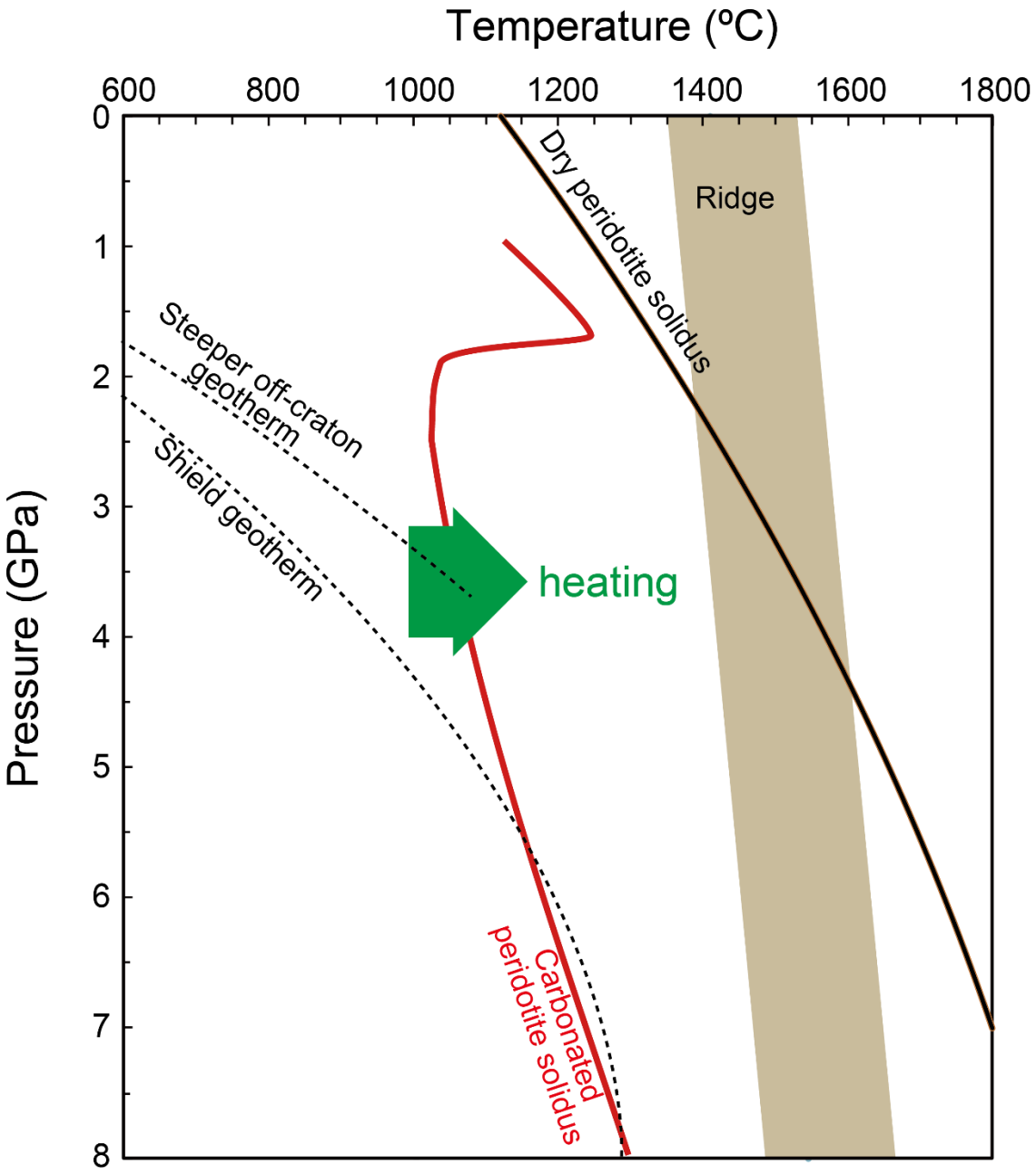

Figure 5-23| Pressure-temperature estimation for the magma source of the CVL. Shield geotherm and Steeper off craton geotherm: Moore et al. (2008), Carbonated peridotite solidus: Dasgupta et al. (2013), and Dry peridotite solidus: Hirschmann et al. (2000).

Table 7 | Average major and trace element compositions of compiled African Kimberlite and carbonatitic melt inclusions

	Kimberlite				High-Mg cabonatitic melt	
	Group 1 average		Group 2 average		Udachnaya	Kankan
SiO_2 (wt.%)	32.1 ± 0.5	(155)	34.2 ± 0.5	(77)	8.3	9.9
TiO_2	2.02 ± 0.08	(155)	1.43 ± 0.08	(77)	1.4	1.6
Al_2O_3	3.7 ± 0.2	(155)	3.5 ± 0.2	(77)	1.4	1.9
Fe_2O_3T	10.2 ± 0.2	(155)	8.6 ± 0.2	(77)	7.4	11.84
Cr_2O_3	0.177 ± 0.005	(155)	0.24 ± 0.01	(77)	0.7	0.4
CaO	9.4 ± 0.3	(155)	9.7 ± 0.6	(77)	19.1	22.2
MgO	25.6 ± 0.4	(155)	24.1 ± 0.8	(77)	21.4	23.0
MnO	0.18 ± 0.006	(155)	0.20 ± 0.01	(77)	0.7	0.6
NiO	0.114 ± 0.007	(35)	0.142 ± 0.006	(69)		
K_2O	0.86 ± 0.06	(155)	2.9 ± 0.2	(77)	19.5	9.8
Na_2O	0.18 ± 0.01	(155)	0.18 ± 0.02	(73)	11.1	10.0
P_2O_5	1.08 ± 0.07	(155)	1.12 ± 0.07	(77)		
CO_2	6.48 ± 0.3	(87)	6.0 ± 0.6	(61)		
Li (µg/g)	16 ± 3	(6)	-			
Rb	52 ± 3	(155)	127 ± 6	(79)	744	170
Sr	858 ± 46	(155)	1301 ± 66	(79)	5299	4809
Y	17.2 ± 0.6	(145)	16.0 ± 0.8	(79)	22.3	34.5
Zr	301 ± 22	(155)	292 ± 14	(76)	446	498
Nb	150 ± 8	(155)	142 ± 7	(77)	1567	1415
Cs	1.4 ± 0.5	(53)			13.8	4.06
Ba	885 ± 59	(155)	2996 ± 188	(79)	14684	29176
La	117 ± 7	(153)	185 ± 8	(79)	1126	2068
Ce	233 ± 15	(153)	360 ± 14	(79)	1475	2427
Pr	26 ± 2	(153)	37 ± 1	(79)	155	217
Nd	94 ± 5	(153)	131 ± 5	(79)	558	693
Sm	13.5 ± 0.7	(153)	15.6 ± 0.6	(79)	58.7	50.5
Eu	3.5 ± 0.2	(153)	3.7 ± 0.1	(79)	15.4	10.8
Gd	8.8 ± 0.4	(153)	9.1 ± 0.3	(79)	31.6	27.6
Tb	1.01 ± 0.04	(153)	1.01 ± 0.04	(79)		
Dy	4.3 ± 0.2	(153)	4.1 ± 0.2	(79)	5.38	10.1
Ho	0.68 ± 0.02	(153)	0.63 ± 0.03	(79)		
Er	1.52 ± 0.04	(153)	1.43 ± 0.07	(79)	2.58	1.96
Tm	0.18 ± 0.005	(140)	0.175 ± 0.009	(73)		4.77
Yb	1.00 ± 0.03	(153)	0.98 ± 0.05	(79)		
Lu	0.132 ± 0.004	(153)	0.128 ± 0.007	(79)		
Hf	6.5 ± 0.5	(153)	6.7 ± 0.3	(79)	9.01	9.7
Ta	7.7 ± 0.3	(140)	7.0 ± 0.4	(73)	83.9	43.1
Pb	7.6 ± 0.5	(153)	26.6 ± 1.8	(79)		
Th	14.9 ± 1.0	(153)	26 ± 1	(79)	153	251
U	3.5 ± 0.2	(153)	5.4 ± 0.3	(79)	25.1	49.6

The average value of Group 1 and Group 2 kimberlite from Africa are from (Becker and le Roex, 2006; Becker et al., 2007; Coe et al., 2008; Donnelly et al., 2011; Galloway et al., 2009; Harris et al., 2004; Le Roex et al., 2003; Wu et al., 2013) and High-Mg carbonatitic high-density fluids (HDFs) from Udachanaya and Kankan (Weiss et al., 2011; Weiss et al., 2009).

Table 8 | Elemental and isotopic compositions of DMM and E-DMM

	DMM	E-DMM
concentration		
Rb (μg/g)	0.05	0.108
Sr	7.664	9.718
Sm	0.239	0.273
Nd	0.581	0.703
Lu	0.058	0.06
Hf	0.157	0.186
U	0.0032	0.0052
Th	0.0079	0.0157
Pb	0.018	0.024
ratio		
$^{87}Sr/^{86}Sr$	0.70255	0.70295
$^{143}Nd/^{144}Nd$	0.51313	0.51290
$^{176}Hf/^{177}Hf$	0.28320	0.28305
$^{206}Pb/^{204}Pb$	18.720	19.80
$^{207}Pb/^{204}Pb$	15.538	15.63
$^{208}Pb/^{204}Pb$	38.277	39.50

Concentration is after (Workman and Hart, 2005).
The isotopic ratio of DMM is average value of Atlantic MORB (Supplementary Table 1) and of E-DMM are nearly the enriched end of the Atlantic MORB.

Table 9 | Partition coefficients and mineral mode for partial melting calculations

	olivine	opx	cpx	garnet	reference
Rb	0.0002	0.0002	0.011	0.0002	Zindler and Jagoutz (1988), McKenzie and O'Nions (1991), Halliday et al. (1995)
Sr	0.00001	0.003	0.1283	0.007	Kelemen et al. (2003)
Sm	0.0007	0.02	0.291	0.217	Kelemen et al. (2003)
Nd	0.00007	0.009	0.1873	0.057	Kelemen et al. (2003)
Lu	0.03	0.12	0.433	9	Kelemen et al. (2003)
Hf	0.004	0.04	0.256	0.5	Kelemen et al. (2003)
U	1.8E-05	0.0057	0.003	0.005	Kelemen et al. (2003), Wittig et al. (2010)
Th	1.2E-05	0.0022	0.001	0.001	Kelemen et al. (2003), Wittig et al. (2010)
Pb	0	0.2	0.072	0.0005	Kelemen et al. (2003), Wittig et al. (2010)
starting mode	0.58	0	0.26	0.16	Walter (1998)
melting proportions	0.25	0	0.51	0.24	Walter (1998)

Table 10 | Calculated Sr, Nd, Hf, and Pb isotopic compositions and parent/daughter elemental compositions of the DMM and E-DMM derived silicate melt compositions

Initial isotope ratio at T						F	Parent-daugther ratio of partial melt at T						Calculated present isotope ratio of melt					
$^{87}Sr/^{86}Sr_i$	$^{143}Nd/^{144}Nd_i$	$^{176}Hf/^{177}Hf_i$	$^{206}Pb/^{204}Pb_i$	$^{207}Pb/^{204}Pb_i$	$^{208}Pb/^{204}Pb_i$		$^{87}Rb/^{86}Sr$	$^{147}Sm/^{144}Nd$	$^{176}Lu/^{177}Hf$	$^{238}U/^{204}Pb$	$^{235}U/^{204}Pb$	$^{232}Th/^{204}Pb$	$^{87}Sr/^{86}Sr$	$^{143}Nd/^{144}Nd$	$^{176}Hf/^{177}Hf$	$^{206}Pb/^{204}Pb$	$^{207}Pb/^{204}Pb$	$^{208}Pb/^{204}Pb$
DMM at T=30Ma																		
0.70254	0.51308	0.28317	18.667	15.535	38.234	0.001	0.167	0.131	0.0050	86	0.647	399	0.70261	0.51310	0.28317	19.069	15.555	38.826
						0.002	0.137	0.132	0.0050	65	0.490	246	0.70260	0.51310	0.28317	18.972	15.550	38.599
						0.004	0.103	0.134	0.0051	46	0.344	147	0.70258	0.51310	0.28317	18.881	15.546	38.453
						0.006	0.084	0.136	0.0052	36.6	0.275	110	0.70257	0.51310	0.28317	18.838	15.544	38.397
						0.008	0.072	0.138	0.0052	31.3	0.235	91	0.70257	0.51311	0.28317	18.813	15.542	38.368
						0.01	0.064	0.140	0.0053	27.8	0.208	79	0.70256	0.51311	0.28317	18.797	15.542	38.350
						0.02	0.044	0.148	0.0056	19.9	0.150	54	0.70256	0.51311	0.28317	18.760	15.540	38.313
						0.04	0.032	0.163	0.0062	15.6	0.117	40.9	0.70255	0.51311	0.28317	18.740	15.539	38.294
						0.06	0.027	0.174	0.0068	14.1	0.106	36.5	0.70255	0.51311	0.28317	18.733	15.539	38.288
						0.08	0.025	0.184	0.0075	13.3	0.100	34.3	0.70255	0.51311	0.28317	18.729	15.538	38.285
						0.1	0.024	0.191	0.0082	12.8	0.096	33.0	0.70255	0.51312	0.28317	18.727	15.538	38.283
DMM at T=130Ma																		
0.70251	0.51292	0.28307	18.490	15.527	38.091	0.001	0.167	0.131	0.0050	86	0.722	397	0.70282	0.51303	0.28308	20.238	15.625	40.654
						0.002	0.137	0.132	0.0050	65	0.546	245	0.70276	0.51303	0.28308	19.813	15.601	39.671
						0.004	0.103	0.134	0.0051	46	0.384	147	0.70270	0.51303	0.28308	19.419	15.579	39.038
						0.006	0.084	0.136	0.0052	36.5	0.307	110	0.70267	0.51303	0.28308	19.233	15.569	38.798
						0.008	0.072	0.138	0.0052	31.1	0.262	90	0.70264	0.51303	0.28308	19.124	15.562	38.673
						0.01	0.064	0.140	0.0053	27.6	0.232	78	0.70263	0.51303	0.28308	19.053	15.558	38.595
						0.02	0.044	0.148	0.0056	19.9	0.167	53	0.70259	0.51304	0.28308	18.894	15.549	38.435
						0.04	0.032	0.163	0.0062	15.5	0.131	40.7	0.70257	0.51305	0.28308	18.806	15.544	38.353
						0.06	0.027	0.174	0.0068	14.0	0.118	36.4	0.70256	0.51306	0.28309	18.775	15.543	38.325
						0.08	0.025	0.184	0.0075	13.2	0.111	34.2	0.70256	0.51307	0.28309	18.759	15.542	38.311
						0.1	0.024	0.191	0.0082	12.8	0.107	32.9	0.70255	0.51308	0.28309	18.750	15.541	38.303

Table 10 | *(continued)*

Initial isotope ratio at T						F	Parent-daugther ratio of partial melt at T						Calculated present isotope ratio of melt					
$^{87}Sr/^{86}Sr_i$	$^{143}Nd/^{144}Nd_i$	$^{176}Hf/^{177}Hf_i$	$^{206}Pb/^{204}Pb_i$	$^{207}Pb/^{204}Pb_i$	$^{208}Pb/^{204}Pb_i$		$^{87}Rb/^{86}Sr$	$^{147}Sm/^{144}Nd$	$^{176}Lu/^{177}Hf$	$^{238}U/^{204}Pb$	$^{235}U/^{204}Pb$	$^{232}Th/^{204}Pb$	$^{87}Sr/^{86}Sr$	$^{143}Nd/^{144}Nd$	$^{176}Hf/^{177}Hf$	$^{206}Pb/^{204}Pb$	$^{207}Pb/^{204}Pb$	$^{208}Pb/^{204}Pb$
DMM at T=280Ma																		
0.70247	0.51267	0.28292	18.218	15.512	37.874	0.001	0.167	0.131	0.0050	85	0.851	395	0.70314	0.51291	0.28294	22.002	15.782	43.378
						0.002	0.137	0.132	0.0050	65	0.644	243	0.70302	0.51291	0.28294	21.083	15.716	41.268
						0.004	0.103	0.134	0.0051	45	0.452	146	0.70288	0.51292	0.28294	20.230	15.655	39.908
						0.006	0.084	0.136	0.0052	36.2	0.361	109	0.70281	0.51292	0.28294	19.826	15.627	39.394
						0.008	0.072	0.138	0.0052	30.9	0.309	90	0.70276	0.51292	0.28294	19.591	15.610	39.124
						0.01	0.064	0.140	0.0053	27.4	0.274	78	0.70272	0.51293	0.28294	19.436	15.599	38.958
						0.02	0.044	0.148	0.0056	19.7	0.197	53	0.70264	0.51294	0.28295	19.094	15.574	38.615
						0.04	0.032	0.163	0.0062	15.4	0.154	40.4	0.70260	0.51297	0.28295	18.903	15.561	38.438
						0.06	0.027	0.174	0.0068	13.9	0.139	36.1	0.70258	0.51299	0.28295	18.836	15.556	38.378
						0.08	0.025	0.184	0.0075	13.1	0.131	33.9	0.70257	0.51301	0.28296	18.802	15.553	38.348
						0.1	0.024	0.191	0.0082	12.7	0.127	32.7	0.70256	0.51302	0.28296	18.781	15.552	38.330
DMM at T=600Ma																		
0.70238	0.51215	0.28259	17.618	15.472	37.408	0.001	0.167	0.131	0.00501	83.9	1.206	389	0.70381	0.51266	0.28265	25.805	16.444	49.114
						0.002	0.137	0.132	0.00504	63.5	0.913	240	0.70356	0.51267	0.28265	23.816	16.208	44.627
						0.004	0.103	0.134	0.00509	44.6	0.641	144	0.70327	0.51268	0.28265	21.970	15.988	41.733
						0.006	0.084	0.136	0.00515	35.7	0.513	107	0.70311	0.51268	0.28265	21.097	15.885	40.641
						0.008	0.072	0.138	0.00521	30.4	0.438	88	0.70300	0.51269	0.28265	20.587	15.824	40.067
						0.01	0.064	0.140	0.00527	27.0	0.388	76	0.70293	0.51270	0.28265	20.253	15.785	39.713
						0.02	0.044	0.148	0.00558	19.4	0.279	52.3	0.70276	0.51273	0.28265	19.512	15.697	38.983
						0.04	0.032	0.163	0.00620	15.2	0.218	39.8	0.70265	0.51279	0.28266	19.099	15.648	38.607
						0.06	0.027	0.174	0.00684	13.7	0.197	35.6	0.70262	0.51283	0.28267	18.954	15.630	38.479
						0.08	0.025	0.184	0.00751	12.9	0.186	33.4	0.70260	0.51287	0.28268	18.880	15.622	38.415
						0.1	0.024	0.191	0.00820	12.5	0.179	32.2	0.70259	0.51290	0.28268	18.835	15.616	38.377

Table 10 | *(continued)*

Initial isotope ratio at T						F	Parent-daugther ratio of partial melt at T						Calculated present isotope ratio of melt					
$^{87}Sr/^{86}Sr_i$	$^{143}Nd/^{144}Nd_i$	$^{176}Hf/^{177}Hf_i$	$^{206}Pb/^{204}Pb_i$	$^{207}Pb/^{204}Pb_i$	$^{208}Pb/^{204}Pb_i$		$^{87}Rb/^{86}Sr$	$^{147}Sm/^{144}Nd$	$^{176}Lu/^{177}Hf$	$^{238}U/^{204}Pb$	$^{235}U/^{204}Pb$	$^{232}Th/^{204}Pb$	$^{87}Sr/^{86}Sr$	$^{143}Nd/^{144}Nd$	$^{176}Hf/^{177}Hf$	$^{206}Pb/^{204}Pb$	$^{207}Pb/^{204}Pb$	$^{208}Pb/^{204}Pb$
E-DMM at T=30Ma																		
0.70294	0.51285	0.28298	19.734	15.622	39.434	0.001	0.285	0.124	0.0044	108	0.814	614	0.70306	0.51288	0.28299	20.239	15.646	40.346
						0.002	0.234	0.125	0.0044	82	0.616	379	0.70304	0.51288	0.28299	20.117	15.640	39.996
						0.004	0.176	0.126	0.0044	58	0.433	227	0.70301	0.51288	0.28299	20.003	15.635	39.771
						0.006	0.144	0.128	0.0045	46	0.346	170	0.70300	0.51288	0.28299	19.949	15.632	39.686
						0.008	0.123	0.130	0.0046	39	0.295	139	0.70299	0.51288	0.28299	19.917	15.631	39.641
						0.01	0.109	0.132	0.0046	34.9	0.262	121	0.70298	0.51288	0.28299	19.897	15.630	39.614
						0.02	0.075	0.140	0.0049	25.1	0.188	83	0.70297	0.51288	0.28299	19.851	15.628	39.557
						0.04	0.054	0.154	0.0054	19.6	0.147	63	0.70296	0.51288	0.28299	19.825	15.626	39.527
						0.06	0.046	0.165	0.0060	17.7	0.133	56.2	0.70296	0.51289	0.28299	19.816	15.626	39.518
						0.08	0.043	0.173	0.0066	16.7	0.125	52.8	0.70295	0.51289	0.28299	19.812	15.626	39.513
						0.1	0.040	0.181	0.0072	16.1	0.121	50.8	0.70295	0.51289	0.28299	19.809	15.626	39.510
E-DMM at T=130Ma																		
0.70289	0.51270	0.28289	19.510	15.611	39.214	0.001	0.285	0.124	0.0044	108	0.907	610	0.70342	0.51281	0.28291	21.706	15.735	43.151
						0.002	0.234	0.125	0.0044	82	0.686	376	0.70332	0.51281	0.28291	21.172	15.705	41.641
						0.004	0.176	0.126	0.0044	57	0.482	225	0.70322	0.51281	0.28291	20.678	15.677	40.668
						0.006	0.144	0.128	0.0045	46	0.385	168	0.70316	0.51281	0.28291	20.443	15.664	40.301
						0.008	0.123	0.130	0.0046	39	0.329	139	0.70312	0.51281	0.28291	20.307	15.656	40.108
						0.01	0.109	0.132	0.0046	34.7	0.292	120	0.70309	0.51281	0.28291	20.217	15.651	39.989
						0.02	0.075	0.140	0.0049	24.9	0.210	82	0.70303	0.51282	0.28291	20.018	15.640	39.743
						0.04	0.054	0.154	0.0054	19.5	0.164	62	0.70299	0.51283	0.28291	19.908	15.633	39.617
						0.06	0.046	0.165	0.0060	17.6	0.148	55.8	0.70298	0.51284	0.28291	19.869	15.631	39.574
						0.08	0.043	0.173	0.0066	16.6	0.140	52.5	0.70297	0.51285	0.28291	19.849	15.630	39.553
						0.1	0.040	0.181	0.0072	16.0	0.135	50.5	0.70296	0.51285	0.28291	19.837	15.629	39.540

Table 10 | *(continued)*

Initial isotope ratio at T						F	Parent-daugther ratio of partial melt at T						Calculated present isotope ratio of melt					
$^{87}Sr/^{86}Sr_i$	$^{143}Nd/^{144}Nd_i$	$^{176}Hf/^{177}Hf_i$	$^{206}Pb/^{204}Pb_i$	$^{207}Pb/^{204}Pb_i$	$^{208}Pb/^{204}Pb_i$		$^{87}Rb/^{86}Sr$	$^{147}Sm/^{144}Nd$	$^{176}Lu/^{177}Hf$	$^{238}U/^{204}Pb$	$^{235}U/^{204}Pb$	$^{232}Th/^{204}Pb$	$^{87}Sr/^{86}Sr$	$^{143}Nd/^{144}Nd$	$^{176}Hf/^{177}Hf$	$^{206}Pb/^{204}Pb$	$^{207}Pb/^{204}Pb$	$^{208}Pb/^{204}Pb$
E-DMM at T=280Ma																		
0.70282	0.51247	0.28276	19.169	15.592	38.881	0.001	0.285	0.124	0.0044	107	1.066	605	0.70396	0.51270	0.28279	23.910	15.931	47.314
						0.002	0.234	0.125	0.0044	81	0.807	373	0.70375	0.51270	0.28279	22.758	15.848	44.081
						0.004	0.176	0.126	0.0044	57	0.567	223	0.70352	0.51270	0.28279	21.689	15.772	41.997
						0.006	0.144	0.128	0.0045	45	0.453	167	0.70339	0.51271	0.28279	21.183	15.736	41.210
						0.008	0.123	0.130	0.0046	39	0.387	137	0.70331	0.51271	0.28279	20.888	15.715	40.796
						0.01	0.109	0.132	0.0046	34.4	0.343	119	0.70326	0.51271	0.28279	20.695	15.701	40.542
						0.02	0.075	0.140	0.0049	24.7	0.247	81	0.70312	0.51273	0.28279	20.266	15.671	40.016
						0.04	0.054	0.154	0.0054	19.3	0.193	62	0.70304	0.51275	0.28279	20.026	15.653	39.745
						0.06	0.046	0.165	0.0060	17.4	0.174	55.3	0.70301	0.51277	0.28279	19.943	15.647	39.653
						0.08	0.043	0.173	0.0066	16.5	0.164	52.0	0.70299	0.51279	0.28280	19.900	15.644	39.607
						0.1	0.040	0.181	0.0072	15.9	0.159	50.0	0.70298	0.51280	0.28280	19.874	15.643	39.579
E-DMM at T=600Ma																		
0.70267	0.51198	0.28248	18.413	15.542	38.163	0.001	0.285	0.124	0.00437	105	1.504	592	0.70511	0.51246	0.28253	28.618	16.753	56.006
						0.002	0.234	0.125	0.00440	79.2	1.138	365	0.70468	0.51247	0.28253	26.138	16.459	49.166
						0.004	0.176	0.126	0.00445	55.6	0.799	219	0.70418	0.51247	0.28253	23.838	16.186	44.756
						0.006	0.144	0.128	0.00450	44.5	0.639	164	0.70390	0.51248	0.28253	22.749	16.057	43.091
						0.008	0.123	0.130	0.00455	37.9	0.545	135	0.70373	0.51249	0.28253	22.114	15.981	42.216
						0.01	0.109	0.132	0.00460	33.7	0.484	117	0.70361	0.51250	0.28253	21.698	15.932	41.677
						0.02	0.075	0.140	0.00487	24.2	0.348	80	0.70331	0.51253	0.28253	20.774	15.822	40.564
						0.04	0.054	0.154	0.00541	18.9	0.272	60.6	0.70314	0.51258	0.28254	20.259	15.761	39.990
						0.06	0.046	0.165	0.00597	17.1	0.245	54.2	0.70307	0.51262	0.28255	20.079	15.740	39.796
						0.08	0.043	0.173	0.00656	16.1	0.232	51.0	0.70304	0.51266	0.28255	19.987	15.729	39.699
						0.1	0.040	0.181	0.00716	15.6	0.224	49.0	0.70302	0.51269	0.28256	19.931	15.722	39.640

Table 11 | Calculated Sr, Nd, Hf, and Pb isotopic compositions and parent/daughter elemental compositions of the DMM and E-DMM derived carbonatite melt compositions

Initial isotope ratio at T						F	Parent-daugther ratio of partial melt at T						Calculated present isotope ratio of melt					
$^{87}Sr/^{86}Sr_i$	$^{143}Nd/^{144}Nd_i$	$^{176}Hf/^{177}Hf_i$	$^{206}Pb/^{204}Pb_i$	$^{207}Pb/^{204}Pb_i$	$^{208}Pb/^{204}Pb_i$		$^{87}Rb/^{86}Sr$	$^{147}Sm/^{144}Nd$	$^{176}Lu/^{177}Hf$	$^{238}U/^{204}Pb$	$^{235}U/^{204}Pb$	$^{232}Th/^{204}Pb$	$^{87}Sr/^{86}Sr$	$^{143}Nd/^{144}Nd$	$^{176}Hf/^{177}Hf$	$^{206}Pb/^{204}Pb$	$^{207}Pb/^{204}Pb$	$^{208}Pb/^{204}Pb$
DMM at T=30Ma																		
0.70254	0.51308	0.28317	18.667	15.535	38.234	0.001	0.133	0.075	0.0173	24	0.178	73	0.70259	0.51309	0.28318	18.778	15.541	38.343
						0.002	0.129	0.075	0.0173	23	0.176	72	0.70259	0.51309	0.28318	18.777	15.541	38.341
						0.004	0.122	0.076	0.0173	23	0.172	70	0.70259	0.51309	0.28318	18.774	15.541	38.337
						0.006	0.116	0.077	0.0173	22.4	0.168	68	0.70259	0.51309	0.28318	18.772	15.540	38.334
						0.008	0.111	0.078	0.0173	21.9	0.164	66	0.70258	0.51309	0.28318	18.769	15.540	38.331
						0.01	0.106	0.079	0.0173	21.5	0.161	64	0.70258	0.51309	0.28318	18.767	15.540	38.329
						0.02	0.088	0.084	0.0174	19.8	0.148	57	0.70257	0.51309	0.28318	18.759	15.540	38.319
						0.04	0.068	0.094	0.0175	17.6	0.132	49.2	0.70257	0.51310	0.28318	18.749	15.539	38.307
						0.06	0.057	0.102	0.0176	16.3	0.122	44.7	0.70256	0.51310	0.28318	18.743	15.539	38.300
						0.08	0.050	0.109	0.0177	15.5	0.116	41.9	0.70256	0.51310	0.28318	18.739	15.539	38.296
						0.1	0.045	0.116	0.0177	14.8	0.111	39.8	0.70256	0.51310	0.28318	18.736	15.539	38.293
DMM at T=130Ma																		
0.70251	0.51292	0.28307	18.490	15.527	38.091	0.001	0.133	0.075	0.0173	24	0.199	73	0.70276	0.51298	0.28311	18.972	15.554	38.561
						0.002	0.129	0.075	0.0173	23	0.196	72	0.70275	0.51298	0.28311	18.965	15.553	38.553
						0.004	0.122	0.076	0.0173	23	0.192	69	0.70274	0.51298	0.28311	18.954	15.553	38.538
						0.006	0.116	0.077	0.0173	22.3	0.187	67	0.70272	0.51298	0.28311	18.944	15.552	38.524
						0.008	0.111	0.078	0.0173	21.8	0.183	65	0.70271	0.51298	0.28311	18.934	15.552	38.512
						0.01	0.106	0.079	0.0173	21.4	0.180	64	0.70271	0.51298	0.28311	18.925	15.551	38.501
						0.02	0.088	0.084	0.0174	19.7	0.165	57	0.70267	0.51299	0.28311	18.890	15.549	38.457
						0.04	0.068	0.094	0.0175	17.5	0.147	49.0	0.70264	0.51300	0.28311	18.847	15.547	38.407
						0.06	0.057	0.102	0.0176	16.2	0.137	44.5	0.70262	0.51300	0.28311	18.821	15.545	38.378
						0.08	0.050	0.109	0.0177	15.4	0.129	41.7	0.70260	0.51301	0.28311	18.803	15.544	38.359
						0.1	0.045	0.116	0.0177	14.8	0.124	39.7	0.70259	0.51301	0.28311	18.791	15.544	38.347

Table 11 | *(continued)*

Initial isotope ratio at T						F	Parent-daugther ratio of partial melt at T						Calculated present isotope ratio of melt					
$^{87}Sr/^{86}Sr_i$	$^{143}Nd/^{144}Nd_i$	$^{176}Hf/^{177}Hf_i$	$^{206}Pb/^{204}Pb_i$	$^{207}Pb/^{204}Pb_i$	$^{208}Pb/^{204}Pb_i$		$^{87}Rb/^{86}Sr$	$^{147}Sm/^{144}Nd$	$^{176}Lu/^{177}Hf$	$^{238}U/^{204}Pb$	$^{235}U/^{204}Pb$	$^{232}Th/^{204}Pb$	$^{87}Sr/^{86}Sr$	$^{143}Nd/^{144}Nd$	$^{176}Hf/^{177}Hf$	$^{206}Pb/^{204}Pb$	$^{207}Pb/^{204}Pb$	$^{208}Pb/^{204}Pb$
DMM at T=280Ma																		
0.70247	0.51267	0.28292	18.218	15.512	37.874	0.001	0.133	0.075	0.01730	23.5	0.234	72	0.70300	0.51281	0.28301	19.261	15.586	38.886
						0.002	0.129	0.075	0.01730	23.2	0.231	71	0.70298	0.51281	0.28301	19.248	15.585	38.868
						0.004	0.122	0.076	0.01731	22.6	0.226	69	0.70296	0.51281	0.28301	19.223	15.584	38.835
						0.006	0.116	0.077	0.01732	22.1	0.221	67	0.70293	0.51281	0.28301	19.201	15.582	38.805
						0.008	0.111	0.078	0.01733	21.7	0.216	65	0.70291	0.51282	0.28301	19.180	15.580	38.779
						0.01	0.106	0.079	0.01734	21.2	0.212	63	0.70289	0.51282	0.28301	19.161	15.579	38.755
						0.02	0.088	0.084	0.01738	19.5	0.195	56.5	0.70282	0.51283	0.28301	19.085	15.574	38.662
						0.04	0.068	0.094	0.01748	17.4	0.174	48.7	0.70274	0.51284	0.28301	18.991	15.567	38.553
						0.06	0.057	0.102	0.01757	16.1	0.161	44.2	0.70270	0.51286	0.28301	18.934	15.563	38.492
						0.08	0.050	0.109	0.01766	15.3	0.152	41.4	0.70267	0.51287	0.28301	18.897	15.560	38.452
						0.1	0.045	0.116	0.01775	14.7	0.146	39.4	0.70265	0.51288	0.28301	18.870	15.558	38.424
DMM at T=600Ma																		
0.70238	0.51215	0.28259	17.618	15.472	37.408	0.001	0.133	0.075	0.01730	23.1	0.332	71	0.70352	0.51244	0.28279	19.874	15.740	39.559
						0.002	0.129	0.075	0.01730	22.8	0.328	70	0.70349	0.51245	0.28279	19.845	15.736	39.521
						0.004	0.122	0.076	0.01731	22.3	0.320	68	0.70343	0.51245	0.28279	19.792	15.730	39.451
						0.006	0.116	0.077	0.01732	21.8	0.313	66	0.70338	0.51245	0.28279	19.743	15.724	39.388
						0.008	0.111	0.078	0.01733	21.3	0.307	64	0.70333	0.51246	0.28279	19.699	15.719	39.332
						0.01	0.106	0.079	0.01734	20.9	0.301	62	0.70329	0.51246	0.28279	19.658	15.714	39.281
						0.02	0.088	0.084	0.01738	19.2	0.276	55.6	0.70314	0.51248	0.28279	19.494	15.694	39.084
						0.04	0.068	0.094	0.01748	17.1	0.246	47.9	0.70296	0.51252	0.28279	19.289	15.670	38.852
						0.06	0.057	0.102	0.01757	15.9	0.228	43.6	0.70287	0.51255	0.28279	19.167	15.656	38.721
						0.08	0.050	0.109	0.01766	15.0	0.216	40.8	0.70281	0.51258	0.28279	19.085	15.646	38.636
						0.1	0.045	0.116	0.01775	14.5	0.208	38.8	0.70277	0.51261	0.28280	19.027	15.639	38.577

Table 11 | *(continued)*

Initial isotope ratio at T						F	Parent-daugther ratio of partial melt at T						Calculated present isotope ratio of melt					
$^{87}Sr/^{86}Sr_i$	$^{143}Nd/^{144}Nd_i$	$^{176}Hf/^{177}Hf_i$	$^{206}Pb/^{204}Pb_i$	$^{207}Pb/^{204}Pb_i$	$^{208}Pb/^{204}Pb_i$		$^{87}Rb/^{86}Sr$	$^{147}Sm/^{144}Nd$	$^{176}Lu/^{177}Hf$	$^{238}U/^{204}Pb$	$^{235}U/^{204}Pb$	$^{232}Th/^{204}Pb$	$^{87}Sr/^{86}Sr$	$^{143}Nd/^{144}Nd$	$^{176}Hf/^{177}Hf$	$^{206}Pb/^{204}Pb$	$^{207}Pb/^{204}Pb$	$^{208}Pb/^{204}Pb$
E-DMM at T=30Ma																		
0.70294	0.51285	0.28298	19.734	15.627	39.434	0.0001	0.226	0.071	0.0151	30	0.224	113	0.70303	0.51287	0.28299	19.873	15.634	39.602
						0.0002	0.219	0.071	0.0151	30	0.221	111	0.70303	0.51287	0.28299	19.871	15.634	39.599
						0.0004	0.208	0.072	0.0151	29	0.216	107	0.70302	0.51287	0.28299	19.868	15.633	39.593
						0.0006	0.198	0.073	0.0151	28	0.211	104	0.70302	0.51287	0.28299	19.865	15.633	39.588
						0.0008	0.189	0.074	0.0151	28	0.207	101	0.70302	0.51287	0.28299	19.862	15.633	39.584
						0.001	0.181	0.075	0.0151	27.0	0.203	98	0.70301	0.51287	0.28299	19.860	15.633	39.580
						0.002	0.150	0.080	0.0152	24.8	0.186	88	0.70300	0.51287	0.28299	19.850	15.632	39.565
						0.004	0.116	0.088	0.0153	22.1	0.166	76	0.70299	0.51287	0.28299	19.837	15.632	39.547
						0.006	0.097	0.096	0.0153	20.5	0.154	68.8	0.70298	0.51287	0.28299	19.829	15.632	39.536
						0.008	0.085	0.103	0.0154	19.4	0.146	64.4	0.70297	0.51287	0.28299	19.824	15.631	39.530
						0.01	0.076	0.109	0.0155	18.7	0.140	61.3	0.70297	0.51288	0.28299	19.821	15.631	39.525
E-DMM at T=130Ma																		
0.70289	0.51270	0.28289	19.510	15.611	39.214	0.0001	0.226	0.071	0.0151	30	0.250	112	0.70331	0.51276	0.28293	20.115	15.645	39.937
						0.0002	0.219	0.071	0.0151	29	0.247	110	0.70330	0.51276	0.28293	20.108	15.645	39.924
						0.0004	0.208	0.072	0.0151	29	0.241	106	0.70327	0.51276	0.28293	20.093	15.644	39.901
						0.0006	0.198	0.073	0.0151	28	0.235	103	0.70326	0.51276	0.28293	20.080	15.643	39.880
						0.0008	0.189	0.074	0.0151	27	0.230	100	0.70324	0.51276	0.28293	20.068	15.642	39.861
						0.001	0.181	0.075	0.0151	26.9	0.226	98	0.70322	0.51276	0.28293	20.057	15.642	39.844
						0.002	0.150	0.080	0.0152	24.7	0.208	87	0.70317	0.51277	0.28293	20.013	15.639	39.777
						0.004	0.116	0.088	0.0153	22.0	0.185	75	0.70310	0.51278	0.28293	19.959	15.636	39.699
						0.006	0.097	0.096	0.0153	20.4	0.172	68.4	0.70307	0.51278	0.28293	19.926	15.634	39.655
						0.008	0.085	0.103	0.0154	19.3	0.163	64.0	0.70305	0.51279	0.28293	19.904	15.633	39.627
						0.01	0.076	0.109	0.0155	18.6	0.156	60.9	0.70303	0.51279	0.28293	19.888	15.632	39.607

Table 11 | *(continued)*

Initial isotope ratio at T						F	Parent-daugther ratio of partial melt at T						Calculated present isotope ratio of melt					
$^{87}Sr/^{86}Sr_i$	$^{143}Nd/^{144}Nd_i$	$^{176}Hf/^{177}Hf_i$	$^{206}Pb/^{204}Pb_i$	$^{207}Pb/^{204}Pb_i$	$^{208}Pb/^{204}Pb_i$		$^{87}Rb/^{86}Sr$	$^{147}Sm/^{144}Nd$	$^{176}Lu/^{177}Hf$	$^{238}U/^{204}Pb$	$^{235}U/^{204}Pb$	$^{232}Th/^{204}Pb$	$^{87}Sr/^{86}Sr$	$^{143}Nd/^{144}Nd$	$^{176}Hf/^{177}Hf$	$^{206}Pb/^{204}Pb$	$^{207}Pb/^{204}Pb$	$^{208}Pb/^{204}Pb$
E-DMM at T=280Ma																		
0.70282	0.51247	0.28276	19.169	15.592	38.881	0.0001	0.226	0.071	0.015	29	0.294	111	0.70372	0.51260	0.28284	20.475	15.686	40.430
						0.0002	0.219	0.071	0.0151	29	0.290	109	0.70370	0.51260	0.28284	20.459	15.684	40.403
						0.0004	0.208	0.072	0.0151	28	0.283	105	0.70365	0.51260	0.28284	20.428	15.682	40.353
						0.0006	0.198	0.073	0.0151	28	0.277	102	0.70361	0.51260	0.28284	20.400	15.680	40.308
						0.0008	0.189	0.074	0.0151	27	0.271	99	0.70357	0.51261	0.28284	20.374	15.678	40.267
						0.001	0.181	0.075	0.0151	27	0.266	97	0.70354	0.51261	0.28284	20.350	15.677	40.230
						0.002	0.150	0.080	0.0152	24.5	0.244	87	0.70342	0.51262	0.28284	20.255	15.670	40.088
						0.004	0.116	0.088	0.0153	21.8	0.218	75	0.70328	0.51263	0.28284	20.137	15.661	39.922
						0.006	0.097	0.096	0.0153	20.2	0.202	68	0.70321	0.51265	0.28284	20.066	15.656	39.827
						0.008	0.085	0.103	0.0154	19.1	0.191	63.4	0.70316	0.51266	0.28285	20.019	15.653	39.766
						0.01	0.076	0.109	0.0155	18.4	0.183	60.4	0.70313	0.51267	0.28285	19.985	15.651	39.723
E-DMM at T=600Ma																		
0.70267	0.51198	0.28248	18.413	15.542	38.163	0.0001	0.226	0.071	0.015	29	0.414	109	0.70461	0.51225	0.28265	21.225	15.876	41.441
						0.0002	0.219	0.071	0.015	28	0.409	107	0.70455	0.51226	0.28265	21.190	15.872	41.384
						0.0004	0.208	0.072	0.01512	28	0.399	103	0.70445	0.51226	0.28265	21.123	15.864	41.277
						0.0006	0.198	0.073	0.01513	27.2	0.390	100	0.70437	0.51226	0.28265	21.062	15.856	41.182
						0.0008	0.189	0.074	0.01513	26.6	0.382	97	0.70429	0.51227	0.28265	21.007	15.850	41.096
						0.001	0.181	0.075	0.01514	26.1	0.375	95	0.70422	0.51227	0.28265	20.955	15.844	41.018
						0.002	0.150	0.080	0.01518	24.0	0.345	85	0.70396	0.51229	0.28265	20.751	15.819	40.717
						0.004	0.116	0.088	0.01526	21.4	0.307	73	0.70366	0.51232	0.28265	20.496	15.789	40.365
						0.006	0.097	0.096	0.01534	19.8	0.285	66	0.70350	0.51236	0.28265	20.344	15.771	40.164
						0.008	0.085	0.103	0.01542	18.8	0.270	62.1	0.70340	0.51238	0.28266	20.242	15.759	40.035
						0.01	0.076	0.109	0.01550	18.0	0.259	59.1	0.70333	0.51241	0.28266	20.170	15.750	39.945

CHAPTER 6: CONCLUSIONS

One of the representative intraplate magmatism occures along the passive continental margin, which is most widely distributed at the western offshore of African continent and their closely related continenal regions. These west African passive margin intraplate basalts (WAPM-IB) are characterized by the large distribution of highly alkaline volcanics including carbonatite and the prolonged volcanic activities in the same volcanic region. The heterogeneous elemental and isotopic compositions of the WAPM-IB have been generally explained by the mixing of the upwelling mantle plume that contains lower mantle material and recycled ancient crustal or lithospheric mantle materials; depleted MORB source mantle; and the delaminated SCLM. However, no clear age propagation of the hot-spot tracks despite their extended eruptive activity in each archipelago, suggest the difficulty to explain their magma genesis by a model involving a simple long-lived upwelling mantle plume.

In order to constrain the magma genensis of the WAPM-IB, I analyzed major and trace elements and Sr, Nd, Hf, and Pb isotopic compositions for 90 mafic samples collected from five volcanic centers (Annobon, Sao Tome, Principe, Bioko, and Etinde) in the Cameroon Volcanic Line. The data from Mt. Cameroon samples which were published previously in the same laboratory (N = 26) are also used for discussion. Most of the samples are classified as basanite with minor amount of basalt, trachybasalt, picrobasalt, phonoetphrite, tephriphonolite, and foidite. These highly alkaline magmas should be formed by relatively low degree of melting, which is inconsistent to have generated by the long-lived upwelling mantle plume. The general trace element pattern of CVL samples show highly enriched in incompatible elements. Most of the samples show unique trace element patters having negative anomalies of K, Pb, P, Zr, Hf, and Ti which is distinct from the MORB or OIB except for HIMU basalts. The negative anomalies of Zr, Hf, and Ti indicate the influence of melt derived from the carbonatite-metasomatized SCLM or CO_2-rich melt formed at the garnet-peridotite stability condition because of their high partition coefficients relative to REE between carbonatite and garnet. To evaluate the influence of carbonatitic melt in the source, the CVL samples are classified into Type 1 and Type 2 based on the Hf/Sm and Ti/Gd. Among the Type 1 samples, those from the SW sections (Annobon, Sao Tome, and Principe) shows relatively flat pattern for P and positive anomaly for Ba, while those for NE sections (Etinde and Mt.

Cameroon) show negative anomalies of P and Ba. By these geochemical differences, the type 1 samples are further classified into Type 1 NE and Type 1 SW. Type 2 are mostly derived from SW sections. The Sr, Nd, Hf, and Pb isotpoic compsition consisntetly show distinct trends among the Type 1 NE, Type 1 SW, and Type 2 samples, suggestig that the CVL magma has been formed basically from three distinct source materials. The geochemical and isotopic data of Type 1 Bioko shows intermediate values among the Type 1 NE and Type 1 SW.

Geophysical data revealed the CVL are located along the NW edge of the Congo craton. The continental rift model also demonstrated the wide distribution of African SCLM beneath the Atlantic Ocean. Thus, it is plausible that these SCLM can be a source for the CVL magma. To decipher the source materials for the identified three components, the Pb isotopic systemtaitc of the CVL samples were evaluated and relative contributions from the following magma sources are examined: (1) MORB-source asthenospheric mantle, (2) rerfertilized kimberlite source lower cratonic subcontinental lithspheric mantle (SCLM), (3) ancient asthenospheric mantle-derived melt that could have rejuvenated the lithospheric mantle, and (4) mafic mantle and crustal xenoliths, and (5) external material which corresponds to upwelling mantle plume component.

The Sr, Nd, and Hf isotopic compositions reveals that the parental magma of the CVL lavas could not have formed by simple melting of the current MORB-source asthenospheric mantle. Melting of the Group 1 SCLM can explain the Pb isotopic variation of Type 1 SW component at the plausible $^{238}U/^{204}Pb$ (μ) and $^{232}Th/^{238}U$ (κ) values. Most of the Nd and Hf isotopic compositions of the Type 1 SW samples also accord with the range of Group 1 SCLM. On the other hand, the $^{207}Pb/^{204}Pb$ of the Type 1 NE and Type 2 samples are lower and higher than those range of Group 1 SCLM at a given $^{206}Pb/^{204}Pb$, respectively. Thus, Group 1 SCLM cannot be a primary source of Type 1 NE and Type 2 samples. The ancient asthenospheric mantle-derived melt can be a source of Type 1 NE samples. As the trace element pattern indicated, the source for Type 1 samples must be influenced by carbonatitic or ultra-low degree of melt. Thus, it is likely that the metasomatic agent to form the rejuvenated lithospheric mantle was initially fertile and isotopically enriched composition. The model calculation suggests that the Pb,Sr,Nd

and Hf isotopic range of the Type 1 NE samples can be reproduced by lithosphere metasomatized low-degree melt that derived from the fertile asthenospheric mantle during the continental breakup at ~130Ma. On the other hand, the ancient asthenospheric mantle–derived melt younger than ~130Ma cannot explain the isotope systematics of the Type 1 SW and Type 2 samples. The elemental and isotopic trend which extends from Type 1 SW to Type 2 could be influenced by the mixing of the third component. The compiled data for all the lower crustal and pyroxenite xenoliths from Africa and its vicinity show that only the pyroxenite xenolith which was derived from pyroxenite vein or layer that formed during Proterozoic at the base of eastern edge of Congo SCLM can explain the trend of the Sr, Nd, and Pb isotopic compositions for Type 2 samples. All of these data deciphered that the external plume component is not necessary to explain the isotopic variations of the CVL magmas.

To investigate this model for other volcanic locations along the western edge of African continents, compiled Sr, Nd, Hf, and Pb isotopic composition of other WAPM-IB (Madeira Islands, Canary Islands, Atlas Mountains, Cape Verde Islands, and continental sector of CVL) and Atlantic MORB are compared with those of CVL. The principal component analysis for these samples (N=707) demonstrates that all the analyzed samples except for Madeira can be explained by the mixing of the same identified three components. The published geophysical data and numerical models revealed that the these WAPM-IB except for Madeira are located on or near the edge of cratonic SCLM which is widely distributed beneath the Atlantic Ocean. The reconstructed continent and rift zones during Jurassic and Cretaceous periods shows that the location of Canary, Atlas, Cape Verde, and CVL are on or near the rift axis during the breakup of Pangea supercontinent. Thus, it is likely that the magmas issued from these locations can be generated by the melting of refertilized SCLM, rejuvenated lithospheric mantle, and pyroxenite vein/layer in the SCLM. The Sr, Nd, Hf, and Pb isotopic compositions suggests that the source of Madeira can be composed of mixture of asthenospheric-mantle-derived metasomatic agent at <~130 Ma and the current asthenospheric mantle. The geophysically revealed absence of SCLM beneath the Madeira Island is consistent with the isotope systematics.

The tomographic model images and the continental rift model for the passive continental margin suggest that the widespread continental crust and the cratonic SCLM beneath the western offshore of Atlantic Ocean was generated by the underplating of the buoyant lower cratonic lithospheric mantle during the continental breakup. During the initial stage of continental breakup, upwelling of asthenospheric mantle can form the partial melt, which can metasomatize the lower part of the lithospheric mantle, forming the rejuvenated SCLM. After breaking up the upwelled SCLM at ridge axis, and separating the continent for more than >~40 My from the initial breakup, the counter flow, proposed as edge-driven convection including in these regions, of the asthenospheric mantle near the asthenosphere-SCLM boundary can be occurred. This edge-driven convection can heat the SCLM beneath the Atlantic Ocean, selectively melting the low solidus material of the SCLM. The coincident distribution of CVL and Canary-Atlas chains at the NW edge of the cratonic lithospheric mantle suggests that the heating of the SCLM by the edge-driven convection can be the most effective where the mantle flow collide near the edge of the SCLM rather than at the front collision. The edge-driven convection can occur more than several tens Mys at the same location, forming the long duration of magmatism without showing the time-progressive linear hot spot track. Thus, intraplate magmatism at the passive continental margin can be explained by melting of previously melt-reacted SCLM heated by the edge-driven mantle convection without considering the mantle plume. This study concludes that the plume hypothesis is not necessary to form the chemical and isotopic characteristics for the passive continental margin hot spot magmatism.

CHAPTER 7: REFERENCES

Abdel-Monem, A., Watkins, N. D., and Gast, P. W. (1971). Potassium-argon ages, volcanic stratigraphy, and geomagnetic polarity history of the Canary Islands; Lanzarote, Fuerteventura, Gran Canaria, and La Gomera. *American Journal of Science*, **271(5),** 490-521.

Abratis, M., Schmincke, H.U. and Hansteen, T. (2002) Composition and evolution of submarine volcanic rocks from the central and western Canary Islands. *Int J Earth Sci* **91,** 562-582.

Adams, A.N., Wiens, D.A., Nyblade, A.A., Euler, G.G., Shore, P.J. and Tibi, R. (2015) Lithospheric instability and the source of the Cameroon Volcanic Line: Evidence from Rayleigh wave phase velocity tomography. *Journal of Geophysical Research-Solid Earth* **120,** 1708-1727.

Agranier, A., Blichert-Toft, J., Graham, D., Debaille, V., Schiano, P. and Albarède, F. (2005) The spectra of isotopic heterogeneities along the mid-Atlantic Ridge. *Earth Planet. Sci. Lett.* **238,** 96-109.

Aka, F. T., K. Nagao, M. Kusakabe, and N. Nfomou (2009), Cosmogenic helium and neon in mantle xenoliths from the Cameroon Volcanic Line (West Africa): Preliminary observations, *J. Afr. Earth Sci*., **55,** 175–184.

Aka, F.T., Nagao, K., Kusakabe, M., Sumino, H., Tanyileke, G., Ateba, B., Hell, J.V., (2004) Symmetrical helium isotope distribution on the Cameroon Volcanic Line. West Africa. *Chemical Geology* **203,** 205-223.

Aka, F.T., Yokoyama, T., Kusakabe, M., Nakamura, E., Tanyileke, G., Ateba, B., Ngako, V., Nnange, J.M., Hell, J.V. (2008) U-series dating of Lake Nyos maar basalts, Cameroon (West Africa); implications for potential hazards on the Lake Nyos dam. *Journal of Volcanology and Geothermal Research* **176,** 212-224.

Allègre, C.J., Dupré, B., Lambret, B., Richard, P., 1981. The subcontinental versus suboceanic debate, I Lead-neodymium-strontium isotopes in primary alkali basalts from a shield area the Ahaggar volcanic suite. *Earth Planet. Sci. Lett.* **52,** 85–92.

Ancochea E, Fuster JM, Ibarrola E, Cendrero A, Hernán F, Cantagrel JM, Jamond C (1990) Volcanic evolution of the island of Tenerife (Canary Islands) in the light of new K-Ar data. *J Volcanol Geotherm Res* **44**:231–249.

Ancochea, E., Barrera, J. L., Bellido, F., Benito, R., Brändle, J. L., Cebriá, J. M., ... and Gómez, J. A. (2004). Canarias y el vulcanismo neógeno peninsular. *Geología de España,* 635-682.

Ancochea, E., Hernán, F., Huertas, M. J., Brändle, J. L., and Herrera, R. (2006). A new chronostratigraphical and evolutionary model for La Gomera: implications for the overall evolution of the Canarian Archipelago. *Journal of Volcanology and Geothermal Research,* **157(4),** 271-293.

Anderson, D.L. (1998) The EDGES of the Mantle, The Core-Mantle Boundary Region. *American Geophysical Union,* pp. 255-271.

Andres, M., Blichert-Toft, J. and Schilling, J.-G. (2004) Nature of the depleted upper mantle beneath the Atlantic: evidence from Hf isotopes in normal mid-ocean ridge basalts from 79°N to 55°S. *Earth Planet. Sci. Lett.* **225,** 89-103.

Anguita F, Hernán F (2000) The Canary Islands origin: a unifying model. *J Volcanol Geotherm Res* **103**:1–26.

Annor, A.E., Freeth, S.J., 1985. Thermo-tectonic evolution of the basement complex around Okene, Nigeria, with special reference to deformation mechanism. *Precambrian Research* **28,** 269-281.

Aparicio, A., Tassinari, C.C.G., García, R. and Araña, V. (2010) Sr and Nd isotope composition of the metamorphic, sedimentary and ultramafic xenoliths of Lanzarote (Canary Islands): Implications for magma sources. *J. Volcanol. Geotherm. Res.* **189,** 143-150.

Arndt, N.T., Christensen, U., 1992. The role of lithospheric mantle in continental flood volcanism: Thermal and geochemical constraints. *J. Geophys. Res.* **97,** 10967.

Asaah, A. N., Yokoyama, T., Aka, F. T., Usui, T., Wirmvem, M. J., Tchamabe, B. C., ... and Hell, J. V. (2015). A comparative review of petrogenetic processes beneath the Cameroon Volcanic Line: *Geochemical constraints. Geoscience Frontiers,* **6(4),** 557-570.

Asaah, A.N.E., Yokoyama, T., Aka, F.T., Usui, T., Kuritani, T., Wirmvem, M.J., Iwamori, H., Fozing, E.M., Tamen, J., Mofor, G.Z., Ohba, T., Tanyileke, G. and Hell, J.V. (2015) Geochemistry of lavas from maar-bearing volcanoes in the Oku Volcanic Group of the Cameroon Volcanic Line. *Chem. Geol.* **406,** 55-69.

Ateba, B., and N. Ntepe (1997), Post-eruptive seismic activity of Mount Cameroon (Cameroon), West Africa: A statistical analysis, *J. Volcanol. Geotherm. Res.,* **79(1–2),** 25–45.

Ateba, B., C. Dorbath, L. Dorbath, N. Ntepe, M. Frogneux, J. Delmond, and D. Manguelle (2009), Eruptive and earthquake activities related to the 2000 eruption of Mount Cameroon volcano (West Africa), *J. Volcanol. Geotherm. Res.,* **179(3–4),** 206–216.

Aulinas, M., Gimeno, D., Fernandez-Turiel, J.L., Font, L., Perez-Torrado, F.J., Rodriguez-Gonzalez, A. and Nowell, G.M. (2010) Small-scale mantle heterogeneity on the source of the Gran Canaria (Canary Islands) Pliocene–Quaternary magmas. *Lithos* **119,** 377-392.

Ballentine, C.J., Lee, D.C. and Halliday, A.N. (1997) Hafnium isotopic studies of the Cameroon line and new HIMU paradoxes. *Chem. Geol.* **139,** 111-124.

Barfod, D. N., Ballentine, C. J., Halliday, A. N., and Fitton, J. G. (1999). Noble gases in the cameroon line and the he, ne, and ar isotopic compositions of high μ (himu) mantle. *Journal of Geophysical Research: Solid Earth (1978–2012),***104(B12),** 29509–29527.

Barker, A.K., Holm, P.M. and Troll, V.R. (2014) The role of eclogite in the mantle heterogeneity at Cape Verde. Contrib. *Mineral. Petrol.* **168,** 1052.

Barker, A.K., Holm, P.M., Peate, D.W. and Baker, J.A. (2009) Geochemical Stratigraphy of Submarine Lavas (3–5 Ma) from the Flamengos Valley, Santiago, Southern Cape Verde Islands. *J. Petrol.* **50,** 169-193.

Barker, A.K., Holm, P.M., Peate, D.W. and Baker, J.A. (2010) A 5-million-year record

of compositional variations in mantle sources to magmatism on Santiago, southern Cape Verde archipelago. *Contrib. Mineral. Petrol.* **160,** 133-154.

Basseka, C., Y. Shandini, and J. Tadjou (2011), Subsurface structural mapping using gravity data of the northern edge of the Congo Craton, South Cameroon, *Geofizika*, 28(2), 229–245.

Beaumont, C. and Ings, S.J. (2012) Effect of depleted continental lithosphere counterflow and inherited crustal weakness on rifting of the continental lithosphere: General results. *Journal of Geophysical Research: Solid Earth* **117,** n/a-n/a.

Beccaluva, L., Azzouni-Sekkal, A., Benhallou, A., Bianchini, G., Ellam, R.M., Marzola, M., Siena, F. and Stuart, F.M. (2007) Intracratonic asthenosphere upwelling and lithosphere rejuvenation beneath the Hoggar swell (Algeria): Evidence from HIMU metasomatised lherzolite mantle xenoliths. *Earth Planet. Sci. Lett.* **260,** 482-494.

Becker, M. and le Roex, A.P. (2006) Geochemistry of South African On- and Off-craton, Group I and Group II Kimberlites: Petrogenesis and Source Region Evolution. *J. Petrol.* **47,** 673-703.

Becker, M., le Roex, A.P. and Class, C. (2007) Geochemistry and petrogenesis of South African transitional kimberlites located on and off the Kaapvaal Craton. *South African Journal of Geology* **110,** 631-646.

Begg, G.C., Griffin, W.L., Natapov, L.M., O'Reilly, S.Y., Grand, S.P., O'Neill, C.J., Hronsky, J.M.A., Djomani, Y.P., Swain, C.J., Deen, T. and Bowden, P. (2009) The lithospheric architecture of Africa: Seismic tomography, mantle petrology, and tectonic evolution. *Geosphere* **5,** 23-50.

Beier, C., Stracke, A., and Haase, K. M. (2007). The peculiar geochemical signatures of s˜ao miguel (azores) lavas: Metasomatised or recycled mantle sources. *Earth and Planetary Science Letters,* **259(1),** 186–199.

Berger, J., Ennih, N. and Liégeois, J.-P. (2014) Extreme trace elements fractionation in Cenozoic nephelinites and phonolites from the Moroccan Anti-Atlas (Eastern Saghro). *Lithos* **210–211,** 69-88.

Bianchini, G., Bryce, J.G., Blichert-Toft, J., Beccaluva, L. and Natali, C. (2014) Mantle dynamics and secular variations beneath the East African Rift: Insights from peridotite xenoliths (Mega, Ethiopia). *Chem. Geol.* **386,** 49-58.

Bonadiman, C., Beccaluva, L., Coltorti, M. and Siena, F. (2005) Kimberlite-like Metasomatism and 'Garnet Signature' in Spinel-peridotite Xenoliths from Sal, Cape Verde Archipelago: Relics of a Subcontinental Mantle Domain within the Atlantic Oceanic Lithosphere. *J. Petrol.* **46,** 2465-2493.

Bosch, D., Maury, R.C., El Azzouzi, M.h., Bollinger, C., Bellon, H. and Verdoux, P. (2014) Lithospheric origin for Neogene–Quaternary Middle Atlas lavas (Morocco): Clues from trace elements and Sr–Nd–Pb–Hf isotopes. *Lithos* **205,** 247-265.

Brede, R., Hauptmann, M., and Herbig, H.-G., 1992, Plate tectonics and the intracratonic mountain ranges in Morocco—The Mesozoic-Cenozoic development of the Central High Atlas and the Middle Atlas: *Geologische Rundschau,* **v. 81,**

p.127–141.

Bull, A.L., McNamara, A.K. and Ritsema, J. (2009) Synthetic tomography of plume clusters and thermochemical piles. *Earth Planet. Sci. Lett.* **278,** 152-162.

Burke, K., 2001. Origin of the Cameroon Line of volcano-capped swells. *The Journal of Geology* **109,** 349-362.

Cantagrel, J. M., Cendrero, A., Fuster, J. M., Ibarrola, E., and Jamond, C. (1984). K-Ar chronology of the volcanic eruptions in the Canarian archipelago: island of La Gomera. *Bulletin of Volcanology,* **47(3),** 597-609.

Cantagrel, J.M., Fúster, J.M., Pin, C., Renaud, U., and Ibarrola, E., 1993, Age Miocène inférieur des carbonatites de Fuerteventura (23 Ma: U-Pb zircon) et le magmatisme précoce d'une île oceanique (îles Canaries): *Paris, Comptes Rendus de l'Académie des Sciences,* **sér. 2, v. 316**, p. 1147–1153.

Carracedo, J. C., Badiola, E. R., and Soler, V. (1992). The 1730–1736 eruption of Lanzarote, Canary Islands: a long, high-magnitude basaltic fissure eruption. *Journal of Volcanology and Geothermal Research,* **53(1-4),** 239-250.

Chauvel, C., Hofmann, A. W., and Vidal, P. (1992). Himu-em: the french polynesian connection. *Earth and Planetary Science Letters,***110(1),** 99–119.

Christensen, B.P., Holm, P.M., Jambon, A. and Wilson, J.R. (2001) Helium, argon and lead isotopic composition of volcanics from Santo Antão and Fogo, Cape Verde Islands. *Chem. Geol.* **178,** 127-142.

Clague, D.A., Frey, F.A., 1982. Petrology and trace element geochemistry of the Honolulu Volcanics, Oahu: implications for the oceanic mantle below Hawaii. *Journal of Petrology* **23,** 447-504.

Clift, P. D., and Lorenzo, J. M. (1999). Flexural unloading and uplift along the Côte d'Ivoire-Ghana Transform Margin, equatorial Atlantic. *Journal of Geophysical Research: Solid Earth*, *104*(B11), 25257-25274.

Coe, N., le Roex, A., Gurney, J., Pearson, D.G. and Nowell, G. (2008) Petrogenesis of the Swartruggens and Star Group II kimberlite dyke swarms, South Africa: constraints from whole rock geochemistry. Contrib. *Mineral. Petrol.* **156,** 627.

Coello, J., Cantagrel, J. M., Hernan, F., Fuster, J. M., Ibarrola, E., Ancochea, E., Casquet, C., Jamond, C., Diaz de Teran, J. R., and Cendrero, A., 1992, Evolution of the eastern volcanic ridge of the Canary Islands based on new K-Ar data: *Journal of Volcanology and Geothermal Research,* **v. 53**, p. 1–4.

Cohen, R. and O'Nions, R. (1982). Identification of recycled continental material in the mantle from sr, nd and pb isotope investigations. *Earth and Planetary Science Letters,* **61(1),** 73–84.

Cohen, R.S., Onions, R.K. and Dawson, J.B. (1984) Isotope geochemistry of xenoliths from East Africa: Implications for development of mantle reservoirs and their interaction. *Earth Planet. Sci. Lett.* **68,** 209-220.

Coltorti, M., Bonadiman, C., O'Reilly, S.Y., Griffin, W.L. and Pearson, N.J. (2010) Buoyant ancient continental mantle embedded in oceanic lithosphere (Sal Island,

Cape Verde Archipelago). *Lithos* **120,** 223-233.

Conrad, C.P., Wu, B., Smith, E.I., Bianco, T.A. and Tibbetts, A. (2010) Shear-driven upwelling induced by lateral viscosity variations and asthenospheric shear: A mechanism for intraplate volcanism. *Physics of the Earth and Planetary Interiors* **178,** 162-175.

Cornen, G., and R. C. Maury (1980), Petrology of the volcanic island of Annobón, Gulf of Guinea, *Mar. Geol.,* **36(3–4),** 253–267.

Coulon, C., Vidal, P., Dupuy, C., Baudin, P., Popoff, M., Maluski, H., and Hermitte, D. (1996). The Mesozoic to early Cenozoic magmatism of the Benue Trough (Nigeria); geochemical evidence for the involvement of the St Helena plume. *Journal of Petrology*, *37*(6), 1341-1358.

Courtillot, V., Davaille, A., Besse, J. and Stock, J. (2003) Three distinct types of hotspots in the Earth's mantle. *Earth Planet. Sci. Lett.* **205,** 295-308.

Cousens, B.L., Spera, F.J. and Tilton, G.R. (1990) Isotopic patterns in silicic ignimbrites and lava flows of the Mogan and lower Fataga Formations, Gran Canaria, Canary Islands: temporal changes in mantle source composition. *Earth Planet. Sci. Lett.* **96,** 319-335.

Dasgupta, R., Hirschmann, M.M., McDonough, W.F., Spiegelman, M. and Withers, A.C. (2009) Trace element partitioning between garnet lherzolite and carbonatite at 6.6 and 8.6 GPa with applications to the geochemistry of the mantle and of mantle-derived melts. *Chem. Geol.* **262,** 57-77.

Dasgupta, R., Mallik, A., Tsuno, K., Withers, A. C., Hirth, G., and Hirschmann, M. M. (2013). Carbon-dioxide-rich silicate melt in the Earth's upper mantle. *Nature*, ***493*(7431),** 211.

Dash, B. P., Ball, M. M., King, G. A., Butler, L. W., and Rona, P. A. (1976). Geophysical investigation of the Cape Verde archipelago. *Journal of Geophysical Research*, **81(29),** 5249-5259.

Davies, G. R., Cliff, R. A., Norry, M. J., and Gerlach, D. C. (1989). A combined chemical and Pb-Sr-Nd isotope study of the Azores and Cape Verde hot-spots: the geodynamic implications. *Geological Society, London, Special Publications,* **42(1),** 231-255.

Davies, G.R. and Lloyd, F.E. (1989) Pb–Sr–Nd isotope and trace element data bearing on the origin of the potassic subcontinental lithosphere beneath south-west Uganda, Kimberlites and Related Rocks, 2, *Geological Society of Australia Special Publication,* pp. 784-794.

Davies, G.R., Spriggs, A.J. and Nixon, P.H. (2001) A Non-Cognate Origin for the Gibeon Kimberlite Megacryst Suite, Namibia: Implications for the Origin of Namibian Kimberlites. *J. Petrol.* **42,** 159-172.

Day, J.M.D., Pearson, D.G., Macpherson, C.G., Lowry, D. and Carracedo, J.C. (2010) Evidence for distinct proportions of subducted oceanic crust and lithosphere in HIMU-type mantle beneath El Hierro and La Palma, Canary Islands. *Geoch. Cosmoch. Acta* **74,** 6565-6589.

De Bruin, D. (2005) Multiple compositional megacryst groups from the Uintjiesberg and Witberg kimberlites, South Africa. *South African Journal of Geology* **108,** 233-246.

De Plaen, R., Bastow, I., Chambers, E., Keir, D., Gallacher, R., and Keane, J. (2014). The development of magmatism along the cameroon volcanic line: Evidence from seismicity and seismic anisotropy. *Journal of Geophysical Research: Solid Earth,* **119(5),** 4233–4252.

Debaille, V., Blichert-Toft, J., Agranier, A., Doucelance, R., Schiano, P. and Albarede, F. (2006) Geochemical component relationships in MORB from the Mid-Atlantic Ridge, 22–35°N. *Earth Planet. Sci. Lett.* **241,** 844-862.

Deegan, F.M., Troll, V.R., Barker, A.K., Harris, C., Chadwick, J.P., Carracedo, J.C. and Delcamp, A. (2012) Crustal versus source processes recorded in dykes from the Northeast volcanic rift zone of Tenerife, Canary Islands. *Chem. Geol.* **334,** 324-344.

Del Moro, S., Di Roberto, A., Meletlidis, S., Pompilio, M., Bertagnini, A., Agostini, S., Ridolfi, F. and Renzulli, A. (2015) Xenopumice erupted on 15 October 2011 offshore of El Hierro (Canary Islands): a subvolcanic snapshot of magmatic, hydrothermal and pyrometamorphic processes. *Bull. Volcanol.* **77,** 53.

DePaolo, D.J., 1981. Trace elements and isotopic effects of combined wallrock assimilation and fractional crystallization. *Earth and Planetary Science Letters* **53,** 189-202.

Deruelle, B., Moreau, C., Nkoubou, C., Kambou, R., Lissom, J., Njonfang, E., Ghogomu, R.T., Nono, A., 1991. The Cameroon line: a review. In: Kampunzu, A.B., Lubala, R.T. (Eds.), Magmatism in Extensional Structural Settings: The Phanerozoic African Plate. *Springer, Berlin,* pp. 275-327.

Deruelle, B., N'ni, J., Kambou, R., 1987. Mount Cameroon: an active volcano of the Cameroon Line. *Journal of African Earth Sciences* **6,** 197-214.

Déruelle, B., Ngounouno, I., Demaiffe, D., 2007. The "Cameroon Hot Line" (CHL): A unique example of active alkaline intraplate structure in both oceanic and continental lithospheres. *Comptes Rendus Geosci.* **339,** 589–600.

Djomani, Y.H.P., Nnange, J.M., Diament, M., Ebinger, C.J. and Fairhead, J.D. (1995) Effective elastic thickness and crustal thickness variations in west central Africa inferred from gravity data. *Journal of Geophysical Research: Solid Earth* **100,** 22047-22070.

Dongmo, A., D. Nkouathio, A. Pouclet, J.-M. Bardintzeff, P. Wandji, A. Nono, and H. Guillou (2010), The discovery of late Quaternary basalt on Mount Bambouto: Implications for recent widespread volcanic activity in the southern Cameroon Line, *J. Afr. Earth Sci.,* **57**, 96–108.

Donnelly, C.L., Griffin, W.L., O'Reilly, S.Y., Pearson, N.J. and Shee, S.R. (2011) The Kimberlites and related rocks of the Kuruman Kimberlite Province, Kaapvaal Craton, South Africa. *Contrib. Mineral. Petrol.* **161,** 351-371.

Donnelly, C.L., Griffin, W.L., Yang, J.-H., O'Reilly, S.Y., Li, Q.-L., Pearson, N.J. and Li, X.-H. (2012) In situ U–Pb Dating and Sr–Nd Isotopic Analysis of Perovskite:

Constraints on the Age and Petrogenesis of the Kuruman Kimberlite Province, Kaapvaal Craton, South Africa. *J. Petrol.* **53,** 2497-2522.

Dorbath, C., L. Dorbath, J. Fairhead, and G. Stuart (1986), A teleseismic delay time study across the central African shear zone in the AdamawaRegion of Cameroon, West Africa, Geophys. *J. R. Astron. Soc.,* **86(3),** 751–766.

Dosso, L., Hanan, B.B., Bougault, H., Schilling, J.-G. and Joron, J.-L. (1991) SrNdPb geochemical morphology between 10° and 17°N on the Mid-Atlantic Ridge: A new MORB isotope signature. *Earth Planet. Sci. Lett.* **106,** 29-43.

Doucelance, R., Bellot, N., Boyet, M., Hammouda, T. and Bosq, C. (2014) What coupled cerium and neodymium isotopes tell us about the deep source of oceanic carbonatites. *Earth Planet. Sci. Lett.* **407,** 175-186.

Doucelance, R., Escrig, S., Moreira, M., Gariépy, C. and Kurz, M.D. (2003) Pb-Sr-He isotope and trace element geochemistry of the Cape Verde Archipelago. *Geoch. Cosmoch. Acta* **67,** 3717-3733.

Doucelance, R., Hammouda, T., Moreira, M. and Martins, J.C. (2010) Geochemical constraints on depth of origin of oceanic carbonatites: The Cape Verde case. *Geoch. Cosmoch. Acta* **74,** 7261-7282.

Driscoll, E. M., Tinkler, K. J., and Hendry, G. L. (1965). The geology and geomorphology of Los Ajaches, Lanzarote. *Geological Journal,* **4(2),** 321-334.

Duggen, S., Hoernle, K., Van Den Bogaard, P. and Garbe-SchÖNberg, D. (2005) Post-Collisional Transition from Subduction- to Intraplate-type Magmatism in the Westernmost Mediterranean: Evidence for Continental-Edge Delamination of Subcontinental Lithosphere. *J. Petrol*. **46,** 1155-1201.

Duggen, S., Hoernle, K.A., Hauff, F., Klugel, A., Bouabdellah, M. and Thirlwall, M.F. (2009) Flow of Canary mantle plume material through a subcontinental lithospheric corridor beneath Africa to the Mediterranean. *Geology* **37,** 283-286.

Dunlop, H. M. (1983), Strontium isotope geochemistry and potassium-argon studies on volcanic rocks from the Cameroon Line, West Africa, PhD thesis, Univ. of Edinburgh, Edinburgh, U. K.

Dunlop, H. M., and J. G. Fitton (1979), K-Ar and Sr-isotopic study of the volcanic-rocks of the island of Prìncipe, West Africa—Evidence for mantle heterogeneity beneath the Gulf of Guinea. Contrib. *Mineral. Petrol.,* **71(2),** 125–131.

Duprat, H. I., Friis, J., Holm, P. M., Grandvuinet, T., and Sørensen, R. V. (2007). The volcanic and geochemical development of São Nicolau, Cape Verde Islands: constraints from field and 40 Ar/39 Ar evidence. *Journal of Volcanology and Geothermal Research,* **162(1),** 1-19.

Ebinger, C., A. Ayele, D. Keir, J. Rowland, G. Yirgu, T. Wright, M. Belachew, and I. Hamling (2010), Length and timescales of rift faulting and magma intrusion: The Afar rifting cycle from 2005 to present. Annu. Rev. *Earth Planet. Sci.,* **38,** 439–466.

Ebinger, C., and N. Sleep (1998), Cenozoic magmatism throughout East Africa resulting from impact of a single plume. *Nature,* **395,** 788–791.

El Azzouzi, M.h., Bernard-Griffiths, J., Bellon, H., Maury, R.C., Piqué, A., Fourcade, S., Cotten, J. and Hernandez, J. (1999) Évolution des sources du volcanisme marocain au cours du Néogène. Comptes Rendus de l'Académie des Sciences - Series IIA - *Earth and Planetary Science* **329,** 95-102.

Elliott, T., Blichert-Toft, J., Heumann, A., Koetsier, G., and Forjaz, V. (2007). The origin of enriched mantle beneath s˜ao miguel, azores. *Geochimica et Cosmochimica Acta,* **71(1),** 219–240.

Elliott, T., Zindler, A., and Bourdon, B. (1999). Exploring the kappa conundrum: the role of recycling in the lead isotope evolution of the mantle. *Earth and Planetary Science Letters,* **169(1),** 129–145.

Elsheikh, A., Gao, S., and Liu, K. (2014). Formation of the cameroon volcanic line by lithospheric basal erosion: Insight from mantle seismic anisotropy. *Journal of African Earth Sciences,* **100,** 96–108.

Emery, K.O., Uchupi, E., 1984. The Geology of the Atlantic Ocean. *Springer, New York*.

Escrig, S., Doucelance, R., Moreira, M. and Allègre, C.J. (2005) Os isotope systematics in Fogo Island: Evidence for lower continental crust fragments under the Cape Verde Southern Islands. *Chem. Geol.* **219,** 93-113.

Fagny, A.M., Nkouandou, O.F., Déruelle, B., Ngounouno, I., 2012. Revised petrology and new chronological data on the peralkaline felsic lavas of Ngaoundéré volcanism (Adamawa plateau, Cameroon, Central Africa): evidence of opensystem magmatic processes. *Analele Stiintifice ale Universitatii "Al. I. Cuza" din Iasi, Seria Geologie* **58 (2),** 5-22.

Fairhead, J., and C. Okereke (1987), A regional gravity study of the West African rift system in Nigeria and Cameroon and its tectonic interpretation. *Tectonophysics,* **143(1–3),** 141–159.

Fairhead, J., Green, C., Masterton, S., and Guiraud, R. (2013). The role that plate tectonics, inferred stress changes and stratigraphic unconformities have on the evolution of the west and central african rift system and the atlantic continental margins. *Tectonophysics,* **594(0),** 118 – 127.

Fairhead, J.D. (1988) Mesozoic plate tectonic reconstructions of the central South Atlantic Ocean: The role of the West and Central African rift system. *Tectonophysics* **155,** 181-191.

Fairhead, J.D., Binks, R.M., 1991. Differential opening of the Central and South Atlantic Oceans and the opening of the West African system. *Tectonophysics* **187,** 191-203.

Féraud, G., Giannérini, G., Campredon, R., and Stillman, C. J., 1985, Geochronology of some dyke swarms: A contribution to the volcano-tectonic evolution of the archipelago. *Journal of Volcanology and Geothermal Research,* **v. 25,** p. 29–52.

Fishwick, S. (2010), Surface wave tomography: Imaging of the lithosphere-asthenosphere boundary beneath central and southern Africa. *Lithos,* **120(1–2),** 63–73.

Fishwick,S.,and I.Bastow (2011),Towards a better understanding of AfricanTopography,

a review of passive-source seismic studies of the African crust and upper mantle, in The Formation and Evolution of Africa: A Synopsis of 3.8 Ga of Earth History, edited by D. Van Hinsbergen et al., *Geol. Soc. Spec. Publ.,* **357,** 343–371.

Fitton, J.D., 1980. The Benue Trough and the Cameroon line e a migrating rift system in West Africa. *Earth and Planetary Science Letters* **51,** 132-138.

Fitton, J.D., Kilburn, C.R.J., Thirwall, M.F., Hughes, D.J., 1983. 1982 eruption of Mt. Cameroon, West Africa. *Nature* **306,** 327-332.

Fitton, J.G., 1987. The Cameroon Line, West Africa: a comparison between oceanic and continental alkaline volcanism. In: Fitton, J.G., Upton, B.G.J. (Eds.), Alkaline Igneous Rocks, 30. *Geological Society London Special Publications,* pp. 273-291.

Fitton, J.G., Dunlop, H.M., 1985. The Cameroon line, West Africa, and its bearing on the origin of oceanic and continental alkali basalt. *Earth Planet. Sci. Lett.* **72,** 23–38.

Fonseca, P.E., Mata, J. and Munhá, J. (1998) Tectonic lineaments from Madeira island evidenced from Satellite Image analysis and preliminary geological data. *Actas do V Congresso Nacional de Geologia, Lisboa, Comun. Inst. Geol. Min.* **84,** D101-104.

Fontignie, D. and Schilling, J.-G. (1996) Mantle heterogeneities beneath the South Atlantic: a Nd Sr Pb isotope study along the Mid-Atlantic Ridge (3°S–46°S). *Earth Planet. Sci. Lett.* **142,** 209-221.

Forte, A. M., Qu´er´e, S., Moucha, R., Simmons, N. A., Grand, S. P., Mitrovica, J. X., and Rowley, D. B. (2010). Joint seismic-geodynamic-mineral physical modelling of african geodynamics: A reconciliation of deep-mantle convection with surface geophysical constraints. *Earth and Planetary Science Letters,***295(3),** 329–341.

Foulger, G.R. and Natland, J.H. (2003) Is "Hotspot" Volcanism a Consequence of Plate Tectonics. *Science* **300,** 921-922.

Fourel, L., Milelli, L., Jaupart, C. and Limare, A. (2013) Generation of continental rifts, basins, and swells by lithosphere instabilities. *Journal of Geophysical Research: Solid Earth* **118,** 3080-3100.

Freeth, S.J., 1978. A model for tectonic activity in West Africa and the Gulf of Guinea during the last 90 m.y. based on membrane tectonics. *Geology Rundsch* **67,** 675-688.

French, S.W. and Romanowicz, B. (2015) Broad plumes rooted at the base of the Earth's mantle beneath major hotspots. *Nature* **525,** 95-99.

Frey, F.A., Green, D.H., Roy, S.D., 1978. Integrated models of basalt petrogenesis: a study of quartz tholeiites to olivine melilitites from South Eastern Australia utilizing geochemical and experimental petrological data. *Journal of Petrology* **19,** 463-513.

Fúster, J. M., Cendrero, A., Gastesi, P., Ibarrola, E., and Lopez, R.J., 1968, Geologia y volcanologia de las Islas Canarias, Fuerteventura: Madrid, Istituto Lucas Mallada, Consejo Superior de Investigaciones Cientificas, 239 p.

Galer, S.and O'Nions,R.(1985). Residence time of thorium, uranium and lead in the mantle with implications for mantle convection. *Nature,***316,** 778–782.

Gallacher, R. and Bastow, I. (2012). The development of magmatism along the cameroon volcanic line: Evidence from teleseismic receiver functions. *Tectonics,***31(3).**

Galloway, M., Nowicki, T., van Coller, B., Mukodzani, B., Siemens, K., Hetman, C., Webb, K. and Gurney, J. (2009) Constraining kimberlite geology through integration of geophysical, geological and geochemical methods: A case study of the Mothae kimberlite, northern Lesotho. *Lithos* **112, Supplement 1,** 130-141.

Geldmacher, J. and Hoernle, K. (2000) The 72 Ma geochemical evolution of the Madeira hotspot (eastern North Atlantic): recycling of Paleozoic (≤500 Ma) oceanic lithosphere. *Earth Planet. Sci. Lett.* **183,** 73-92.

Geldmacher, J., Hoernle, K., Bogaard, P.v.d., Duggen, S. and Werner, R. (2005) New 40Ar / 39Ar age and geochemical data from seamounts in the Canary and Madeira volcanic provinces: Support for the mantle plume hypothesis. *Earth Planet. Sci. Lett.* **237,** 85-101.

Geldmacher, J., Hoernle, K., Hanan, B.B., Blichert-Toft, J., Hauff, F., Gill, J.B. and Schmincke, H.-U. (2011) Hafnium isotopic variations in East Atlantic intraplate volcanism. *Contrib. Mineral. Petrol.* **162,** 21-36.

Geldmacher, J., Hoernle, K., Klügel, A., van den Bogaard, P. and Duggen, S. (2006) A geochemical transect across a heterogeneous mantle upwelling: Implications for the evolution of the Madeira hotspot in space and time. *Lithos* **90,** 131-144.

Geldmacher, J., Hoernle, K., van den Bogaard, P., Zankl, G. and Garbe-Schönberg, D. (2001) Earlier history of the ≥70-Ma-old Canary hotspot based on the temporal and geochemical evolution of the Selvagen Archipelago and neighboring seamounts in the eastern North Atlantic. *J. Volcanol. Geotherm. Res.* **111,** 55-87.

Geldmacher, J., van den Bogaard, P., Hoernle, K. and Schmincke, H.-U. (2000) The 40Ar/39Ar age dating of the Madeira Archipelago and hotspot track (eastern North Atlantic). *Geochemistry, Geophysics, Geosystems* **1,** n/a-n/a.

Gerlach, D. C., Stormer Jr, J. C., and Mueller, P. A. (1987). Isotopic geochemistry of fernando de noronha. *Earth and Planetary Science Letters,***85(1),** 129–144.

Gerlach, D.C., Cliff, R.A., Davies, G.R., Norry, M. and Hodgson, N. (1988) Magma sources of the Cape Verdes archipelago: Isotopic and trace element constraints. *Geoch. Cosmoch. Acta* **52,** 2979-2992.

Gerstenberger, H., Haase, G., 1997. A highly effective emitter substance for mass spectrometric Pb isotope ratio determinations. *Chem. Geol.* **136,** 309–312.

Geze, B., 1943. Geographie physique et geologie du Cameroun occidental, 17. *Mem. Mus. natl Hist. nat. Paris, Nouv. Ser,* pp. 1-272.

Giuliani, A., Phillips, D., Fiorentini, M., Kendrick, M., Maas, R., Wing, B., Woodhead, J., Bui, T., and Kamenetsky,V.(2013). Mantle oddities: A sulphate fluid preserved in a marid xenolith from the bultfontein kimberlite (kimberley, south africa). *Earth and Planetary Science Letters*,**376,** 74–86.

Globig, J., Fernàndez, M., Torne, M., Vergés, J., Robert, A. and Faccenna, C. (2016) New insights into the crust and lithospheric mantle structure of Africa from

elevation, geoid, and thermal analysis. *Journal of Geophysical Research: Solid Earth* **121,** 5389-5424.

Gomez, F., Beauchamp, W., and Barazangi, M. (2000). Role of the Atlas Mountains (northwest Africa) within the African-Eurasian plate-boundary zone. *Geology,* **28(9),** 775-778.

Gorini, M.A., Bryan, G.M., 1976. The tectonic fabric of Equatorial Atlantic and adjoining continental margins: Gulf of Guinea to northeastern Brazil. *Anais da Academia Brasileira de Ciências* **48,** 10-119.

Gouhier, J., Nougier, J., Nougier, R., 1974. Contribution a l'etude volcanologique du Cameroun (Ligne du Cameroun" e Adamaoua). *Annales de la Faculté des Sciences,* 3-48.

Gr´egoire, M., Bell, D., and Le Roex, A. (2002). Trace element geochemistry of phlogopite-rich mafic mantle xenoliths: their classification and their relationship to phlogopite-bearing peridotites and kimberlites revisited. *Contributions to Mineralogy and Petrology*,**142(5),** 603–625.

Grant, N. K., D. C. Rex, and S. J. Freeth (1972), Potassium-argon ages and strontium isotope ration measurements from volcanic rocks in northeastern Nigeria. *Contrib. Mineral. Petrol.,* **35(4),** 277–292.

Griffin, W.L., Batumike, J.M., Greau, Y., Pearson, N.J., Shee, S.R. and O'Reilly, S.Y. (2014) Emplacement ages and sources of kimberlites and related rocks in southern Africa: U–Pb ages and Sr–Nd isotopes of groundmass perovskite. *Contrib. Mineral. Petrol.* **168,** 1032.

Griffin, W.L., Begg, G.C. and O'Reilly, S.Y. (2013) Continental-root control on the genesis of magmatic ore deposits. *Nature Geosci* **6,** 905-910.

Griffin, W.L., O'Reilly, S.Y., Afonso, J.C., Begg, G.C., 2008. The Composition and Evolution of Lithospheric Mantle: a Re-evaluation and its Tectonic Implications. *J. Petrol.* **50,** 1185–1204.

Grunau, H.R., Lehner, P., Cleintuar, M.R., Allenbach, A., Bakker, G., 1975. New radiometric ages and seismic data from Fuerteventura (Canary Islands), Maio (Cape Verde Island) and Sao Tome (Gulf of Guinea). In: Borradaile, G.J., Ritsema, A.R., Rondeel, H.E., Simon, O.J. (Eds.), *Progress in Geodynamics. NorthHolland, Amsterdam,* pp. 90-118.

Guillou H, Carracedo JC, Day S (1998) Dating of the upper Pleistocene-Holocene volcanic activity of La Palma using the unspiked K-Ar technique. *J Volcanol Geotherm Res* **86:**137–149.

Guillou H, Carracedo JC, Duncan RA (2001) K-Ar, 40Ar-39Ar ages and magnetostratigraphy of Brunhes and Matuyama lava sequences from La Palma Island. *J Volcanol Geotherm Res* **106:**175–194.

Guillou H, Carracedo JC, Perez Torrado FJ, Rodriguez Badiola E (1996) K-Ar ages and magnetic stratigraphy of a hotspotinduced, fast grown oceanic island; El Hierro, Canary Islands. *J Volcanol Geotherm Res* **73:**141–155.

Guiraud, R., Binks, R. M., Fairhead, J. D., and Wilson, M. (1992). Chronology and

geodynamic setting of Cretaceous-Cenozoic rifting in West and Central Africa. *Tectonophysics*, *213*(1-2), 227-234.

Gurenko, A.A., Hoernle, K.A., Hauff, F., Schmincke, H.U., Han, D., Miura, Y.N. and Kaneoka, I. (2006) Major, trace element and Nd–Sr–Pb–O–He–Ar isotope signatures of shield stage lavas from the central and western Canary Islands: Insights into mantle and crustal processes. *Chem. Geol.* **233,** 75-112.

Gurenko, A.A., Hoernle, K.A., Sobolev, A.V., Hauff, F. and Schmincke, H.-U. (2010) Source components of the Gran Canaria (Canary Islands) shield stage magmas: evidence from olivine composition and Sr–Nd–Pb isotopes. *Contrib. Mineral. Petrol.* **159,** 689-702.

Gurenko, A.A., Sobolev, A.V., Hoernle, K.A., Hauff, F. and Schmincke, H.-U. (2009) Enriched, HIMU-type peridotite and depleted recycled pyroxenite in the Canary plume: A mixed-up mantle. *Earth Planet. Sci. Lett.* **277,** 514-524.

Haase, K.M., Brandl, P.A., Devey, C.W., Hauff, F., Melchert, B., Garbe-Schönberg, D., Kokfelt, T.F. and Paulick, H. (2016) Compositional variation and 226Ra-230Th model ages of axial lavas from the southern Mid-Atlantic Ridge, 8°48S. *Geochemistry, Geophysics, Geosystems* **17,** 199-218.

Halliday, A.N., Davidson, J.P., Holden, P., DeWolf, C., Lee, D.-C. and Fitton, J.G. (1990) Trace-element fractionation in plumes and the origin of HIMU mantle beneath the Cameroon line. *Nature* **347,** 523-528.

Halliday, A.N., Davies, G.R., Lee, D.-C., Tommasini, S., Paslick, C.R., Fitton, J.G. and James, D.E. (1992) Lead isotope evidence for young trace element enrichment in the oceanic upper mantle. *Nature* **359,** 623-627.

Halliday, A.N., Dicken, A.P., Fallick, A.E., Fitton, J.D., 1988. Mantle dynamics: a Nd, Sr, Pb and Os isotope study of the Cameroon line volcanic chain. *Journal of Petrology* **29,** 181-211.

Halliday, A.N., Lee, D.-C., Tommasini, S., Davies, G.R., Paslick, C.R., Fitton, J.G. and James, D.E. (1995) Incompatible trace elements in OIB and MORB and source enrichment in the sub-oceanic mantle. *Earth Planet. Sci. Lett.* **133,** 379-395.

Hanan,B. and Graham,D.(1996). Lead and helium isotope evidence from oceanic basalts for a common deep source of mantle plumes. *Science,* **272(5264),** 991–995.

Hansteen TH, Andersen T, Neumann E-R, Jelsma H (1991) Fluid and silicate glass inclusions in ultramafic and mafic xenoliths from Hierro, Canary Islands; implications for mantle metasomatism. *Contrib Mineral Petrol* **107:** 242–254.

Hanyu, T., Kawabata, H., Tatsumi, Y., Kimura, J.-I., Hyodo, H., Sato, K., Miyazaki, T., Chang, Q., Hirahara,Y., Takahashi, T., et al. (2014). Isotope evolution in the himu reservoir beneath st. helena: Implications for the mantle recycling of U and Th. *Geochimica et Cosmochimica Acta,* **143,** 232-252.

Harris, M., le Roex, A. and Class, C. (2004) Geochemistry of the Uintjiesberg kimberlite, South Africa: petrogenesis of an off-craton, group I, kimberlite. *Lithos* **74,** 149-165.

Hart, S., Hauri, E., Oschmann, L., and Whitehead, J. (1992). Mantle plumes and

entrainment: isotopic evidence. *Science*, **256(5056),** 517–520.

Hart, S.R., 1984. A large-scale isotope anomaly in the Southern Hemisphere mantle. *Nature* **309,** 753-757.

Hawkesworth, C., Kempton, P., Rogers, N., Ellam, R., and Van Calsteren, P. (1990). Continental mantle lithosphere, and shallow level enrichment processes in the earth's mantle. *Earth and Planetary Science Letters,* **96(3),** 256–268.

Hayes, D. E., and Rabinowitz, P. D. (1975). Mesozoic magnetic lineations and the magnetic quiet zone off northwest Africa. *Earth and Planetary Science Letters,* **28(2),** 105-115.

Hedberg, J. (1969), A geological analysis of the Cameroon trend, PhD thesis, Princeton Univ., Princeton, New Jersey.

Hiess, J., Condon, D. J., McLean, N., and Noble, S. R. (2012). 238U/235U systematics in terrestrial uranium bearing minerals. *Science,* **335(6076),** 1610–1614.

Hildner, E., Klügel, A. and Hansteen, T.H. (2012) Barometry of lavas from the 1951 eruption of Fogo, Cape Verde Islands: Implications for historic and prehistoric magma plumbing systems. *J. Volcanol. Geotherm. Res.* **217–218,** 73-90.

Hirschmann, M. M. (2000). Mantle solidus: Experimental constraints and the effects of peridotite composition. *Geochemistry, Geophysics, Geosystems,* ***1*****(10)**.

Hoal, K.O. (2003) Samples of Proterozoic iron-enriched mantle from the Premier kimberlite. *Lithos* **71,** 259-272.

Hoernle K, Schmincke H-U (1993a) The petrology of the tholeiites through melilite nephelinites on Gran Canaria, Canary Islands: crystal fractionation, accumulation, and depths of melting. *J Petrol* **34:**573–597.

Hoernle K, Schmincke H-U (1993b) The role of partial melting in the 15-Ma geochemical evolution of Gran Canaria: a blob model for the Canary hotspot. *J Petrol* **34:**599–626.

Hoernle K, Tilton G, Schmincke H-U (1991) Sr-Nd-Pb isotopic evolution of Gran Canaria: evidence for shallow enriched mantle beneath the Canary Islands. *Earth Planet Sci Lett* **106:** 44–63.

Hoernle, K., Hauff, F., Kokfelt, T.F., Haase, K., Garbe-Schönberg, D. and Werner, R. (2011) On- and off-axis chemical heterogeneities along the South Atlantic Mid-Ocean-Ridge (5–11°S): Shallow or deep recycling of ocean crust and/or intraplate volcanism. *Earth Planet. Sci. Lett.* **306,** 86-97.

Hofmann, A.W. and White, W.M. (1982) Mantle plumes from ancient oceanic crust. *Earth Planet. Sci, Lett.* **57,** 421-436.

Hofmann, A. W., Jchum K. P., Seufer M. and White W. M (1986). Nb and Pb in oceanic basalts: new constraints on mantle evolution. *Earth Planet. Sci. Lett.,* **79:** 33-45.

Hofmann, A.W., 1988. Chemical differentiation of the Earth: the relationship between mantle, continental crust, and the oceanic crust. *Earth and Planetary Science Letters* **90,** 297-314.

Holik JS, Rabinowitz PD, Austin JA (1991) Effects of Canary hotspot volcanism on structure of oceanic crust off Morocco. *J Geophys Res* **96:** 12039–12067.

Holm, P.M., Wilson, J.R., Christensen, B.P., Hansen, L., Hansen, S.L., Hein, K.M., Mortensen, A.K., Pedersen, R., Plesner, S. and Runge, M.K. (2006) Sampling the Cape Verde Mantle Plume: Evolution of Melt Compositions on Santo Antão, Cape Verde Islands. *J. Petrol.* **47,** 145-189.

Huismans, R. and Beaumont, C. (2011) Depth-dependent extension, two-stage breakup and cratonic underplating at rifted margins. *Nature* **473,** 74-78.

Ibrahim, A.E., Ebinger, C.J., Fairhead, J.D., 1996. Lithospheric extension northwest of the Central African Shear Zone in Sudan from potential field studies. *Tectonophysics* **255,** 79–97.

Irvine, T., and Baragar, W. (1971). A guide to the chemical classification of the common volcanic rocks. *Canadian journal of earth sciences,* **8(5),** 523-548.

Johansen, T.S., Hauff, F., Hoernle, K., Klugel, A. and Kokfelt, T.F. (2005) Basanite to phonolite differentiation within 1550–1750 yr: U-Th-Ra isotopic evidence from the A.D. 1585 eruption on La Palma, Canary Islands. *Geology* **33,** 897-900.

Jørgensen, J.Ø. and Holm, P.M. (2002) Temporal variation and carbonatite contamination in primitive ocean island volcanics from São Vicente, Cape Verde Islands. *Chem. Geol.* **192,** 249-267.

Jung, S., Masberg, P., 1998. Major-and-trace element systematics and isotope geochemistry of Cenozoic mafic volcanic rocks from the Vogelsberg (Central Germany) constraints on the origin of continental alkaline and tholeiitic basalts and their mantle sources. *Journal of Volcanology and Geothermal Research* **86,** 151-177.

Kaczmarek, M.A., Bodinier, J.L., Bosch, D., Tommasi, A., Dautria, J.M. and Kechid, S.A. (2016) Metasomatized Mantle Xenoliths as a Record of the Lithospheric Mantle Evolution of the Northern Edge of the Ahaggar Swell, In Teria (Algeria). *J. Petrol.* **57,** 345-382.

Kagou, D.A., Nkouathio, D., Pouclet, A., Bardintzeff, J.M., Wandji, P., Nono, A., Guillou, H., 2010. The discovery of late Quaternary basalt on Mount Bambouto: implications for recent widespread volcanic activity in the southern Cameroon Line. *Journal of African Earth Sciences* **57,** 96-108.

Kaislaniemi, L. and van Hunen, J. (2014) Dynamics of lithospheric thinning and mantle melting by edge-driven convection: Application to Moroccan Atlas Mountains. *Geochemistry, Geophysics, Geosystems* **15,** 3175-3189.

Kamenetsky, V.S., Belousova, E.A., Giuliani, A., Kamenetsky, M.B., Goemann, K. and Griffin, W.L. (2014) Chemical abrasion of zircon and ilmenite megacrysts in the Monastery kimberlite: Implications for the composition of kimberlite melts. *Chem. Geol.* **383,** 76-85.

Kamgang, P., Chazot, G., Njonfang, E., Ngongang, N.B.T., Tchoua, F.M., 2013. Mantle sources and magma evolution beneath the Cameroon Volcanic Line: geochemistry of mafic rocks from the Bamenda Mountains (NW Cameroon).

Gondwana Research **24,** 727-741.

Kamgang, P., Chazot, G., Njonfang, E., Tchoua, F., 2008. Geochemistry and geochronology of mafic rocks from Bamenda Mountains (Cameroon): source composition and crustal contamination along the Cameroon Volcanic Line. *Comptes Rendus Geoscience* **340,** 850-857.

Kamgang, P., Njonfang, E., Nono, A., Gountie, D.M., Tchoua, F., 2010. Petrogenesis of a silicic magma system: geochemical evidence from Bamenda Mountains, NW Cameroon, Cameroon Volcanic Line. *Journal of African Earth Sciences* **58,** 285-304.

Keir,D., I.Bastow, K.Whaler, E.Daly, D.Cornwell, and S. Hautot (2009), Lower crustal earthquakes near the Ethiopian rift induced by magmatic processes. *Geochem. Geophys. Geosyst.,* **10(6)**.

Kelemen, P.B., Yogodzinski, G.M. and Scholl, D.W. (2003) Along-Strike Variation in the Aleutian Island Arc: Genesis of High Mg# Andesite and Implications for Continental Crust, Inside the Subduction Factory. *American Geophysical Union,* pp. 223-276.

Kellogg, L.H., Hager, B.H. and van der Hilst, R.D. (1999) Compositional Stratification in the Deep Mantle. *Science* **283,** 1881-1884.

Keskin, M., 2013. AFC-Modeler: a Microsoft Excel workbook program for modeling assimilation combined with fractional crystallization (AFC) process in magmatic systems by using equations of DePaolo (1981). *Turkish Journal of Earth Sciences* **22,** 304-319.

King, S.D. (2007) Hotspots and edge-driven convection. *Geology* **35,** 223-226.

King, S.D. and Anderson, D.L. (1998) Edge-driven convection. *Earth Planet. Sci. Lett.* **160,** 289-296.

King, S.D. and Ritsema, J. (2000) African Hot Spot Volcanism: Small-Scale Convection in the Upper Mantle Beneath Cratons. *Science* **290,** 1137-1140.

King, S.D., Anderson, D.L., 1995. An alternative mechanism of flood basalt formation. *Earth and Planetary Science Letters* **136,** 269-279.

Kleine, T., M¨unker, C., Mezger, K., and Palme, H. (2002). Rapid accretion and early core formation on asteroids and the terrestrial planets from Hf–W chronometry. *Nature,* **418(6901),** 952–955.

Klerkx, J., and De Paepe, P. (1977). The main characteristics of the magmatism of the Cape Verde Islands. *Annales de la Société géologique de Belgique.*

Klitgord KD, Schouten H (1986) Plate kinematics of the central Atlantic. In: Vogt PR, Tucholke BE (eds) The western North Atlantic region. The geology of North America, vol M. *Geol Soc Am,* pp 351–378

Klügel A, Schmincke H-U, White JDL, Hoernle KA (1999) Chronology and volcanology of the 1949 multi-vent rift-zone eruption on La Palma (Canary Islands). *J Volcanol Geotherm Res* **94:** 267–282.

Koch, F. W., Wiens, D.A., Nyblade, A. A., Shore, P. J., Tibi, R., Ateba,B., Tabod, C.,

and Nnange, J. (2012).Upper-mantle anisotropy beneath the cameroon volcanic line and congo craton from shear wave splitting measurements. *Geophysical Journal International,* **190(1),** 75–86.

Koide, Y., Nakamura, E., 1990. Lead isotope analyses of standard rock samples. *Mass Spectrosc.* **38,** 241–252.

Konzett, J., Rhede, D. and Frost, D.J. (2012) The high P-T stability of apatite and Cl partitioning between apatite and hydrous potassic phases in peridotite: an experimental study to 19 GPa with implications for the transport of P, Cl and K in the upper mantle. *Contrib. Mineral. Petrol.* **163,** 277-296.

Kramers, J., Roddick, J., and Dawson, J. (1983). Trace element and isotope studies on veined, metasomatic and marid xenoliths from bultfontein, south africa. *Earth and Planetary Science Letters,* **65(1),** 90–106.

Kramers, J.D. (1977) Lead and strontium isotopes in Cretaceous kimberlites and mantle-derived xenoliths from Southern Africa. *Earth Planet. Sci. Lett.* **34,** 419-431.

Kuritani, T., and Nakamura, E. (2002). Precise isotope analysis of nanogram-level Pb for natural rock samples without use of double spikes. *Chemical Geology,* **186(1),** 31-43.

Kuritani, T., and Nakamura, E. (2003). Highly precise and accurate isotopic analysis of small amounts of Pb using 205 Pb–204 Pb and 207 Pb-204 Pb, two double spikes. *Journal of Analytical Atomic Spectrometry*, *18*(12), 1464-1470.

Lasserre, M., 1966. Confirmation de l'existence d'une séries de granites tertiaires au Cameroun. *Bull BRGM* **3,** 141-148.

Lasserre, M., 1978. Mise au point sue les granitoïdes dits "ultime" du Cameroun: gisement, petrographie et geochronologie. *Bull BRGM* **(2) IV,** 143-159.

Lawrence, S. R., Munday, S., and Bray, R. (2002). Regional geology and geophysics of the eastern Gulf of Guinea (Niger Delta to Rio Muni). *The leading edge*, *21*(11), 1112-1117.

Le Bas, M.J., LeMaitre, R.W., Streckeisen, A., Zanettin, B., 1986. A chemical classification of volcanic rocks based on the total alkali silica diagram. *Journal of Petrology* **27,** 745-750.

Le Maitre, R. W., Bateman, P., Dudek, A., Keller, J., Lameyre, J., LeBas, M. J., ... and Woolley, A. R. 1989, A classification of igneous rocks and glossary of terms: Recommendations of the International Union of Geological Sciences Subcommission on the Systematics of Igneous Rocks.

Le Maitre, R.W. (Ed.), 2002. Igneous Rocks. A Classification and Glossary of Terms. Recommendations of the International Union of Geological Sciences Subcommission on the Systematics of Igneous Rocks.

Le Marechal, A., 1976. Geologie et Géochimie des sources thermo minérales du Cameroun. No. 59. *Collection des Memoires de l'ORSTOM, Paris*.

Le Roex, A.P., Bell, D.R. and Davis, P. (2003) Petrogenesis of Group I Kimberlites from Kimberley, South Africa: Evidence from Bulk-rock Geochemistry. *J. Petrol.* **44,**

2261-2286.

Lee, D.C., Halliday, A.N., Davies, G.R., Essene, E.J., Fitton, J.G., Temdjim, R., 1996. Melt enrichment of shallow depleted mantle: a detailed petrological, trace element and isotopic study of mantle-derived xenoliths and megacrysts from the Cameroon Line. *Journal of Petrology* **37,** 415-441.

Lee, D.C., Halliday, A.N., Fitton, J.F., Poli, G., 1994. Isotopic variation with distance and time in the volcanic Islands of the Cameroon line: evidence for a mantle plume origin. *Earth and Planetary Science Letters* **123,** 119-138.

Liu, C.-Z., Yang, L.-Y., Li, X.-H. and Tchouankoue, J.P. (2016) Age and Sr-Nd-Hf isotopes of the sub-continental lithospheric mantle beneath the Cameroon Volcanic Line: Constraints from the Nyos mantle xenoliths. *Chem. Geol*.

Liu, X. and Zhao, D. (2014) Seismic evidence for a mantle plume beneath the Cape Verde hotspot. *International Geology Review* **56,** 1213-1225.

Llanes, P., Herrera, R., Gómez, M., Muñoz, A., Acosta, J., Uchupi, E., and Smith, D. (2009). Geological evolution of the volcanic island La Gomera, Canary Islands, from analysis of its geomorphology. *Marine Geology,* **264(3),** 123-139.

Lloyd, F.E., Woolley, A.R., Stoppa, F. and Eby, G.N. (1999) Rift Valley magmatism — is there evidence for laterally variable alkali clinopyroxenite mantle. *Geolines* **9,** 76-83.

Lu, Y., Makishima, A., and Nakamura, E. (2007). Purification of Hf in silicate materials using extraction chromatographic resin, and its application to precise determination of 176 Hf/177 Hf by MC-ICP-MS with 179 Hf spike. *Journal of Analytical Atomic Spectrometry,* **22(1),** 69-76.

Lugmair, G.W., Galer, S.J.G., 1992. Age and isotopic relationships among the angrites Lewis Cliff 86010 and Angra dos Reis. *Geochim. Cosmochim. Acta* **56,** 1673–1694.

Makishima, A., and Nakamura, E. (2006). Determination of Major/Minor and Trace Elements in Silicate Samples by ICP-QMS and ICP-SFMS Applying Isotope Dilution-Internal Standardisation (ID-IS) and Multi-Stage Internal Standardisation. *Geostandards and Geoanalytical Research*, *30*(3), 245-271.

Makishima, A., Tanaka, R., and Nakamura, E. (2009) Precise Elemental and Isotopic Analyses in Silicate Samples Employing ICP-MS: Application of Hydrofluoric Acid Solution and Analytical Techniques. *Analytical Sciences,* **25,** 1181-1187.

Marcantonio, F., Zindler, A., Elliott, T. and Staudigel, H. (1995) Os isotope systematics of La Palma, Canary Islands: Evidence for recycled crust in the mantle source of HIMU ocean islands. *Earth Planet. Sci. Lett.* **133,** 397-410.

Martins, S., Mata, J., Munhá, J., Mendes, M.H., Maerschalk, C., Caldeira, R. and Mattielli, N. (2010) Chemical and mineralogical evidence of the occurrence of mantle metasomatism by carbonate-rich melts in an oceanic environment (Santiago Island, Cape Verde). *Mineralogy and Petrology* **99,** 43-65.

Marzoli, A., P. Renne, E. Piccirillo, C. Francesca, G. Bellieni, A. Melfi, J. Nyobe, and J. N'ni (1999), Silicic magmas from the continental Cameroon Volcanic Line (Oku, Bambouto and Ngaoundere): 40Ar-39Ar dates, petrology, Sr-Nd-O isotopes and

their petrogenetic significance. *Contrib. Mineral. Petrol.,* **135,** 133–150.

Marzoli, A., Peccirillo, E.M., Renne, P.R., Bellieni, G., Iacumin, M., Nyobe, J.B., Tongwa, A.T., 2000. The Cameroon Volcanic Line revisited: petrogenesis of continental basaltic magmas from lithospheric and asthenospheric mantle sources. *Journal of Petrology* **41,** 87-109.

Mata, J., Kerrich, R., MacRae, N.D. and Wu, T.W. (1998) Elemental and isotopic (Sr, Nd, and Pb) characteristics of Madeira Island basalts: evidence for a composite HIMU - EM I plume fertilizing lithosphere. *Canadian Journal of Earth Sciences* **35,** 980-997.

Mathieu, L., Kervyn, M., and Ernst, G. G. (2011). Field evidence for flank instability, basal spreading and volcano-tectonic interactions at Mt Cameroon, West Africa. *Bulletin of volcanology,* **73(7),** 851-867.

Mbassa, B.J., Njonfang, E., Benoit, M., Kamgang, P., Grégoire, M., Duchene, S., Brunet, P., Ateba, B., Tchoua, F.M., 2012. Mineralogy, geochemistry and petrogenesis of the recent magmatic formations from Mbengwi, a continental sector of the Cameroon Volcanic Line (CVL), Central Africa. *Mineralogy and Petrology* **106,** 217-242.

Mbowou, G. I. B., Lagmet, C., Nomade, S., Ngounouno, I., Deruelle, B., and Ohnenstetter, D. (2012). Petrology of the Late Cretaceous peralkaline rhyolites (pantellerite and comendite) from Lake Chad, Central Africa. *Journal of GEOsciences*, *57*(2), 127-141.

McBirney, A.R., Noyes, R.M., 1979. Crystallisation and layering of the Skaergard intrusion. *Journal of Petrology* **20,** 487-554.

McCulloch, M. T. and Bennett, V. C. (1994). Progressive growth of the earth's continental crust and depleted mantle: geochemical constraints. *Geochimica et Cosmochimica Acta,* **58(21),** 4717–4738.

McDonough, W.F., Sun, S., 1995. The composition of the Earth. *Chemical Geology* **120,** 223-253.

McKenzie, D. and O'Nions, R.K. (1991) Paritial melt distributions from inversion of rare earth element concentratjions. *J. Petrol.* **32,** 1021-1091.

Meshesha, D., Shinjo, R., Matsumura, R. and Chekol, T. (2011) Metasomatized lithospheric mantle beneath Turkana depression in southern Ethiopia (the East Africa Rift): geochemical and Sr–Nd–Pb isotopic characteristics. *Contrib. Mineral. Petrol.* **162,** 889-907.

Meyers, J., Rosendalh, B.R., Harrison, C.G., Ding, Z.D., 1998. Deep-imaging seismic and gravity results from the offshore Cameroon Volcanic Line, and speculation of African hotlines. *Tectonophysics* **284,** 31-63.

Meyers, J.B., Rosendahl, B.R., 1991. Seismic reflection character of the Cameroon volcanic line: Evidence for uplifted oceanic crust. *Geology* **19,** 1072.

Milelli, L., Fourel, L., Jaupart, C., 2012. A lithospheric instability origin for the Cameroon Volcanic Line. *Earth and Planetary Science Letters* **335,** 80-87.

Miller, D.M., Goldstein, S.L. and Langmuir, C.H. (1994) Cerium/lead and lead isotope ratios in arc magmas and the enrichment of lead in the continents. *Nature* **368,** 514-520.

Millet, M.-A., Doucelance, R., Schiano, P., David, K. and Bosq, C. (2008) Mantle plume heterogeneity versus shallow-level interactions: A case study, the São Nicolau Island, Cape Verde archipelago. *J. Volcanol. Geotherm. Res.* **176,** 265-276.

Missenard, Y. and Cadoux, A. (2012) Can Moroccan Atlas lithospheric thinning and volcanism be induced by Edge-Driven Convection. *Terra Nova* **24,** 27-33.

Mitchell, J. G., Le Bas, M. J., Zielonka, J., and Furnes, H. (1983). On dating the magmatism of Maio, Cape Verde islands. *Earth and Planetary Science Letters,* **64(1),** 61-76.

Mitchell, R.H. (1995) Melting Experiments on a Sanidine Phlogopite Lamproite at 4–7 GPa and their Bearing on the Sources of Lamproitic Magmas. *J. Petrol.* **36,** 1455-1474.

Moeller, H. (2002) Magma genesis and mantle sources at the Mid-Atlantic Ridge east of Ascension Island. *Christian-Albrechts Universität, Kiel,* p. 149.

Montelli, R., Nolet, G., Dahlen, F.A., Masters, G., Engdahl, E.R. and Hung, S.-H. (2004) Finite-Frequency Tomography Reveals a Variety of Plumes in the Mantle. *Science* **303,** 338-343.

Moore JG, Clague DA (1992) Volcano growth and evolution of the Island of Hawaii. *Geol Soc Am Bull* **104:**1471–1484.

Moore, A., and Blenkinsop, T. (2008). Controls on post-Gondwana alkaline volcanism in Southern Africa. *Earth and Planetary Science Letters*, ***268*(1),** 151-164.

Moreau, C., Regnoult, J.M., Deruelle, B., Robineau, B., 1987. A new tectonic model for the Cameroon Line, Central Africa. *Tectonophysics* **139,** 317-334.

Morgan JW (1972) Plate motions and deep mantle convection. *Geol Soc Am Mem* **132:**7–22.

Morgan, W.J. (1971) Convection plumes in the lower mantle. *Nature* **230,** 42-43.

Morgan, W.J., 1983. Hotspot tracks and the early rifting of the Atlantic. *Tectonophysics* **94,** 123-139.

Mourão, C., Mata, J., Doucelance, R., Madeira, J., Millet, M.-A. and Moreira, M. (2012) Geochemical temporal evolution of Brava Island magmatism: Constraints on the variability of Cape Verde mantle sources and on carbonatite–silicate magma link. *Chem. Geol.* **334,** 44-61.

M¨uller, R. D. and Roest, W. R. (1992). Fracture zones in the north atlantic from combined geosat and seasat data. *Journal of Geophysical Research: Solid Earth (1978–2012),* **97(B3),** 3337–3350.

Mundl, A., Touboul, M., Jackson, M.G., Day, J.M.D., Kurz, M.D., Lekic, V., Helz, R.T. and Walker, R.J. (2017) Tungsten-182 heterogeneity in modern ocean island basalts. *Science* **356,** 66-69.

Nagao, K., Ogata, A., Miura, Y. N., and Yamaguchi, K. (1996). Ar isotope analysis for K-Ar dating using two Modified-VG5400 mass spectrometers—I: Isotope dilution method. *Journal of the Mass Spectrometry Society of Japan, **44*****(1),** 39-61.

Nakamura, E., Makishima, A., Moriguti, T., Kobayashi, K., Sakaguchi, C., Yokoyama, T., Tanaka, R., Kuritani, T., Takei, H., (2003). Comprehensive geochemical analyses of small amounts (< 100mg) of extraterrestrial samples for the analytical competition related to the sample return mission MUSES-C, *Inst. Space Astronaut. Sci. Rep.* **SP. 16,** 49–101.

Natali, C., Beccaluva, L., Bianchini, G., Ellam, R.M., Siena, F. and Stuart, F.M. (2013) Carbonated alkali-silicate metasomatism in the North Africa lithosphere: Evidence from Middle Atlas spinel-lherzolites, Morocco. *Journal of South American Earth Sciences* **41,** 113-121.

Neumann E-R (1991) Ultramafic and mafic xenoliths from Hierro, Canary Islands; evidence for melt infiltration in the upper mantle. *Contrib Mineral Petrol* **106**: 236–252.

Neumann E-R, Wulff-Pedersen E (1997) The origin of highly silicic glass in mantle xenoliths from the Canary Islands. *J Petrol* **38:**1513–1539.

Neumann E-R, Wulff-Pedersen E, Simonsen SL, Pearson NJ, Marti J, Mitjavila J (1999) Evidence for fractional crystallization of periodically refilled magma chambers in Tenerife, Canary Islands. *J Petrol* **40:**1089–1123.

Ngako, V., Njonfang, E., Aka, F.T., Affaton, P., Nnange, J.M., 2006. The North-South Paleozoic to Quaternary trend of alkaline magmatism from Niger-Nigeria to Cameroon: complex interaction between hotspots and Precambrian faults. *Journal of African Earth Sciences* **45 (3),** 241-256.

Ngounouno, I., B. Déruelle, D. Demaiffe, and R. Montigny (1997), New data on the Cenozoic volcanism of the Garoua valley (Upper Benue trough, northern Cameroon). *C. R. Acad. Sci., Ser. II*, **325(2),** 87–94.

Ngounouno, I., B. Déruelle, D. Demaiffe, and R. Montigny (2001), Petrology of the alkaline undersaturated complex of Kokoumi (Cameroon), *Bull. Soc. Geol. France.,* **172(6),** 675–686.

Ngounouno, I., B. Déruelle, D. Demaiffe, and R. Montigny (2003), The monchiquites from Tchircotche, Upper Benue valley (northern Cameroon), *C. R. Geosci.,* **335(3),** 289-296.

Ngounouno, I., B. Déruelle, R. Montigny, and D. Demaiffe (2005), Petrology and geochemistry of monchiquites from Tchircotche (Garoua rift, north Cameroon, Central Africa), *Mineral. Petrol.,* **83(3–4),** 167–190.

Ngounouno, I., B. Déruelle, R. Montigny, and D. Demaiffe (2006), The camptonites from Mount Cameroon, Cameroon, Africa, *C. R. Geosci.,* **338(8),** 537–544.

Ngounouno, I., Déruelle, D., Demaiffe, D., 2000. Petrology of the bimodal Cenozoïc volcanism of the Kapsiki Plateau (northernmost Cameroon, Central Africa). *Journal of Volcanology and Geothermal Research* **102,** 21-44.

Njilah, I., H. Ajonina, D. Kamgang, and M. Tchindjang (2004), K-Ar ages, mineralogy,

major and trace element geochemistry of the Tertiary-Quaternary lavas from the Ndu Volcanic Ridge N.W. Cameroon, *Afr. J. Sci. Technol.,* **5(1),** 47–56.

Njilah, K., Temdjim, R., Nzolang, C., Tchuitchou, R., Ajonina, H., 2007. Geochemistry of Tertiary-Quartenary lavas of Mt. Oku, Northwest Cameroon, 040. *Revisita facultad de ingeenieria Univeridad de Antioquia, Junio,* pp. 59-75.

Njonfang, E., Nono, A., Kamgang, P., Ngako, V., Tchoua, F.M., 2011. Cameroon line magmatism (Central Africa): a reappraisal. In: Beccaluva, L., Bianchini, G., Wilson, M. (Eds.), Volcanism and Evolution of the African Lithosphere. *GSA, Special Paper,* **478,** pp. 173-191.

Nkouandou, O.F., Ngounouno, I., Déruelle, B., Ohnenstetter, D., Montigny, R. and Demaiffe, D. (2008) Petrology of the Mio-Pliocene volcanism to the North and East of Ngaoundéré (Adamawa, Cameroon). *Comptes Rendus Geoscience* **340,** 28-37.

Nkouandou, O.F., Temdjim, R., 2011. Petrology of spinel lherzolite xenoliths and host basaltic lava from Ngao Voglar volcano, Adamawa Massif (Cameroon Volcanic Line, West Africa): equilibrium conditions and mantle characteristics. *Journal of Geoscience* **56,** 375-387.

Nkouathio, D.G., Kagou Dongmo, A., Bardintzeff, J.M., Wandji, P., Bellon, H., Pouclet, A., 2008. Evolution of volcanism in graben and horst structures alongthe Cenozoic Cameroon Line (Africa): implications for tectonic evolution and mantle source composition. *Mineralogy and Petrology* **94,** 287-303.

Nkoumbou, C., Deruelle, B., Velde, D., 1995. Petrology of Mt. Etinde Nephelinite series. *Journal of Petrology* **36,** 373-395.

Nnange, J., Y. Poudjom Djomani, J. Fairhead, and C. Ebinger (2001), Determination of the isostatic compensation mechanism of the region of the Adamawa Dome, west central Africa using the admittance technique of gravity data, *Afr. J. Sci. Technol., Sci. Eng. Ser.,* **1(4),** 29–35.

Nono, A., Njonfang, E., Kagou Dongmo, A., Nkouathio, D.G., Tchoua, F.M., 2004. Pyroclastic deposits of the Bambouto volcano (Cameroon Line, Central Africa): evidence of an initial strombolian phase. *Journal of African Earth Sciences* **39,** 409-414.

Nowell, G.M., Pearson, D.G., Bell, D.R., Carlson, R.W., Smith, C.B., Kempton, P.D. and Noble, S.R. (2004) Hf Isotope Systematics of Kimberlites and their Megacrysts: New Constraints on their Source Regions. *J. Petrol*. **45,** 1583-1612.

O'Connor, J.M., le Roex, A.P., 1992. South Atlantic hot spot-plume systems: 1. Distribution of volcanism in time and space. *Earth Planet. Sci. Lett.* **113,** 343–364.

O'Reilly, S.Y., Zhang, M., Griffin, W.L., Begg, G. and Hronsky, J. (2009) Ultradeep continental roots and their oceanic remnants: A solution to the geochemical "mantle reservoir" problem. *Lithos* **112, Supplement 2,** 1043-1054.

Ovchinnikiva, G.V., Belyatsky, B.V., Vasil'eva, I.M., Levskii, L.K., Grachev, A.F., Arana, V. and Mithavila, J. (1995) Sr-Nd-Pb isotope characteristics of the mantle sources of basalts from the Canary Islands. *Petrology* **3,** 172-182.

Palme, H., O'Neill, H. StC., 2003. Cosmochemical Estimates of mantle composition. In: Carlson, R.W. (Eds.). The Mantle and Core. In: Holland, H.D., Turekian, K.K. (Eds.), *Treatise on Geochemistry, vol. 2, Elsevier-Pergamon, Oxford*, pp. 1-38.

Pasyanos,M., and A. Nyblade (2007),A toptobottom lithospheric study of Africa and Arabia, *Tectonophysics,* **444(1–4),** 27–44.

Paulick, H., Münker, C. and Schuth, S. (2010) The influence of small-scale mantle heterogeneities on Mid-Ocean Ridge volcanism: Evidence from the southern Mid-Atlantic Ridge (7°30'S to 11°30'S) and Ascension Island. *Earth Planet. Sci. Lett*. **296,** 299-310.

Pérez-Gussinyé, M., M. Metois, M. Fernández, J. Vergés, J. Fullea, and A. Lowry (2009), Effective elastic thickness of Africa and its relationship to other proxies for lithospheric structure and surface tectonics. *Earth Planet. Sci. Lett.,* **287(1–2),** 152–167.

Pilet, S., Baker, M. B., and Stolper, E. M. (2008). Metasomatized lithosphere and the origin of alkaline lavas. *Science,***320(5878),** 916–919.

Pilet, S., Hernandez, J., Sylvester, P., and Poujol, M. (2005). The metasomatic alternative for ocean island basalt chemical heterogeneity. *Earth and Planetary Science Letters,* **236(1),** 148–166.

Piper, J.D.A., Richardson, A., 1972. The paleomagnetism of the Gulf of Guinea volcanic province, West Africa. *Geophysical Journal of the Royal Astronomical Society* **29,** 147-171.

Plomerova, J., V. Babuška, C. Dorbath, L. Dorbath, and R. Lillie (1993), Deep lithospheric structure across the central African shear zone in Cameroon, *Geophys. J. Int.,* **115(2),** 381–390.

Pollitz, F. F. (1991). Two-stage model of African absolute motion during the last 30 million years. *Tectonophysics,* **194(1-2),** 91-106.

Poudjom Djomani, Y., J. Nnange, M. Diament, C. Ebinger, and J. Fairhead (1995), Effective elastic thickness and crustal thickness variations in west central Africa inferred from gravity data. *J. Geophys. Res.,* **100(B11),** 22047–22070.

Poudjom Djomani, Y.H., Diament, M., Albouy, Y., 1992. Mechanical behavior of the lithosphere beneath the Adamawa uplift (Cameroon, West Africa) based on gravity data. *Journal of African Earth Sciences* **15,** 81-90.

Poudjom Djomani, Y.H., Diament, M., Wilson, M., 1997. Lithospheric structure across the Adamawa Plateau (Cameroon) from gravity studies. *Tectonophysics* **273,** 317-327.

Prægel, N.O. and Holm, P.M. (2006) Lithospheric contributions to high-MgO basanites from the Cumbre Vieja Volcano, La Palma, Canary Islands and evidence for temporal variation in plume influence. *J. Volcanol. Geotherm. Res.* **149,** 213-239.

Priestley, K., D. McKenzie, E. Debayle, and S. Pilidou (2008), The African upper mantle and its relationship to tectonics and surface geology. *Geophys. J. Int.,* **175(3),** 1108–1126.

Princivalle, F., Salviulo, G., Marzoli, A., and Piccirillo, E. M. (2000). Clinopyroxene of spinel-peridotite mantle xenoliths from lake nji (cameroon volcanic line, w africa): crystal chemistry and petrological implications. *Contributions to Mineralogy and Petrology,* **139(5),** 503–508.

Rankenburg, K., 2004. The Role of Continental Crust and Lithospheric Mantle in the Genesis of Cameroon Volcanic Line Lavas: Constraints from Isotopic Variations in Lavas and Megacrysts from the Biu and Jos Plateaux. *J. Petrol.* **46,** 169–190.

Rankenburg, K., Lassiter, J., and Brey, G. (2004). Origin of megacrysts in volcanic rocks of the cameroon volcanic chain–constraints on magma genesis and crustal contamination. *Contributions to Mineralogy and Petrology,* **147(2),** 129–144.

Reusch, A. M., Nyblade, A. A., Tibi, R., Wiens, D. A., Shore, P. J., Bekoa, A., Tabod, C. T., and Nnange, J. M. (2011). Mantle transition zone thickness beneath cameroon: evidence for an upper mantle origin for the cameroon volcanic line. *Geophysical Journal International*,**187(3),** 1146–1150.

Reusch, A.M., Nyblade, A.A., Wiens, D.A., Shore, P.J., Ateba, B., Tabod, C.T., Nnange, J.M., 2010. Upper mantle structure beneath Cameroon from body wave tomography and the origin of the Cameroon Volcanic Line. *Geochemistry, Geophysics, Geosystems* **11(10).**

Richards, M.A., Duncan, R.A. and Courtillot, V.E. (1989) Flood Basalts and Hot-Spot Tracks: Plume Heads and Tails. *Science* **246,** 103-107.

Ritsema, J. and Allen, R.M. (2003) The elusive mantle plume. *Earth Planet. Sci. Lett.* **207,** 1-12.

Robertson, A. H. F., and Bernoulli, D., 1982, Stratigraphy, facies, and significance of late Mesozoic and early Tertiary sedimentary rocks of Fuerteventura (Canary Islands) and Maio (Cape Verde Islands), in von Rad, U., Hinz, K., Sarnthein, M., and Seibold, E., eds., Geology of the northwest African continental margin: Berlin, *Springer-Verlag,* p. 498–525.

Roeser HA (1982) Magnetic anomalies in the magnetic quiet zones off Morocco. In: von Rad U, Hinz K, Sarnthein M, Seibold E (eds) Geology of the Northwest African continental margin. *Springer, Berlin Heidelberg New York,* pp 61–68.

Rosenthal, A., Foley, S.F., Pearson, D.G., Nowell, G.M. and Tappe, S. (2009) Petrogenesis of strongly alkaline primitive volcanic rocks at the propagating tip of the western branch of the East African Rift. *Earth Planet. Sci. Lett.* **284,** 236-248.

Rudge, J.F., Maclennan, J., Stracke, A., 2013. The geochemical consequences of mixing melts from a heterogeneous mantle. *Geochim. Cosmochim. Acta* **114,** 112–143.

Rudnick, R.L., and Gao, S., 2003. Composition of the continental crust, pp. 1e64. In the crust (ed. R.L. Rudnick) vol. 3. *Treatise on Geochemistry (eds. H.D. Holland and K.K. Turekian), Elsevier-Pergamon, Oxford.*

Sato, H., Aramaki, S., Kusakabe, M., Hirabayashi, J., Sano, Y., Nojiri, V., Tchoua, F.M., 1990. Geochemical difference of basalts between polygenetic and monogenetic volcanoes in the central part of the Cameroon volcanic line.

Geochemical Journal **24,** 357-370.

Schettino, A. and Turco, E. (2009) Breakup of Pangaea and plate kinematics of the central Atlantic and Atlas regions. *Geophysical Journal International* **178,** 1078-1097.

Schilling, J.G., Hanan, B.B., McCully, B., Kingsley, R.H. and Fontignie, D. (1994) Influence of the Sierra Leone mantle plume on the equatorial Mid-Atlantic Ridge: A Nd-Sr-Pb isotopic study. *Journal of Geophysical Research: Solid Earth* **99,** 12005-12028.

Schmincke H-U (1998) Zeitliche, strukturelle und vulkanische Entwicklung der Kanarischen Inseln, der Selvagens Inseln und des Madeira-Archipels. In: Böhme W (ed) Handbuch der Reptilien und Amphibien Europas. Die Reptilien der Kanarischen Inseln, der Selvagens-Inseln und des Madeira-Archipels 6. *Aula, Wiesbaden,* pp 27–69.

Schmincke H-U, Sumita M (1998) Volcanic evolution of Gran Canaria reconstructed from apron sediments: synthesis of Vicap Project Drilling. In: Weaver PPE, Schmincke H-U, Firth JV, Duffield W (eds) *Proceedings Ocean Drilling Program, Sci Res* **157,** pp 443–469.

Schmincke, H. U. (1982). Volcanic and chemical evolution of the Canary Islands. In Geology of the Northwest African continental margin (pp. 273-306). *Springer, Berlin, Heidelberg.*

Sebai, A., Stutzmann, E., Montagner, J.-P., Sicilia, D., and Beucler, E. (2006). Anisotropic structure of the african upper mantle from rayleigh and love wave tomography. *Physics of the Earth and Planetary Interiors,* **155(1),** 48–62.

Shandini, Y., J. Tadjou, C. Tabod, and J. Fairhead (2010), Gravity data interpretation in the northern edge of the Congo Craton, South Cameroon, Anuário do Instituto de *Geociências,* **33(1),** 73–82.

Shaw, H.F. (1970) Trace element fractionation during anatexis. *Geoch. Cosmoch. Acta* **34,** 237-243.

Sibuet, J.C., Mascle, J., 1978. Plate kinematic implications Atlantic Equatorial fracture zone trends. *Journal of Geophysical Research* **83,** 3401-3421.

Simonsen SL, Neumann E-R, Seim K (2000) Sr-Nd-Pb isotope and trace-element geochemistry evidence for a young HIMU source and assimilation at Tenerife (Canary Island). *J Volcanol Geotherm Res* **103:** 299–312.

Sleep, N.H. (2005) Evolution of the continental lithosphere. *Annual Review of Earth and Planetary Sciences* **33,** 369-393.

Smith, C.B. (1983) Pb, Sr and Nd isotopic evidence for sources of Southern Africa Cretaceous kimberlites. *Nature* **304,** 51-54.

Staudigel H, Schmincke H-U (1984) The Pliocene seamount series of La Palma/Canary Islands. *J Geophys Res* **89:** 11195–11215.

Steiger, R.and J¨ager, E. (1977). Subcommission on geochronology: convention on the use of decay constants in geo-and cosmochronology. *Earth and planetary science*

*letters,***36(3),** 359–362.

Steiner, C., Hobson, A., Favre, P., Stampfli, G. M., and Hernandez, J. (1998). Mesozoic sequence of Fuerteventura (Canary Islands): Witness of Early Jurassic sea-floor spreading in the central Atlantic. *Geological Society of America Bulletin,* **110(10),** 1304-1317.

Stillman, C. J., Furnes, H., LeBas, M. J., Robertson, A. H. F., and Zielonka, J. (1982). The geological history of Maio, Cape Verde islands. *Journal of the Geological Society,* **139(3),** 347-361.

Stracke, A. (2012) Earth's heterogeneous mantle: A product of convection-driven interaction between crust and mantle. *Chem. Geol.* **330–331,** 274-299.

Stracke, A., Bizimis, M., and Salters, V. J. (2003). Recycling oceanic crust: quantitative constraints. *Geochemistry, Geophysics, Geosystems,***4(3)**.

Stracke, A., Hofmann, A.W., Hart, S.R., 2005. FOZO, HIMU, and the rest of the mantle zoo. *Geochemistry, Geophys. Geosystems* **6**.

Strelow, F.W.E., 1978. Distribution coefficients and anion exchange behavior of some elements in hydrobromic–nitric acid mixtures. *Anal. Chem.* **50,** 1359–1361.

Stroncik, N.A. and Niedermann, S. (2016) Atmospheric contamination of the primary Ne and Ar signal in mid-ocean ridge basalts and its implications for ocean crust formation. *Geoch. Cosmoch. Acta* **172,** 306-321.

Stuart, G., J. Fairhead, L. Dorbath, and C. Dorbath (1985), Crustal structure of the Adamawa Plateau Cameroon, *Rev. Sci. Technol. Ser. Sci. Terre,* **1(1–2),** 25–35.

Suh, C.E., Ayonghe, S.N., Sparks, R.S.J., Annen, C., Fitton, J.G., Nana, R., Luckman, a., 2003. The 1999 and 2000 eruptions of Mount Cameroon: eruption behaviour and petrochemistry of lava. *Bull. Volcanol.* **65,** 267–281.

Suh, C.E., Luhr, J.F., Njome, M.S., 2008. Olivine-hosted glass inclusions from Scoriae erupted in 1954-2000 at Mount Cameroon volcano, West Africa. *Journal of Volcanology and Geothermal Research* **169,** 1-33.

Sun, S., Hanson, G.N., 1975. Origin of Ross Island basanitoids and limitations upon the heterogeneity of mantle sources for alkali basalts and nephelinites. *Contributions to Mineralogy and Petrology* **52,** 77-106.

Sun, S., McDonough, W., 1989. Chemical and isotopic systematics of oceanic basalts: implications for mantle composition and processes. *Geological Society of London Special Publications* **42,** 313-345.

Tabod, C., J. Fairhead, G. Stuart, B. Ateba, and N. Ntepe (1992), Seismicity of the Cameroon Volcanic Line, 1982–1990, *Tectonophysics,* **212(3–4),** 303–320.

Tadjou, J., R. Nouayou, J. Kamguia, H. Kande, and E. Manguelle-Dicoum (2009), Gravity analysis of the boundary between the Congo Craton and the Pan-African belt of Cameroon, *Austrian J. Earth Sci.,* **102(1),** 71–79.

Takei, H. (2002) Development of precise analytical techniques for major and trace element concentrations in rock samples and their application to the Hishikari Gold Mine, southern Kyushu, Japan. PhD Thesis, Okayama University.

Tanaka, R., Makishima, A., Kitagawa, H., Nakamura, E., 2003. Suppression of Zr , Nb , Hf and Ta coprecipitation in fluoride compounds for determination in Ca-rich materials. *Journal of Analytical Atomic Spectrometry,* **18(12),** 1458-1463.

Tappe,S.,Foley,S.F.,Kjarsgaard,B.A.,Romer,R.L.,Heaman,L.M.,Stracke,A.,and Jenner,G.A.(2008).Between carbonatite and lamproite diamondiferous torngat ultrama?c lamprophyres formed by carbonate- fluxed melting of cratonic marid-type metasomes. *Geochimica et Cosmochimica Acta,***72(13),** 3258–3286.

Tatsumoto, M., Knight, R. J., and Allegre, C. J. (1973). Time differences in the formation of meteorites as determined from the ratio of lead-207 to lead-206. *Science,***180(4092),** 1279–1283.

Taylor, S. R., and McLennan, S. M. (1985). The continental crust: its compostion and evolution. An examination of geochemical record preserved in sedimentary rocks. *Blackwell Scientific publications, Oxford,* 312pp.

Tchouankoue, J.P., Wambo, N.A.S., Kagou, D.A., Wörner, G., 2012. Petrology, geochemistry, and Geodynamic implications of basaltic Dyke Swarms from the southern Continental part of the Cameroon volcanic line, Central Africa. *The Open Geology Journal* **6,** 72-84.

Tchuimegnie Ngongang, N.B., Kamgang, P., Chazot, G., Agranier, A., Bellon, H. and Nonnotte, P. (2015) Age, geochemical characteristics and petrogenesis of Cenozoic intraplate alkaline volcanic rocks in the Bafang region, West Cameroon. *J. Afr. Earth Sci.* **102,** 218-232.

Thirlwall MF, Singer BS, Marriner GF (2000) 39Ar – 40Ar ages and geochemistry of the basaltic shield stage of Tenerife, Canary Islands, *Spain. J Volcanol Geotherm Res* **103:** 247–297.

Thirlwall, M.F., Jenkins, C., Vroon, P.Z. and Mattey, D.P. (1997) Crustal interaction during construction of ocean islands: Pb-Sr-Nd-O isotope geochemistry of the shield basalts of Gran Canaria, Canary Islands. *Chem. Geol.* **135,** 233-262.

Thirlwall,M.(1997). Pb isotopic and elemental evidence for oib derivation from young himu mantle. *Chemical Geology,***139(1),** 51–74.

Thomas, L.E., Hawkesworth, C.J., Van Calsteren, P., Turner, S.P. and Rogers, N.W. (1999) Melt generation beneath ocean islands: a U-Th-Ra isotope study from Lanzarote in the Canary Islands. *Geoch. Cosmoch. Acta* **63,** 4081-4099.

Thompson, R. N. (1984). Dispatches from the basalt front. I. Experiments. *Proceedings of the Geologists' Association,* **95(3),** 249-262.

Thompson, R. N., Gibson S.A., Dickin A.P., Smith P.M. (2001) Early Cretaceous basalt and picrite dykes of the Southern Etendeka region, NW Namibia: windows into the role of the Tristan mantle plume in Parana-Etendeka magmatism. *J. Petrol*. **42,** 2049-2081.

Tokam, A., C. Tabod, A. Nyblade, J. Julià, D. Wiens, and M. Pasyanos (2010), Structure of the crust beneath Cameroon, West Africa, from the joint inversion of Rayleigh wave group velocities and receiver functions, *Geophys. J. Int.,* **183(2),** 1061–1076.

Torsvik, T.H. and Cocks, L.R.M. (2011) The Palaeozoic palaeogeography of central Gondwana. *Geological Society, London, Special Publications* **357,** 137-166.

Toteu, S., J. Penaye, and Y. Djomani (2004), Geodynamic evolution of the Pan-African belt in central Africa with special reference to Cameroon, *Can. J. Earth Sci.,* **41(1),** 73–85.

Tsafack, T.J.P., Wandji, P., Bardintzeff, J.M., Bellon, H., Guillou, H., 2009. The Mount Cameroon stratovolcano (Cameroon volcanic line, Central Africa): petrology, geochemistry, isotope and age data. *Geochemistry, Mineralogy and Petrology. SOFIA* **47**, 65-78.

Turcotte, D.L. and Oxburgh, E.R. (1973) Mid-plate Tectonics. *Nature* **244,** 337-339.

Turner, S., Hoernle, K., Hauff, F., Johansen, T.S., Klügel, A., Kokfelt, T. and Lundstrom, C. (2015) 238 U– 230 Th– 226 Ra Disequilibria Constraints on the Magmatic Evolution of the Cumbre Vieja Volcanics on La Palma, Canary Islands. *J. Petrol*. **56,** 1999-2024.

Ulrich, M., Hémond, C., Nonnotte, P. and Jochum, K.P. (2012) OIB/seamount recycling as a possible process for E-MORB genesis. *Geochemistry, Geophysics, Geosystems* **13,** n/a-n/a.

Van den Bogaard, P. (2013) The origin of the Canary Island Seamount Province - New ages of old seamounts. *Scientific Reports* **3,** 2107.

Wagner, C., Mokhtari, A., Deloule, E. and Chabaux, F. (2003) Carbonatite and Alkaline Magmatism in Taourirt (Morocco): Petrological, Geochemical and Sr–Nd Isotope Characteristics. *J. Petrol*. **44,** 937-965.

Walker, R.J., Carlson, R.W., Shirey, S.B. and Boyd, F.R. (1989) Os, Sr, Nd, and Pb isotope systematics of southern African peridotite xenoliths: Implications for the chemical evolution of subcontinental mantle. *Geoch. Cosmoch. Acta* **53,** 1583-1595.

Walter, M.J. (1998) Melting of garnet peridotite and the origin of komatiite and depleted lithosphere. *J. Petrol.* **39,** 29-60.

Weaver, B.L., 1991. The origin of ocean island basalt end-member compositions: trace element and isotopic constraints. *Earth and Planetary Science Letters* **104,** 381-397.

Wedepohl, K.H., Gohn, E., Hartmann, G., 1994. Cenozoic alkali basaltic magmas of western Germany and their products of differentiation. *Contributions to Mineralogy and Petrology* **115,** 253-278.

Weis, D. (1983). Pb isotopes in Ascension Island rocks: oceanic origin for the gabbroic to granitic plutonic xenoliths. *Earth and Planetary Science Letters*,**62(2),** 273–282.

Weis, D. and Demaiffe, D. (1985) A depleted mantle source for kimberlites from Zaire: Nd, Sr, and Pb isotopic evidence. *Earth Planet. Sci. Lett.* **73,** 269-277.

Weiss, Y., Griffin, W.L., Bell, D.R. and Navon, O. (2011) High-Mg carbonatitic melts in diamonds, kimberlites and the sub-continental lithosphere. *Earth Planet. Sci. Lett*. **309,** 337-347.

Weiss, Y., Kessel, R., Griffin, W.L., Kiflawi, I., Klein-BenDavid, O., Bell, D.R., Harris, J.W. and Navon, O. (2009) A new model for the evolution of diamond-

forming fluids: Evidence from microinclusion-bearing diamonds from Kankan, Guinea. *Lithos* **112,** Supplement 2, 660-674.

White, W.M. and Schilling, J.-G. (1978) The nature and origin of geochemical variation in Mid-Atlantic Ridge basalts from the Central North Atlantic. *Geoch. Cosmoch. Acta* **42,** 1501-1516.

Whitehouse MJ, Neumann E-R (1995) Sr-Nd-Pb isotope data for ultramafic xenoliths from Hierro, Canary Islands: Melt infiltration processes in the upper mantle. *Contrib Mineral Petrol* **119:** 239–246.

Widom, E., Carlson, R., Gill, J., and Schmincke, H.-U. (1997). Th-sr-nd-pb isotope and trace element evidence for the origin of the sao miguel, azores, enriched mantle source. *Chemical Geology,* **140(1),** 49–68.

Wiesmaier, S., Deegan, F.M., Troll, V.R., Carracedo, J.C., Chadwick, J.P. and Chew, D.M. (2011) Magma mixing in the 1100 AD Montaña Reventada composite lava flow, Tenerife, Canary Islands: interaction between rift zone and central volcano plumbing systems. *Contrib. Mineral. Petrol.* **162,** 651-669.

Willbold, M. and Stracke, A. (2006) Trace element composition of mantle end-members: Implications for recycling of oceanic and upper and lower continental crust. *Geochemistry, Geophysics, Geosystems* **7,** n/a-n/a.

Wilson, M., 1992. Magmatism and continental rifting during the opening of the South Atlantic Ocean: a consequence of Lower Cretaceous super-plume activity? in: magmatism and the causes of continental Break-up. *Geological Society Special Publications* **68,** 241-255.

Wilson, M., Downes, H., 1991. Tertiary-Quaternary extension-related alkaline magmatism in Western and Central Europe. *Journal of Petrology* **32(4),** 811-849.

Wilson, M., and Guiraud, R. (1992). Magmatism and rifting in Western and Central Africa, from Late Jurassic to Recent times. *Tectonophysics*, *213*(1-2), 203-225.

Wilson, S.C., Murton, B.J. and Taylor, R.N. (2013) Mantle composition controls the development of an Oceanic Core Complex. *Geochemistry, Geophysics, Geosystems* **14,** 979-995.

Wittig, N., Pearson, D.G., Duggen, S., Baker, J.A. and Hoernle, K. (2010) Tracing the metasomatic and magmatic evolution of continental mantle roots with Sr, Nd, Hf and and Pb isotopes: A case study of Middle Atlas (Morocco) peridotite xenoliths. *Geoch. Cosmoch. Acta* **74,** 1417-1435.

Workman, R.K. and Hart, S.R. (2005) Major and trace element composition of the depleted MORB mantle (DMM). *Earth Planet. Sci. Lett.* **231,** 53-72.

Wright, J. (1970). High pressure phases in nigerian cenozoic lavas distribution and geotectonic setting. *Bulletin Volcanologique,***34(4),** 833–847.

Wu, F.-Y., Mitchell, R.H., Li, Q.-L., Sun, J., Liu, C.-Z. and Yang, Y.-H. (2013) In situ U-Pb age determination and Sr-Nd isotopic analysis of perovskite from the Premier (Cullinan) kimberlite, South Africa. *Chem. Geol.* **353,** 83-95.

Wulff-Pedersen E, Neumann E-R, Jensen BB (1996) The upper mantle under La Palma,

Canary Islands: formation of Si-KNa-rich melt and its importance as a metasomatic agent. *Contrib Mineral Petrol* **125:**113–139.

Yamgouot, F. N., Déruelle, B., Mbowou, I. B. G., Ngounouno, I., Demaiffe, D. (2016) Geochemistry of the volcanic rocks from Bioko Island ("Cameroon Hot Line"): Evidence for plume-lithosphere interaction. Geoscience Frontiers, 7, 743-757.

Ye, J., Chardon, D., Rouby, D., Guillocheau, F., Dall'asta, M., Ferry, J.-N. and Broucke, O. (2017) Paleogeographic and structural evolution of northwestern Africa and its Atlantic margins since the early Mesozoic. *Geosphere* **13**.

Yokoyama, T., Aka, F.T., Kusakabe, M., Nakamura, E., 2007. Plume-lithosphere interaction beneath Mt. Cameroon volcano, West Africa: constraints from 238U-230Th-226Ra and Sr-Nd-Pb isotopic systematics. *Geochimica et Cosmochimica Acta* **71,** 1835-1854.

Yokoyama, T., Makishima, A., and Nakamura, E. (1999). Evaluation of the coprecipitation of incompatible trace elements with fluoride during silicate rock dissolution by acid digestion. *Chemical Geology*, **157(3),** 175-187.

Yoshikawa, M, and Nakamura, E., 1993. Precise isotope determination of trace amount of Sr in magnesium-rich samples, *Journal of Mineralogist and Petrologist and Economic Geologist*,**88,** 548-561.

Yokoyama, T., and Nakamura, E. (2002). Precise determination of ferrous iron in silicate rocks. *Geochimica et Cosmochimica Acta*, *66*(6), 1085-1093.

Yu, D. (1993) Rare earth element chromatographic separation and application to the Mid-Atlantic Ridge basalts (28°N-65°N) geochemistry. *Univ. Geneva.*

Zindler, A. and Jagoutz, E. (1988) Mantle cryptology. *Geoch. Cosmoch. Acta* **52,** 319-333.

Zindler, A., Hart, S.R., 1986. Chemical geodynamics. *Annual Review of Earth and Planetary Sciences* **14,** 493-571.

Zou, H., Zindler, A., Xu, X., Qi, Q., 2000. Major, trace element, and Nd, Sr and Pb isotope studies of Cenozoic basalts in SE China: mantle sources, regional variations, and tectonic significance. *Chemical Geology* **171,** 33-47.

APPENDIX

Supplementary Table 1 | Compiled Sr, Nd, Hf, and Pb isotopic data of Atlantic MORB (30°N – 30°S)

Sample name	Lat (°N)	Long (°W)	depth (mbsl)	$^{87}Sr/^{86}Sr$	$^{143}Nd/^{144}Nd$	$^{176}Hf/^{177}Hf$	$^{206}Pb/^{204}Pb$	$^{207}Pb/^{204}Pb$	$^{208}Pb/^{204}Pb$	ref.
M13	29.93	-42.77			0.513093	0.283200	18.638	15.507	38.086	14
V3 (1)	29.62	-43.00			0.513104	0.283156	18.591	15.504	38.048	14
V3 (2)	29.62	-43.00			0.513092	0.283180	18.583	15.506	38.056	14
M14b	29.28	-43.08			0.513153	0.283223	18.364	15.490	37.858	14
P-1	29.07	-43.02	2212			0.283218				15
N-1	28.88	-43.33	3658	0.702706	0.513079	0.283176				8,10,15
M15	27.77	-44.08			0.513160	0.283195	18.250	15.479	37.714	14
M16	25.27	-45.33			0.513171	0.283172	18.359	15.495	37.835	14
M17(1)	24.47	-46.25			0.513118	0.283175	18.400	15.496	37.915	14
V4a	23.70	-45.43			0.513187	0.283171	18.158	15.468	37.559	14
V5	23.42	-44.98			0.513141	0.283189	18.361	15.499	37.783	14
CHRRI88-031	23.13	-44.59				0.283205	18.238	15.482	37.672	15
R30	21.82	-45.22			0.513199	0.283194	18.445	15.508	37.851	14
VR30	21.82	-45.22			0.513175	0.283212	18.454	15.514	37.877	14
CHRRI88-030	21.82	-45.22				0.283171	18.456	15.512	37.851	15
CHHRl88 27	20.00	-45.70				0.283293	18.379	15.504	37.833	15
CHRRI88-026	19.58	-45.95				0.283174	18.282	15.494	37.686	15
CHRRI88-024	19.38	-45.98				0.283154	18.326	15.487	37.719	15
CHRRI88-022	19.12	-46.02				0.283265	18.523	15.506	38.141	15
CHRRI88-022	19.12	-46.02				0.283177	18.359	15.497	37.739	15
CHRRI88-021	18.82	-46.27				0.283175	18.235	15.484	37.614	15
CHRRI88-020	18.66	-46.28				0.283171	18.276	15.489	37.650	15
CHRRI88-018	18.26	-46.67				0.283218	18.009	15.460	37.373	15
CHRRI88-016	17.46	-46.43				0.283376	17.503	15.387	36.920	15
CHRRI88-015	17.31	-46.43				0.283371	17.519	15.383	36.927	15
CHRRI88-014	17.13	-46.45				0.283259	17.604	15.412	37.045	15
2pD 48-1	16.35	-46.66	3500	0.702407	0.513244	0.283328				9,13
CHRRI88-010	16.16	-46.66				0.283267	18.328	15.505	37.854	15
2pD 47-1	15.87	-46.58	3760		0.513149	0.283259				15
CHRRI88-009	15.74	-46.59				0.283254	18.485	15.511	38.052	15
SHK0415-005	15.66	-46.64		0.702606	0.513163		18.407	15.501	37.971	6
SHK0415-004	15.66	-46.64	4170	0.702624	0.513127		18.495	15.516	38.084	6
NAUFARA-021	15.62	-46.67				0.283268	18.399	15.499	37.944	15
NAUFARA-011	15.59	-46.61				0.283284	18.340	15.493	37.910	15
SHK0421-001	15.54	-46.63	4748	0.702492	0.513163		18.375	15.497	37.933	6
SHK0417-001	15.54	-46.58	4022	0.702637	0.513132		18.577	15.519	38.182	6
NAUFARA-017	15.52	-46.68				0.283262	18.587	15.506	37.971	15
NAUFARA-018	15.51	-46.64				0.283207	18.430	15.500	37.977	15
NAUFARA-016	15.50	-46.66				0.283318	18.342	15.489	37.893	15
NAUFARA-013	15.48	-46.56				0.283334	18.209	15.517	37.812	15
NAUFARA-015	15.44	-46.58				0.283257	18.457	15.514	38.013	15
SHK0419-011	15.44	-46.68	3703	0.702533	0.513114		18.573	15.521	38.159	6

Supplementary Table 1 | *(continued)*

Sample name	Lat (°N)	Long (°W)	depth (mbsl)	$^{87}Sr/^{86}Sr$	$^{143}Nd/^{144}Nd$	$^{176}Hf/^{177}Hf$	$^{206}Pb/^{204}Pb$	$^{207}Pb/^{204}Pb$	$^{208}Pb/^{204}Pb$	ref.
SHK0419-004	15.43	-46.67	4751	0.702652	0.513122		18.572	15.514	38.129	6
SHK0420-007	15.39	-46.58	4201	0.702542	0.513138		18.491	15.507	38.038	6
SHK0418-001A	15.36	-46.62	5232	0.702523	0.513160		18.464	15.504	38.019	6
SHK0418-003	15.36	-46.64	4915	0.702532	0.513148		18.479	15.499	37.994	6
SHK0428-003	15.15	-44.83	5092	0.702762	0.512962		19.238	15.578	38.905	6
SHK0428-004	15.14	-44.85	5001	0.702737	0.512967		19.237	15.577	38.902	6
SHK0428-005	15.14	-44.85	4854	0.702758	0.512976		19.252	15.575	38.885	6
NAUFARA-007	15.03	-44.93				0.283138	19.200	15.566	38.850	15
CHRRI88-007	14.68	-45.52				0.283118	18.693	15.558	38.637	15
2pD 45-2	14.50	-44.84	3720	0.702736	0.512948	0.283107				9,13
2pD 44-2	14.33	-45.04	3295		0.512995	0.283133				15
CHR0077-006-145	14.12	-45.00	2954	0.702794	0.512978		19.228	15.575	38.894	6
CHR0077-006	14.12	-45.00				0.283161	19.225	15.573	38.876	15
CH 77 DR6 157	14.12	-45.00	2954	0.702783	0.512995	0.283166				9,15
JCK0007-030-005	14.09	-45.02	2970	0.702783	0.512990		19.132	15.565	38.769	6
JCK0007-029-010	13.90	-45.03	3181	0.702933			19.220	15.554	38.903	6
JCK0007-028-012	13.84	-44.94	2768		0.513080		18.882	15.555	38.382	6
JCK0007-027-001	13.80	-44.96	3164	0.702773			19.228	15.581	38.848	6
JCK0007-027-002	13.80	-44.96	3164	0.702823			19.218	15.582	38.835	6
2pD 43-2	13.77	-45.01	3770		0.513099	0.283168				15
JCK0007-026-003	13.66	-44.97	3496		0.513020		19.145	15.595	38.796	6
JCK0007-023-011	13.51	-44.90	2854				18.950	15.539	38.489	6
JCK0007-023-013	13.51	-44.90	2854	0.702813	0.513040		18.974	15.556	38.528	6
JCK0007-025-001-001	13.40	-44.89	3857	0.702693	0.513060		18.860	15.571	38.398	6
JCK0007-025-003-001	13.40	-44.89	3857		0.513080		18.874	15.537	38.331	6
JCK0007-024-009	13.35	-44.90	3011	0.702743			18.891	15.543	38.427	6
JCK0007-010-038-002	13.34	-44.89	3187				18.427	15.504	37.932	6
JCK0007-014-001-004	13.33	-44.86	3500				18.751	15.529	38.282	6
JCK0007-014-001-010	13.33	-44.86	3500	0.702703	0.513100		19.209	15.594	38.879	6
JCK0007-009-008-002	13.32	-44.93	2354		0.513110		18.622	15.504	38.148	6
JCK0007-009-011-008	13.32	-44.93	2354				18.457	15.505	37.960	6
JCK0007-013-012	13.32	-44.89	3196				18.779	15.528	38.235	6
JCK0007-012-001-002	13.30	-44.78	3457	0.702883	0.512990		19.247	15.609	38.745	6
JCK0007-012-002-002	13.30	-44.78	3457	0.702623			18.500	15.505	38.020	6
JCK0007-012-003-001	13.30	-44.78	3457				18.512	15.539	38.077	6
JCK0007-012-005	13.30	-44.78	3457	0.702573	0.513130		18.478	15.493	37.995	6
JCK0007-012-006-002G	13.30	-44.78	3457	0.702863	0.513030		19.252	15.598	38.727	6
JCK0007-012-008	13.30	-44.78	3457	0.702523			18.455	15.503	37.973	6
JCK0007-006-001-010	13.30	-44.96	2526		0.512910		19.457	15.603	38.736	6
JCK0007-006-001-012	13.30	-44.96	2526				19.459	15.605	38.743	6
JCK0007-006-007-004	13.30	-44.96	2526				18.693	15.524	38.215	6
JCK0007-005-001-002	13.30	-44.96	2612	0.702643	0.513060		18.640	15.516	38.099	6

Supplementary Table 1 | *(continued)*

Sample name	Lat (°N)	Long (°W)	depth (mbsl)	$^{87}Sr/^{86}Sr$	$^{143}Nd/^{144}Nd$	$^{176}Hf/^{177}Hf$	$^{206}Pb/^{204}Pb$	$^{207}Pb/^{204}Pb$	$^{208}Pb/^{204}Pb$	ref.
JCK0007-005-001A	13.30	-44.96	2612				18.630	15.500	38.094	6
JCK0007-005-002-006	13.30	-44.96	2612	0.702843	0.512930		19.283	15.614	38.744	6
JCK0007-005-002-007	13.30	-44.96	2612	0.702633			18.644	15.519	38.137	6
JCK0007-005-005-002	13.30	-44.96	2612	0.702883	0.513010		19.281	15.614	38.742	6
JCK0007-005-005-003	13.30	-44.96	2612	0.702863	0.512970		19.273	15.607	38.721	6
JCK0007-011-001	13.27	-44.87	3740		0.513040		18.835	15.498	38.288	6
JCK0007-011-005	13.27	-44.87	3740		0.513050		18.846	15.501	38.299	6
JCK0007-015-001	13.07	-44.09	4496	0.702763	0.513020		19.031	15.564	38.646	6
JCK0007-015-010	13.07	-44.09	4496	0.702793			19.053	15.591	38.736	6
JCK0007-016-013	13.03	-44.84	4820	0.702623	0.513090		18.689	15.538	38.194	6
JCK0007-016-017	13.03	-44.84	4820		0.513110		18.684	15.533	38.178	6
JCK0007-020-018	12.99	-44.93	2866		0.513200		18.259	15.484	37.710	6
JCK0007-019-001-001	12.78	-44.84	4094		0.513140		18.590	15.528	38.051	6
JCK0007-019-005	12.78	-44.84	4094	0.702603	0.513130		18.586	15.524	38.060	6
2pD 40-2	12.40	-44.10	4375		0.513226	0.283228				13,15
NADVE89-008	10.72	-40.93				0.283172	18.332	15.496	37.854	15
NADVE89-016	10.71	-40.89				0.283180	18.482	15.511	37.999	15
CHR0078-010	10.68	-41.00				0.283158	18.699	15.513	38.231	15
NADVE89-006	10.67	-40.96				0.283182	18.390	15.492	37.795	15
NADVE89-003	10.66	-42.73				0.283169				15
CHR0078-008	10.62	-40.83				0.283157	18.332	15.492	37.855	15
CH 78 DR 08-20	10.62	-40.83	4339	0.702684	0.513126	0.283197				9,15
NADVE89-007	10.41	-40.55				0.283181	18.353	15.498	37.878	15
RC2806 55D-2g	4.91	-32.69	3530	0.702720	0.513013	0.283188	19.356	15.593	38.968	11,15
RC2806 55D-3g	4.91	-32.69	3530	0.702664	0.513031		19.348	15.579	38.941	11,15
RC2806 56D-3g	4.61	-32.67	3417	0.702683	0.513105		18.870	15.544	38.429	11,15
RC2806 57D-1g	4.37	-32.58	3885	0.702630	0.513053		19.036	15.549	38.600	11,15
RC2806 59D-1g	4.20	-32.58	4120	0.702583	0.513090	0.283204	18.743	15.530	38.308	11,15
RC2806 53D-4g	3.97	-31.55	4430	0.702687	0.513095	0.283199	19.042	15.553	38.598	11,15
RC2806 54D-1g	3.93	-31.56	4471	0.702669	0.513174		18.896	15.541	38.467	11,15
RC2806 50D-1g	3.91	-31.52	4130	0.702620	0.513105		19.050	15.554	38.623	11,15
RC2806 49D-1g	3.70	-31.51	3738	0.702586	0.513176	0.283254	18.744	15.527	38.301	11,15
RC2806 4D-2g	3.70	-31.51	3738				18.768	15.588	38.352	15
RC2806 48D-9g	3.46	-31.49	3896	0.702740	0.513110		19.121	15.579	38.744	11,15
RC2806 47D-1g	3.13	-31.36	3815	0.702659	0.513113	0.283206	19.105	15.557	38.658	11,15
RC2806 45D-1g	2.87	-31.35	3070	0.702813	0.512984	0.283205	19.561	15.607	39.165	11,15
RC2806 44D-1g	2.87	-31.27	3513	0.702614	0.513070		19.541	15.623	39.172	11,15
RC2806 46D-1g	2.81	-31.29	3682	0.702550	0.513145	0.283277				11,15
RC2806 43D-5g	2.39	-30.77	3674	0.702871	0.512973	0.283188	19.783	15.622	39.395	11,15
RC2806 42D-7g	2.18	-30.68	3440	0.702894	0.512953		19.643	15.609	39.281	11,15
RC2806 41D-1g	1.93	-30.64	3190	0.702915	0.512932	0.283157	20.034	15.637	39.666	11,15
RC2806 40D-9g	1.70	-30.64	3515	0.703003	0.512906		20.085	15.647	39.733	11,15

Supplementary Table 1 | *(continued)*

Sample name	Lat (°N)	Long (°W)	depth (mbsl)	$^{87}Sr/^{86}Sr$	$^{143}Nd/^{144}Nd$	$^{176}Hf/^{177}Hf$	$^{206}Pb/^{204}Pb$	$^{207}Pb/^{204}Pb$	$^{208}Pb/^{204}Pb$	ref.
RC2806 40D-3g	1.70	-30.64	3515	0.702956	0.512880	0.283089	20.099	15.651	39.749	11,15
RC2806 39D-1g	1.51	-30.67	3450	0.702886	0.512939	0.283087	19.766	15.631	39.479	11,15
RC2806 38D-1g	1.29	-30.54	3690	0.702746	0.512974		19.366	15.612	39.049	11,15
RC2806 37D-1g	1.10	-30.44	3345	0.702919	0.512960	0.283054	19.631	15.620	39.321	11,15
RC2806 34D-1g	1.02	-27.70	4530	0.702830	0.512985	0.283084	19.527	15.626	38.998	11,15
RC2806 33D-1g	0.99	-27.69	4470	0.702724	0.513004	0.283084	19.512	15.626	38.982	11,15
RC2806 36D-1g	0.95	-30.42	3285	0.702801	0.512998	0.283201	19.361	15.609	39.102	11,15
RC2806 32D-1g	0.82	-26.35	4665	0.702536	0.513203	0.283249				11,15
RC2806 35D-1g	0.79	-30.40	3740	0.702796	0.512962	0.283122	19.342	15.602	39.053	11,15
RC2806 35D-2g	0.79	-30.40	3740	0.702792	0.512932		19.345	15.608	39.074	11,15
RC2806 35D-4g	0.79	-30.40	3740	0.702804	0.512955	0.283122	19.347	15.607	39.083	11,15
RC2806 35D-8g	0.79	-30.40	3740	0.702832	0.512949		19.342	15.604	39.068	11,15
RC2806 31D-1g	0.65	-25.46	4414	0.702670	0.513138	0.283246				11,15
RC2806 29D-3g	0.48	-25.03	3975	0.702534	0.513148		18.889	15.555	38.338	11,15
RC2806 28D-1Ag	0.37	-24.97	3989	0.702541	0.513122	0.283199				11,15
RC2806 27D-4g	0.18	-24.91	3944	0.702489	0.513166		18.930	15.554	38.348	11,15
RC2806 18D-1g	-0.04	-16.47	3837	0.702595	0.513193	0.283365				11,15
RC2806 7D-1g	-0.14	-16.43	4000	0.702874	0.512899	0.282997				11,15
RC2806 25D-2g	-0.15	-24.81	3845	0.702502	0.513097	0.283148	18.928	15.555	38.347	11,15
RC2806 16D-1g	-0.27	-16.24	4095	0.702460	0.513180		18.691	15.540	38.214	11,15
RC2806 16D-10g	-0.27	-16.24	4095	0.702692	0.513095	0.283216	18.795	15.573	38.424	11,15
RC2806 24D-1g	-0.33	-24.76	2957	0.702531	0.513099	0.283166				11,15
RC2806 8D-1g	-0.41	-16.09	4220	0.702811	0.513079	0.283187				11,15
RC2806 23D-1g	-0.57	-24.61	3363	0.702505	0.513039	0.283153				11,15
RC2806 9D-3g	-0.74	-16.08	4305	0.702568	0.513137		18.664	15.544	38.207	11,15
RC2806 22D-4g	-0.79	-24.61	3895	0.702558	0.513094	0.283133	18.968	15.566	38.403	11,15
RC2806 21D-1g	-0.89	-24.58	4275	0.702586	0.513113	0.283145	18.900	15.559	38.360	11,15
RC2806 19D-1g	-1.01	-24.60	3690	0.702537	0.513099		18.925	15.562	38.371	11,15
RC2806 7D-3g	-1.05	-13.11	4175			0.283005	19.483	15.670	39.077	11,15
RC2806 6D-7	-1.05	-13.11	4175	0.702767	0.513073	0.283112				11,15
RC2806 6D-1g	-1.05	-13.11	4175	0.702472	0.513213		18.105	15.490	37.673	11,15
RC2806 6D-2g	-1.05	-13.11	4175			0.283192	18.166	15.502	37.754	11,15
RC2806 10D-6g	-1.06	-15.98	4000	0.702504	0.513089	0.283190	18.662	15.539	38.196	11,15
RC2806 14D-2g	-1.16	-15.94	3930	0.702585	0.513119	0.283188				11,15
RC2806 5D-1g	-1.16	-13.07	3975	0.702498	0.513173	0.283207				11,15
RC2806 11D-1g	-1.26	-15.92	4355	0.702483	0.513155	0.283208				11,15
RC2806 13D-3g	-1.37	-15.92	4580	0.702631	0.513122		18.582	15.536	38.144	11,15
EN061 1D-1g	-1.41	-13.18	2600	0.702466	0.513256	0.283261				11,15
RC2806 4D-1g	-1.41	-13.01	3950	0.702885	0.513074	0.283205				11,15
RC2806 4D-3g	-1.41	-13.01	3950	0.702923	0.513072	0.283206				11,15
RC2806 12D-1g	-1.54	-15.89	4376	0.702575	0.513109	0.283171				11,15
RC2806 3D-2g	-1.84	-12.96	3800	0.702591	0.513151	0.283241	18.362	15.518	37.971	11,15

Supplementary Table 1 | *(continued)*

Sample name	Lat (°N)	Long (°W)	depth (mbsl)	$^{87}Sr/^{86}Sr$	$^{143}Nd/^{144}Nd$	$^{176}Hf/^{177}Hf$	$^{206}Pb/^{204}Pb$	$^{207}Pb/^{204}Pb$	$^{208}Pb/^{204}Pb$	ref.
RC2806 2D-1g	-2.18	-12.64	3858	0.702190	0.513246		17.890	15.450	37.346	11,15
EN061 2D-1g	-2.24	-12.40	3885	0.702136	0.513283	0.283238				11,15
RC2806 1D-1g	-2.54	-12.23	3740	0.702125	0.513259	0.283269				11,15
EN061 3D-1g	-3.43	-12.23	3045	0.702176	0.513287	0.283260				11,15
EN061 3D-1	-3.43	-12.23	3045	0.702176	0.513287	0.283226				11,15
EN061 4D-1g	-4.27	-12.20	2300	0.702263	0.513311	0.283269	17.695	15.441	37.172	11,15
MET64/1-119	-4.80	-12.36	2980	0.702104	0.513315		17.576	15.416	37.028	2
MET64/1-118	-4.80	-12.37	3000	0.702104	0.513321		17.562	15.414	37.023	2
MET64/1-146-002	-4.81	-12.38	3024	0.702129	0.513309		17.631	15.422	37.089	2,4
MET64/1-123-008	-4.81	-12.37	2985	0.702157	0.513311		17.648	15.426	37.111	2
MET64/1-124-001A	-4.81	-12.37	2998	0.702142	0.513305		17.645	15.430	37.121	2
MET64/1-131-001	-4.81	-12.37	2999	0.702157	0.513306		17.650	15.427	37.113	2
MET64/1-125-006	-4.81	-12.37	2986	0.702141	0.513302		17.631	15.422	37.091	2
MET64/1-109-001	-4.81	-12.37	2998	0.702142	0.513302		17.632	15.424	37.094	2
MET64/1-125-008	-4.81	-12.37	2985	0.702134	0.513316		17.604	15.420	37.066	2
MET64/1-135	-4.82	-12.38	3001	0.702154	0.513306		17.655	15.427	37.116	2,4
EN061 5D-1Ag	-5.19	-11.52	3300	0.702156	0.513335	0.283363				11,15
EN061 5D-3A	-5.19	-11.52	3300				17.660	15.429	37.140	15
MET41/2-119-001	-6.27	-11.38	3242	0.702173	0.513331		17.669	15.435	37.157	1,2
EN061 6D-1Cg	-6.31	-11.32	3218	0.702270	0.513322	0.283280				11,15
MET41/2-120-002	-6.40	-11.34	3523	0.702241	0.513285		17.860	15.451	37.333	1,2
MET41/2-121-001	-6.54	-11.31	3749	0.702193	0.513315		17.688	15.437	37.178	1,2
MET41/2-126-002	-7.14	-13.05	4514	0.702126	0.513279		17.822	15.437	37.309	1,2
EN061 07D-1g	-7.51	-13.46	4025	0.702426	0.513184		18.862	15.564	38.473	12,15
MET41/2-130-001	-7.58	-13.47	3925	0.702318	0.513342		17.882	15.460	37.434	2
MET41/2-130-003	-7.58	-13.47	3925	0.702307	0.513309	0.283389	17.909	15.482	37.512	1,2,3,4
MET41/2-141-001	-7.58	-13.47	3925	0.702312	0.513285		18.059	15.476	37.598	1,2
MET41/2-132-001	-7.67	-13.46	3925	0.702489	0.513148		18.852	15.554	38.389	1,2
MET41/2-132-005	-7.67	-13.46	3925	0.702544	0.513148	0.283255	18.847	15.551	38.384	1,2
MET41/2-133-007	-7.72	-13.44	3980	0.702386	0.513189		18.661	15.534	38.196	1,2
MET41/2-136-001	-7.77	-13.43	3727	0.702394	0.513176		18.571	15.523	38.128	1,2
MET41/2-137-002	-7.82	-13.43	3405	0.702305	0.513241		18.353	15.497	37.863	1,2
MET41/2-138-001	-7.87	-13.43	3451	0.702689	0.513050	0.283131	19.424	15.610	39.000	1,2,3
MET41/2-138-002	-7.87	-13.43	3451	0.702653	0.513066		19.359	15.603	38.930	1,2
MET41/2-138-003	-7.87	-13.43	3451	0.702701	0.513048		19.495	15.617	39.072	1,2
MET41/2-139-001	-7.92	-13.41	3631	0.702279	0.513222		18.364	15.498	37.891	2
MET41/2-139-003	-7.92	-13.41	3631	0.702408	0.513183		18.657	15.530	38.217	1,2
MET41/2-140-001	-7.97	-13.40	3670	0.702253	0.513259	0.283374	18.192	15.488	37.722	1,2,3
EN061 08D-2Ag	-8.01	-13.40	3390	0.702323	0.513246	0.283295	18.393	15.500	37.917	12,15
EN061 08D-1Ag	-8.01	-13.40	3390	0.702392	0.513148		18.936	15.567	38.532	12,15
MET41/2-142-002	-8.02	-13.43	3576	0.702289			18.396	15.503	37.918	1,2,4
MET41/2-143-002	-8.05	-13.42	3457	0.702216	0.513225	0.283224	18.198	15.487	37.672	1,2,3

Supplementary Table 1 | *(continued)*

Sample name	Lat (°N)	Long (°W)	depth (mbsl)	$^{87}Sr/^{86}Sr$	$^{143}Nd/^{144}Nd$	$^{176}Hf/^{177}Hf$	$^{206}Pb/^{204}Pb$	$^{207}Pb/^{204}Pb$	$^{208}Pb/^{204}Pb$	ref.
MET41/2-144-001	-8.09	-13.45	3522	0.702069			18.333	15.494	37.870	1,2
MET41/2-145-001	-8.12	-13.41	3470	0.702301	0.513224		18.391	15.501	37.908	1,2
MET41/2-146-002	-8.17	-13.45	3401	0.702328	0.513197		18.462	15.510	38.002	1,2
MET41/2-147-001	-8.31	-13.61	3055	0.702376	0.513220		18.635	15.535	38.172	1,2
MET41/2-153-001	-8.55	-13.55	2552	0.702462	0.513194		18.892	15.561	38.445	1,2
EN061 09D-1	-8.62	-13.27	2205	0.702934	0.512985	0.283070	19.111	15.616	38.994	12,15
MET41/2-155-001	-8.69	-13.54	2380	0.702370	0.513216	0.283161	18.767	15.545	38.261	1,3
MET64/1-163	-8.76	-13.51	2287	0.702498	0.513177		18.995	15.574	38.548	2,5
MET64/1-162	-8.77	-13.51	2273	0.702372	0.513264		18.566	15.529	38.113	2,5
MET64/1-160	-8.78	-13.51	2208	0.702481	0.513191		18.989	15.573	38.519	2,5
MET64/1-159-010	-8.79	-13.50	2219	0.702498	0.513169		19.005	15.574	38.583	2,5
MET64/1-159-006	-8.80	-13.50	2151	0.702273	0.513200		18.737	15.544	38.206	2,5
MET64/1-159-004	-8.80	-13.50	2201	0.702459	0.513205		18.904	15.565	38.425	2,5
MET64/1-159-003	-8.80	-13.50	2198	0.702453	0.513209		18.909	15.569	38.439	2,5
MET64/1-159-001	-8.80	-13.50	2204	0.702465	0.513185		18.960	15.571	38.502	2,5
MET41/2-157-003	-8.81	-13.50	2212	0.702459	0.513213	0.283183	18.933	15.563	38.417	1,2,3,5
MET64/1-155-001	-8.82	-13.51	2161	0.702376	0.513225		18.901	15.553	38.260	2,5
MET64/1-155-007	-8.82	-13.50	2221	0.702466	0.513217		18.935	15.562	38.413	2,5
MET64/1-155-004	-8.82	-13.51	2149	0.702461	0.513202		18.901	15.561	38.416	2,5
MET41/2-158-001	-8.84	-13.50	2139	0.702458			18.983	15.570	38.527	1,2,5
MET41/2-160-001	-8.97	-13.46	2166	0.702347	0.513186		18.957	15.553	38.375	1,2
MET41/2-160-002	-8.97	-13.46	2166	0.702344	0.513193		18.963	15.562	38.404	1,2
MET41/2-160-003	-8.97	-13.46	2166	0.702395	0.513145	0.283144	19.009	15.569	38.566	1,2,3
MET41/2-161-001	-9.01	-13.46	2232	0.702408	0.513178	0.283161	18.959	15.562	38.455	1,2,3
MET41/2-162-001	-9.08	-13.45	2460	0.702454	0.513159		19.114	15.586	38.640	1,2
EN061 10D-1	-9.11	-13.33	2663	0.702470	0.513183		18.972	15.584	38.678	12,15
MET41/2-166-004	-9.24	-13.42	2460	0.702660	0.513053		19.198	15.599	38.930	1,2
MET68/1-036	-9.53	-13.21	1439	0.702677	0.513047		19.193	15.600	38.939	2
MET64/1-203	-9.55	-13.21	1509	0.702691	0.513053		19.170	15.599	38.934	2
MET64/1-214-001	-9.55	-13.21	1511	0.702670	0.513048		19.193	15.599	38.937	2
MET64/1-209-001	-9.55	-13.21	1511	0.702665	0.513052		19.195	15.602	38.944	2
MET64/1-200-006	-9.55	-13.21	1505	0.702672	0.513059		19.193	15.602	38.943	2
MET64/1-205	-9.56	-13.21	1497	0.702679	0.513053		19.178	15.599	38.937	2
MET41/2-172-003	-9.56	-13.21	1488	0.702683	0.513044		19.190	15.600	38.938	1,2
MET64/1-211	-9.57	-13.21	1488	0.702672	0.513048		19.197	15.606	38.956	2
MET64/1-194ROV-007	-9.57	-13.21	1448	0.702681	0.513074	0.283121	19.069	15.595	38.814	3
MET64/1-194-007	-9.57	-13.21	1448	0.702682	0.513063		19.195	15.603	38.943	2
MET64/1-194-011	-9.57	-13.21	1470	0.702683	0.513053		19.196	15.605	38.953	2
MET64/1-194-009	-9.57	-13.21	1465	0.702668	0.513062		19.195	15.602	38.943	2
EN061 11D-1Ag	-9.62	-13.23	1680	0.702744	0.513203		19.286	15.617	39.083	12,15
MET41/2-176-002	-9.68	-13.02	1543	0.702721	0.513056		19.134	15.594	38.848	1,2
MET41/2-175-002	-9.69	-13.09	1726	0.702512	0.513078	0.283106	19.047	15.582	38.723	1,2,3

Supplementary Table 1 | *(continued)*

Sample name	Lat (°N)	Long (°W)	depth (mbsl)	$^{87}Sr/^{86}Sr$	$^{143}Nd/^{144}Nd$	$^{176}Hf/^{177}Hf$	$^{206}Pb/^{204}Pb$	$^{207}Pb/^{204}Pb$	$^{208}Pb/^{204}Pb$	ref.
MET41/2-183-001	-9.71	-12.14	2297	0.702625	0.513054		19.239	15.591	38.867	1,2
MET41/2-183-003	-9.71	-12.14	2297	0.702607	0.513056		19.269	15.597	38.887	2
MET41/2-188-001	-9.77	-13.16	1603	0.702654			19.180	15.595	38.925	1,2
MET41/2-186-001	-9.77	-12.15	918	0.702660	0.513058		19.191	15.586	38.803	1,2
MET41/2-190-004	-9.89	-13.09	2052	0.702691	0.513046		19.211	15.604	38.992	1,2
EN061 12D-1g	-9.93	-13.13	2205	0.702682	0.513063		19.170	15.603	38.934	12,15
MET41/2-191-003	-9.95	-13.07	2188	0.702660	0.513067		19.126	15.591	38.867	1,2
MET41/2-194-001	-10.07	-13.20	2953	0.702513	0.513099		18.839	15.557	38.513	1,2
MET41/2-195-001	-10.13	-13.20	3091	0.702425	0.513221	0.283325	18.437	15.521	38.063	1,3
MET41/2-195-002	-10.13	-13.20	3091	0.702432	0.513203		18.434	15.517	38.050	1,2
MET41/2-196-003	-10.23	-13.19	3241	0.702604	0.513079		18.976	15.580	38.706	1,2
MET41/2-197-003	-10.29	-13.18	3100	0.702612	0.513084		19.052	15.589	38.799	1,2
MET41/2-198-001	-10.38	-13.18	3500	0.702492	0.513189		18.460	15.530	38.132	1,2
MET41/2-199-002	-10.48	-13.17	3528	0.702328	0.513262	0.283403	18.107	15.484	37.719	1,2,3
EN061 13D-1g	-10.55	-13.01	3288	0.702420	0.513216	0.283334	18.388	15.523	38.057	12,15
MET41/2-200-001	-10.61	-13.09	3791	0.702424	0.513188		18.496	15.528	38.152	1,2
MET41/2-201-005	-10.68	-13.07	3712	0.702554	0.513111		19.075	15.589	38.593	1,2
MET41/2-202-001	-10.78	-13.05	3463	0.702372	0.513126		18.517	15.510	38.044	1,2
MET41/2-203-002	-10.88	-13.04	3639	0.702371	0.513201		18.447	15.518	38.021	1,2
EN061 15D-1	-12.03	-14.41	3258	0.702400	0.513200		18.494	15.510	37.893	12,15
EN061 16D-1g	-12.68	-14.66	3575	0.702547	0.513182		18.622	15.516	38.113	12,15
RC16 3D-1	-12.90	-14.73	2303	0.702415	0.513224	0.283235				12,15
RC16 6D-1A	-13.47	-14.75	2752	0.702450	0.513101		18.221	15.480	37.819	12,15
RC16 7D-1g	-14.08	-14.46	3534	0.702277	0.513224	0.283222				12,15
EN061 18D-1g	-15.46	-13.26	2860	0.702845	0.512996	0.283032	18.896	15.571	38.492	12,13,15
EN061 20D-1g	-17.33	-14.18	3765	0.702373	0.513220		18.548	15.569	38.099	12,15
EN061 22D-1g	-18.38	-12.84	3675	0.702338	0.513179		18.705	15.534	38.056	12,15
EN063 01D-6g	-20.79	-11.60	3460	0.702331	0.513098	0.283160				12,15
EN063 02D-5g	-21.50	-11.82	3460	0.702301	0.513177	0.283188				12,13
EN063 03D-5g	-22.96	-13.49	2105	0.702355	0.513220	0.283140				12,15
EN063 07D-5g	-23.49	-13.40	3630	0.702291	0.513148		18.322	15.503	37.839	12,15
EN063 08D-5g	-24.01	-13.30	3370	0.702443	0.513025	0.283155				12,15
EN063 09D-5	-24.52	-13.36	4010	0.702627	0.513108		18.305	15.531	38.006	12,15
EN063 10D-5g	-24.95	-13.19	3105	0.702869	0.513082		18.342	15.513	37.965	12,15
EN063 12D-5g	-26.00	-13.90	2670	0.702423			18.309	15.506	37.927	12,15
EN063 13D-5g	-26.52	-13.64	3935	0.702478	0.513080	0.283134				12,15
EN063 14D-5g	-26.99	-13.52	3610	0.702427	0.513086		18.306	15.505	37.910	12,15
EN063 17D-5g	-28.54	-12.54	3890	0.702670	0.513025		18.135	15.503	37.873	12,15
EN063 19D-5g	-28.96	-13.50	4140	0.702681	0.513099	0.283171				12,15

The isotopic compositions were normalized to $^{87}Sr/^{86}Sr = 0.71024$ for SRM 987, $^{143}Nd/^{144}Nd = 0.51186$ for La Jolla, $^{176}Hf/^{177}Hf = 0.28216$ for JMC-475, $^{206}Pb/^{204}Pb = 16.9424$, $^{207}Pb/^{204}Pb = 15.5003$, and $^{208}Pb/^{204}Pb = 36.7266$ for SRM 981.

Supplementary Table 2 | Compiled Sr, Nd, Hf, and Pb isotopic data of Canary Islands, Mount Atlas, Cape Verde Islands, Madeira Islands, and continental section of Cameroon Volcanic Line

location	Sample	$^{87}Sr/^{86}Sr$	$^{143}Nd/^{144}Nd$	$^{176}Hf/^{177}Hf$	$^{206}Pb/^{204}Pb$	$^{207}Pb/^{204}Pb$	$^{208}Pb/^{204}Pb$	method	ref.
Canary Islands									
El Hierro (S)	JMDD EH 01	0.702959	0.512980		19.366	15.607	39.042	Tl	31
El Hierro (S)	JMDD EH 03	0.702943	0.512964		19.400	15.582	39.051	Tl	31
El Hierro (S)	JMDD EH 07	0.703025	0.512991		19.142	15.578	38.906	Tl	31
El Hierro (S)	JMDD EH 10	0.702973	0.512940		19.605	15.595	39.272	Tl	31
El Hierro (S)	JMDD EH 11	0.703003	0.512928		19.642	15.621	39.362	Tl	31
El Hierro (S)	JMDD EH 12	0.703023	0.512957		19.299	15.542	38.961	Tl	31
El Hierro (S)	JMDD EH 13	0.702996	0.512938		19.540	15.607	39.237	Tl	31
El Hierro (S)	JMDD EH 14	0.702967	0.512966		19.340	15.573	39.046	Tl	31
El Hierro (S)	JMDD EH 15	0.703027	0.512971		19.470	15.604	39.195	Tl	31
El Hierro (S)	JMDD EH 16	0.702854	0.513001		19.117	15.572	38.754	Tl	31
El Hierro (S)	JMDD EH 17	0.702972	0.512954		19.417	15.581	39.117	Tl	31
El Hierro (S)	JMDD EH 18	0.703127	0.512950		19.674	15.628	39.376	Tl	31
El Hierro (S)	JMDD LP 01	0.703040	0.512912		19.767	15.638	39.732	Tl	31
El Hierro (S)	JMDD LP 02	0.703133	0.512928		20.160	15.670	39.910	Tl	31
El Hierro (S)	JMDD LP 04	0.703074	0.512895		19.917	15.638	39.723	Tl	31
El Hierro (S)	JMDD LP 05	0.703045	0.512918		19.728	15.630	39.496	Tl	31
El Hierro (S)	JMDD LP 07	0.703045	0.512894		19.850	15.637	39.749	Tl	31
El Hierro (S)	JMDD LP 09	0.703204	0.512903		20.149	15.668	40.042	Tl	31
El Hierro (S)	JMDD LP 14	0.703100	0.512921		19.535	15.603	39.305	Tl	31
El Hierro	EH9	0.702948	0.512978	0.283016	*19.188*	*15.564*	*38.825*	conv.	32
El Hierro	EH 11	0.702951	0.512950	0.283005	*19.363*	*15.571*	*39.032*	conv.	32
El Hierro	EH4	0.703010	0.512984	0.282981	*19.422*	*15.577*	*39.090*	conv.	32
El Hierro	EH 8	0.702914	0.512984	0.282993	*19.404*	*15.600*	*39.067*	conv.	32
El Hierro	H1-60/61	0.702930	0.512960		*19.442*	*15.624*	*39.136*	conv.	19
El Hierro	668-2	0.702974	0.512971		*19.253*	*15.580*	*38.905*	conv.	27
El Hierro	669-3	0.703140	0.512912		*19.920*	*15.636*	*39.657*	conv.	27
El Hierro	675-2	0.702961	0.512949		*19.390*	*15.573*	*39.017*	conv.	27
El Hierro	EH8	0.702922	0.512979		*19.402*	*15.602*	*39.063*	conv.	28
El Hierro	EH 11	0.702952	0.512956		*19.365*	*15.575*	*39.038*	conv.	28
El Hierro	TRAC 2	0.703058	0.512958		*19.459*	*15.590*	*39.124*	conv.	35
Fuerteventura	EF1	0.702972	0.513032	0.283065	*19.106*	*15.560*	*38.889*	conv.	32
Fuerteventura	EF5	0.703018	0.512971	0.283044	*19.209*	*15.552*	*38.889*	conv.	32
Fuerteventura	EF6	0.703178	0.512914	0.283017	*19.202*	*15.570*	*39.025*	conv.	32
Fuerteventura	EF7	0.703042	0.512966	0.283041	*19.168*	*15.552*	*38.972*	conv.	32
Fuerteventura	EF12	0.703177	0.512894	0.283009	*19.210*	*15.584*	*39.136*	conv.	32
Fuerteventura	KFS240	0.703015	0.512959						21
Fuerteventura	KFS96	0.703146	0.512958						21
Fuerteventura	KFS69	0.703186	0.512922						21
Fuerteventura	KFS110	0.702988	0.512980						21
Fuerteventura	KFS140	0.703001	0.512962						21
Fuerteventura	KFS34A	0.703041	0.512954						21
Fuerteventura	KFS46	0.703119	0.512923						21
Fuerteventura	KFS53	0.703113	0.512924						21
Fuerteventura	KFS54	0.703086	0.512917						21
Fuerteventura	KFS55	0.703283	0.512913						21
Gran Canaria (S)	GCR-47	0.703169	0.512899		19.538	15.612	39.454	black.	30
Gran Canaria (S)	GCR-36	0.703159	0.512952						30
Gran Canaria (S)	GCR-60	0.703189	0.512892		19.535	15.616	39.451	black.	30
Gran Canaria (S)	GCR-45	0.703138	0.512849						30
Gran Canaria (S)	GCR-6	0.703149	0.512909						30
Gran Canaria (S)	GCR-38	0.703142	0.512910		19.568	15.607	39.474	black.	30
Gran Canaria (S)	GCR-20	0.703160	0.512911						30
Gran Canaria (S)	GCR-62	0.703221	0.512889		19.500	15.613	39.422	black.	30
Gran Canaria (S)	GCR-63	0.703217	0.512873		19.558	15.643	39.497	black.	30
Gran Canaria (S)	GCR-27	0.703109	0.512931						30
Gran Canaria (S)	GCR-2	0.703347	0.512884						30
Gran Canaria (S)	GCR-14	0.703167	0.512903						30
Gran Canaria (S)	GCR-19	0.703195	0.512892						30
Gran Canaria (S)	GCR-35	0.703136	0.512919		19.414	15.599	39.316	black.	30
Gran Canaria (S)	GCR-34	0.703298	0.512916		19.383	15.590	39.264	black.	30
Gran Canaria (S)	GCR-50	0.703273	0.512923						30
Gran Canaria (S)	GCR-39	0.703093	0.512927		19.203	15.571	39.060	black.	30
Gran Canaria (S)	GCR-42	0.703117	0.512882						30
Gran Canaria (S)	GCR-21	0.703081	0.512919						30
Gran Canaria (S)	GCR-18	0.703154	0.512923		19.363	15.579	39.268	black.	30
Gran Canaria (S)	GCR-A10	0.703187	0.512960						30
Gran Canaria (S)	GCR-16	0.703098	0.512932						30
Gran Canaria (S)	GCR-37	0.703122	0.512937		19.382	15.575	39.247	black.	30
Gran Canaria (S)	GCRN-4	0.703130	0.512917		19.488	15.588	39.403	black.	30

Supplementary Table 2 | *(continued)*

location	Sample	$^{87}Sr/^{86}Sr$	$^{143}Nd/^{144}Nd$	$^{176}Hf/^{177}Hf$	$^{206}Pb/^{204}Pb$	$^{207}Pb/^{204}Pb$	$^{208}Pb/^{204}Pb$	method	ref.
Gran Canaria (S)	GCR-15	0.703088	0.512917						30
Gran Canaria (S)	GCR-30	0.703077	0.512960		19.418	15.584	39.284	black.	30
Gran Canaria (S)	GCR-41	0.703162	0.512892		19.540	15.593	39.483	black.	30
Gran Canaria (S)	GCR-46	0.703063	0.512976		19.461	15.588	39.347	black.	30
Gran Canaria (S)	GCR-A8	0.703029	0.512960						30
Gran Canaria (S)	GCR-52	0.703116	0.512918		19.549	15.672	39.520	black.	30
Gran Canaria (S)	GCR-24	0.703162	0.512862		19.288	15.573	39.204	black.	30
Gran Canaria (S)	GCR-48	0.703377	0.512781		19.517	15.577	39.592	black.	30
Gran Canaria (S)	GCR-X7	0.703161	0.512915		19.342	15.571	39.222	black.	30
Gran Canaria (S)	GCR-1	0.703157	0.512931		19.405	15.574	39.303	black.	30
Gran Canaria (S)	GCR-A3	0.703002	0.512968						30
Gran Canaria (S)	GCR-A5	0.703107	0.512910						30
Gran Canaria (S)	GCR-3	0.703082	0.512892						30
Gran Canaria	EGC1	0.703199	0.512888	0.282981	*19.489*	*15.595*	*39.368*	conv.	32
Gran Canaria	EGC3	0.703151	0.512933	0.282995	*19.602*	*15.590*	*39.410*	conv.	32
Gran Canaria	EGC6	0.703162	0.512948	0.282980	*19.564*	*15.590*	*39.411*	conv.	32
Gran Canaria	EGC8	0.703143	0.512910	0.282992	*19.388*	*15.582*	*39.236*	conv.	32
Gran Canaria	GCQ 1369	0.703137	0.512897	0.282986	*19.366*	*15.586*	*39.209*	conv.	32
Gran Canaria	GC664	0.703380			*19.532*	*15.584*	*39.276*	conv.	17
Gran Canaria	GC665	0.703350			*19.482*	*15.574*	*39.226*	conv.	17
Gran Canaria	GC666	0.703360			*19.502*	*15.584*	*39.246*	conv.	17
Gran Canaria	GC667	0.703390			*19.542*	*15.594*	*39.296*	conv.	17
Gran Canaria	GC668	0.703370			*19.492*	*15.574*	*39.166*	conv.	17
Gran Canaria	GC669	0.703390			*19.502*	*15.584*	*39.196*	conv.	17
Gran Canaria	GC670	0.703400			*19.542*	*15.584*	*39.226*	conv.	17
Gran Canaria	W1	0.703310	0.512920						17
Gran Canaria (S)	A6_leach	0.703226	0.512924		*19.681*	*15.622*	*39.459*	conv.	16
Gran Canaria (S)	A16	0.703335	0.512920		*19.565*	*15.620*	*39.348*	conv.	16
Gran Canaria (S)	A2	0.703330	0.512930						16
Gran Canaria (S)	T8	0.703200	0.512923		*19.616*	*15.616*	*39.392*	conv.	16
Gran Canaria (S)	GC35	0.703225	0.512922		*19.671*	*15.622*	*39.427*	conv.	26
Gran Canaria	750-3	0.703284	0.512927		*19.593*	*15.619*	*39.356*	conv.	27
Gran Canaria	780-2	0.703271	0.512920		*19.646*	*15.592*	*39.352*	conv.	27
Gran Canaria	783-1	0.703321	0.512924		*19.555*	*15.583*	*39.238*	conv.	27
Gran Canaria	790-1	0.703320	0.512885		*19.883*	*15.649*	*39.717*	conv.	27
Gran Canaria (S)	GCR-13								30
Gran Canaria (PS)	GC682	0.703170			*19.872*	*15.604*	*39.596*	conv.	17
Gran Canaria (PS)	I1	0.703330	0.512900						17
Gran Canaria (PS)	GC619	0.703320			*19.702*	*15.604*	*39.436*	conv.	17
Gran Canaria (PS)	GC615	0.703360			*19.582*	*15.604*	*39.336*	conv.	17
Gran Canaria (PS)	GC612	0.703330			*19.662*	*15.594*	*39.386*	conv.	17
Gran Canaria (PS)	2D	0.703360			*19.412*	*15.584*	*39.166*	conv.	17
Gran Canaria (PS)	J9	0.703310	0.512910						17
Gran Canaria (PS)	K16	0.703320	0.512900						17
La Gomera (S)	LG1	0.703106	0.512919		*19.882*	*15.637*	*39.570*	conv.	26
La Gomera (S)	LG11	0.703114	0.512912		*19.886*	*15.640*	*39.576*	conv.	26
La Gomera (S)	LG35	0.703042	0.512945		*19.575*	*15.603*	*39.240*	conv.	26
La Gomera	LG50	0.703106	0.512924		*19.740*	*15.617*	*39.437*	conv.	26
La Gomera (S)	LG53	0.703048	0.512933		*19.782*	*15.634*	*39.459*	conv.	26
La Gomera (S)	LG59	0.703180	0.512914		*19.931*	*15.651*	*39.644*	conv.	26
La Gomera (S)	LG65	0.703162	0.512906		*20.050*	*15.666*	*39.761*	conv.	26
La Gomera (S)	LG58	0.703140	0.512920		*19.824*	*15.626*	*39.505*	conv.	26
La Palma	TLP 79-1	0.703101	0.512908		19.600	15.603	39.392	DS	36
La Palma	TLP 43-1	0.703091	0.512903		19.645	15.613	39.467	DS	36
La Palma	TLP 58-1	0.703090	0.512903		19.650	15.605	39.461	DS	36
La Palma	TLP 23-1	0.703071	0.512911		19.554	15.598	39.298	DS	36
La Palma	TLP 38-1	0.703100	0.512899		19.665	15.605	39.490	DS	36
La Palma	TLP 64-1	0.703085	0.512903		19.719	15.610	39.497	DS	36
La Palma	TLP 108-1	0.703082	0.512898		19.672	15.607	39.530	DS	36
La Palma	TLP 69-1	0.703065	0.512910		19.649	15.607	39.436	DS	36
La Palma	TLP 116-1	0.703110	0.512908		19.673	15.609	39.506	DS	36
La Palma	TLP 19-2	0.703108	0.512908		19.656	15.599	39.463	DS	36
La Palma	ELP1	0.703068	0.512907	0.282941	*19.643*	*15.607*	*39.463*	conv.	32
La Palma	LP71-7L	0.703108	0.512932	0.282951	*19.619*	*15.611*	*39.420*	conv.	32
La Palma	ELP4	0.703047	0.512921	0.282958	*19.495*	*15.584*	*39.216*	conv.	32
La Palma	ELP7	0.703100	0.512906	0.282962	*19.668*	*15.599*	*39.465*	conv.	32
La Palma	LP124794	0.703087	0.512913	0.282958	*19.626*	*15.615*	*39.441*	conv.	32
La Palma	LP261925	0.703111	0.512921	0.282964	*19.681*	*15.631*	*39.543*	conv.	32
La Palma	LP30A				*19.658*	*15.651*	*39.540*	conv.	18
La Palma	LP63C				*19.502*	*15.599*	*39.317*	conv.	18

Supplementary Table 2 | *(continued)*

location	Sample	$^{87}Sr/^{86}Sr$	$^{143}Nd/^{144}Nd$	$^{176}Hf/^{177}Hf$	$^{206}Pb/^{204}Pb$	$^{207}Pb/^{204}Pb$	$^{208}Pb/^{204}Pb$	method	ref.
La Palma	LP104				*19.838*	*15.638*	*39.763*	conv.	18
La Palma	LP105				*19.858*	*15.655*	*39.814*	conv.	18
La Palma	LP106				*19.940*	*15.657*	*39.770*	conv.	18
La Palma	LP107				*20.012*	*15.675*	*39.744*	conv.	18
La Palma	LP110				*19.814*	*15.655*	*39.639*	conv.	18
La Palma	LP111				*19.227*	*15.596*	*39.007*	conv.	18
La Palma	LP113				*19.879*	*15.673*	*39.780*	conv.	18
La Palma	LP115				*19.954*	*15.673*	*39.839*	conv.	18
La Palma	LP116				*19.523*	*15.629*	*39.395*	conv.	18
La Palma	LP120				*19.838*	*15.657*	*39.679*	conv.	18
La Palma	LP129				*19.917*	*15.668*	*39.815*	conv.	18
La Palma	LP-1	0.703163	0.513018		*18.973*	*15.631*	*38.802*	conv.	20
La Palma	LP-2	0.703150	0.512925		*19.485*	*15.674*	*39.327*	conv.	20
La Palma	LP-3	0.703001	0.512937		*19.790*	*15.652*	*39.616*	conv.	20
La Palma	LP-4	0.703112	0.512949		*19.640*	*15.629*	*39.503*	conv.	20
La Palma	LP-5A	0.703072	0.512934		*19.003*	*15.635*	*39.930*	conv.	20
La Palma	LP-5B	0.703049	0.512921		*19.394*	*15.615*	*39.224*	conv.	20
La Palma	LP-6A	0.703105	0.512908		*19.330*	*15.619*	*39.168*	conv.	20
La Palma	LP-6B	0.703089	0.512903		*19.406*	*15.612*	*39.234*	conv.	20
La Palma	LP-6C	0.703079	0.512920		*19.266*	*15.612*	*39.092*	conv.	20
La Palma	LP-6D	0.703146	0.512922		*19.429*	*15.624*	*39.266*	conv.	20
La Palma	AD-7	0.703070	0.512913		*19.664*	*15.622*	*39.450*	conv.	20
La Palma	ND-1	0.703045	0.512947		*19.821*	*15.636*	*39.446*	conv.	20
La Palma	116525	0.703079	0.512880		*19.502*	*15.606*	*39.295*	conv.	25
La Palma	116526	0.703073	0.512880		*19.536*	*15.603*	*39.306*	conv.	25
La Palma	116527	0.703041	0.512865		*19.583*	*15.618*	*39.373*	conv.	25
La Palma	116528	0.703061	0.512851		*19.575*	*15.594*	*39.307*	conv.	25
La Palma	116529	0.703065	0.512863		*19.580*	*15.596*	*39.320*	conv.	25
La Palma	116530	0.703069	0.512879		*19.533*	*15.601*	*39.291*	conv.	25
La Palma	116538	0.703067	0.512894		*19.470*	*15.557*	*39.187*	conv.	25
La Palma	116531	0.703089	0.512881		*19.602*	*15.614*	*39.408*	conv.	25
La Palma	116532	0.703073	0.512884		*19.597*	*15.616*	*39.418*	conv.	25
La Palma	116533	0.703079	0.512874		*19.579*	*15.600*	*39.357*	conv.	25
La Palma	116534	0.703078	0.512886		*19.594*	*15.617*	*39.419*	conv.	25
La Palma	116535	0.703057	0.512912		*19.574*	*15.587*	*39.355*	conv.	25
La Palma	116536	0.703109	0.512875		*19.652*	*15.619*	*39.555*	conv.	25
La Palma	116545	0.703092	0.512910		*19.535*	*15.595*	*39.285*	conv.	25
La Palma	116506	0.703082	0.512888		*19.563*	*15.595*	*39.401*	conv.	25
La Palma	116507	0.703083	0.512887		*19.537*	*15.606*	*39.346*	conv.	25
La Palma	116508	0.703069	0.512890		*19.493*	*15.588*	*39.252*	conv.	25
La Palma	116512	0.703127	0.512871		*19.653*	*15.599*	*39.450*	conv.	25
La Palma	116515	0.703061	0.512895		*19.594*	*15.617*	*39.408*	conv.	25
La Palma	116516	0.703073	0.512855		*19.478*	*15.583*	*39.211*	conv.	25
La Palma	116520	0.703030	0.512872		*19.681*	*15.610*	*39.497*	conv.	25
La Palma (S)	LP25	0.703059	0.512909		*19.841*	*15.624*	*39.645*	conv.	26
La Palma	LP47	0.703031	0.512911		*19.842*	*15.619*	*39.672*	conv.	26
La Palma	LP1	0.703078	0.512913		*19.500*	*15.609*	*39.277*	conv.	26
La Palma (S)	LP48	0.703047	0.512914		*19.874*	*15.622*	*39.668*	conv.	26
La Palma (S)	LP81	0.703053	0.512902		*19.901*	*15.625*	*39.695*	conv.	26
La Palma	639-1	0.702995	0.512943		*19.217*	*15.565*	*38.946*	conv.	27
La Palma	646-1	0.702971	0.512916		*19.796*	*15.632*	*39.488*	conv.	27
La Palma	648-2	0.702975	0.512915		*19.794*	*15.635*	*39.484*	conv.	27
La Palma	657-4	0.703088	0.512875		*19.701*	*15.602*	*39.520*	conv.	27
La Palma	658-7	0.703005	0.512964		*19.232*	*15.576*	*38.982*	conv.	27
La Palma	658-8	0.703011	0.512952		*19.238*	*15.585*	*39.012*	conv.	27
La Palma	660-1A	0.703003	0.512962		*19.224*	*15.573*	*38.972*	conv.	27
La Palma	665-2	0.703139	0.512895		*19.574*	*15.611*	*39.403*	conv.	27
La Palma	666-3	0.703094	0.512897		*19.674*	*15.607*	*39.495*	conv.	27
La Palma	667-2	0.703022	0.512894		*19.586*	*15.649*	*39.414*	conv.	27
La Palma	TLP 50-2	0.703065	0.512910		*19.652*	*15.602*	*39.443*	conv.	37
La Palma	TLP 51-3								
Lanzarote	EL3	0.703144	0.512939	0.283017	*19.171*	*15.575*	*39.027*	conv.	32
Lanzarote	EL11	0.703008	0.512997	0.283036	*19.232*	*15.563*	*39.019*	conv.	32
Lanzarote	EL13	0.703126	0.512956	0.283013	*19.170*	*15.573*	*39.045*	conv.	32
Lanzarote	EL1	0.703248	0.512905	0.283032	*19.348*	*15.587*	*39.206*	conv.	32
Lanzarote	EL5	0.703040	0.512930	0.283010	*19.196*	*15.569*	*39.002*	conv.	32
Lanzarote	EL8	0.703042	0.512931	0.283026	*19.233*	*15.567*	*39.078*	conv.	32
Lanzarote	EL10	0.703030	0.513006	0.283056	*19.235*	*15.560*	*38.992*	conv.	32
Lanzarote	EL17	0.703226	0.512896	0.282985	*19.361*	*15.586*	*39.210*	conv.	32
Lanzarote	ND7	0.703198	0.512944		*19.379*	*15.675*	*39.566*	conv.	20

Supplementary Table 2 | *(continued)*

location	Sample	$^{87}Sr/^{86}Sr$	$^{143}Nd/^{144}Nd$	$^{176}Hf/^{177}Hf$	$^{206}Pb/^{204}Pb$	$^{207}Pb/^{204}Pb$	$^{208}Pb/^{204}Pb$	method	ref.
Lanzarote	L6	0.703259	0.512951		*19.495*	*15.633*	*39.304*	conv.	20
Lanzarote	L5	0.703138	0.512944		*19.508*	*15.607*	*38.967*	conv.	20
Lanzarote	A560	0.703212	0.512963		*19.328*	*15.606*	*39.287*	conv.	20
Lanzarote	L-89-3	0.703230	0.512901		*19.066*	*15.626*	*39.008*	conv.	20
Lanzarote	L-1(1)	0.703199	0.512906		*19.133*	*15.619*	*39.082*	conv.	20
Lanzarote	L-1(2)	0.703213	0.512915		*19.122*	*15.616*	*39.058*	conv.	20
Lanzarote	L-1(2)	0.703156	0.513006		*19.234*	*15.632*	*39.230*	conv.	20
Lanzarote	L-5^	0.703136							20
Lanzarote	L-92-2	0.703107	0.512991		*19.088*	*15.589*	*38.993*	conv.	20
Lanzarote	L-92-3	0.703232	0.512960		*19.334*	*15.601*	*39.209*	conv.	20
Lanzarote	L-92-4	0.703202	0.513037		*19.171*	*15.639*	*39.181*	conv.	20
Lanzarote	EN-4B	0.703188	0.512791		*19.155*	*15.626*	*39.101*	conv.	20
Lanzarote	LAN16	0.703240	0.512363		*19.292*	*15.537*	*39.059*	conv.	22
Lanzarote	LAN11	0.703200	0.512473		*19.152*	*15.549*	*38.912*	conv.	22
Lanzarote	LAN2	0.703230	0.512743		*19.047*	*15.538*	*38.814*	conv.	22
Lanzarote	LAN12	0.703290	0.512783		*19.087*	*15.538*	*38.843*	conv.	22
Lanzarote	LAN7	0.703180	0.512803		*19.147*	*15.526*	*38.886*	conv.	22
Lanzarote	LAN1	0.703240	0.512823		*19.065*	*15.559*	*38.837*	conv.	22
Lanzarote	LAN13	0.703280	0.512833		*19.266*	*15.521*	*38.967*	conv.	22
Lanzarote	LAN4	0.703200	0.512833		*19.007*	*15.502*	*38.692*	conv.	22
Lanzarote	LAN10	0.703220	0.512833		*19.135*	*15.541*	*38.893*	conv.	22
Lanzarote	LAN15	0.703220	0.512833		*19.264*	*15.517*	*38.993*	conv.	22
Lanzarote	LAN6	0.703190	0.512843		*19.201*	*15.537*	*38.970*	conv.	22
Lanzarote	LAN3	0.703200	0.512853		*18.997*	*15.512*	*38.709*	conv.	22
Lanzarote	LAN14	0.703340	0.512853		*19.274*	*15.517*	*38.993*	conv.	22
Lanzarote	LAN5	0.703190	0.512863		*19.109*	*15.518*	*38.817*	conv.	22
Lanzarote	LAN9	0.703080	0.512863		*19.084*	*15.509*	*38.787*	conv.	22
Lanzarote	LAN8	0.703110	0.512883		*19.100*	*15.507*	*38.793*	conv.	22
Lanzarote	LAN17	0.703220			*19.092*	*15.543*	*38.849*	conv.	22
Lanzarote	L1-28-2	0.703240							22
Lanzarote	L1-28-3	0.703240							22
Lanzarote	11596	0.703029	0.512911						29
Lanzarote	11597	0.703126	0.512927						29
Lanzarote	15598	0.703090	0.512901						29
Lanzarote	11599	0.703086	0.512855						29
Lanzarote	11591	0.703373	0.512924						29
Lanzarote	11590	0.703392	0.512894						29
Lanzarote	11600	0.703225	0.512867						29
Lanzarote	11601	0.703209	0.512900						29
Lanzarote	11589	0.702808	0.512906						29
Tenerife	205-1	0.703050	0.512906		19.741	15.611	39.557	black.	33
Tenerife	205-2	0.703050	0.512877		19.739	15.615	39.564	black.	33
Tenerife	205-3	0.703042	0.512887		19.734	15.620	39.569	black.	33
Tenerife	E 206A	0.703046	0.512909		19.763	15.618	39.582	black.	33
Tenerife	E 206B	0.703069	0.512881		19.752	15.610	39.557	black.	33
Tenerife	E 206D	0.703042	0.512885		19.758	15.616	39.575	black.	33
Tenerife	E 204F	0.703049	0.512885		19.765	15.613	39.567	black.	33
Tenerife	NER-12	0.703082	0.512864		19.706	15.611	39.581	black.	34
Tenerife	NER-22	0.703085	0.512904		19.774	15.616	39.677	black.	34
Tenerife	NER-29	0.703076	0.512976		19.714	15.619	39.601	black.	34
Tenerife	NER-37W	0.703115	0.512902		19.802	15.618	39.665	black.	34
Tenerife	NER-37A	0.703081	0.512886		19.810	15.625	39.694	black.	34
Tenerife	NER-40	0.703100	0.512856		19.779	15.619	39.665	black.	34
Tenerife	NER-47	0.703118	0.512938						34
Tenerife	NER-57B	0.703126	0.512901		19.833	15.622	39.714	black.	34
Tenerife	NER-61	0.703088	0.512825		19.838	15.625	39.727	black.	34
Tenerife	NER-65	0.703090	0.512907						34
Tenerife	NER-66	0.703066	0.512812		19.796	15.624	39.701	black.	34
Tenerife	NER-70A	0.703080	0.512957		19.779	15.619	39.668	black.	34
Tenerife	NER-77	0.703141	0.512968		19.656	15.624	39.590	black.	34
Tenerife	NER-81	0.703067	0.512818		19.704	15.603	39.582	black.	34
Tenerife	G2-D11	0.703073	0.512882		19.680	15.610	39.564	black.	34
Tenerife	G2-D19	0.703070	0.512914		19.591	15.603	39.417	black.	34
Tenerife	G2-D20	0.703194	0.512903		19.669	15.636	39.587	black.	34
Tenerife	LO-25	0.703068	0.512880		19.779	15.619	39.629	black.	34
Tenerife	LC-7	0.703150	0.512908		19.740	15.616	39.609	black.	34
Tenerife	TF 1577	0.703056	0.512913	0.282961	*19.738*	*15.626*	*39.566*	conv.	32
Tenerife	ET2	0.703028	0.512911	0.282962	*19.726*	*15.608*	*39.518*	conv.	32
Tenerife	ET6	0.703093	0.512917	0.282961	*19.721*	*15.610*	*39.504*	conv.	32
Tenerife	ET8	0.703139	0.512895	0.282964	*19.747*	*15.610*	*39.519*	conv.	32

Supplementary Table 2 | *(continued)*

location	Sample	$^{87}Sr/^{86}Sr$	$^{143}Nd/^{144}Nd$	$^{176}Hf/^{177}Hf$	$^{206}Pb/^{204}Pb$	$^{207}Pb/^{204}Pb$	$^{208}Pb/^{204}Pb$	method	ref.
Tenerife	ND4	0.703068	0.512902		*19.720*	*15.655*	*39.551*	conv.	20
Tenerife	AD9	0.703110	0.512947		*19.570*	*15.615*	*39.351*	conv.	20
Tenerife	ND3	0.703116	0.512931		*19.693*	*15.633*	*39.546*	conv.	20
Tenerife	ND-5	0.703122	0.512932		*19.779*	*15.626*	*39.623*	conv.	20
Tenerife	ND-7	0.703124	0.512920		*19.656*	*15.622*	*39.485*	conv.	20
Tenerife	S-9	0.703169	0.512914		*19.463*	*15.614*	*39.294*	conv.	20
Tenerife	T-89	0.703259	0.512874		*18.997*	*15.561*	*38.961*	conv.	20
Tenerife	T-3-3	0.703141	0.512802		*19.848*	*15.660*	*39.809*	conv.	20
Tenerife	TF70	0.702856	0.512933		*19.907*	*15.631*	*39.607*	conv.	23
Tenerife	TF102-1	0.702923	0.512892		*20.087*	*15.640*	*39.562*	conv.	23
Tenerife	TF93	0.702924	0.512925		*20.001*	*15.627*	*39.655*	conv.	23
Tenerife	TF80	0.702933	0.512853		*19.739*	*15.599*	*39.563*	conv.	23
Tenerife	TF88	0.702967	0.512967		*20.023*	*15.625*	*39.773*	conv.	23
Tenerife	TF61	0.702974	0.512877						23
Tenerife	TF1	0.702977	0.512906		*19.890*	*15.599*	*39.505*	conv.	23
Tenerife	TF68	0.702982	0.512906		*19.951*	*15.630*	*39.632*	conv.	23
Tenerife	TF78	0.702985	0.512872		*19.761*	*15.583*	*39.486*	conv.	23
Tenerife	TF55	0.702989	0.512871						23
Tenerife	TF120	0.702992	0.512854		*19.668*	*15.593*	*39.498*	conv.	23
Tenerife	TF118	0.702993	0.512813						23
Tenerife	TF66	0.702994	0.512963		*19.817*	*15.627*	*39.567*	conv.	23
Tenerife	TF121	0.703012	0.512895		*19.655*	*15.592*	*39.457*	conv.	23
Tenerife	TF94	0.703019	0.512903		*19.898*	*15.614*	*39.530*	conv.	23
Tenerife	TF77	0.703020	0.512864		*19.733*	*15.622*	*39.546*	conv.	23
Tenerife	TF41-2	0.703023	0.512880		*19.716*	*15.585*	*39.458*	conv.	23
Tenerife	TF23-2	0.703025	0.512886						23
Tenerife	TF65	0.703028			*19.325*	*15.602*	*39.052*	conv.	23
Tenerife	TF86	0.703031	0.512897		*19.928*	*15.619*	*39.714*	conv.	23
Tenerife	TF65	0.703035	0.512857		*19.331*	*15.605*	*39.067*	conv.	23
Tenerife	TF100	0.703036	0.512896		*19.755*	*15.596*	*39.528*	conv.	23
Tenerife	TF59-2	0.703037	0.512863		*19.655*	*15.607*	*39.478*	conv.	23
Tenerife	TF33-1	0.703037	0.512866		*19.766*	*15.633*	*39.645*	conv.	23
Tenerife	TF53-1	0.703040	0.512866						23
Tenerife	TF24	0.703043	0.512876		*19.691*	*15.590*	*39.413*	conv.	23
Tenerife	TF27-1	0.703050	0.512873						23
Tenerife	TF75-3	0.703053	0.512872						23
Tenerife	TF117	0.703055	0.512881						23
Tenerife	TF23-1	0.703060	0.512838						23
Tenerife	TF20	0.703061	0.512858		*19.795*	*15.597*	*39.512*	conv.	23
Tenerife	TF101	0.703065	0.512915		*19.782*	*15.608*	*39.560*	conv.	23
Tenerife	TF72-1	0.703068	0.512872						23
Tenerife	TF21-1	0.703072	0.512870						23
Tenerife	TF57	0.703074	0.512848						23
Tenerife	TF59-1	0.703081	0.512874		*19.787*	*15.617*	*39.594*	conv.	23
Tenerife	TF74	0.703093	0.512880		*19.750*	*15.612*	*39.514*	conv.	23
Tenerife	TF-73-1	0.703097	0.512905						23
Tenerife	TF116	0.703098	0.512875		*19.480*	*15.521*	*39.337*	conv.	23
Tenerife	TF38-1	0.703103	0.512869						23
Tenerife	TF45	0.703105	0.512885						23
Tenerife	TF54	0.703107	0.512884						23
Tenerife	TF50	0.703108	0.512892						23
Tenerife	TF82	0.703110	0.512868		*19.749*	*15.593*	*39.553*	conv.	23
Tenerife	TF98	0.703115	0.512863		*19.701*	*15.589*	*39.496*	conv.	23
Tenerife	TF102-2	0.703120	0.512892		*19.770*	*15.626*	*39.485*	conv.	23
Tenerife	TF87	0.703151	0.512850		*19.601*	*15.648*	*39.431*	conv.	23
Tenerife	TF-114	0.703151	0.512807		*19.457*	*15.578*	*39.482*	conv.	23
Tenerife	TF111	0.703175	0.512849		*19.581*	*15.574*	*39.507*	conv.	23
Tenerife	TF3C-1	0.703188	0.512838		*19.587*	*15.577*	*39.494*	conv.	23
Tenerife	TF109	0.703190	0.512772		*19.564*	*15.590*	*39.540*	conv.	23
Tenerife	TF4	0.703216	0.512829		*19.747*	*15.598*	*39.709*	conv.	23
Tenerife	TF71	0.703218	0.512887		*19.728*	*15.594*	*39.484*	conv.	23
Tenerife	TF115	0.703231	0.512854		*19.536*	*15.560*	*39.444*	conv.	23
Tenerife	TF123	0.703255	0.512860		*19.669*	*15.576*	*39.415*	conv.	23
Tenerife	TF87				*19.607*	*15.644*	*39.422*	conv.	23
Tenerife	TF109				*19.579*	*15.600*	*39.569*	conv.	23
Tenerife	TF7	0.702957	0.512940		*19.880*	*15.631*	*39.592*	conv.	26
Tenerife	TF9	0.703025	0.512923		*19.737*	*15.627*	*39.448*	conv.	26
Tenerife	TF51	0.703079	0.512935		*20.277*	*15.659*	*39.830*	conv.	26
Tenerife	TF51				*20.273*	*15.661*	*39.837*	conv.	26
Tenerife	TF4	0.702989	0.512932		*19.938*	*15.629*	*39.665*	conv.	26

Supplementary Table 2 | *(continued)*

location	Sample	$^{87}Sr/^{86}Sr$	$^{143}Nd/^{144}Nd$	$^{176}Hf/^{177}Hf$	$^{206}Pb/^{204}Pb$	$^{207}Pb/^{204}Pb$	$^{208}Pb/^{204}Pb$	method	ref.
Tenerife (S)	TF23	0.703057	0.512920		*19.658*	*15.615*	*39.313*	conv.	26
Tenerife (S)	TF64	0.702995	0.512905		*19.719*	*15.624*	*39.461*	conv.	26
Tenerife (S)	TF16	0.702979	0.512940		*19.899*	*15.638*	*39.553*	conv.	26
Tenerife (S)	731-1	0.703003	0.512915		*19.972*	*15.634*	*39.744*	conv.	27
Tenerife (S)	733-1	0.703105	0.512883		*19.717*	*15.609*	*39.556*	conv.	27
Tenerife (S)	773-1	0.703228	0.512821		*19.581*	*15.593*	*39.577*	conv.	27
Tenerife (S)	776-1	0.703242	0.512807		*19.514*	*15.529*	*39.549*	conv.	27
Selvagen, Grande	J-49	0.703062	0.512926		19.378	15.577	39.218	conv.	24
Selvagen, Grande	J-30	0.703138	0.512922	0.283025	19.367	15.571	39.177	conv.	24,32
Selvagen, Grande	J-8A	0.703026	0.512924		19.407	15.575	39.205	conv.	24
Selvagen, Grande	J-36	0.703140	0.512922		19.391	15.588	39.257	conv.	24
Selvagen, Grande	J-42	0.703154	0.512920		19.342	15.575	39.164	conv.	24
Selvagen, Grande	SG10	0.703027	0.512930	0.283027	19.403	15.574	39.200	conv.	24,32
Selvagen, Grande	J-45	0.703091	0.512928		19.367	15.574	39.200	conv.	24
Selvagen, Grande	J-35G	0.703060	0.512928	0.283041	19.916	15.625	40.133	conv.	24,32
Selvagen, Grande	J-9	0.703649	0.512927		19.724	15.618	39.651	conv.	24
Selvagen, Grande	J-32	0.703137	0.512918		19.911	15.614	39.814	conv.	24
Selvagen, Grande	J-41A	0.703277	0.512938	0.283042	19.658	15.609	39.498	conv.	24,32
Selvagen, Pequena	SP-1	0.703087	0.512922		19.730	15.628	39.585	conv.	24
Selvagen, Pequena	J-51	0.703103	0.512927		19.812	15.608	39.584	conv.	24
Selvagen, Pequena	J-56	0.703238	0.512904	0.283031	19.714	15.619	39.528	conv.	24,32
Selvagen, Pequena	J-58	0.703110	0.512919		19.630	15.596	39.424	conv.	24
Selvagen, Pequena	SP-2	0.703174	0.512922		19.764	15.622	39.602	conv.	24
Altas Mountains & Maghrebides									
Middle Atlas	MA401	0.703220	0.512844	0.282996	19.634	15.631	39.367	conv.	42
Middle Atlas	MA414	0.703202	0.512897	0.282980	19.822	15.624	39.428	conv.	42
Middle Atlas	MA427	0.703213	0.512847	0.282950	19.973	15.629	39.772	conv.	42
Middle Atlas	MA514	0.703161	0.512876		19.420	15.642	39.270	conv.	42
Middle Atlas	MA522	0.703207	0.512883	0.282984	19.576	15.629	39.288	conv.	42
Middle Atlas	MA524	0.703150	0.512925	0.282981	19.684	15.629	39.401	conv.	42
Middle Atlas	MA531	0.703234	0.512859	0.282921	20.279	15.650	39.900	conv.	42
Middle Atlas	KH36	0.703452	0.512791	0.282943	19.700	15.633	39.535	conv.	42
Middle Atlas	AZ21	0.703191	0.512859		19.843	15.627	39.494	conv.	42
Middle Atlas	AZ25	0.703152	0.512869	0.282986	19.582	15.624	39.302	conv.	42
Middle Atlas	MA406	0.703232	0.512855	0.283032	19.525	15.627	39.325	conv.	42
Middle Atlas	MA407	0.703196	0.512860	0.282990	19.558	15.609	39.316	conv.	42
Middle Atlas	MA421	0.703476	0.512855		19.261	15.641	39.275	conv.	42
Middle Atlas	MA516	0.703335	0.512843		19.914	15.638	39.599	conv.	42
Middle Atlas	MA528	0.703439	0.512821	0.282952	19.285	15.641	39.246	conv.	42
Middle Atlas	KH33	0.703208	0.512840	0.282991	19.485	15.624	39.300	conv.	42
Middle Atlas	KH41	0.703651	0.512756	0.282827	20.276	15.680	40.065	conv.	42
Middle Atlas	MA405	0.703563	0.512806	0.282960	19.118	15.641	39.107	conv.	42
Middle Atlas	MA405		0.512799	0.282974					42
Middle Atlas	MA409	0.703368	0.512866	0.282954	19.491	15.648	39.340	conv.	42
Middle Atlas	MA412	0.703817	0.512816		19.230	15.666	39.205	conv.	42
Middle Atlas	MA426	0.703595	0.512899		19.230	15.639	39.371	conv.	42
Middle Atlas	MA502	0.703232	0.512893	0.282980	19.463	15.636	39.264	conv.	42
Middle Atlas	MA505	0.703693	0.512808	0.282964	19.416	15.648	39.078	conv.	42
Middle Atlas	MA520	0.703613	0.512812	0.282966	19.404	15.667	39.219	conv.	42
Middle Atlas	AZ31	0.703640	0.512811	0.282936	19.143	15.643	39.172	conv.	42
Middle Atlas	MA506	0.704119	0.512767	0.282931	19.397	15.663	38.984	conv.	42
Middle Atlas	KH33	0.703224	0.512846		19.470	15.611	39.283	conv.	42
Middle Atlas	KH41	0.703669	0.512727		20.271	15.678	40.057	conv.	42
Middle Atlas	TZ1	0.703170	0.512882						39
Middle Atlas	AZ25	0.703170	0.512878						39
Middle Atlas	AZ31	0.703670	0.512811						39
Middle Atlas	AZ21	0.703240	0.512869						39
Middle Atlas	KH41	0.703740	0.512757						39
Middle Atlas	CH31	0.703393	0.512784						40
Middle Atlas	AT 7 HOST	0.703220	0.512920						41
High Atlas	TAF 7	0.703277	0.512862						43
High Atlas	FN 4	0.703060	0.512884		19.567	15.634	39.187	conv.	43
High Atlas	TL 6	0.703270	0.512821		19.534	15.613	39.312	conv.	43
High Atlas	FS 5	0.703199	0.512836		19.421	15.624	39.121	conv.	43
High Atlas	TAB 3	0.703353	0.512883						43
Maghrebides	74-252	0.706270	0.512517						39
Maghrebides	74-270	0.703590	0.512847						39
Maghrebides	74-123	0.703050	0.512905						39
Maghrebides	GZ040400-4	0.704130	0.512852		18.939	15.642	39.041	conv.	38

Supplementary Table 2 | *(continued)*

location	Sample	$^{87}Sr/^{86}Sr$	$^{143}Nd/^{144}Nd$	$^{176}Hf/^{177}Hf$	$^{206}Pb/^{204}Pb$	$^{207}Pb/^{204}Pb$	$^{208}Pb/^{204}Pb$	method	ref.
Maghrebides	GZ280300-3B	0.704926	0.512766		18.844	15.642	38.998	conv.	38
Maghrebides	GZ280300-4	0.704925	0.512778		18.831	15.639	38.977	conv.	38
Maghrebides	GZ280300-1	0.704739			18.997	15.627	38.997	conv.	38
Maghrebides	GZ160699-5	0.703263	0.513036		19.361	15.612	39.116	conv.	38
Maghrebides	GZ040400-8	0.702921	0.513047		19.324	15.587	38.972	conv.	38
Maghrebides	GZ170699-4	0.703153	0.512842		18.910	15.608	38.933	conv.	38
Maghrebides	GZ160699-1	0.703561	0.512851		19.114	15.612	38.941	conv.	38
Maghrebides	GZ180699-4	0.703362	0.512975		19.321	15.627	39.117	conv.	38
Maghrebides	GZ150699-1	0.703849	0.512891		19.112	15.634	39.039	conv.	38
Maghrebides	GZ180699-5	0.703554	0.512813						38
Maghrebides	AF 1	0.710186	0.512247		18.776	15.655	38.913	conv.	38
Maghrebides	OD260599-10	0.703583	0.512889		20.320	15.677	40.080	conv.	38
Maghrebides	OD260599-12	0.703608	0.512890		20.299	15.679	40.070	conv.	38
Maghrebides	OD260599-1	0.703732	0.512749		19.940	15.654	39.734	conv.	38
Maghrebides	OD300599-4	0.703832	0.512915		20.023	15.661	39.806	conv.	38
Maghrebides	OD260599-13	0.703848	0.512911		19.985	15.655	39.791	conv.	38
Maghrebides	OD190699-1A	0.703880	0.512918		20.032	15.660	39.839	conv.	38
Maghrebides	OD020699-2B	0.000000	0.512890		20.113	15.671	39.936	conv.	38
Maghrebides	OD020699-1B	0.704221	0.512890		19.346	15.650	39.371	conv.	38
Maghrebides	PR020400-1B	0.703093	0.513010		19.344	15.565	39.083	conv.	38
Maghrebides	PR020400-4A	0.703023	0.513017		20.786	15.669	40.332	conv.	38
Maghrebides	PR020400-5	0.703047	0.512984		20.632	15.656	40.462	conv.	38
Maghrebides	GZ160699-1	0.703566	0.512978						38
Maghrebides	OD190699-1A				20.028	15.657	39.830	conv.	38
Cape Verde Islands									
Sao Antao	NA51	0.703168	0.512859		*19.653*	*15.627*	*39.287*	conv.	44
Sao Antao	N17	0.703649	0.512741		*19.015*	*15.567*	*38.865*	conv.	44
Sao Antao	NA2	0.703096	0.512863		*19.717*	*15.630*	*39.340*	conv.	45
Sao Antao	NA15	0.702919	0.513035		*19.608*	*15.627*	*39.198*	conv.	45
Sao Antao	NA48	0.703192	0.512904		*19.671*	*15.623*	*39.326*	conv.	45
Sao Antao	NA60	0.703020	0.512958		*19.685*	*15.625*	*39.289*	conv.	45
Sao Antao	NA63	0.703086	0.512891		*19.734*	*15.628*	*39.341*	conv.	45
Sao Antao	NA69	0.703050	0.512999		*19.672*	*15.615*	*39.262*	conv.	45
Sao Antao	NA73	0.703157	0.512906		*19.769*	*15.627*	*39.451*	conv.	45
Sao Antao	NA79	0.703105	0.512964		*19.611*	*15.619*	*39.191*	conv.	45
Sao Antao	NA80	0.702943	0.513002		*19.277*	*15.591*	*38.908*	conv.	45
Sao Antao	SA-110062				*19.598*	*15.621*	*39.158*	conv.	46
Sao Antao	SA-111822				*19.578*	*15.611*	*39.298*	conv.	46
Sao Antao	SA-111827				*19.458*	*15.631*	*39.058*	conv.	46
Sao Antao	SA-111832				*19.178*	*15.561*	*39.188*	conv.	46
Sao Antao	SA-111837				*19.608*	*15.621*	*38.848*	conv.	46
Sao Antao	SA-111940				*19.638*	*15.631*	*39.248*	conv.	46
Sao Antao	111827	0.703050			*19.457*	*15.632*	*39.056*	conv.	50
Sao Antao	114528	0.703229			*19.710*	*15.649*	*39.568*	conv.	50
Sao Antao	114533	0.703253	0.512870		*19.681*	*15.609*	*39.436*	conv.	50
Sao Antao	111743	0.703332	0.512882		*19.892*	*15.610*	*39.676*	conv.	50
Sao Antao	109901	0.703037	0.512944		*19.935*	*15.616*	*39.366*	conv.	50
Sao Antao	109994	0.703127	0.512900		*19.702*	*15.608*	*39.342*	conv.	50
Sao Antao	109995	0.703138	0.512879		*19.547*	*15.591*	*39.175*	conv.	50
Sao Antao	109997	0.703074			*19.879*	*15.618*	*39.316*	conv.	50
Sao Antao	110062	0.702959	0.512946		*19.618*	*15.622*	*39.180*	conv.	50
Sao Antao	114816	0.703046			*19.368*	*15.647*	*39.007*	conv.	50
Sao Antao	109502	0.703105	0.512908		*19.552*	*15.586*	*39.173*	conv.	50
Sao Antao	109557	0.703080	0.512949		*19.513*	*15.590*	*39.079*	conv.	50
Sao Antao	110033	0.703123	0.512912		*19.686*	*15.647*	*39.316*	conv.	50
Sao Antao	111768	0.703252	0.512932		*19.544*	*15.604*	*39.114*	conv.	50
Sao Antao	111840	0.703036	0.512934		*19.756*	*15.624*	*39.329*	conv.	50
Sao Antao	109556	0.703147	0.512918		*19.633*	*15.610*	*39.164*	conv.	50
Sao Antao	109508	0.703115	0.512936		*19.612*	*15.601*	*39.227*	conv.	50
Sao Antao	109563	0.702988	0.512934		*19.538*	*15.606*	*39.117*	conv.	50
Sao Antao	109545	0.702985	0.512909		*19.544*	*15.597*	*39.110*	conv.	50
Sao Antao	109546	0.703073	0.512917		*19.697*	*15.602*	*39.272*	conv.	50
Sao Antao	114811	0.703023			*19.694*	*15.605*	*39.233*	conv.	50
Sao Antao	111767	0.702972	0.512968		*19.394*	*15.593*	*39.092*	conv.	50
Sao Antao	109551	0.703055	0.512943		*19.765*	*15.600*	*39.238*	conv.	50
Sao Antao	106459	0.703008	0.512683		*19.497*	*15.595*	*39.079*	conv.	50
Sao Antao	109568	0.703024						conv.	50
Sao Antao	111813	0.703237	0.512913		*19.900*	*15.639*	*39.325*	conv.	50
Sao Antao	111718	0.703162	0.512911		*19.739*	*15.642*	*39.340*	conv.	50

Supplementary Table 2 | *(continued)*

location	Sample	$^{87}Sr/^{86}Sr$	$^{143}Nd/^{144}Nd$	$^{176}Hf/^{177}Hf$	$^{206}Pb/^{204}Pb$	$^{207}Pb/^{204}Pb$	$^{208}Pb/^{204}Pb$	method	ref.
Sao Antao	106452	0.703085	0.512952					conv.	50
Sao Antao	111712	0.703002	0.512985		*19.713*	*15.617*	*39.212*	conv.	50
Sao Antao	111709	0.703020	0.512947		*19.719*	*15.625*	*39.220*	conv.	50
Sao Antao	111725	0.703005	0.512933		*19.505*	*15.602*	*39.080*	conv.	50
Sao Antao	111705	0.703040	0.512967		*19.696*	*15.616*	*39.214*	conv.	50
Sao Antao	111713	0.703003	0.512949		*19.578*	*15.604*	*39.094*	conv.	50
Sao Antao	111832	0.703164	0.512905		*19.181*	*15.559*	*38.848*	conv.	50
Sao Antao	114522				*19.767*	*15.630*	*39.441*	conv.	50
Sao Antao	114521	0.703119	0.512903		*19.782*	*15.635*	*39.475*	conv.	50
Sao Antao	111828	0.703116	0.512901		*19.754*	*15.616*	*39.378*	conv.	50
Sao Antao	110049	0.703121	0.512927		*19.696*	*15.624*	*39.253*	conv.	50
Sao Antao	110041	0.703093	0.512919		*19.173*	*15.611*	*38.816*	conv.	50
Sao Antao	111832	0.703174						conv.	50
Sao Antao	106454	0.703275	0.512895		*19.819*	*15.633*	*39.588*	conv.	50
Sao Antao	111753	0.703267	0.512856		*19.660*	*15.606*	*39.394*	conv.	50
Sao Antao	109965	0.703318	0.512818		*19.598*	*15.596*	*39.335*	conv.	50
Sao Antao	109564				*19.552*	*15.594*	*39.253*	conv.	50
Sao Antao	111750	0.703262	0.512898		*19.696*	*15.605*	*39.466*	conv.	50
Sao Antao	111757	0.703207	0.512890		*19.700*	*15.609*	*39.430*	conv.	50
Sao Antao	111822	0.703276	0.512861		*19.574*	*15.611*	*39.300*	conv.	50
Sao Antao	111762				*19.797*	*15.610*	*39.533*	conv.	50
Sao Antao	111756	0.703168	0.512901		*19.574*	*15.594*	*39.303*	conv.	50
Sao Antao	111748	0.703259	0.512869		*19.850*	*15.617*	*39.623*	conv.	50
Sao Antao	111751	0.703277	0.512862		*19.826*	*15.612*	*39.583*	conv.	50
Sao Antao	114531	0.703243	0.512867		*19.459*	*15.627*	*39.170*	conv.	50
Sao Antao	111745				*19.842*	*15.608*	*39.597*	conv.	50
Sao Antao	109521	0.703178			*19.576*	*15.586*	*39.248*	conv.	50
Sao Antao	109957	0.703200						conv.	50
Sao Antao	109527	0.703213	0.512923		*19.569*	*15.608*	*39.261*	conv.	50
Sao Antao	109962	0.703045	0.512894		*19.683*	*15.603*	*39.409*	conv.	50
Sao Antao	106453	0.703174	0.512920		*19.666*	*15.584*	*39.264*	conv.	50
Sao Antao	109952	0.703184	0.512884		*19.784*	*15.597*	*39.444*	conv.	50
Sao Antao	109558	0.703024						conv.	50
Sao Antao	110028	0.703046	0.512899		*19.591*	*15.630*	*39.216*	conv.	50
Sao Antao	111721	0.703020	0.512916		*19.618*	*15.642*	*39.260*	conv.	50
Sao Antao	111737	0.703060	0.512892		*19.615*	*15.629*	*39.218*	conv.	50
Sao Antao	111717	0.703104	0.512948		*19.633*	*15.634*	*39.222*	conv.	50
Sao Antao	111701	0.703100	0.512918		*19.671*	*15.647*	*39.304*	conv.	50
Sao Antao	110021	0.703044	0.512912		*19.330*	*15.607*	*38.923*	conv.	50
Sao Antao	111837				*19.699*	*15.631*	*39.321*	conv.	50
Sao Antao	111764	0.703127	0.512921		*19.781*	*15.614*	*39.384*	conv.	50
Sao Antao	111763	0.703108	0.512916		*19.771*	*15.622*	*39.407*	conv.	50
Sao Antao	106456				*19.421*	*15.604*	*39.016*	conv.	50
Sao Antao	111759	0.703059	0.512911		*19.697*	*15.609*	*39.281*	conv.	50
Sao Antao	106455	0.703226	0.512929		*19.447*	*15.616*	*39.040*	conv.	50
Sao Antao	110029	0.703088	0.512903		*19.598*	*15.628*	*39.214*	conv.	50
Sao Antao	110026	0.703111	0.512915		*19.640*	*15.655*	*39.319*	conv.	50
Sao Antao	110030	0.703081	0.512915		*19.623*	*15.643*	*39.257*	conv.	50
Sao Antao	110052	0.703068	0.512881		*19.661*	*15.632*	*39.271*	conv.	50
Sao Antao	106457	0.703095	0.512904		*19.642*	*15.627*	*39.248*	conv.	50
Sao Antao	111940				*19.638*	*15.631*	*39.248*	conv.	50
Sao Vicente	NV6	0.703205	0.512974		*19.145*	*15.575*	*38.756*	conv.	45
Sao Vicente	SV-01	0.703202			19.641	15.598	39.367	Ti, conv.	48
Sao Vicente	SV-02	0.703212			19.275	15.623	39.001	Ti, conv.	48
Sao Vicente	SV-03	0.703151			19.189	15.575	38.769	Ti, conv.	48
Sao Vicente	SV-05	0.703246			19.694	15.614	39.276	Ti, conv.	48
Sao Vicente	SV-09				19.678	15.622	39.343	Ti, conv.	48
Sao Vicente	SV-10	0.703105			19.359	15.582	38.970	Ti, conv.	48
Sao Vicente	SV-12	0.703269			19.679	15.612	39.407	Ti, conv.	48
Sao Vicente	SV-178								55
Sao Vicente	CV-98-SV-01								58
Sao Vicente	CV-98-SV-12								58
Sao Vicente	115-097	0.703140	0.512920		*19.963*	*15.612*	*39.670*	conv.	47
Sao Vicente	115-098	0.703090	0.512960		*19.486*	*15.569*	*39.030*	conv.	47
Sao Vicente	115-100				*19.611*	*15.572*	*39.219*	conv.	47
Sao Vicente	115-107	0.703180	0.512910		*19.752*	*15.583*	*39.241*	conv.	47
Sao Vicente	115-109	0.703160	0.512900		*20.019*	*15.631*	*39.583*	conv.	47
Sao Vicente	115-110				*19.869*	*15.572*	*39.414*	conv.	47
Sao Vicente	115-113	0.703130	0.512930		*19.479*	*15.564*	*39.049*	conv.	47
Sao Vicente	115-051				*19.833*	*15.584*	*39.496*	conv.	47

Supplementary Table 2 | *(continued)*

location	Sample	$^{87}Sr/^{86}Sr$	$^{143}Nd/^{144}Nd$	$^{176}Hf/^{177}Hf$	$^{206}Pb/^{204}Pb$	$^{207}Pb/^{204}Pb$	$^{208}Pb/^{204}Pb$	method	ref.
Sao Vicente	115-073				*19.741*	*15.593*	*39.449*	conv.	47
Sao Vicente	115-074	0.703230	0.512930		*19.482*	*15.574*	*39.126*	conv.	47
Sao Vicente	115-077	0.703200	0.512850		*19.788*	*15.600*	*39.487*	conv.	47
Sao Vicente	115-079	0.703190	0.512860		*19.754*	*15.596*	*39.484*	conv.	47
Sao Vicente	115-080	0.703190	0.512870		*19.739*	*15.592*	*39.444*	conv.	47
Sao Vicente	115-093				*19.729*	*15.576*	*39.415*	conv.	47
Sao Vicente	115-094				*19.723*	*15.587*	*39.409*	conv.	47
Sao Vicente	115-103				*19.412*	*15.564*	*38.879*	conv.	47
Sao Vicente	115-104		0.512970		*19.412*	*15.572*	*38.793*	conv.	47
Sao Vicente	115-117				*19.152*	*15.552*	*38.700*	conv.	47
Sao Nicolao	SN-02	0.702980			19.528	15.607	38.990	Ti, conv.	48
Sao Nicolao	SN-03	0.703346			19.408	15.574	38.952	Ti, conv.	48
Sao Nicolao	SN-05	0.703057			19.491	15.577	38.959	Ti, conv.	48
Sao Nicolao	SN-10	0.703040			19.540	15.590	38.970	Ti, conv.	48
Sao Nicolao	SN-11	0.703120			19.466	15.584	38.967	Ti, conv.	48
Sao Nicolao	SN-18	0.703212			19.448	15.584	38.945	Ti, conv.	48
Sao Nicolao	SN01	0.702964	0.512998		19.516	15.610	39.013	Tl	51
Sao Nicolao	SN02	0.702971	0.512987		19.516	15.605	39.001	Tl	51
Sao Nicolao	SN03	0.702975	0.512992		19.407	15.571	38.949	Tl	51
Sao Nicolao	SN04	0.703006	0.512979		19.535	15.606	39.061	Tl	51
Sao Nicolao	SN05	0.703019	0.512968		19.490	15.574	38.956	Tl	51
Sao Nicolao	SN06	0.703026	0.512954		19.452	15.612	39.027	Tl	51
Sao Nicolao	SN07	0.703031	0.512977		19.668	15.616	39.167	Tl	51
Sao Nicolao	SN08	0.703009	0.513002		19.358	15.595	38.878	Tl	51
Sao Nicolao	SN09	0.703073	0.512954		19.653	15.616	39.154	Tl	51
Sao Nicolao	SN10	0.702976	0.512978		19.539	15.587	38.967	Tl	51
Sao Nicolao	SN11	0.703063	0.512956		19.465	15.581	38.964	Tl	51
Sao Nicolao	SN12	0.703098	0.512967		19.438	15.601	38.997	Tl	51
Sao Nicolao	SN13	0.703035	0.512966		19.473	15.590	38.984	Tl	51
Sao Nicolao	SN14	0.703049	0.512975		19.434	15.600	38.988	Tl	51
Sao Nicolao	SN15	0.703029	0.512979		19.441	15.605	39.007	Tl	51
Sao Nicolao	SN16	0.703050	0.512971		19.492	15.607	39.090	Tl	51
Sao Nicolao	SN17	0.702998	0.512972		19.503	15.606	39.095	Tl	51
Sao Nicolao	SN18	0.703020	0.512970		19.451	15.595	38.999	Tl	51
Sao Nicolao	SN19	0.703013	0.512973		19.477	15.598	39.019	Tl	51
Sao Nicolao	SN-13	0.703105			19.474	15.593	38.987	Ti, conv.	48
Sal	S-03	0.703121			19.444	15.579	38.933	Ti, conv.	48
Sal	S-06				19.362	15.568	38.996	Ti, conv.	48
Sal	S-07				19.365	15.586	39.010	Ti, conv.	48
Maio	NV9	0.702922	0.512990		*19.441*	*15.594*	*39.088*	conv.	45
Maio	NV1(1)	0.703054	0.512948						45
Maio	NV2(1)	0.703127	0.512938						45
Maio	NV2(2)	0.703086	0.512955						45
Maio	NV3(1)	0.703124	0.512940						45
Maio	HV4	0.703029	0.512930						45
Maio	HV210	0.703137	0.512885						45
Maio	ZM159	0.703749	0.512702		*19.035*	*15.564*	*39.121*	conv.	45
Maio	ZM189	0.703795	0.512684		*18.956*	*15.524*	*38.822*	conv.	45
Maio	ZM191	0.703600	0.512725		*19.262*	*15.586*	*39.287*	conv.	45
Maio	ZM55	0.703249	0.512891		*19.289*	*15.585*	*39.066*	conv.	44
Maio	ZM53	0.703386	0.512876		*19.269*	*15.579*	*39.021*	conv.	45
Maio	ZM32	0.703299	0.512887		*19.175*	*15.590*	*38.978*	conv.	45
Maio	ZM60	0.703720	0.512801		*19.203*	*15.568*	*39.060*	conv.	44
Maio	ZM69	0.703653	0.512801		*19.187*	*15.587*	*39.020*	conv.	45
Maio	ZM63	0.703754	0.512775		*19.201*	*15.582*	*39.084*	conv.	45
Santiago	Z150	0.703280	0.512850		*19.120*	*15.581*	*39.976*	conv.	44
Santiago	Z147	0.703250	0.512600		*18.745*	*15.536*	*38.666*	conv.	44
Santiago	ZM150	0.703748	0.512682		*18.972*	*15.564*	*38.849*	conv.	45
Santiago	ST-02	0.703476			19.310	15.571	39.007	Ti, conv.	48
Santiago	ST-06	0.703506			19.376	15.579	39.103	Ti, conv.	48
Santiago	ST-08				19.400	15.584	39.196	Ti, conv.	48
Santiago	ST-09	0.703500			19.218	15.553	39.020	Ti, conv.	48
Santiago	ST-10				19.097	15.543	38.911	Ti, conv.	48
Santiago	S16	0.702881	0.513140		19.383	15.592	39.159	Tl	51
Santiago	S17	0.702962	0.513123		19.406	15.596	39.054	Tl	51
Santiago	S56	0.702883	0.513172		19.418	15.594	39.096	Tl	51
Santiago	ZI47	0.703934	0.512596		*18.745*	*15.541*	*38.693*	conv.	45
Santiago	ZI46	0.703844	0.512683		*18.932*	*15.550*	*38.824*	conv.	45
Santiago	ST-18	0.703420	0.512811	0.282946					53
Santiago	ST-19	0.703418	0.512803	0.282977					53

Supplementary Table 2 | *(continued)*

location	Sample	$^{87}Sr/^{86}Sr$	$^{143}Nd/^{144}Nd$	$^{176}Hf/^{177}Hf$	$^{206}Pb/^{204}Pb$	$^{207}Pb/^{204}Pb$	$^{208}Pb/^{204}Pb$	method	ref.
Santiago	ST-21	0.703818	0.512643	0.282899					53
Santiago	114918	0.703850	0.512711						54
Santiago	NI126	0.703410	0.512768						45
Santiago	117425	0.703551	0.512642						54
Santiago	117413		0.512736						54
Santiago	366	0.703513	0.512787	0.282930	19.102	15.570	39.016	DS	52,54
Santiago	367	0.703596	0.512788	0.282925	19.092	15.567	38.978	DS	52,54
Santiago	368	0.703493	0.512762		19.094	15.565	38.990	DS	52
Santiago	369	0.703498	0.512775		19.126		39.051	DS	52
Santiago	370	0.703508	0.512768	0.282927	19.088	15.560	38.984	DS	52,54
Santiago	371	0.703515	0.512770		19.095	15.568	38.992	DS	52
Santiago	114915	0.704026	0.512630						54
Santiago	114916	0.703992	0.512650	0.282864	18.847	15.546	38.814	DS	54
Santiago	114957		0.512766					DS	54
Santiago	114959	0.703508	0.512832	0.282932	19.284	15.585	39.126	DS	54
Santiago	114881	0.703984	0.512623	0.282866	18.819	15.546	38.782	DS	54
Santiago	114883	0.703654	0.512771	0.282911	19.380	15.598	39.125	DS	54
Santiago	ZI60	0.703192	0.512898		*19.440*	*15.599*	*39.106*	conv.	45
Santiago	ZI59	0.703278	0.512852		*19.120*	*15.581*	*38.972*	conv.	45
Santiago	ZI54	0.703383	0.512807						45
Santiago	ZI3	0.703224	0.512844		*19.126*	*15.581*	*38.991*	conv.	45
Santiago	NI39	0.703589	0.512732						45
Santiago	NI43	0.703801	0.512763						45
Santiago	301	0.703356		0.282912	19.237	15.578	39.141	DS	52,54
Santiago	302	0.703415	0.512758		19.160	15.571	39.086	DS	52
Santiago	303	0.703373			19.299	15.591	39.192	DS	52
Santiago	304	0.703442	0.512739	0.282901	19.143	15.569	39.099	DS	52,54
Santiago	305	0.703469	0.512804		19.144	15.571	39.103	DS	52
Santiago	306	0.703428	0.512763		19.140	15.571	39.097	DS	52
Santiago	307	0.703398		0.282913	19.305	15.590	39.199	DS	52,54
Santiago	308	0.703366	0.512776						52
Santiago	309	0.703366	0.512782		19.293	15.581	39.169	DS	52
Santiago	311	0.703453	0.512759		19.191	15.572	39.131	DS	52
Santiago	312	0.703491	0.512760		19.181	15.571	39.158	DS	52
Santiago	313	0.703496	0.512756		19.182	15.571	39.158	DS	52
Santiago	314	0.703420	0.512793	0.282870	19.069	15.570	38.988	DS	52,54
Santiago	315	0.703147	0.512853	0.282989	19.387	15.596	39.224	DS	52,54
Santiago	316	0.703424	0.512755		19.180	15.573	39.103	DS	52
Santiago	317	0.703406	0.512768		19.280	15.583	39.203	DS	52
Santiago	318	0.703488	0.512781		19.149	15.571	39.092	DS	52
Santiago	319	0.703455	0.512773		19.192	15.574	39.124	DS	52
Santiago	321				19.298	15.583	39.172	DS	52
Santiago	322				19.243	15.577	39.133	DS	52
Santiago	323				19.282	15.580	39.200	DS	52
Santiago	324	0.703376	0.512785		19.262	15.588	39.108	DS	52
Santiago	325	0.703366	0.512788	0.282948	19.211	15.578	39.116	DS	52,54
Santiago	326	0.703348		0.282928	19.211	15.578	39.127	DS	52,54
Santiago	328	0.703387	0.512788	0.282893					52,54
Santiago	329	0.703391	0.512770		19.271	15.582	39.185	DS	52
Santiago	351	0.703240	0.512841		19.352	15.585	39.211	DS	52
Santiago	352	0.703341	0.512793		19.245	15.583	39.145	DS	52
Santiago	353				19.294	15.588	39.196	DS	52
Santiago	354				19.485	15.598	39.307	DS	52
Santiago	355	0.703496	0.512727		19.464	15.606	39.314	DS	52
Santiago	356	0.703306	0.512820						52
Santiago	357			0.282972	19.224	15.584	39.099	DS	52,54
Santiago	358	0.703439	0.512758	0.282867	19.295	15.581	39.199	DS	52,54
Santiago	359	0.703551	0.512774	0.282883	19.251	15.582	39.136	DS	52,54
Santiago	361	0.703674	0.512708	0.282913	19.042	15.562	38.976	DS	52,54
Santiago	304	0.703453							52
Santiago	310	0.703430	0.512764		19.226	15.579	39.170	DS	52
Santiago	310				19.224	15.577	39.166	DS	52
Santiago	310				19.230	15.581	39.179	DS	52
Santiago	327A	0.703373	0.512800		19.210	15.581	39.130	DS	52
Santiago	327D				19.214	15.577	39.118	DS	52
Santiago	327C				19.213	15.578	39.119	DS	52
Santiago	327B				19.212	15.580	39.116	DS	52
Santiago	327E				19.214	15.577	39.106	DS	52
Santiago	314				19.060	15.567	38.961	DS	52
Santiago	ST-5	0.703173	0.512898	0.282986					53

Supplementary Table 2 | *(continued)*

location	Sample	$^{87}Sr/^{86}Sr$	$^{143}Nd/^{144}Nd$	$^{176}Hf/^{177}Hf$	$^{206}Pb/^{204}Pb$	$^{207}Pb/^{204}Pb$	$^{208}Pb/^{204}Pb$	method	ref.
Santiago	ST-34	0.703439	0.512735	0.282954					53
Santiago	ST-12	0.703396	0.512802	0.282987					53
Santiago	360	0.703656			19.048	15.563	38.991	DS	52
Santiago	362	0.703726	0.512697	0.282926	19.050	15.561	38.991	DS	52,54
Santiago	363				19.043	15.563	38.987	DS	52
Santiago	364	0.703624	0.512722	0.282940	19.038	15.564	38.984	DS	52,54
Santiago	365	0.703716	0.512717		19.036	15.559	38.976	DS	52
Santiago	114-856	0.703412		0.282922	19.429	15.595	39.219	DS	54
Santiago	114-858	0.703675			19.242	15.583	39.007	DS	54
Santiago	114-859	0.703434	0.512805		19.189	15.580	38.964	DS	54
Santiago	114-860	0.703485	0.512766		19.199	15.578	39.024	DS	54
Santiago	114890	0.703866	0.512642		18.840	15.551	38.827	DS	54
Santiago	114921	0.703829	0.512649		18.867	15.546	38.818	DS	54
Santiago	114954	0.703755	0.512682	0.282905	19.236	15.586	39.006	DS	54
Santiago	114955	0.703784	0.512711						54
Santiago	ST-16	0.703619	0.512710	0.282949					53
Santiago	ST-24	0.703758	0.512664	0.282904					53
Santiago	114891	0.703471	0.512832						54
Santiago	114944	0.703748	0.512716						54
Santiago	114947		0.512804	0.282947	19.238	15.577	39.063	DS	54
Santiago	114951	0.703511	0.512790	0.282972	19.257	15.576	39.024	DS	54
Santiago	114952				19.144	15.575	38.988	DS	54
Santiago	114958	0.703576	0.512758	0.282837	19.430	15.599	39.168	DS	54
Santiago	114962	0.703652	0.512778						54
Santiago	NI77	0.703611	0.512774						45
Santiago	N171	0.703546	0.512768						45
Santiago	N161	0.703822	0.512676		*18.968*	*15.552*	*38.805*	conv.	45
Santiago	N160	0.703821	0.512628		*18.975*	*15.546*	*38.797*	conv.	45
Santiago	N113	0.703835	0.512648						45
Santiago	N14	0.703721	0.512751		*19.001*	*15.554*	*38.855*	conv.	45
Santiago	NI185	0.703511	0.512818		*19.137*	*15.577*	*38.894*	conv.	45
Santiago	N178	0.703515	0.512701		*19.199*	*15.582*	*38.968*	conv.	45
Santiago	ZI53	0.703512	0.512780		*19.209*	*15.574*	*38.980*	conv.	45
Santiago	NI176	0.703875	0.512664		*18.885*	*15.554*	*38.803*	conv.	45
Santiago	Z0I7	0.703506	0.512794						45
Santiago	N0I74	0.703463	0.512820						45
Santiago	ST-27	0.703607	0.512726	0.282919					53
Santiago	ST-48	0.703358	0.512803	0.282962					53
Santiago	ST-50	0.703360	0.512811	0.282968					53
Santiago	ST-37	0.703545	0.512732	0.282973					53
Santiago	ST-40	0.703523	0.512779	0.282966					53
Santiago	ST-44	0.703525	0.512758	0.282950					53
Santiago	ST-59	0.703903	0.512664	0.282865					53
Santiago	ST-42	0.703534	0.512751	0.282961					53
Santiago	ST-30	0.703539	0.512758	0.282959					53
Santiago	ST-74	0.703537	0.512709	0.282930					53
Santiago	114869	0.703612	0.512800	0.282926	19.373	15.585	39.125	DS	54
Santiago	114874	0.703898	0.512662	0.282877	19.127	15.572	39.035	DS	54
Santiago	114876	0.703794	0.512745						54
Santiago	117408	0.704056							54
Santiago	117417	0.703995							54
Santiago	117419	0.703633	0.512773						54
Santiago	117422	0.703857			19.118	15.572	39.043	DS	54
Santiago	117438	0.703700	0.512755						54
Santiago	PST13	0.703700	0.512717						54
Fogo	NF34	0.703420	0.512741		*18.928*	*15.555*	*38.827*	conv.	44
Fogo	NF8	0.703693	0.512776		*18.934*	*15.558*	*38.807*	conv.	45
Fogo	NF16	0.703646	0.512769		*18.945*	*15.548*	*38.800*	conv.	45
Fogo	ZF30	0.703647	0.512776		*18.940*	*15.560*	*38.784*	conv.	45
Fogo	NF19	0.703552	0.512794					conv.	45
Fogo	ZF29	0.703522	0.512773		*18.950*	*15.558*	*38.823*	conv.	45
Fogo	NF60	0.703223	0.512968		*19.883*	*15.644*	*39.460*	conv.	45
Fogo	F-106403				*19.408*	*15.581*	*39.058*	conv.	46
Fogo	F-106444				*18.908*	*15.541*	*38.717*	conv.	46

Supplementary Table 2 | *(continued)*

location	Sample	$^{87}Sr/^{86}Sr$	$^{143}Nd/^{144}Nd$	$^{176}Hf/^{177}Hf$	$^{206}Pb/^{204}Pb$	$^{207}Pb/^{204}Pb$	$^{208}Pb/^{204}Pb$	method	ref.
Fogo	F-07	0.703779	0.512722		*18.884*	*15.534*	*38.707*	conv.	48,49
Fogo	F-10	0.703606	0.512745		*19.135*	*15.564*	*38.923*	conv.	49
Fogo	F-12	0.703615	0.512758		*19.144*	*15.582*	*38.981*	conv.	49
Fogo	F-22	0.703646	0.512765		*19.096*	*15.565*	*38.904*	conv.	49
Fogo	F-06	0.703728	0.512726		*18.902*	*15.543*	*38.737*	conv.	48,49
Fogo	F-14	0.703748	0.512725		*18.937*	*15.553*	*38.778*	conv.	49
Fogo	F-15	0.703728	0.512728		*18.932*	*15.555*	*38.796*	conv.	49
Fogo	F-21	0.703717	0.512736		*19.022*	*15.558*	*38.838*	conv.	49
Fogo	F-16	0.703754	0.512737		*18.934*	*15.541*	*38.758*	conv.	49
Fogo	F-08	0.703724	0.512737		*18.947*	*15.566*	*38.833*	conv.	49
Fogo	F-24	0.703751	0.512728		18.971	15.566	38.810	conv. Ti,	48
Fogo	F-08A	0.703724			18.956	15.567	38.842	conv. Ti,	48
Fogo	CV-98-F-07								58
Fogo	CV-98-F-10								58
Fogo	CV-98-F-16								58
Fogo	CV-98-F-18								58
Fogo	F-11	0.703655	0.512759		*19.078*	*15.570*	*38.954*	conv.	49
Fogo	F-13	0.703705	0.512733		*19.111*	*15.556*	*38.907*	conv.	49
Fogo	F-01	0.703675	0.512760		*19.107*	*15.557*	*38.890*	conv.	48,49
Fogo	F-02	0.703713	0.512727		*19.066*	*15.571*	*38.887*	conv.	48,49
Fogo	F-18	0.703536	0.512764		*19.222*	*15.567*	*38.920*	conv.	49
Fogo	F-20	0.703712	0.512735		19.064	15.552	38.828	conv. Ti,	48
Brava	CY-25	0.703173	0.512914		19.635	15.607	39.084	DS	57
Brava	CY-174	0.703264	0.512910		20.021	15.613	39.205	DS	57
Brava	CY-11	0.703271	0.512915		20.252	15.645	39.364	DS	57
Brava	CY-19	0.703305	0.512908		19.874	15.616	39.153	DS	57
Brava	CY-82	0.703241	0.512903		19.793	15.611	39.190	DS	57
Brava	CY-165	0.703342	0.512920		19.848	15.615	39.131	DS	57
Brava	CY-31	0.703621	0.512788		19.465	15.589	39.154	DS	57
Brava	CY-138	0.703652	0.512806		19.623	15.596	39.226	DS	57
Brava	CY-197	0.703561	0.512811		19.656	15.598	39.209	DS	57
Brava	CY-27	0.703592	0.512812		19.434	15.594	39.144	DS	57
Brava	CY-193	0.703572	0.512805		19.556	15.593	39.175	DS	57
Brava	CY-8	0.703305	0.512916		20.018	15.620	39.194	DS	57
Brava	CY-32	0.703691	0.512781		19.255	15.568	39.038	DS	57
Brava	CY-99	0.703611	0.512800		19.557	15.587	39.133	DS	57
Brava	CY-200	0.703621	0.512793		19.431	15.588	39.134	DS	57
Brava	CY-80	0.703644	0.512795		19.360	15.584	39.115	DS	57
Brava	CY-188	0.703658	0.512788		19.258	15.570	39.037	DS	57
Brava	CY-215	0.703672	0.512772		19.394	15.578	39.102	DS	57
Brava	CY-95	0.703585	0.512797		19.658	15.602	39.250	DS	57
Brava	CY-222	0.703547	0.512821		19.678	15.596	39.243	DS	57
Brava	CY-238	0.703570	0.512806		19.661	15.603	39.258	DS	57
Brava	CY-165								58
Brava	Brav 02	0.703671	0.512807		19.520	15.595	39.195	DS	56
Brava	Brav02*	0.703674	0.512803		19.523	15.599	39.204	DS	56
Brava	Brav 05	0.703539	0.512845		19.551	15.601	39.196	DS	56
Brava	Brav 06	0.703646	0.512830		19.599	15.608	39.200	DS	56
Brava	Brav 07	0.703524	0.512839		19.595	15.614	39.183	DS	56
Brava	Brav 08	0.703692	0.512793		19.444	15.597	39.173	DS	56
Brava	Brav 17	0.703433	0.512914		19.912	15.630	39.175	DS	56
Brava	Brav 18	0.703299	0.512928		19.894	15.637	39.147	DS	56
Brava	Brav 20	0.703582	0.512826		19.434	15.596	39.117	DS	56
Brava	Brav 21	0.703641	0.512803		19.342	15.601	39.075	DS	56
Brava	Brav 24	0.703626	0.512802		19.287	15.598	39.020	DS	56
Brava	Brav 25	0.703690	0.512797		19.453	15.595	39.173	DS	56
Brava	Brav 28	0.703583	0.512806		19.462	15.598	39.117	DS	56
Brava	Fogo 19	0.703510	0.512815		19.274	15.580	39.017	DS	56
Brava	Fogo 35	0.703509	0.512807		19.264	15.578	39.002	DS	56
Continental section of CVL and Nenue Trough									
CVL, Adamawa	NG105				*19.978*	*15.690*	*39.569*	conv.	59
CVL, Adamawa	NG14				*19.987*	*15.710*	*39.783*	conv.	59
CVL, Adamawa	NG1X				*19.504*	*15.685*	*39.706*	conv.	59
CVL, Adamawa	NG9				*20.237*	*15.730*	*39.811*	conv.	59
CVL, Adamawa	NG18				*19.040*	*15.690*	*39.017*	conv.	59
CVL, Adamawa	NG20				*19.298*	*15.699*	*39.429*	conv.	59
CVL, Bafang	BAF 22	0.703219	0.512951	0.282935	20.041	15.675	39.728	Tl	62
CVL, Bafang	BAF 34	0.703328	0.512921	0.282908	20.062	15.674	39.899	Tl	62
CVL, Bafang	BAF 44	0.703282	0.512916	0.282928	19.921	15.659	39.619	Tl	62
CVL, Bafang	BAF 45	0.703101	0.512912	0.282910	20.056	15.677	39.653	Tl	62
CVL, Bafang	BAF 15	0.704096	0.512892	0.282896	19.467	15.635	39.348	Tl	62
CVL, Bafang	BAF 18	0.704098	0.512893	0.282890	19.298	15.644	39.285	Tl	62
CVL, Bafang	BAF 36	0.703466	0.512923	0.282937	20.080	15.649	39.668	Tl	62
CVL, Bafang	BAF 42	0.703323	0.512891	0.282913	19.893	15.664	39.615	Tl	62

Supplementary Table 2 | *(continued)*

location	Sample	$^{87}Sr/^{86}Sr$	$^{143}Nd/^{144}Nd$	$^{176}Hf/^{177}Hf$	$^{206}Pb/^{204}Pb$	$^{207}Pb/^{204}Pb$	$^{208}Pb/^{204}Pb$	method	ref.
CVL, Bafang	BAF 43	0.704079	0.512895	0.282902	19.505	15.644	39.387	Tl	62
CVL, Bafang	BAF 2	0.704097	0.512852	0.282890	19.870	15.656	39.709	Tl	62
CVL, Bafang	BAF 10	0.704151	0.512824	0.282875	19.045	15.551	38.679	Tl	62
CVL, Bafang	BAF 3	0.703214	0.512845	0.282876	19.853	15.653	39.670	Tl	62
CVL, Bafang	BAF 37	0.703835	0.512875	0.282885	19.854	15.659	39.624	Tl	62
CVL, Oku	OVG20	0.703220	0.512922		19.573	15.627	39.292	DS	63
CVL, Oku	OVG32	0.703210	0.512922		19.613	15.628	39.387	DS	63
CVL, Oku	OVG38	0.703170	0.512912		19.710	15.635	39.356	DS	63
CVL, Oku	OVG40	0.703320	0.512882		19.337	15.600	39.080	DS	63
CVL, Oku	OVG214b				19.527	15.598	39.187	DS	63
CVL, Oku	OVG215	0.703260			19.378	15.598	39.119	DS	63
CVL, Oku	OVG216	0.703440	0.512872		18.982	15.587	39.095	DS	63
CVL, Oku	OVG2	0.703370	0.512882		19.626	15.653	39.451	DS	63
CVL, Oku	OVG4	0.703220	0.512912		19.743	15.642	39.355	DS	63
CVL, Oku	OVG6	0.703210	0.512912		19.810	15.646	39.461	DS	63
CVL, Oku	OVG12	0.703240	0.512902		19.802	15.657	39.406	DS	63
CVL, Oku	OVG13b	0.703260	0.512912		19.821	15.670	39.546	DS	63
CVL, Oku	OVGLW2	0.703290	0.512902		19.702	15.637	39.384	DS	63
CVL, Oku	OVG70	0.703470	0.512822		19.229	15.582	38.845	DS	63
CVL, Oku	OVG79	0.703550	0.512852		19.985	15.667	39.850	DS	63
CVL, Oku	OVG80	0.703340	0.512882		19.450	15.623	39.244	DS	63
CVL, Oku	OVG81	0.703560	0.512832		19.349	15.619	39.017	DS	63
CVL, Manengouba	C55	0.703158	0.512962		19.796	15.613	39.366	Tl	60
CVL, Manengouba	C69	0.703148	0.512928		19.711	15.617	39.356	Tl	60
CVL, Manengouba	C51	0.703078	0.512934		19.922	15.615	39.526	Tl	60
CVL, Manengouba	C59	0.703068	0.512909		20.137	15.669	39.876	Tl	60
CVL, Manengouba	C72	0.703028	0.512872		20.184	15.698	39.876	Tl	60
CVL, Manengouba	C70	0.702998	0.512945		19.636	15.629	39.276	Tl	60
CVL, Manengouba	C56	0.702988	0.512964		19.574	15.656	39.306	Tl	60
CVL, Manengouba	C68	0.702978	0.512991		19.797	15.639	39.506	Tl	60
CVL, Manengouba	C135	0.703074	0.512967	0.283026	19.700	15.672	39.387	Tl	61
CVL, Manengouba	C240	0.703069	0.512945	0.283022	19.880	15.639	39.647	Tl	61
CVL, Bambouto	C256	0.703284	0.512899	0.282738	19.590	15.633	39.272	Tl	61
CVL, Bambouto	C286	0.703163	0.512945	0.282810	19.781	15.662	39.458	Tl	61
CVL, Oku	C274	0.703333	0.512913	0.282944	19.634	15.640	39.380	Tl	61
CVL, Oku	C281	0.703511	0.512988	0.282949	19.608	15.658	39.428	Tl	61
Biu Plateau	ZAGU	0.702951	0.512976		*19.679*	*15.644*	*39.386*	conv.	64
Biu Plateau	JIGU 1	0.703504	0.512880		*19.097*	*15.627*	*39.214*	conv.	64
Biu Plateau	JIGU-M	0.702892	0.513015		*19.834*	*15.653*	*39.499*	conv.	64
Biu Plateau	X	0.703183	0.512936		*19.386*	*15.624*	*39.265*	conv.	64
Biu Plateau	KOROKO	0.703193	0.512928		*20.105*	*15.697*	*39.723*	conv.	64
Biu Plateau	BUGOR	0.702922	0.512962		*19.672*	*15.659*	*39.490*	conv.	64
Biu Plateau	SE BUGOR	0.702927	0.512986		*19.625*	*15.641*	*39.380*	conv.	64
Biu Plateau	TAMZA	0.702890	0.512968		*20.041*	*15.678*	*39.753*	conv.	64
Biu Plateau	GUFKA	0.703079	0.512968		*19.418*	*15.638*	*39.267*	conv.	64
Biu Plateau	GULD-UMBUR	0.702914	0.512988		*20.008*	*15.673*	*39.718*	conv.	64
Biu Plateau	WIGA	0.702941	0.513004		*19.783*	*15.644*	*39.518*	conv.	64
Biu Plateau	ZUMTA	0.703105	0.512958		*20.164*	*15.688*	*40.287*	conv.	64
Biu Plateau	HIZSHI	0.702904	0.512963		*20.111*	*15.674*	*39.785*	conv.	64
Biu Plateau	TUM	0.703003	0.512968		*20.020*	*15.678*	*39.850*	conv.	64
Biu Plateau	ETUM	0.702856	0.512984		*19.880*	*15.647*	*39.526*	conv.	64
Biu Plateau	TILA 1	0.703140	0.512949		*19.559*	*15.648*	*39.428*	conv.	64
Biu Plateau	TILA STR	0.702900	0.512997		*19.775*	*15.644*	*39.512*	conv.	64
Biu Plateau	BIU4	0.702884	0.512996		*19.851*	*15.652*	*39.622*	conv.	64
Biu Plateau	BIU5	0.702934	0.512991		*19.744*	*15.639*	*39.520*	conv.	64
Biu Plateau	BIU8	0.703341	0.512923		*19.033*	*15.636*	*39.181*	conv.	64
Biu Plateau	BIU9	0.702942	0.512972		*19.707*	*15.646*	*39.423*	conv.	64
Biu Plateau	DAM	0.702995	0.512963		*19.519*	*15.633*	*39.312*	conv.	64
Biu Plateau	DAM2	0.703171	0.512961		*19.656*	*15.659*	*39.700*	conv.	64
Biu Plateau	MIR	0.703061	0.512947		*20.328*	*15.696*	*40.360*	conv.	64
Biu Plateau	GUMJA	0.702890	0.512991		*19.713*	*15.660*	*39.476*	conv.	64
Biu Plateau	GWARAM	0.702981	0.512973		*20.020*	*15.676*	*39.804*	conv.	64
Biu Plateau	HILIA 1	0.702923	0.512987		*19.777*	*15.659*	*39.546*	conv.	64
Biu Plateau	HILIA 2	0.702888	0.512989		*19.643*	*15.641*	*39.426*	conv.	64
Biu Plateau	PELA JUNG	0.703351	0.512901		*19.483*	*15.651*	*39.511*	conv.	64
Biu Plateau	PELA ALT	0.703192	0.512928		*19.862*	*15.685*	*39.959*	conv.	64
Biu Plateau	PELA 2	0.703090	0.512957		*19.659*	*15.647*	*39.368*	conv.	64
Jos Plateau	DAI	0.703379	0.512881		*19.328*	*15.650*	*39.325*	conv.	64
Jos Plateau	AMPANG	0.703588	0.512875		*19.266*	*15.664*	*39.310*	conv.	64
Jos Plateau	KERANG	0.703393	0.512896		*19.656*	*15.676*	*39.483*	conv.	64
Jos Plateau	PIDONG-M	0.703370	0.512902		*19.624*	*15.666*	*39.495*	conv.	64
Jos Plateau	PIDONG-S	0.703173	0.512872		*19.686*	*15.673*	*39.649*	conv.	64
Madeira Islands									
Madeira (PE)	MD-33	0.702634	0.513175		18.787	15.516	38.402	conv.	65
Madeira (PE)	191292-5	0.702709	0.513154		18.893	15.528	38.570	conv.	65
Madeira (PE)	191292-6	0.702652	0.513167		18.848	15.534	38.495	conv.	65
Madeira (PE)	191292-8	0.702640	0.513205		18.804	15.525	38.421	conv.	65
Madeira (PE)	MA-85	0.702644	0.513194	0.283333	18.739	15.513	38.354	conv.	32,65
Madeira (PE)	MA-87	0.702692	0.513162		18.889	15.516	38.485	conv.	65
Madeira (PE)	MA-88	0.702682	0.513139	0.283319	18.884	15.516	38.494	conv.	32,65

Supplementary Table 2 | *(continued)*

location	Sample	$^{87}Sr/^{86}Sr$	$^{143}Nd/^{144}Nd$	$^{176}Hf/^{177}Hf$	$^{206}Pb/^{204}Pb$	$^{207}Pb/^{204}Pb$	$^{208}Pb/^{204}Pb$	method	ref.
Madeira (PE)	MA-218A	0.702743	0.513136	0.283299	18.975	15.526	38.622	conv.	32,65
Madeira (LR)	MD-1	0.702890	0.513081		19.271	15.546	38.955	conv.	65
Madeira (LR)	MD-3	0.702882	0.513081		19.428	15.553	39.100	conv.	65
Madeira (LR)	MD-5	0.702865	0.513064		19.040	15.544	38.757	conv.	65
Madeira (LR)	MD-9	0.702810	0.513063		19.408	15.554	39.079	conv.	65
Madeira (LR)	MD-12	0.702849	0.513065		19.355	15.552	39.039	conv.	65
Madeira (LR)	MD-21	0.702862	0.513071		19.342	15.557	39.038	conv.	65
Madeira (LR)	MA-16	0.702936	0.513058		19.449	15.569	39.162	conv.	65
Madeira (S)	MA-17	0.702827	0.513071	0.283224	19.312	15.554	38.998	conv.	32,65
Madeira (S)	MA-23	0.702900	0.513041	0.283205	19.415	15.559	39.105	conv.	32,65
Madeira (LR)	MA-53	0.702931	0.513056		19.312	15.555	39.025	conv.	65
Madeira (S)	MA-66	0.702840	0.513088		19.100	15.547	38.807	conv.	65
Madeira (S)	MA-75B	0.702876	0.513044	0.283203	19.608	15.571	39.305	conv.	32,65
Madeira (LR)	MA-115	0.702873	0.513020		19.795	15.575	39.475	conv.	65
Madeira (LR)	MA-137	0.702757	0.513117		18.928	15.524	38.561	conv.	65
Madeira (S)	MA-142	0.702733	0.513131		18.943	15.523	38.570	conv.	65
Madeira (S)	MA-160	0.702769	0.513128	0.283306	19.004	15.535	38.658	conv.	32,65
Madeira (LR)	MA-162	0.702805	0.513084		19.141	15.531	38.783	conv.	65
Desertas	DGR-2	0.702876	0.513062		19.529	15.572	39.234	conv.	65
Desertas (S)	DGR-14	0.702906	0.513040		19.628	15.567	39.306	conv.	65
Desertas (S)	DGR-47	0.702965	0.513023	0.283130	19.688	15.577	39.416	conv.	32,65
Desertas	K-11	0.702904	0.513049	0.283151	19.541	15.560	39.204	conv.	32,65
Desertas	K-18	0.702953	0.513026		19.356	15.562	39.110	conv.	65
Desertas	K-22	0.702970	0.513017		19.361	15.571	39.162	conv.	65
Desertas (S)	K-26	0.702976	0.513025		19.659	15.581	39.386	conv.	65
Madeira	MA-120	0.702932	0.513034		19.476	15.567	39.151	conv.	65
Madeira	MA-123	0.702862	0.513051		19.523	15.574	39.215	conv.	65
Madeira	MA-208	0.702846	0.513063		19.178	15.535	38.868	conv.	65
Madeira	MA-215	0.702858	0.513032	0.283166	19.797	15.587	39.499	conv.	32,65
Madeira (S)	MA-227	0.702808	0.513079	0.283225	19.067	15.539	38.800	conv.	32,65
Porto Santo	PS161292-2	0.702816	0.513101		19.269	15.563	38.936	conv.	65
Porto Santo	PS-2	0.702946	0.513060		18.947	15.523	38.637	conv.	65
Porto Santo	PS-3	0.703025	0.512995		19.249	15.549	38.988	conv.	65
Porto Santo	PS-4	0.702924	0.513035		19.324	15.558	39.058	conv.	65
Porto Santo	K-43	0.702826	0.513075	0.283237	19.107	15.539	38.793	conv.	32,65
Porto Santo	K-55	0.702868	0.513052		19.290	15.552	38.954	conv.	65
Porto Santo	K-67	0.702906	0.513047		18.965	15.534	38.685	conv.	65
Porto Santo	DS790-1	0.702934	0.512996		19.486	15.588	39.147	conv.	65
Porto Santo	PS-36	0.702855	0.513102		19.304	15.553	38.958	conv.	65
Porto Santo	PS-37.1	0.702937	0.513023		19.338	15.557	39.038	conv.	65
Porto Santo	PS-41	0.702826	0.513090		18.886	15.519	38.514	conv.	65
Porto Santo	PS-53	0.702827	0.513100		18.859	15.519	38.505	conv.	65
Madeira	13796-1			0.283168					32
Madeira	436DR-1	0.702992	0.513084		19.175	15.533	38.817	conv.	67
Madeira	436DR-2	0.702809	0.513081		19.193	15.549	38.873	conv.	67
Madeira	437DR-1	0.702881	0.513029		19.664	15.571	39.346	conv.	67
Madeira	438DR-1	0.702870	0.513026		19.676	15.582	39.373	conv.	67
Madeira	438DR-1	0.702870	0.513021		19.667	15.568	39.320	conv.	67
Madeira	439DR-1	0.702879	0.513028		19.663	15.564	39.328	conv.	67
Madeira	440DR-1	0.702903	0.513021		19.640	15.575	39.347	conv.	67
Madeira	441DR-1	0.702903	0.513028		19.662	15.559	39.316	conv.	67
Madeira	442DR-1	0.702940	0.513006		19.562	15.572	39.322	conv.	67
Madeira	442DR-3	0.702941	0.513009		19.582	15.581	39.355	conv.	67
Madeira (PE)	MA 143	0.702731	0.513125		18.940	15.511	38.540	conv.	67
Madeira	MF 15	0.702939	0.513017		19.409	15.573	39.148	conv.	67
Madeira	MF 4	0.702837	0.513060		19.398	15.553	39.074	conv.	67
Madeira	MF 5	0.702892	0.513066		19.397	15.549	39.068	conv.	67
Madeira	M-19	0.702686							66
Madeira	M-141	0.702706	0.513107						66
Madeira	M-209	0.702876	0.513000		19.168	15.553	38.910	conv.	66
Madeira	M-67	0.702926	0.513047		19.060	15.498	38.669	conv.	66
Madeira	PM-7	0.702906	0.512839		19.514	15.574	39.218	conv.	66
Madeira	M-390	0.702836			19.587	15.665	39.450	conv.	66
Madeira	M-245	0.702726	0.513081		19.003	15.501	38.730	conv.	66
Madeira	M-347	0.702306	0.513212		18.871	15.534	38.381	conv.	66
Madeira	M-370	0.702836	0.512955		19.289	15.547	38.928	conv.	66

(S): shield stage, (PS): post shield stage, (LR): late rift stage, Tl: Tl-doping ICP-MS method, conv.: conventional TIMS method, black.: blanketing ICP-MS method, DS: double spike method. Red color: not used for plot and principal component analysis.

Supplementary Table 3 | Compiled Sr, Nd, Hf, and Pb isotopic data of mafic xenolith from Africa

Location	Sample	rock	material	$^{87}Sr/^{86}Sr$	$^{143}Nd/^{144}Nd$	$^{176}Hf/^{177}Hf$	$^{206}Pb/^{204}Pb$	$^{207}Pb/^{204}Pb$	$^{208}Pb/^{204}Pb$	ref.
CVL, continental section										
Adamawa	YK-01	Clinopyroxenite	cpx	0.702661	0.513057					68
Adamawa	YK-12	Websterite	cpx	0.702849	0.512892					68
Adamawa	YK-13	Websterite	cpx	0.702763	0.512967					68
Adamawa	P12	Websterite	cpx	0.702293	0.513234		18.13	15.51	37.58	69
Adamawa	P12	Websterite	opx	0.702460			18.93	15.71	38.4	69
Adamawa	P6	Websterite	cpx	0.702761	0.512910		18.91	15.54	38.67	69
Adamawa	P6	Websterite	amp	0.702974	0.512961		18.92	15.54	38.64	69
Adamawa	P6	Websterite	garnet		0.512975		19.38	15.75	38.79	69
Atlas Mountains, Middle Atlas										
Azrou-Timhadite	TAK4	Clinopyroxenite	cpx	0.703166	0.512865					70
Azrou-Timhadite	TAK4	Clinopyroxenite	cpx	0.703185	0.512863					68
Azrou-Timhadite	IBA 18	Hormblendite	cpx	0.703147	0.512857					71
Azrou-Timhadite	TAK3	Websterite	cpx	0.703113	0.513253					70
Azrou-Timhadite	TAK5	Websterite	cpx	0.702739	0.513050					70
Azrou-Timhadite	TAK6	Websterite	cpx	0.703193	0.512966					70
Azrou-Timhadite	TAK10	Websterite	cpx	0.703229	0.513051					70
Azrou-Timhadite	IBA 21	Websterite	cpx	0.702909	0.513195					70
Azrou-Timhadite	TAK3	Websterite	cpx	0.703143	0.513269					68
Middle Atlas	AT 4	Websterite	cpx	0.703340	0.513100					41
Azrou-Timhadite	IBA 28	Websterite	cpx	0.702569	0.513375					71
Azrou-Timhadite	TAK13	Websterite	cpx	0.702508	0.512904					70
Azrou-Timhadite	TAK14	Websterite	cpx	0.702507	0.512908					70
Azrou-Timhadite	IBA 5	Websterite	cpx	0.703551	0.512813					71
Azrou-Timhadite	IBA 32	Websterite	cpx	0.703441	0.512823					71
Azrou-Timhadite	IBA 41	Websterite	cpx	0.703536	0.512810					71
Azrou-Timhadite	IBA 53	Websterite	cpx	0.703494	0.512939					71
Azrou-Timhadite	IBA 69	Websterite	cpx	0.703430	0.512824					71
Azrou-Timhadite	IBA 5	Websterite	amp	0.703490	0.512873					71
Azrou-Timhadite	IBA 41	Websterite	amp	0.703445	0.512822					71
Hogger Swell										
In Teria	IL-17-16	Clinopyroxenite	WR	0.704696	0.512936		19.803	15.663	39.395	72
In Teria	IL-17-16	Clinopyroxenite	WR	0.704550	0.512940		19.814	15.662	39.329	72
In Teria	IL-17-22	Pyroxenite	WR	0.703267	0.512955		19.646	15.642	39.255	72
In Teria	IL-17-24	Pyroxenite	WR	0.703448	0.512936		19.738	15.655	39.331	72
In Teria	IL-17-27	Pyroxenite	WR	0.703495	0.512917		19.469	15.666	39.210	72
In Teria	INT-17-89-100	Pyroxenite	WR	0.704991	0.512965		19.519	15.670	39.289	72
In Teria	INT-14-6	Websterite	WR	0.703836	0.512912		18.705	15.614	38.481	72
In Teria	LL-17-21	Websterite	WR	0.703391	0.512939		19.892	15.669	39.449	72
Canary Islands										
Gran Canaria	BM1965P8151	Clinopyroxenite	cpx	0.703198	0.512887					73
Fuerteventura	TF14-51	Clinopyroxenite	WR	0.703136	0.512915					74
Fuerteventura	TF14-46	Clinopyroxenite	WR	0.703121	0.512871					74
El Hierro	H1-15leach	Pyroxenite	WR	0.702990	0.512980		19.31	15.55	38.89	19
El Hierro	H1-35leach	Pyroxenite	WR	0.702920	0.513000					19
El Hierro	H1-15unleach	Pyroxenite	WR	0.703150	0.512930					19
El Hierro	H1-35unleach	Pyroxenite	WR	0.703140	0.512960					19
Fuerteventura	TF14-46	Wehrlite	WR	0.703139	0.512954					74
El Hierro	H1-18leach	Wehrlite	WR	0.702950	0.512980		19.41	15.6	39.07	19
El Hierro	H1-38leach	Wehrlite	WR	0.702960	0.512970		19.19	15.55	38.82	19
El Hierro	H1-18unleach	Wehrlite	WR	0.703350	0.512940					19
El Hierro	H1-38unleach	Wehrlite	WR	0.703270	0.512920					19
Fuerteventura	FT9-1_leach	Wehrlite	WR	0.703285	0.512967					75
East African Rift										
Afar	AE11/06	Pyroxenite	cpx	0.704048	0.512882	0.283107				76
Afar	AE17/06	Pyroxenite	cpx	0.704091	0.512855	0.283105				76

Supplementary Table 3 | *(continued)*

Location	Sample	rock	material	$^{87}Sr/^{86}Sr$	$^{143}Nd/^{144}Nd$	$^{176}Hf/^{177}Hf$	$^{206}Pb/^{204}Pb$	$^{207}Pb/^{204}Pb$	$^{208}Pb/^{204}Pb$	ref.
Afar	AE14/06	Pyroxenite	cpx	0.703694	0.512911	0.283136				76
Afar	AE15/06	Pyroxenite	cpx	0.703774	0.512950	0.283258				76
Afar	AE16/06	Pyroxenite	cpx	0.703104	0.513042	0.283349				76
Afar	AE16/06	Pyroxenite	cpx	0.703140	0.513050					76
Afar	AE14/06	Pyroxenite	opx	0.705827		0.283200				76
Lashine	BD-816	Clinopyroxenite	cpx	0.703960	0.511780		17.36	15.62	38.13	77
Oldoinyo Lengai	BD77	Pyroxenite	WR	0.708610	0.511740					78
Oldoinyo Lengai	BD93	Pyroxenite	WR	0.705290	0.512440					78
Labait	AT41	Wehrlite	cpx	0.703522	0.512757					79
Labait	AT57	Wehrlite	cpx	0.703584	0.512778					79
Olmani	89-777	Wehrlite	cpx	0.703468	0.512798					80
Olmani	89-777	Wehrlite	WR	0.703502	0.512840					80
Lashaine	BD-727	Granulite	WR	0.704140	0.512100		15.77	15.39	35.92	77
Lashaine	BD-528	Granulite	WR	0.704150	0.512290		16.36	15.46	36.47	77
Lashaine	BD-798	Granulite	WR	0.703590	0.511540		17.5	15.65	37.94	77
Lashaine	BD-526	Granulite	WR	0.704290	0.512160		17.39	15.5	37.54	77
Lashaine	BD-728	Granulite	WR	0.704050	0.512360		16.65	15.44	36.72	77
Lashaine	BD-786	Granulite	WR	0.704340	0.512090		16.42	15.46	36.42	77
Lashaine	89-726	Granulite	WR	0.704055	0.512288					81
Lashaine	89-729	Granulite	WR	0.703665	0.511700					81
Lashaine	89-730	Granulite	WR	0.703834	0.512445					81
Lashaine	89-733	Granulite	WR	0.716532	0.511689					81
Lashaine	89-745	Granulite	WR	0.721067	0.511761					81
Labait	LB-04-19	Granulite	WR	0.703979	0.511452					81
Labait	LB-04-52	Granulite	WR	0.703909	0.511539					81
Labait	LB-04-07	Granulite	WR	0.705147	0.512222					81
Labait	LB-04-82	Granulite	WR	0.704131	0.511607					81
Labait	LB-04-39	Granulite	WR	0.704834	0.512081					81
Labait	LB-04-91	Granulite	WR	0.703987	0.511683					81
Naibor Soito	NS04-01	Granulite	WR	0.711056	0.511311					81
Naibor Soito	NS04-05	Granulite	WR	0.702671	0.510970					81
Naibor Soito	NS04-13	Granulite	WR	0.705456	0.511328					81
Naibor Soito	NS04-83	Granulite	WR	0.703268	0.511078					81
Naibor Soito	NS04-91	Granulite	WR	0.705486	0.511042					81
Naibor Soito	NS04-61	Granulite	WR	0.703837	0.511873					81
Naibor Soito	NS04-80	Granulite	WR	0.703231	0.512273					81
Western East African Rift (Tanganyika Rift)										
Tanganyika	23208	Pyroxenite	cpx	0.705032	0.512545		18.032	15.586	38.258	82
Tanganyika	23209	Pyroxenite	cpx	0.705018			18.705	15.661	39.145	82
Tanganyika	23210	Pyroxenite	cpx				18.035	15.595	38.238	82
Tanganyika	23211	Pyroxenite	cpx	0.705044	0.512537		18.638	15.651	39.106	82
Tanganyika	23215	Pyroxenite	cpx	0.704868	0.512563		17.951	15.580	38.127	82
Tanganyika	23255	Pyroxenite	cpx	0.704919	0.512550		17.123	15.497	36.914	82
Tanganyika	23256	Pyroxenite	cpx	0.704758	0.512576		17.007	15.490	36.800	82
Tanganyika	23262	Pyroxenite	cpx	0.704705			18.368	15.623	38.773	82
Tanganyika	23266	Pyroxenite	cpx	0.705685	0.512563		18.171	15.596	38.470	82
Tanganyika	23267	Pyroxenite	cpx	0.704819	0.512563		18.954	15.686	39.653	82
Tanganyika	23268	Pyroxenite	cpx	0.704742	0.512554		18.103	15.603	38.228	82
Tanganyika	23212	Pyroxenite	amp	0.704991			18.907	15.675	39.583	82
Tanganyika	LU 196/1	Pyroxenite	WR	0.703990	0.512217					83
Kaapvaal craton (Kimberlite xenolith)										
Bultfontein	PHN 2768/3	Clinopyroxenite	phl				19.529	15.733	39.184	84
Bultfontein	PHN 2768/3	Clinopyroxenite	phl				19.995	15.74	39.538	84
Kaalvallei	276	Websterite	cpx	0.703675	0.512839					85
Kaalvallei	431	Websterite	cpx	0.703662	0.512784					85
Kaalvallei	431	Websterite	cpx	0.703697						85

Supplementary Table 4 | Present Sr, Nd, Hf, and Pb isotopic compositions of kimberlite-source

Sample Name	Age T (Ma)	Initial isotope ratio at T						Present isotope ratio										ref.
		$^{87}Sr/^{86}Sr$	$^{143}Nd/^{144}Nd$	$^{176}Hf/^{177}Hf$	$^{206}Pb/^{204}Pb$	$^{207}Pb/^{204}Pb$	$^{208}Pb/^{204}Pb$	$^{87}Sr/^{86}Sr$	$^{143}Nd/^{144}Nd$	$^{176}Hf/^{177}Hf$	$^{206}Pb/^{204}Pb$			$^{207}Pb/^{204}Pb$			$^{208}Pb/^{204}Pb$	
											μ =80	μ =50	μ =10	μ =80	μ =50	μ =10	κ =4	
Group 1 Kimberlite																		
KK-3	90	0.70421	0.51256					0.70425	0.51268									86
KK-6	90	0.70478	0.51256					0.70482	0.51268									86
JJG2151	86	0.70527	0.51252					0.70531	0.51264									86
ROM312	88	0.70328	0.51262					0.70332	0.51274									86
LKF-1	74	0.70338	0.51259					0.70341	0.51269									86
ADF 1	74	0.70364	0.51264					0.70368	0.51273									86
JJG-4282	74	0.70369	0.51269					0.70372	0.51279									86
JAR-30012	74	0.70359	0.51269					0.70362	0.51279									86
JJG-3118	150	0.70398	0.51250					0.70405	0.51270									86
JJG-1906	150	0.70416	0.51249					0.70423	0.51269									86
GNF-2	74	0.70387	0.51266					0.70390	0.51275									86
HEB-1A	74	0.70368	0.51271					0.70372	0.51280									86
JJG-4323	74	0.70383	0.51268					0.70387	0.51278									86
JAR 31012	74	0.70386	0.51268					0.70390	0.51277									86
COL6	84	0.70450	0.51261					0.70454	0.51272									86
K8/17	84	0.70398	0.51261					0.70402	0.51272									86
K8/115	84	0.70537	0.51258					0.70541	0.51269									86
C16	84	0.70483	0.51254					0.70487	0.51265									86
K3/608	84	0.70460	0.51257					0.70463	0.51268									86
K6/55	84	0.70490	0.51259					0.70494	0.51270									86
C07	84	0.70432	0.51260					0.70435	0.51271									86
K119/2	84	0.70467	0.51257					0.70471	0.51268									86
K119/3	84	0.70462	0.51255					0.70466	0.51266									86

Supplementary Table 4 | *(continued)*

Sample Name	Age T (Ma)	Initial isotope ratio at T						Present isotope ratio										ref.
		$^{87}Sr/^{86}Sr$	$^{143}Nd/^{144}Nd$	$^{176}Hf/^{177}Hf$	$^{206}Pb/^{204}Pb$	$^{207}Pb/^{204}Pb$	$^{208}Pb/^{204}Pb$	$^{87}Sr/^{86}Sr$	$^{143}Nd/^{144}Nd$	$^{176}Hf/^{177}Hf$	$^{206}Pb/^{204}Pb$			$^{207}Pb/^{204}Pb$			$^{208}Pb/^{204}Pb$	
											μ =80	μ =50	μ =10	μ =80	μ =50	μ =10	κ =4	
K5/1	84	0.70404	0.51262					0.70408	0.51273									86
UB 1	101	0.70455	0.51254					0.70459	0.51268									86
UB 6	101	0.70456	0.51252					0.70460	0.51266									86
K2/W1/M	71.2	0.70442	0.51274		18.648	15.608	38.329	0.70445	0.51283		19.537	19.203	18.759	15.654	15.636	15.614	39.458	87
K2/W1/X	71.2	0.70442	0.51273					0.70445	0.51282									87
K2/W2/M	71.2	0.70440	0.51268		18.783	15.624	38.384	0.70444	0.51277		19.672	19.338	18.894	15.670	15.653	15.630	39.513	87
K2/W2/X	71.2	0.70433	0.51271					0.70436	0.51281									87
K2/W3/M	71.2	0.70431	0.51266					0.70434	0.51276									87
K2/W3/X	71.2	0.70430	0.51270					0.70434	0.51280									87
K2/3/M	71.2	0.70502	0.51268		18.667	15.620	38.471	0.70505	0.51277		19.556	19.223	18.778	15.666	15.648	15.626	39.601	87
K2/3/X	71.2	0.70532	0.51272					0.70535	0.51281									87
K35/W/X	71.6	0.70362	0.51263		18.932	15.635	38.537	0.70365	0.51272		19.825	19.490	19.043	15.681	15.663	15.640	39.672	87
K35/W/M	71.6	0.70361	0.51267		18.951	15.638		0.70364	0.51276		19.845	19.509	19.063	15.684	15.667	15.644		87
K39/W/M	71	0.70392	0.51268		19.104	15.658	38.838	0.70395	0.51277		19.990	19.657	19.214	15.703	15.686	15.663	39.964	87
K39/W/X	71	0.70390	0.51263					0.70393	0.51272									87
K39/1/M	71	0.70389	0.51264		18.839	15.631	38.593	0.70393	0.51274		19.725	19.393	18.950	15.677	15.660	15.637	39.719	87
K39/1/X	71	0.70387	0.51267		19.051	15.654		0.70390	0.51277		19.937	19.605	19.162	15.699	15.682	15.659		87
K53/W/M	64	0.70367	0.51265		19.091	15.633	38.741	0.70370	0.51274		19.889	19.590	19.191	15.673	15.658	15.638	39.756	87
K53/W/X	64	0.70366	0.51270					0.70369	0.51278									87
JAG-K10	86				18.993	15.536	38.671				20.067	19.664	19.127	15.592	15.571	15.543	40.035	88
UIN-1	100	0.70412	0.51273		19.035	15.691	38.947	0.70416	0.51286		20.286	19.817	19.191	15.758	15.733	15.699	40.534	88
RJ53+54K	90	0.70329	0.51276		19.093	15.547	38.699	0.70333	0.51288		20.217	19.795	19.233	15.606	15.584	15.554	40.127	88
BFK-1	90	0.70484	0.51274		18.673	15.518	38.283	0.70488	0.51286		19.798	19.376	18.814	15.578	15.556	15.526	39.711	88
K7/10B	90	0.70374	0.51277		19.006	15.570		0.70378	0.51289		20.131	19.709	19.147	15.630	15.607	15.578		88

Supplementary Table 4 | *(continued)*

Sample Name	Age T (Ma)	Initial isotope ratio at T						Present isotope ratio										ref.
		$^{87}Sr/^{86}Sr$	$^{143}Nd/^{144}Nd$	$^{176}Hf/^{177}Hf$	$^{206}Pb/^{204}Pb$	$^{207}Pb/^{204}Pb$	$^{208}Pb/^{204}Pb$	$^{87}Sr/^{86}Sr$	$^{143}Nd/^{144}Nd$	$^{176}Hf/^{177}Hf$	$^{206}Pb/^{204}Pb$			$^{207}Pb/^{204}Pb$			$^{208}Pb/^{204}Pb$	
											μ=80	μ=50	μ=10	μ=80	μ=50	μ=10	κ=4	
K61/35	114	0.70493			19.044	15.638	38.982	0.70498			20.472	19.936	19.223	15.717	15.687	15.648	40.792	88
P-PIEBALD	1180	0.70340	0.51126	0.28193				0.70394	0.51283	0.28271								89
CBS 1087-4	1180	0.70530	0.51123	0.28197				0.70584	0.51280	0.28275								89
FS-K1	114	0.70458	0.51252	0.28259	19.017	15.650	39.057	0.70463	0.51267	0.28266	20.444	19.909	19.195	15.729	15.699	15.660	40.867	88,89
MON-1	90	0.70410	0.51267	0.28276				0.70414	0.51279	0.28282								89
MON GREEN	90	0.70414	0.51265	0.28270				0.70418	0.51277	0.28275								89
BEN-1	90	0.70508	0.51263	0.28276				0.70513	0.51275	0.28281								89,90
KAA-1	85	0.70340	0.51266	0.28272				0.70343	0.51278	0.28278								89
WESS 423	86	0.70380	0.51262	0.28260				0.70384	0.51273	0.28265								89
LQ-7	90	0.70360	0.51264	0.28273				0.70364	0.51276	0.28279								89
P200	90	0.70315	0.51272	0.28274				0.70319	0.51283	0.28280								89
27/K16/6	103	0.70466	0.51255	0.28271				0.70470	0.51268	0.28278								89
GNS-13	100	0.70388	0.51268	0.28271				0.70392	0.51282	0.28277								89
26/K46/3	90	0.70348	0.51268	0.28270				0.70352	0.51279	0.28276								89
27/K1/16	74	0.70367	0.51271	0.28283				0.70371	0.51281	0.28288								89
26/K35	74		0.51269	0.28276					0.51279	0.28281								89
33/K5	71.5	0.70431	0.51275	0.28293				0.70435	0.51285	0.28298								89
K3-2	1787	0.70434	0.51018	0.28169				0.70516	0.51257	0.28288								91
K4-5-1	1787	0.70314	0.51025	0.28171				0.70396	0.51264	0.28290								91
K5-451	1787	0.70309	0.51034	0.28170				0.70390	0.51273	0.28289								91
K6-10-2	1787	0.70312	0.51038	0.28168				0.70394	0.51277	0.28286								91
K6-15-5	1787	0.70250	0.51032	0.28172				0.70332	0.51271	0.28291								91
K10-10-2	1787	0.70318		0.28161				0.70400		0.28280								91
K12-13-1	1787	0.70433	0.51019	0.28157				0.70515	0.51257	0.28276								91

Supplementary Table 4 | *(continued)*

Sample Name	Age T (Ma)	Initial isotope ratio at T						Present isotope ratio									ref.
		$^{87}Sr/^{86}Sr$	$^{143}Nd/^{144}Nd$	$^{176}Hf/^{177}Hf$	$^{206}Pb/^{204}Pb$	$^{207}Pb/^{204}Pb$	$^{208}Pb/^{204}Pb$	$^{87}Sr/^{86}Sr$	$^{143}Nd/^{144}Nd$	$^{176}Hf/^{177}Hf$	$^{206}Pb/^{204}Pb$			$^{207}Pb/^{204}Pb$			$^{208}Pb/^{204}Pb$	
											μ =80	μ =50	μ =10	μ =80	μ =50	μ =10	κ =4	
K12-12-1	1787	0.70458	0.51021	0.28157				0.70540	0.51260	0.28276								91
K13-13-1	1787	0.70455	0.51021	0.28167				0.70537	0.51260	0.28286								91
K14-5	1787	0.70345	0.51026	0.28166				0.70427	0.51265	0.28285								91
K14-11	1787	0.70294		0.28158				0.70376		0.28277								91
K4-2	1787	0.70312	0.51026	0.28165				0.70394	0.51265	0.28284								91
K10-8-7	1787	0.70339	0.51026					0.70420	0.51265									91
LETSENG-LA TERAI	85	0.70370	0.51267					0.70373	0.51278									92
NOD 1 CORE	71	0.70417	0.51269		18.340	15.590		0.70421	0.51279		19.226	18.893	18.450	15.635	15.618	15.595		93
NOD 5	71	0.70456	0.51285					0.70459	0.51294									93
NOD 11 CORE	71	0.70442	0.51264		18.267	15.576	38.182	0.70445	0.51274		19.153	18.821	18.378	15.622	15.605	15.582	39.308	93
NOD 12	71	0.70410	0.51272					0.70414	0.51282									93
NOD 14	71	0.70402						0.70405										93
K1	71	0.70429	0.51278		18.089	15.594		0.70432	0.51288		18.975	18.643	18.200	15.640	15.623	15.600		93
15C	71	0.70374	0.51280		19.254	15.662	38.925	0.70377	0.51289		20.140	19.808	19.365	15.708	15.691	15.668	40.051	93
M1	71	0.70401			18.802	15.631	38.798	0.70404			19.688	19.356	18.913	15.676	15.659	15.637	39.924	93
M3	71	0.70460			18.837	15.640		0.70464			19.723	19.391	18.948	15.686	15.669	15.646		93
PREM-A	1150	0.70382	0.51133					0.70435	0.51286									94
PREM-B	1150	0.70055	0.51124					0.70108	0.51278									94
PREM-C	1150	0.70157	0.51126					0.70210	0.51279									94
PREM-D	1150	0.70460	0.51121					0.70513	0.51274									94
PREM-E	1150	0.70389	0.51114					0.70441	0.51267									94
SHR207	1180	0.70234	0.51187					0.70288	0.51344									95
B-109	90		0.51261						0.51273									96
BEN-1	90		0.51258						0.51270									96

Supplementary Table 4 | *(continued)*

Sample Name	Age T (Ma)	Initial isotope ratio at T						Present isotope ratio										ref.
		$^{87}Sr/^{86}Sr$	$^{143}Nd/^{144}Nd$	$^{176}Hf/^{177}Hf$	$^{206}Pb/^{204}Pb$	$^{207}Pb/^{204}Pb$	$^{208}Pb/^{204}Pb$	$^{87}Sr/^{86}Sr$	$^{143}Nd/^{144}Nd$	$^{176}Hf/^{177}Hf$	$^{206}Pb/^{204}Pb$			$^{207}Pb/^{204}Pb$			$^{208}Pb/^{204}Pb$	
											μ=80	μ=50	μ=10	μ=80	μ=50	μ=10	κ=4	
A	90	0.70492			19.001	15.669	38.824	0.70496			20.125	19.704	19.141	15.728	15.706	15.676	40.252	97
B	90	0.70374			20.009	15.745	39.552	0.70378			21.133	20.712	20.149	15.804	15.782	15.752	40.980	97
C	90	0.70361			19.975	15.755	39.583	0.70365			21.099	20.678	20.115	15.814	15.792	15.762	41.011	97
1	90				19.919	15.709	39.479				21.043	20.621	20.059	15.768	15.746	15.716	40.907	97
2	90				19.643	15.696	39.035				20.768	20.346	19.783	15.755	15.733	15.703	40.463	97
4	90				19.411	15.736	39.460				20.536	20.114	19.551	15.795	15.773	15.743	40.888	97
6	90				19.323	15.642	39.116				20.447	20.026	19.463	15.701	15.679	15.649	40.544	97
8	90				19.187	15.700	39.076				20.311	19.890	19.327	15.760	15.737	15.708	40.504	97
9	90				18.412	15.557	38.060				19.537	19.115	18.553	15.617	15.594	15.565	39.488	97
10	90				19.890	15.724	39.320				21.015	20.593	20.030	15.784	15.761	15.732	40.748	97
11	90				18.846	15.610	38.507				19.971	19.549	18.987	15.669	15.647	15.617	39.935	97
Group 1 Kimberlite																		
JJG-4676	122	0.70799	0.51200															86
NE-K6	126	0.70739	0.51191															86
JJG-24	114	0.70782	0.51196															86
RVK-1	128	0.70814	0.51186															86
RVK-2	128	0.70739	0.51187															86
K2/2	110	0.70727	0.51204															86
K6/11	117	0.70837	0.51194															86
MRK-3	117	0.70837	0.51195															86
COL9	84	0.70748	0.51259															86
NC006SM	150	0.70833	0.51186	0.28223														98
NC010M	150	0.70958	0.51185	0.28216														98

Supplementary Table 4 | *(continued)*

Sample Name	Age T (Ma)	Initial isotope ratio at T						Present isotope ratio										ref.
		$^{87}Sr/^{86}Sr$	$^{143}Nd/^{144}Nd$	$^{176}Hf/^{177}Hf$	$^{206}Pb/^{204}Pb$	$^{207}Pb/^{204}Pb$	$^{208}Pb/^{204}Pb$	$^{87}Sr/^{86}Sr$	$^{143}Nd/^{144}Nd$	$^{176}Hf/^{177}Hf$	$^{206}Pb/^{204}Pb$			$^{207}Pb/^{204}Pb$			$^{208}Pb/^{204}Pb$	
											μ =80	μ =50	μ =10	μ =80	μ =50	μ =10	κ =4	
NC005M	150	0.70915	0.51183	0.28218														98
NC007M	150	0.71047	0.51184	0.28197														98
JJG 3149SM	150	0.70772	0.51184	0.28224														98
JJG 3145M	150	0.70807	0.51183	0.28224														98
JJG 2833	124	0.70736	0.51201	0.28248														98
JJG 6369	124	0.70797	0.51204	0.28249														98
NC050	124	0.70737	0.51204	0.28248														98
JJG 4570	124	0.70729	0.51201	0.28247														98
SJH30	124	0.70818	0.51204	0.28248														98
SJH79SM	124	0.70872	0.51203	0.28248														98
SJH78M	124	0.70795	0.51204															98
NC051M	124	0.70738	0.51207	0.28256														98
NC054M	124	0.70717	0.51208	0.28256														98
VI-A	520	0.70655	0.51016															99
NE-K4	127	0.70745			17.262	15.471	37.528	0.70745			18.854	18.257	17.461	15.561	15.527	15.483	39.580	88
NE-K6	127	0.70755			17.224	15.467	37.563	0.70755			18.816	18.219	17.423	15.557	15.523	15.478	39.580	88
NE-K10	127	0.70744			17.226	15.554	37.538	0.70744			18.818	18.221	17.425	15.643	15.609	15.565	39.555	88
K64/55	120	0.70752	0.51214		17.480	15.502	37.564	0.70752	0.51214		18.983	18.419	17.668	15.585	15.554	15.512	39.469	88
NS	114	0.70737			17.461	15.466		0.70737			18.889	18.353	17.640	15.545	15.515	15.476		88
K56/15	114	0.70771	0.51215															88
FINSCH B	118	0.70875	0.51228		17.629	15.523	37.640	0.70875	0.51228		19.107	18.552	17.814	15.605	15.574	15.533	39.513	88
MALE 14/1	145	0.70991	0.51206		17.636	15.513		0.70991	0.51206		19.456	18.773	17.863	15.618	15.579	15.526		88
KLIP3	150	0.70769			17.386	15.490	37.532	0.70769			19.270	18.563	17.622	15.600	15.559	15.504	39.916	88
FSM-2	114	0.70765	0.51247	0.28260														89

Supplementary Table 4 | *(continued)*

Sample Name	Age T (Ma)	Initial isotope ratio at T						Present isotope ratio										ref.
		$^{87}Sr/^{86}Sr$	$^{143}Nd/^{144}Nd$	$^{176}Hf/^{177}Hf$	$^{206}Pb/^{204}Pb$	$^{207}Pb/^{204}Pb$	$^{208}Pb/^{204}Pb$	$^{87}Sr/^{86}Sr$	$^{143}Nd/^{144}Nd$	$^{176}Hf/^{177}Hf$	$^{206}Pb/^{204}Pb$			$^{207}Pb/^{204}Pb$			$^{208}Pb/^{204}Pb$	
											μ=80	μ=50	μ=10	μ=80	μ=50	μ=10	κ=4	
PHN 2811	86	0.70540	0.51252	0.28256														89
MAIN 14/6	145	0.70865	0.51187	0.28200														89
MAIN 15/1	145	0.71085	0.51185	0.28208														89
PHN2386	127	0.70795	0.51187	0.28228														89
ROVIC-1	127	0.70753	0.51189	0.28227														89
F445	118	0.70868	0.51217	0.28257														89
F756	118	0.70893	0.51207	0.28246	17.796	15.570	37.623	0.70893	0.51207		19.274	18.720	17.981	15.652	15.621	15.580	39.497	89,100
F757	118	0.70877	0.51220	0.28259	17.614	15.497	37.568	0.70877	0.51220		19.092	18.538	17.799	15.579	15.548	15.507	39.442	89,100
F767	118	0.70894	0.51213	0.28259	17.547	15.494	37.485	0.70894	0.51213		19.025	18.471	17.732	15.576	15.546	15.505	39.358	89,100
LACE3	133	0.70722	0.51210	0.28257														89
FRB430M	120	0.70792	0.51202	0.28236														89
26/K24/5	122	0.70859	0.51193	0.28232														89
27/K9	123	0.70650	0.51233	0.28239														89
MW-3	124	0.70631	0.51234	0.28245														89
27/K19/2	125	0.70706	0.51222	0.28216														89
K5-463	1787		0.51030	0.28168														91
K11-2-2	1787		0.51019	0.28167														91
K15-6	124	0.70750	0.51200	0.28238														91
K11-10	1787	0.71637	0.51024	0.28169														91
K13-3-1	1787	0.70722	0.51013	0.28162														91
K15-5	124	0.70804	0.51201	0.28243														91
BELLSBANK	120	0.70788	0.51202															92
JJG 4326	92	0.70630	0.51249															101
JJG 6054	92	0.70748	0.51248															101

Supplementary Table 4 | *(continued)*

Sample Name	Age T (Ma)	Initial isotope ratio at T						Present isotope ratio										ref.
		$^{87}Sr/^{86}Sr$	$^{143}Nd/^{144}Nd$	$^{176}Hf/^{177}Hf$	$^{206}Pb/^{204}Pb$	$^{207}Pb/^{204}Pb$	$^{208}Pb/^{204}Pb$	$^{87}Sr/^{86}Sr$	$^{143}Nd/^{144}Nd$	$^{176}Hf/^{177}Hf$	$^{206}Pb/^{204}Pb$			$^{207}Pb/^{204}Pb$			$^{208}Pb/^{204}Pb$	
											μ=80	μ=50	μ=10	μ=80	μ=50	μ=10	κ=4	
K40/13	140	0.70631	0.51209															101
WIMB 1	90	0.70600	0.51244															101
WIMB 2	90	0.70564	0.51242															101
K19/2	150	0.70646	0.51216															101
MLW 3	143	0.70614	0.51228															101
SLH 9	150	0.70688	0.51215															101
SLH 10	150	0.70670	0.51209															101
K23/3	116	0.70617	0.51229															101
KJW9/WR	148	0.70706	0.51205															102
KJW13/WR	148	0.70714	0.51211															102
CRC1	118	0.70984	0.51211		17.544	15.473	37.488	0.70984	0.51211		19.022	18.467	17.728	15.554	15.524	15.483	39.362	100,103
CRC2	118	0.70869	0.51210		17.585	15.531	37.611	0.70869	0.51210		19.063	18.508	17.769	15.613	15.582	15.541	39.485	100,103
CRC3	118	0.70873			17.678	15.507	37.692	0.70873	0.00000		19.156	18.602	17.863	15.589	15.558	15.517	39.565	100,103
CRC4	118	0.71162	0.51209		18.026	15.563	37.987	0.71162	0.51209		19.504	18.949	18.210	15.645	15.615	15.574	39.860	100,103
CRC6	118	0.70875	0.51217		17.572	15.513	37.614	0.70875	0.51217		19.050	18.496	17.757	15.595	15.564	15.523	39.488	100,103
CRC7	118	0.70883	0.51213		17.640	15.558	37.716	0.70883	0.51213		19.118	18.564	17.825	15.640	15.609	15.568	39.590	100,103
FINSCH B	118	0.70855	0.51210		17.591	15.514	37.693	0.70855	0.51210		19.069	18.515	17.776	15.596	15.566	15.525	39.567	100,103
F653	118	0.70848	0.51212		17.614	15.519	37.561	0.70848	0.51212		19.092	18.538	17.799	15.601	15.571	15.530	39.435	100
F656	118	0.70862	0.51209		17.613	15.489	37.525	0.70862	0.51209		19.091	18.537	17.798	15.571	15.541	15.500	39.398	100
F659	118	0.70873	0.51209		17.619	15.518	37.573	0.70873	0.51209		19.097	18.543	17.804	15.600	15.569	15.529	39.447	100
F664	118	0.70777	0.51212		17.610	15.505	37.580	0.70777	0.51212		19.088	18.534	17.795	15.587	15.556	15.515	39.454	100
F287	118	0.70912	0.51199		17.630	15.541	37.793	0.70912	0.51199		19.107	18.553	17.814	15.623	15.592	15.551	39.667	100
F765	118	0.70922	0.51214		17.634	15.530	37.590	0.70922	0.51214		19.112	18.558	17.819	15.612	15.581	15.540	39.463	100
F766	118	0.70871	0.51215		17.627	15.520	37.588	0.70871	0.51215		19.105	18.551	17.812	15.602	15.571	15.530	39.462	100

Supplementary Table 4 | *(continued)*

Sample Name	Age T (Ma)	Initial isotope ratio at T						Present isotope ratio										ref.
		$^{87}Sr/^{86}Sr$	$^{143}Nd/^{144}Nd$	$^{176}Hf/^{177}Hf$	$^{206}Pb/^{204}Pb$	$^{207}Pb/^{204}Pb$	$^{208}Pb/^{204}Pb$	$^{87}Sr/^{86}Sr$	$^{143}Nd/^{144}Nd$	$^{176}Hf/^{177}Hf$	$^{206}Pb/^{204}Pb$			$^{207}Pb/^{204}Pb$			$^{208}Pb/^{204}Pb$	
											μ=80	μ=50	μ=10	μ=80	μ=50	μ=10	κ=4	
F652	118	0.70841	0.51210		17.616	15.534	37.684	0.70841	0.51210		19.094	18.540	17.801	15.616	15.585	15.545	39.557	100
F660	118	0.70867	0.51212		17.593	15.499	37.517	0.70867	0.51212		19.071	18.517	17.778	15.581	15.550	15.509	39.390	100
F661	118	0.70940	0.51216		17.513	15.431	37.305	0.70940	0.51216		18.991	18.437	17.698	15.513	15.483	15.442	39.179	100
F340	118	0.70948	0.51183		17.559	15.520	37.588	0.70948	0.51183		19.037	18.482	17.743	15.602	15.571	15.530	39.461	100
F557	118	0.70943	0.51190		17.553	15.490	37.462	0.70943	0.51190		19.031	18.476	17.738	15.572	15.541	15.501	39.335	100
F758	118	0.70994	0.51187		17.798	15.530	37.541	0.70994	0.51187		19.276	18.722	17.983	15.612	15.581	15.540	39.414	100
PREM-F	1150	0.70764	0.51100															94
12(Type2)	90				17.625	15.572	37.928	0.00004	0.00012		18.749	18.328	17.765	15.632	15.609	15.580	39.356	97
D	90	0.70917			17.710	15.518	37.678	0.70917			18.835	18.413	17.850	15.578	15.555	15.526	39.106	97
E	90	0.70936			17.695	15.497	37.640	0.70936			18.820	18.398	17.836	15.557	15.534	15.505	39.068	97

Parent-daughter ratios for the present isotope ratio of Sr, Nd, and Hf are calculated using $^{87}Rb/^{87}Rb$=0.03183, $^{147}Sm/^{144}Nd$=0.2032, and $^{176}Hf/^{177}Hf$=0.0339.

References in Appendix Tables

1 Moeller, H. *Magma genesis and mantle sources at the Mid-Atlantic Ridge east of Ascension Island* PhD thesis thesis, Christian-Albrechts Universität, Kiel, (2002).

2 Hoernle, K., Hauff, F., Kokfelt, T. F., Haase, K., Garbe-Schönberg, D. & Werner, R. On- and off-axis chemical heterogeneities along the South Atlantic Mid-Ocean-Ridge (5–11°S): Shallow or deep recycling of ocean crust and/or intraplate volcanism? *Earth Planet. Sci. Lett.* **306**, 86-97, (2011).

3 Paulick, H., Münker, C. & Schuth, S. The influence of small-scale mantle heterogeneities on Mid-Ocean Ridge volcanism: Evidence from the southern Mid-Atlantic Ridge (7°30′S to 11°30′S) and Ascension Island. *Earth Planet. Sci. Lett.* **296**, 299-310, (2010).

4 Stroncik, N. A. & Niedermann, S. Atmospheric contamination of the primary Ne and Ar signal in mid-ocean ridge basalts and its implications for ocean crust formation. *Geoch. Cosmoch. Acta* **172**, 306-321, (2016).

5 Haase, K. M., Brandl, P. A., Devey, C. W., Hauff, F., Melchert, B., Garbe-Schönberg, D., Kokfelt, T. F. & Paulick, H. Compositional variation and 226Ra-230Th model ages of axial lavas from the southern Mid-Atlantic Ridge, 8°48′S. *Geochemistry, Geophysics, Geosystems* **17**, 199-218, (2016).

6 Ulrich, M., Hémond, C., Nonnotte, P. & Jochum, K. P. OIB/seamount recycling as a possible process for E-MORB genesis. *Geochemistry, Geophysics, Geosystems* **13**, n/a-n/a, (2012).

7 Wilson, S. C., Murton, B. J. & Taylor, R. N. Mantle composition controls the development of an Oceanic Core Complex. *Geochemistry, Geophysics, Geosystems* **14**, 979-995, (2013).

8 White, W. M. & Schilling, J.-G. The nature and origin of geochemical variation in Mid-Atlantic Ridge basalts from the Central North Atlantic. *Geoch. Cosmoch. Acta* **42**, 1501-1516, (1978).

9 Dosso, L., Hanan, B. B., Bougault, H., Schilling, J.-G. & Joron, J.-L. SrNdPb geochemical morphology between 10° and 17°N on the Mid-Atlantic Ridge: A new MORB isotope signature. *Earth Planet. Sci. Lett.* **106**, 29-43, (1991).

10 Yu, D. *Rare earth element chromatographic separation and application to the Mid-Atlantic Ridge basalts (28°N-65°N) geochemistry* Ph.D. thesis thesis, Univ. Geneva, (1993).

11 Schilling, J. G., Hanan, B. B., McCully, B., Kingsley, R. H. & Fontignie, D. Influence of the Sierra Leone mantle plume on the equatorial Mid-Atlantic Ridge: A Nd-Sr-Pb isotopic study. *Journal of Geophysical Research: Solid Earth* **99**, 12005-12028, (1994).

12 Fontignie, D. & Schilling, J.-G. Mantle heterogeneities beneath the South Atlantic: a NdSrPb isotope study along the Mid-Atlantic Ridge (3°S–46°S). *Earth Planet. Sci. Lett.* **142**, 209-221, (1996).

13 Andres, M., Blichert-Toft, J. & Schilling, J.-G. Nature of the depleted upper mantle beneath the Atlantic: evidence from Hf isotopes in normal mid-ocean ridge basalts from 79°N to 55°S. *Earth Planet. Sci. Lett.* **225**, 89-103, (2004).

14 Debaille, V., Blichert-Toft, J., Agranier, A., Doucelance, R., Schiano, P. & Albarede, F. Geochemical component relationships in MORB from the Mid-Atlantic Ridge, 22–35°N. *Earth Planet. Sci. Lett.* **241**, 844-862, (2006).

15 Agranier, A., Blichert-Toft, J., Graham, D., Debaille, V., Schiano, P. & Albarède, F. The spectra of isotopic heterogeneities along the mid-Atlantic Ridge. *Earth Planet. Sci. Lett.* **238**, 96-109, (2005).
16 Thirlwall, M. F., Jenkins, C., Vroon, P. Z. & Mattey, D. P. Crustal interaction during construction of ocean islands: Pb□Sr□Nd□O isotope geochemistry of the shield basalts of Gran Canaria, Canary Islands. *Chem. Geol.* **135**, 233-262, (1997).
17 Cousens, B. L., Spera, F. J. & Tilton, G. R. Isotopic patterns in silicic ignimbrites and lava flows of the Mogan and lower Fataga Formations, Gran Canaria, Canary Islands: temporal changes in mantle source composition. *Earth Planet. Sci. Lett.* **96**, 319-335, (1990).
18 Marcantonio, F., Zindler, A., Elliott, T. & Staudigel, H. Os isotope systematics of La Palma, Canary Islands: Evidence for recycled crust in the mantle source of HIMU ocean islands. *Earth Planet. Sci. Lett.* **133**, 397-410, (1995).
19 Whitehouse, M. J. & Neumann, E. R. Sr-Nd-Pb isotope data for ultramafic xenoliths from Hierro, Canary Islands: Melt infiltration processes in the upper mantle. *Contrib. Mineral. Petrol.* **119**, 239-246, (1995).
20 Ovchinnikiva, G. V., Belyatsky, B. V., Vasil'eva, I. M., Levskii, L. K., Grachev, A. F., Arana, V. & Mithavila, J. Sr-Nd-Pb isotope characteristics of the mantle sources of basalts from the Canary Islands. *Petrology* **3**, 172-182, (1995).
21 Hoernle, K., Tilton, G. & Schmincke, H.-U. SrNdPb isotopic evolution of Gran Canaria: Evidence for shallow enriched mantle beneath the Canary Islands. *Earth Planet. Sci. Lett.* **106**, 44-63, (1991).
22 Thomas, L. E., Hawkesworth, C. J., Van Calsteren, P., Turner, S. P. & Rogers, N. W. Melt generation beneath ocean islands: a U-Th-Ra isotope study from Lanzarote in the Canary Islands. *Geoch. Cosmoch. Acta* **63**, 4081-4099, (1999).
23 Simonsen, S. L., Neumann, E. R. & Seim, K. Sr–Nd–Pb isotope and trace-element geochemistry evidence for a young HIMU source and assimilation at Tenerife (Canary Island). *J. Volcanol. Geotherm. Res.* **103**, 299-312, (2000).
24 Geldmacher, J., Hoernle, K., van den Bogaard, P., Zankl, G. & Garbe-Schönberg, D. Earlier history of the ≥70-Ma-old Canary hotspot based on the temporal and geochemical evolution of the Selvagen Archipelago and neighboring seamounts in the eastern North Atlantic. *J. Volcanol. Geotherm. Res.* **111**, 55-87, (2001).
25 Prægel, N. O. & Holm, P. M. Lithospheric contributions to high-MgO basanites from the Cumbre Vieja Volcano, La Palma, Canary Islands and evidence for temporal variation in plume influence. *J. Volcanol. Geotherm. Res.* **149**, 213-239, (2006).
26 Gurenko, A. A., Hoernle, K. A., Hauff, F., Schmincke, H. U., Han, D., Miura, Y. N. & Kaneoka, I. Major, trace element and Nd–Sr–Pb–O–He–Ar isotope signatures of shield stage lavas from the central and western Canary Islands: Insights into mantle and crustal processes. *Chem. Geol.* **233**, 75-112, (2006).
27 Abratis, M., Schmincke, H. U. & Hansteen, T. Composition and evolution of submarine volcanic rocks from the central and western Canary Islands. *Int J Earth Sci* **91**, 562-582, (2002).
28 Gurenko, A. A., Sobolev, A. V., Hoernle, K. A., Hauff, F. & Schmincke, H.-U. Enriched, HIMU-type peridotite and depleted recycled pyroxenite in the Canary plume: A mixed-up mantle. *Earth Planet. Sci. Lett.* **277**, 514-524, (2009).
29 Aparicio, A., Tassinari, C. C. G., García, R. & Araña, V. Sr and Nd isotope

composition of the metamorphic, sedimentary and ultramafic xenoliths of Lanzarote (Canary Islands): Implications for magma sources. *J. Volcanol. Geotherm. Res.* **189**, 143-150, (2010).

30 Aulinas, M., Gimeno, D., Fernandez-Turiel, J. L., Font, L., Perez-Torrado, F. J., Rodriguez-Gonzalez, A. & Nowell, G. M. Small-scale mantle heterogeneity on the source of the Gran Canaria (Canary Islands) Pliocene–Quaternary magmas. *Lithos* **119**, 377-392, (2010).

31 Day, J. M. D., Pearson, D. G., Macpherson, C. G., Lowry, D. & Carracedo, J. C. Evidence for distinct proportions of subducted oceanic crust and lithosphere in HIMU-type mantle beneath El Hierro and La Palma, Canary Islands. *Geoch. Cosmoch. Acta* **74**, 6565-6589, (2010).

32 Geldmacher, J., Hoernle, K., Hanan, B. B., Blichert-Toft, J., Hauff, F., Gill, J. B. & Schmincke, H.-U. Hafnium isotopic variations in East Atlantic intraplate volcanism. *Contrib. Mineral. Petrol.* **162**, 21-36, (2011).

33 Wiesmaier, S., Deegan, F. M., Troll, V. R., Carracedo, J. C., Chadwick, J. P. & Chew, D. M. Magma mixing in the 1100 AD Montaña Reventada composite lava flow, Tenerife, Canary Islands: interaction between rift zone and central volcano plumbing systems. *Contrib. Mineral. Petrol.* **162**, 651-669, (2011).

34 Deegan, F. M., Troll, V. R., Barker, A. K., Harris, C., Chadwick, J. P., Carracedo, J. C. & Delcamp, A. Crustal versus source processes recorded in dykes from the Northeast volcanic rift zone of Tenerife, Canary Islands. *Chem. Geol.* **334**, 324-344, (2012).

35 Del Moro, S., Di Roberto, A., Meletlidis, S., Pompilio, M., Bertagnini, A., Agostini, S., Ridolfi, F. & Renzulli, A. Xenopumice erupted on 15 October 2011 offshore of El Hierro (Canary Islands): a subvolcanic snapshot of magmatic, hydrothermal and pyrometamorphic processes. *Bull. Volcanol.* **77**, 53, (2015).

36 Turner, S., Hoernle, K., Hauff, F., Johansen, T. S., Klügel, A., Kokfelt, T. & Lundstrom, C. 238 U– 230 Th– 226 Ra Disequilibria Constraints on the Magmatic Evolution of the Cumbre Vieja Volcanics on La Palma, Canary Islands. *J. Petrol.* **56**, 1999-2024, (2015).

37 Johansen, T. S., Hauff, F., Hoernle, K., Klügel, A. & Kokfelt, T. F. Basanite to phonolite differentiation within 1550–1750 yr: U-Th-Ra isotopic evidence from the A.D. 1585 eruption on La Palma, Canary Islands. *Geology* **33**, 897-900, (2005).

38 Duggen, S., Hoernle, K., Van Den Bogaard, P. & Garbe-SchÖNberg, D. Post-Collisional Transition from Subduction- to Intraplate-type Magmatism in the Westernmost Mediterranean: Evidence for Continental-Edge Delamination of Subcontinental Lithosphere. *J. Petrol.* **46**, 1155-1201, (2005).

39 El Azzouzi, M. h., Bernard-Griffiths, J., Bellon, H., Maury, R. C., Piqué, A., Fourcade, S., Cotten, J. & Hernandez, J. Évolution des sources du volcanisme marocain au cours du Néogène. *Comptes Rendus de l'Académie des Sciences - Series IIA - Earth and Planetary Science* **329**, 95-102, (1999).

40 Wagner, C., Mokhtari, A., Deloule, E. & Chabaux, F. Carbonatite and Alkaline Magmatism in Taourirt (Morocco): Petrological, Geochemical and Sr–Nd Isotope Characteristics. *J. Petrol.* **44**, 937-965, (2003).

41 Natali, C., Beccaluva, L., Bianchini, G., Ellam, R. M., Siena, F. & Stuart, F. M. Carbonated alkali-silicate metasomatism in the North Africa lithosphere: Evidence from Middle Atlas spinel-lherzolites, Morocco. *Journal of South*

American Earth Sciences **41**, 113-121, (2013).
42 Bosch, D., Maury, R. C., El Azzouzi, M. h., Bollinger, C., Bellon, H. & Verdoux, P. Lithospheric origin for Neogene–Quaternary Middle Atlas lavas (Morocco): Clues from trace elements and Sr–Nd–Pb–Hf isotopes. *Lithos* **205**, 247-265, (2014).
43 Berger, J., Ennih, N. & Liégeois, J.-P. Extreme trace elements fractionation in Cenozoic nephelinites and phonolites from the Moroccan Anti-Atlas (Eastern Saghro). *Lithos* **210–211**, 69-88, (2014).
44 Davies, G. R., Cliff, R. A., Norry, M. J. & Gerlach, D. C. A combined chemical and Pb-Sr-Nd isotope study of the Azores and Cape Verde hot-spots: the geodynamic implications. *Geological Society, London, Special Publications* **42**, 231-255, (1989).
45 Gerlach, D. C., Cliff, R. A., Davies, G. R., Norry, M. & Hodgson, N. Magma sources of the Cape Verdes archipelago: Isotopic and trace element constraints. *Geoch. Cosmoch. Acta* **52**, 2979-2992, (1988).
46 Christensen, B. P., Holm, P. M., Jambon, A. & Wilson, J. R. Helium, argon and lead isotopic composition of volcanics from Santo Antão and Fogo, Cape Verde Islands. *Chem. Geol.* **178**, 127-142, (2001).
47 Jørgensen, J. Ø. & Holm, P. M. Temporal variation and carbonatite contamination in primitive ocean island volcanics from São Vicente, Cape Verde Islands. *Chem. Geol.* **192**, 249-267, (2002).
48 Doucelance, R., Escrig, S., Moreira, M., Gariépy, C. & Kurz, M. D. Pb-Sr-He isotope and trace element geochemistry of the Cape Verde Archipelago. *Geoch. Cosmoch. Acta* **67**, 3717-3733, (2003).
49 Escrig, S., Doucelance, R., Moreira, M. & Allègre, C. J. Os isotope systematics in Fogo Island: Evidence for lower continental crust fragments under the Cape Verde Southern Islands. *Chem. Geol.* **219**, 93-113, (2005).
50 Holm, P. M., Wilson, J. R., Christensen, B. P., Hansen, L., Hansen, S. L., Hein, K. M., Mortensen, A. K., Pedersen, R., Plesner, S. & Runge, M. K. Sampling the Cape Verde Mantle Plume: Evolution of Melt Compositions on Santo Antão, Cape Verde Islands. *J. Petrol.* **47**, 145-189, (2006).
51 Millet, M.-A., Doucelance, R., Schiano, P., David, K. & Bosq, C. Mantle plume heterogeneity versus shallow-level interactions: A case study, the São Nicolau Island, Cape Verde archipelago. *J. Volcanol. Geotherm. Res.* **176**, 265-276, (2008).
52 Barker, A. K., Holm, P. M., Peate, D. W. & Baker, J. A. Geochemical Stratigraphy of Submarine Lavas (3–5 Ma) from the Flamengos Valley, Santiago, Southern Cape Verde Islands. *J. Petrol.* **50**, 169-193, (2009).
53 Martins, S., Mata, J., Munhá, J., Mendes, M. H., Maerschalk, C., Caldeira, R. & Mattielli, N. Chemical and mineralogical evidence of the occurrence of mantle metasomatism by carbonate-rich melts in an oceanic environment (Santiago Island, Cape Verde). *Mineralogy and Petrology* **99**, 43-65, (2010).
54 Barker, A. K., Holm, P. M., Peate, D. W. & Baker, J. A. A 5 million year record of compositional variations in mantle sources to magmatism on Santiago, southern Cape Verde archipelago. *Contrib. Mineral. Petrol.* **160**, 133-154, (2010).
55 Doucelance, R., Hammouda, T., Moreira, M. & Martins, J. C. Geochemical constraints on depth of origin of oceanic carbonatites: The Cape Verde case. *Geoch. Cosmoch. Acta* **74**, 7261-7282, (2010).

56 Hildner, E., Klügel, A. & Hansteen, T. H. Barometry of lavas from the 1951 eruption of Fogo, Cape Verde Islands: Implications for historic and prehistoric magma plumbing systems. *J. Volcanol. Geotherm. Res.* **217–218**, 73-90, (2012).
57 Mourão, C., Mata, J., Doucelance, R., Madeira, J., Millet, M.-A. & Moreira, M. Geochemical temporal evolution of Brava Island magmatism: Constraints on the variability of Cape Verde mantle sources and on carbonatite–silicate magma link. *Chem. Geol.* **334**, 44-61, (2012).
58 Doucelance, R., Bellot, N., Boyet, M., Hammouda, T. & Bosq, C. What coupled cerium and neodymium isotopes tell us about the deep source of oceanic carbonatites. *Earth Planet. Sci. Lett.* **407**, 175-186, (2014).
59 Nkouandou, O. F., Ngounouno, I., Déruelle, B., Ohnenstetter, D., Montigny, R. & Demaiffe, D. Petrology of the Mio-Pliocene volcanism to the North and East of Ngaoundéré (Adamawa, Cameroon). *Comptes Rendus Geoscience* **340**, 28-37, (2008).
60 Halliday, A. N., Davidson, J. P., Holden, P., DeWolf, C., Lee, D.-C. & Fitton, J. G. Trace-element fractionation in plumes and the origin of HIMU mantle beneath the Cameroon line. *Nature* **347**, 523-528, (1990).
61 Ballentine, C. J., Lee, D. C. & Halliday, A. N. Hafnium isotopic studies of the Cameroon line and new HIMU paradoxes. *Chem. Geol.* **139**, 111-124, (1997).
62 Tchuimegnie Ngongang, N. B., Kamgang, P., Chazot, G., Agranier, A., Bellon, H. & Nonnotte, P. Age, geochemical characteristics and petrogenesis of Cenozoic intraplate alkaline volcanic rocks in the Bafang region, West Cameroon. *J. Afr. Earth Sci.* **102**, 218-232, (2015).
63 Asaah, A. N. E., Yokoyama, T., Aka, F. T., Usui, T., Kuritani, T., Wirmvem, M. J., Iwamori, H., Fozing, E. M., Tamen, J., Mofor, G. Z., Ohba, T., Tanyileke, G. & Hell, J. V. Geochemistry of lavas from maar-bearing volcanoes in the Oku Volcanic Group of the Cameroon Volcanic Line. *Chem. Geol.* **406**, 55-69, (2015).
64 Rankenburg, K., Lassiter, J. C. & Brey, G. The Role of Continental Crust and Lithospheric Mantle in the Genesis of Cameroon Volcanic Line Lavas: Constraints from Isotopic Variations in Lavas and Megacrysts from the Biu and Jos Plateaux. *J. Petrol.* **46**, 169-190, (2005).
65 Geldmacher, J. & Hoernle, K. The 72 Ma geochemical evolution of the Madeira hotspot (eastern North Atlantic): recycling of Paleozoic (≤500 Ma) oceanic lithosphere. *Earth Planet. Sci. Lett.* **183**, 73-92, (2000).
66 Mata, J., Kerrich, R., MacRae, N. D. & Wu, T. W. Elemental and isotopic (Sr, Nd, and Pb) characteristics of Madeira Island basalts: evidence for a composite HIMU - EM I plume fertilizing lithosphere. *Canadian Journal of Earth Sciences* **35**, 980-997, (1998).
67 Geldmacher, J., Hoernle, K., Klügel, A., van den Bogaard, P. & Duggen, S. A geochemical transect across a heterogeneous mantle upwelling: Implications for the evolution of the Madeira hotspot in space and time. *Lithos* **90**, 131-144, (2006).
68 France, L., Chazot, G., Kornprobst, J., Dallai, L., Vannucci, R., Grégoire, M., Bertrand, H. & Boivin, P. Mantle refertilization and magmatism in old orogenic regions: The role of late-orogenic pyroxenites. *Lithos* **232**, 49-75, (2015).
69 Lee, D.-C., Halliday, A. N., Davies, G. R., Essene, E. J., Fitton, J. G. & Temdjim, R. Melt Enrichment of Shallow Depleted Mantle: a Detailed Petrological, Trace Element and Isotopic Study of Mantle-Derived Xenoliths and Megacrysts from

the Cameroon Line. *J. Petrol.* **37**, 415-441, (1996).
70 Pezzali, I., France, L., Chazot, G. & Vannucci, R. Analogues of exhumed pyroxenite layers in the Alboran domain sampled as xenoliths by Middle Atlas Cenozoic volcanism. *Lithos* **230**, 184-188, (2015).
71 Raffone, N., Chazot, G., Pin, C., Vannucci, R. & Zanetti, A. Metasomatism in the Lithospheric Mantle beneath Middle Atlas (Morocco) and the Origin of Fe- and Mg-rich Wehrlites. *J. Petrol.* **50**, 197-249, (2009).
72 Kaczmarek, M. A., Bodinier, J. L., Bosch, D., Tommasi, A., Dautria, J. M. & Kechid, S. A. Metasomatized Mantle Xenoliths as a Record of the Lithospheric Mantle Evolution of the Northern Edge of the Ahaggar Swell, In Teria (Algeria). *J. Petrol.* **57**, 345-382, (2016).
73 Vance, D., Stone, J. O. H. & O'Nions, R. K. He, Sr and Nd isotopes in xenoliths from Hawaii and other oceanic islands. *Earth Planet. Sci. Lett.* **96**, 147-160, (1989).
74 Neumann, E. R., Wulff-Pedersen, E., Pearson, N. J. & Spencer, E. A. Mantle Xenoliths from Tenerife (Canary Islands): Evidence for Reactions between Mantle Peridotites and Silicic Carbonatite Melts inducing Ca Metasomatism. *J. Petrol.* **43**, 825-857, (2002).
75 Neumann, E. R., Abu El-Rus, M. A., Tiepolo, M., Ottolini, L., Vannucci, R. & Whitehouse, M. Serpentinization and Deserpentinization Reactions in the Upper Mantle beneath Fuerteventura Revealed by Peridotite Xenoliths with Fibrous Orthopyroxene and Mottled Olivine. *J. Petrol.* **56**, 3-31, (2015).
76 Teklay, M., Scherer, E. E., Mezger, K. & Danyushevsky, L. Geochemical characteristics and Sr–Nd–Hf isotope compositions of mantle xenoliths and host basalts from Assab, Eritrea: implications for the composition and thermal structure of the lithosphere beneath the Afar Depression. *Contrib. Mineral. Petrol.* **159**, 731-751, (2010).
77 Cohen, R. S., Onions, R. K. & Dawson, J. B. Isotope geochemistry of xenoliths from East Africa: Implications for development of mantle reservoirs and their interaction. *Earth Planet. Sci. Lett.* **68**, 209-220, (1984).
78 Bell, K. & Dawson, J. B. in *Carbonatite Volcanism: Oldoinyo Lengai and the Petrogenesis of Natrocarbonatites* (eds Keith Bell & Jörg Keller) 100-112 (Springer Berlin Heidelberg, 1995).
79 Koornneef, J. M., Davies, G. R., Döpp, S. P., Vukmanovic, Z., Nikogosian, I. K. & Mason, P. R. D. Nature and timing of multiple metasomatic events in the sub-cratonic lithosphere beneath Labait, Tanzania. *Lithos* **112, Supplement 2**, 896-912, (2009).
80 Rudnick, R. L., McDonough, W. F. & Chappell, B. W. Carbonatite metasomatism in the northern Tanzanian mantle: petrographic and geochemical characteristics. *Earth Planet. Sci, Lett.* **114**, 463-475, (1993).
81 Mansur, A. T., Manya, S., Timpa, S. & Rudnick, R. L. Granulite-Facies Xenoliths in Rift Basalts of Northern Tanzania: Age, Composition and Origin of Archean Lower Crust. *J. Petrol.* **55**, 1243-1286, (2014).
82 Davies, G. R. & Lloyd, F. E. in *Kimberlites and Related Rocks, 2, Geological Society of Australia Special Publication* Vol. 14 784-794 (1989).
83 Kramm, U., Maravic, H. V. & Morteani, G. Neodymium and Sr isotopic constraints on the petrogenetic relationships between carbonatites and cancrinite

syenites from the Lueshe Alkaline Complex, east Zaire. *J. Afr. Earth Sci.* **25**, 55-76, (1997).
84 Rosenbaum, J. M. Mantle phlogopite: a significant lead repository? *Chem. Geol.* **106**, 475-483, (1993).
85 Viljoen, K. S., Schulze, D. J. & Quadling, A. G. Contrasting Group I and Group II Eclogite Xenolith Petrogenesis: Petrological, Trace Element and Isotopic Evidence from Eclogite, Garnet-Websterite and Alkremite Xenoliths in the Kaalvallei Kimberlite, South Africa. *J. Petrol.* **46**, 2059-2090, (2005).
86 Becker, M. & le Roex, A. P. Geochemistry of South African On- and Off-craton, Group I and Group II Kimberlites: Petrogenesis and Source Region Evolution. *J. Petrol.* **47**, 673-703, (2006).
87 Davies, G. R., Spriggs, A. J. & Nixon, P. H. A Non-cognate Origin for the Gibeon Kimberlite Megacryst Suite, Namibia: Implications for the Origin of Namibian Kimberlites. *J. Petrol.* **42**, 159-172, (2001).
88 Smith, C. B. Pb, Sr, and Nd isotopic evidence for sources of southern African Cretaceous kimberlites. *Nature* **304**, 51-54, (1983).
89 Nowell, G. M., Pearson, D. G., Bell, D. R., Carlson, R. W., Smith, C. B., Kempton, P. D. & Noble, S. R. Hf Isotope Systematics of Kimberlites and their Megacrysts: New Constraints on their Source Regions. *J. Petrol.* **45**, 1583-1612, (2004).
90 Nowell, G. M., Pearson, D. G., Kempton, P. D., Noble, S. R. & Smith, C. B. in *Proceedings 7th International Kimberlite Conference.* (eds J. J. Gurney, J. L. Gurney, M. D. Pascoe, & S. H. Richardson) 616-624 (National Book Printer).
91 Donnelly, C. L., Griffin, W. L., O'Reilly, S. Y., Pearson, N. J. & Shee, S. R. The Kimberlites and related rocks of the Kuruman Kimberlite Province, Kaapvaal Craton, South Africa. *Contrib. Mineral. Petrol.* **161**, 351-371, (2011).
92 Walker, R. J., Carlson, R. W., Shirey, S. B. & Boyd, F. R. Os, Sr, Nd, and Pb isotope systematics of southern African peridotite xenoliths: Implications for the chemical evolution of subcontinental mantle. *Geoch. Cosmoch. Acta* **53**, 1583-1595, (1989).
93 Weis, D. & Demaiffe, D. A depleted mantle source for kimberlites from Zaire: Nd, Sr and Pb isotopic evidence. *Earth Planet. Sci. Lett.* **73**, 269-277, (1985).
94 Wu, F.-Y., Mitchell, R. H., Li, Q.-L., Sun, J., Liu, C.-Z. & Yang, Y.-H. In situ UPb age determination and SrNd isotopic analysis of perovskite from the Premier (Cullinan) kimberlite, South Africa. *Chem. Geol.* **353**, 83-95, (2013).
95 Hoal, K. O. Samples of Proterozoic iron-enriched mantle from the Premier kimberlite. *Lithos* **71**, 259-272, (2003).
96 Basu, A. R. & Tatsumoto, M. Nd-isotopes in selected mantle-derived rocks and minerals and their implications for mantle evolution. *Contrib. Mineral. Petrol.* **75**, 43-54, (1980).
97 Kramers, J. D. Lead and strontium isotopes in Cretaceous kimberlites and mantle-derived xenoliths from Southern Africa. *Earth Planet. Sci. Lett.* **34**, 419-431, (1977).
98 Coe, N., le Roex, A., Gurney, J., Pearson, D. G. & Nowell, G. Petrogenesis of the Swartruggens and Star Group II kimberlite dyke swarms, South Africa: constraints from whole rock geochemistry. *Contrib. Mineral. Petrol.* **156**, 627, (2008).
99 Richardson, S. H., Pöml, P. F., Shirey, S. B. & Harris, J. W. Age and origin of

peridotitic diamonds from Venetia, Limpopo Belt, Kaapvaal–Zimbabwe craton. *Lithos* **112, Supplement 2**, 785-792, (2009).

100 Fraser, K. J. & Hawkesworth, C. J. The petrogenesis of group 2 ultrapotassic kimberlites from Finsch Mine, South Africa. *Lithos* **28**, 327-345, (1992).

101 Becker, M., le Roex, A. P. & Class, C. Geochemistry and petrogenesis of South African transitional kimberlites located on and off the Kaapvaal Craton. *South African Journal of Geology* **110**, 631-646, (2007).

102 Westerlund, K. J., Gurney, J. J., Carlson, R. W., Shirey, S. B., Hauri, E. H. & Richardson, S. H. A metasomatic origin for late Archean eclogitic diamonds: Implications from internal morphology of diamonds and Re-Os and S isotope characteristics of their sulfide inclusions from the late Jurassic Klipspringer kimberlites. *South African Journal of Geology* **107**, 119-130, (2004).

103 Fraser, K. J., Hawkesworth, C. J., Erlank, A. J., Mitchell, R. H. & Scottsmith, B. H. Sr, Nd and Pb isotope and minor element geochemistry of lamproites and kimberlites. *Earth Planet. Sci. Lett.* **76**, 57-70, (1985).